The Gran Sasso National Laboratory

The Gran Sasso National Laboratory (LNGS) is the largest underground laboratory in the world for experiments in particle and astroparticle physics. It is one of four INFN national laboratories and it is used as a worldwide facility by scientists (presently 900 in number) from 24 countries.

Its location is near the town of L'Aquila, about 120 km from Rome. The underground facilities are located on a side of the ten kilometres long freeway tunnel crossing the Gran Sasso Mountain. They consist of three large experimental halls, each about 100 m long, 20 m wide and 15 m high and service tunnels for a total volume of about 180,000 cubic metres.

The average 1400 m rock coverage gives a reduction factor of one million in the cosmic ray flux; moreover, the neutron flux is thousand times less than on the surface, thanks to the smallness of the Uranium and Thorium content of the dolomite rocks of the mountain.

The headquarters and the support facilities including the general electric and safety service, library and meeting halls, canteen, computing and networking services, mechanical, electronic and chemical shops, low radioactivity service, assembly halls, offices and administration department are located on the surface.

The mission of the Laboratory is to host experiments that require a low background environment in the field of astroparticle physics and nuclear astrophysics and other disciplines that can profit of its characteristics and of its infrastructures.

The geographical location (inside the National Park of Gran Sasso - Monti della Laga) and the special operating conditions (underground, near a highway tunnel and in close proximity to a large water basin) demand that special attention is paid to the safety and environmental aspects of the activities.

Main research topics of the present scientific programme are: neutrino physics with neutrinos naturally produced in the Sun and in Supernova explosion and neutrino oscillations with a beam from CERN (CNGS program), search for neutrino mass in neutrinoless double beta decays, dark matter search, nuclear reactions of astrophysical interest.

The activity in the year 2005 was characterized by the interaction of the heavy safety works by the Government Commissioner (to be terminated in the summer 2006) with the installation and operation of the experiments. Thanks to a strong inter-coordination effort of the Commissioner's and the Laboratory staff the unavoidable problems and delays were minimized.

Let us summarise the 2005 activity of the main research lines.

Solar neutrino physics is one of the traditional research sectors of the laboratory. After the glorious life of GALLEX and GNO, the focus is now on Borexino, which is dedicated mainly to the measurement of the Be line component of the solar neutrino spectrum. Thanks to the preparation work in 2005, this experiment is now ready for filling.

The solar models are based on data and extrapolations; in particular the thermonuclear cross sections of the involved reactions are not measured in the relevant energy range but rather extrapolated from higher energies. The direct measurements are made very difficult by the very low values of the cross sections. Using the new 400 kV accelerator, LUNA continued its activity for the measurements of the cross section of nuclear reaction of astrophysical interest.

The detection of low energy neutrinos from the gravitational collapse of galactic objects is the major purpose of the LVD (Large Volume Detector) experiment; the experiment is continuosly monitoring the galaxies with its 1000 tons of liquid scintillator.

LVD participates to the Supernovae Early Warning System of detectors.

Elementary particles are different from their antiparticles because their charges - not only the electric one, but all of them - are opposite. The standard model assumes that neutrinos have only one charge, the lepton number. But, if this charge is not conserved, neutrinos and antineutrinos can be two states of the same particle. In this case well-specified nuclides would decay through the neutrino-less double beta channel. The Laboratory hosts today experiments searching for these very rare decays, employing different and complementary techniques, and is preparing new important activities.

The Heidelberg-Moscow experiment, with a sensitive mass of 11 kg of enriched ^{76}Ge, was the most sensitive experiment in the world, accumulating data for a 75 kg y exposure and claiming for a positive signal.

CUORICINO, which employs TeO_2 bolometers for a total of 42 kg and started taking data data in 2003, has continuously operated in 2005. It is the most sensitive running experiment today.

In this field the Laboratory approved two new experiments representing the state of the art: CUORE, which brings the CUORICINO technique to a mass of more than 400 kg of TeO_2 bolometers, and GERDA planning to employ 500 kg of enriched ^{76}Ge.

From astronomical observations, we know that most of the matter in the Universe is not made of nuclei and electrons as normal matter. It is called dark matter, because it does not emit light, and its nature is unknown. Probably, its constituents, elementary particles that interact only very weakly with the rest (they are called WIMPs,) have not been discovered yet; they are around us, invisible, waiting to be discovered. The search for WIMPs is very difficult and requires a very low background environment and the development of advanced background reduction techniques. The search is going on in many experiments worldwide. At Gran Sasso several experiments, using different techniques, are active and new experiments have been approved and started operating in 2005.

DAMA/LIBRA employs NaI crystals to detect the WIMPs by means of the flash of light produced in the detector by a Iodine nucleus recoiling after having been hit by a WIMP, a very rare phenomenon. To distinguish these events from the background, DAMA searches for an annual modulation of the rate, a behaviour that has several aspects that are peculiar of the searched effect and not of the main backgrounds. With its about 100 kg sensitive mass DAMA was the only experiment world wide sensitive to the annual modulation signature. After the conclusion of the experiment, results were published confirming a signal of annual modulation.

The larger experiment LIBRA, with 250 kg sensitive mass, continued regularly to take data along all the year.

CRESST searches for WIMPs with a cryogenic technique, looking for a very tiny temperature increase in the detector, due to the energy deposited by nuclei hit by the WIMPs. Activity started with the new CRESST2 $CaWO_2$ detector.

The activity of the small test facility GENIUS-TF, with 40 kg of natural Germanium operated in liquid Nitrogen, continued during the year.

Two new dark matter experiments, WARP and XENON are preparing their activity underground. They are based on the simultaneous detection of the ionization and scintillation

signals in, respectively, liquid argon and liquid xenon. WARP performed during the year interesting measurements underground with a small (2.3 l) prototype.

One of the major committments of the Gran Sasso laboratory in the next decennium will be the search of tau neutrino appearance on the artificial neutrino beam being built at CERN in Geneva, the CERN Neutrinos to Gran Sasso (CNGS) project. The beam will be directed through the Earth crust to Gran Sasso at 732 km distance. Beam is foreseen to be ready in the summer of 2006.

The OPERA experiment is designed for the direct observation of tau neutrinos resulting from oscillations of the muon neutrino of the beam. This search requires both micrometer scale resolution, obtained with modern emulsion techniques and large sensitive mass (1800 t) obtained with Pb sheets interleaved by emulsion layers. In 2005 the installation in Hall C has continued regularly, as well as the realization of a dedicated space for the brick assembly machine and other facilities, even in presence of the interference represented by the Commissioner safety works.

ICARUS is a general-purpose detector, with a broad physics programme, based on the novel concept of the liquid Argon time-projection chamber. The 600 ton module was transported from Pavia to our underground Laboratory in december 2004. During 2005 the tender for the reliquefaction system has been launched and the construction of the new insulation panel by Air Liquide has continued.

The main activity of the theory group, staff and visitor scientists, has been focused on astroparticle physics, including solar and Supernova neutrinos, massive neutrinos, ultra high energy cosmic rays, topological defects and relativistic astrophysics. Important activity took place also in particle phenomenology and computer simulations of Lattice Field Theories.

The Gran Sasso laboratory is recognized by Europe as a large scientific infrastructure. An EU contract is involving LNGS as one of the leader paricipants in the Integrated Infrastructure Initiative (I3) called ILIAS within Framework Program 6 (contract RII3-CT-2003-505818).

The main goal of ILIAS (Integrated Large Infrastructures for Astroparticle Physics) is to pull together all of Europe's leading infrastructures in Astroparticle Physics to produce a focused, coherent and integrated project to improve the existing infrastructures and their operation as well as to organise and structure the scientific community to prepare the best infrastructures for the future.

Gran Sasso, July 3 2006

The Director of the Laboratory
Prof. Eugenio Coccia

BOREXINO. SOLAR NEUTRINO PHYSICS

M. Balata[b], A. de Bellefon[o], G. Bellini[a], J. Benziger[c], S. Bonetti[a], B. Caccianiga[a],
F.P. Calaprice[d], D. D'Angelo[h], A. Derbin[m], A. Etenko[s], F. von Feilitzsch[h], R. Ford[b],
D. Franco[a], C. Galbiati[d], S. Gazzana[b], M.G. Giammarchi[a], A. Goretti[a], B. Harding[d],
G. Heusser[j], A. Ianni,[d], A.M. Ianni[c], H. de Kerret[o], G. Korga[a], Y. Kozlov[s], D. Kryn[o],
M. Laubenstein[b], C. Lendvai[h], M. Leung[c], E. Litvinovich[s], P. Lombardi[a], I. Machulin[s],
I. Manno[k], D. Manuzio[i], G. Manuzio[i], F. Masetti[g], U. Mazzucato[g], K. McCarty[d],
E. Meroni[a], L. Miramonti[a], M.E. Monzani[a], V. Muratova[m], L. Niedermeier[h], L. Oberauer[h],
M. Obolensky[o], F. Ortica[g], M. Pallavicini[i], L. Papp[a], L. Perasso[i], A. Pocar[d], R.S. Raghavan[l],
G. Ranucci[a], A. Razeto[i], A. Sabelnikov[s], C. Salvo[i], S. Schönert[j], T. Shutt[d], H. Simgen[j],
M. Skorokhvatov[s], O. Smirnov[m], A. Sotnikov[m], S. Sukhotin[s], Y. Suvorov[s], V. Tarasenkov[s],
R. Tartaglia,[b], G. Testera[i], D. Vignaud[o], B. Vogelaar[n], V. Vyrodov[s], W. Wojcik[q],
O. Zaimidoroga[m], G. Zuzel[q]

[a]Dip. di Fisica dell'Università and Infn Milano - Italy
[b]Laboratori Nazionali del Gras Sasso, Assergi (Aq) - Italy
[c]Dept. of Chemical Engineering, Princeton University - NJ USA
[d]Dept. of Physics, Princeton University - NJ USA
[e]Dip. di Fisica dell'Università and Infn Pavia - Italy
[f]Dept. of Physics, Massachusetts Institute of Technology - MA USA
[g]Dip. di Chimica dell'Università and Infn Perugia - Italy
[h]Technische Universität München - Germany
[i]Dip. di Fisica dell'Università and Infn Genova - Italy
[j]Max Planck Inst. für Kernphysik, Heidelberg - Germany
[k]KFKI-RMKI Research Institute for Particle & Nuclear Physics, Budapest - Hungary
[l]Bell Laboratories, Lucent Technologies, Murray Hill - NJ USA
[m]J.I.N.R. Dubna - Russia
[n]Dept. of Physics, Virginia Polytechnic Institute - VA USA
[o]Laboratoire de Physique Corpusculaire et Cosmologie, Paris - France
[p]I.R.M.M. - EURATOM, Geel - Belgium
[q]Institute of Physics, Jagellonian University, Kracov - Poland
[r]Dept. of Physics, Queen's University, Ontario - Canada
[s]RRC Kurchatov Institute, Moscow - Russia

Abstract

Borexino is a solar neutrino detector in commissioning phase in Hall C of LNGS.
We summarize here the status of the project and the main technical achievements
obtained in these years of development.

1

1 Introduction

Borexino is a real time experiment which plans to study the low energy (sub-MeV) solar neutrinos. The main experimental goal is the study of the 0.862 MeV ^{7} Be solar neutrino line through the neutrino-electron elastic scattering reaction. The maximum energy of the recoiling electron is 664 KeV and the experimental design threshold will be at 250 KeV. The detection reaction will be observed in a large mass of well shielded liquid scintillator. The main problem of a real time experiment with such a low energy threshold is the natural radioactivity which is present in any environment and in any material. For these reasons an intense R&D program has been carried out in the last ten years to develop methods for selecting low radioactivity materials and/or purify them. An effort in this field has to be complemented by a comparably thorough research in the field of detection and measurement of very low radioactivity levels.

The development of purification methods has been focused on the costituents of the liquid scintillator. Four main methods have been developed: distillation, water extraction, stripping with ultrapure N_2, solid gel column (Si gel, Al gel) adsorption. Significant results have been achieved by the Collaboration as for example: $10^{-16} - 10^{-17}$ (g of contaminants/g of material) for ^{232}Th and ^{238}U family and a few microBq of Rn-222 sensitivity in gases and liquids.

In addition the organic solvent selected by the collaboration has been shown to have a ^{14}C presence not exceeding 10^{-18} in its ratio to ^{12}C. This impurity is particularly important because it cannot be removed by chemical purification methods.

For the measurements of these ultralow radioactivity levels, dedicated methods were developed. In addition to small-scale techniques (Ge underground detectors installed in Rn free environment, Inductively Coupled Plasma Mass Spectometer, high sensitivity Neutron Activation, Atomic Absorption Spectroscopy etc...), a Counting Test Facility (CTF), has been constructed on purpose and operated in the Hall C of LNGS. The Counting Test Facility features 4 tonnes of liquid scintillator viewed by 100 photomultipliers and shielded by 1000 tons of ultrapure water.

The sensitivities reached are summarized below and correspond to the lowest radioactivity levels obtained by the Borexino Collaboration, in preparation of the experiment:

- Bulk material radiopurities of 10^{-10} g/g for ^{238}U and ^{232}Th, $\sim 10^{-5}$ for ^{nat}K, few tenths of mBq/kg for ^{60}Co, have been measured with Ge detectors in construction materials such as stainless steel, photomultipliers, metal and plastic gaskets, products for PMT sealing, piping, filters...
- Radon emanations of 10 μBq/m^2 from plastic materials, 0.1 mBq/m^3 for Rn-222 and 1 mBq/m^3 for Ra-226 in water, 1 mBq/m^3 for the N_2 used for scintillator stripping.
- Radiopurity levels of a few times 10^{-15} g/g ^{238}U, ^{232}Th and ^{40}K have been reached with ICMPS in measuring the Borexino shielding water.
- few ppt for ^{238}U and ^{232}Th have been obtained in Nylon bulk measurements.
- The radiopurity of the scintillator itself was measured to be at the level of few 10^{-16} g/g for ^{238}U, ^{232}Th and $\sim 10^{-18}$ for ^{14}C/^{12}C in the Counting Test Facility.
- Bulk radiopurity levels of $10^{-13} - 10^{-14}$ g/g for Au, Ba, Ce, Co, Cr, Cs, Ga, Hg, In, Mo, Rb; less than few 10^{-15} g/g for Cd, Sb, Ta, W; $10^{-16} - 10^{-17}$ g/g for La, Lu, Re, Sc, Th;

less than $1\text{x}10^{-17}$ g/g for U, have been reached by mean of Neutron Activation followed by β-γ coincidence analysis selection applied to the scintillator.
- Kr and Ar contamination in nitrogen at 0.005 ppm (for Ar) and 0.06 ppt (for Kr) were obtained and measured with noble gas mass spectrometry.

These results were a milestone in the development of the Borexino detector and technique. Several of these concepts were incorporated in the construction of the high purity systems for the treatment of the most critical liquid, the scintillator of the experiment.
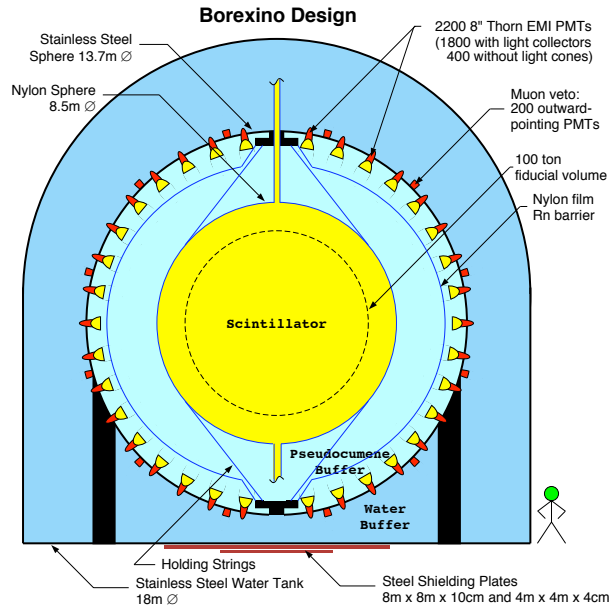
Figure 1: Schematic view of the Borexino detector.

2   The Borexino Detector

Borexino is an unsegmented scintillation detector featuring 300 tonnes of well shielded liquid ultrapure scintillator viewed by 2200 photomultipliers (fig. 1). The detector core is a transparent spherical vessel (Nylon Sphere, 100μm thick), 8.5 m of diameter, filled with 300 tonnes of liquid scintillator and surrounded by 1000 tonnes of high-purity buffer liquid. The scintillator mixture is PC and PPO (1.5 g/l) as a fluor, while the buffer liquid will be PC alone (with the addition of DMP as light quencher). The photomultipliers are supported by a Stainless Steel Sphere, which also separates the inner part of the detector from the external shielding, provided by 2400 tonnes of pure water (water buffer).
An additional containment vessel (Nylon film Radon barrier) is interposed between the Scintillator Nylon Sphere and the photomultipliers, with the goal of reducing Radon diffusion towards the internal part of the detector.
The outer water shield is instrumented with 200 outward-pointing photomultipliers serving as a veto for penetrating muons, the only significant remaining cosmic ray background

at the Gran Sasso depth (about 3500 meters of water equivalent). The innermost 2200 photomultipliers are divided into a set of 1800 photomultipliers equipped with light cones (so that they see light only from the Nylon Sphere region) and a set of 400 PMT's without light cones, sensitive to light originated in the whole Stainless Steel Sphere volume. This design greatly increases the capability of the system to identify muons crossing the PC buffer (and not the scintillator).

The BOREXINO design is based on the concept of a graded shield of progressively lower intrinsic radioactivity as one approaches the sensitive volume of the detector; this culminates in the use of 200 tonnes of the low background scintillator to shield the 100 tonnes innermost Fiducial Volume. In these conditions, the ultimate background will be dominated by the intrinsic contamination of the scintillator, while all backgrounds from the construction materials and external shieldings will be negligible.

BOREXINO also features several external systems and conceived to purify the experimental fluids (water, nitrogen and scintillator) used by the experiment.

3 Status of the project

The Borexino detector and the associated purification and ancillary plants are completed. The whole system is now in commissioning phase.

While waiting for the full operability permission from authorities, air runs are being performed with the Borexino detector while the CTF is taking data to test purification strategies to be used in the experiment.

4 Borexino and Neutrino Physics

Borexino will be studying solar neutrino physics below the 1 MeV threshold, where the Large Mixing Angle suppresion pattern becomes vacuum dominated. This is in contrast with the "matter dominated" situation of the B-8 neutrinos, the only component observed in real-time up to now.

The expected Be-7 solar neutrino rates is close to 30 counts/day. With a sizeable number of real-time expected events, Borexino can also study several time-dependences of the solar neutrino signal, including day-night and seasonal variations.

Finally, a 10% accuracy measurement of the Be-7 line will be of great importance to measure the relative solar model parameter whose uncertainty is at present of the order of 50%.

Other physics topics can be investigated with high sensitivity with the Borexino detector, such as Supernova neutrinos, neutrino magnetic moment, terrestrial neutrinos...

Physics results already obtained with the Counting Test Facility, confirm the validity and the sensitivity of the Borexino technique.

5 List of articles published in year 2004

1. L. Miramonti *European underground facilities: an overview.* AIP Volume 785 (2005).

2. D. Franco on behalf of the Borexino collaboration ^{11}C *measurement and CNO flux at Borexino.* Nucl. Phys. B, 145 (2005).

References

[1] G. Alimonti et al., *Science and technology of Borexino: a real-time detector for low energy solar neutrinos*, Astroparticle Physics 16 (2002) 205.

[2] C. Arpesella et al., *Measurements of extremely low radioactivity levels in BOREX-INO*, Astroparticle Physics 18 (2002) 1.

DAMA. DARK MATTER SEARCH

DAMA collaboration:

P. Belli[a], R. Bernabei[a,@], A. Bussolotti[a,*], F. Montecchia[a], F. Nozzoli[a],
A. d'Angelo[b,e], F. Cappella[b], A. Incicchitti[b], A. Mattei[b,*], D. Prosperi[b],
S. Castellano[c,**], R. Cerulli[c],
C.J. Dai[d], H.L. He[d], H.H. Kuang[d], J.M. Ma[d], Sheng Xiangdong[d],
Wang Ruiguang[d], Zhang Yongjie[d], Z. P. Ye[d,f]

in neutron measurements: M.Angelone[g], P.Batistoni[g], M.Pillon[g]

in some by-product results and small scale experiments: F.A. Danevich[h],
V.V. Kobychev[h], S.S.Nagorny[h], D.V. Poda[h], V.I. Tretyak[h],
S.S. Yurchenko[h], M. Martinez[i]

[a]Dip. di Fisica, Università di Roma "Tor Vergata" and INFN-RomaTor Vergata (gia' INFN-Roma2), 00133 Roma, Italy;

[b]Dip. di Fisica, Università di Roma "La Sapienza" and INFN-Roma, 00185 Roma, Italy;
[c]Laboratorio Nazionale del Gran Sasso, INFN, 67010 Assergi (Aq), Italy;
[d]IHEP, Chinese Academy, P.O. Box 918/3, Beijing 100039, China;
[e]Scuola di Specializzazione in Fisica Sanitaria, Università di Roma "Tor Vergata", 00133 Rome, Italy;
[f]Physics Dept, Jinggangshan University 343009, Ji-an, Jiangxi province, China;
[g]ENEA - C. R. Frascati, P.O. Box 65, 00044 Frascati, Italy;
[h]Institute for Nuclear Research, 252650 Kiev, Ukraine.
[i]Laboratory of Nuclear and High Energy Physics, University of Zaragoza, 50009 Zaragoza, Spain

@ Spokesperson
* technical staff
** and Università degli Studi dell'Aquila

Abstract

DAMA is an observatory for rare processes and it is operative deep underground at the Gran Sasso National Laboratory of the I.N.F.N.. The main experimental set-ups are: i) DAMA/NaI ($\simeq$ 100 kg of highly radiopure NaI(Tl)) which completed its

data taking on July 2002; ii) DAMA/LXe ($\simeq$ 6.5 kg liquid Kr-free Xenon enriched either in ^{129}Xe or in ^{136}Xe); iii) DAMA/R&D, devoted to tests on prototypes and to small scale experiments; iv) the new second generation DAMA/LIBRA set-up ($\simeq$ 250 kg highly radiopure NaI(Tl)) in operation since March 2003. Moreover, in the framework of devoted R&D for radiopure detectors and photomultipliers, sample measurements are carried out by means of the low background DAMA/Ge detector (installed deep underground since more than 10 years) and, in some cases, by means either of mass spectrometers or of other facilities. In the following main arguments on the activity during 2005 are summarised.

1 DAMA/NaI

The DAMA/NaI set-up [1, 2, 3] had as main aim the investigation of the presence of a cold Dark Matter particle component (DM) in the galactic halo by exploiting the model independent annual modulation signature (see refs. [2, 3, 4, 5, 6, 7, 8, 9, 10] and 2005 publication list). The same experimental set-up also achieved several results both on Dark Matter particle investigations with other approaches and on several rare processes (see refs. [11, 12, 13, 14, 15, 16, 17, 18] and the 2005 publication list).

DAMA/NaI has been a pioneer experiment running at LNGS for about a decade and investigating as first the Dark Matter particle annual modulation signature with suitable exposed mass, sensitivity and control of the running parameters.

1.1 On further corollary analyses

1.1.1 Introduction

The presence of particle Dark Matter component(s) at level of our Galaxy in the data of DAMA/NaI has firstly been reported by the DAMA collaboration at the TAUP conference in 1997 [19] and published also in [4], confirmed in [5, 6], further confirmed in [2, 7, 8, 9, 10] and conclusively confirmed, at end of experiment in 2003 (see ref. [3] and the 2005 publication list).

In fact, during seven independent experiments each one of one annual cycle (total exposure: 107731 kg × day), DAMA/NaI has pointed out the presence of an annual modulation in the *single-hit* residual rate in the lowest energy interval (2 – 6) keV, at 6.3 σ C.L., (Fig.1) satisfying all the features expected for a Dark Matter particle component in the galactic halo. No systematic effect or side reaction able to account for the observed effect has been found. This result is model-independent. It represents the first experimental evidence of the presence of DM particles in the halo independently on their nature.

At present, apart from DAMA/LIBRA, no other experiment is sensitive, for mass, radiopurity and control of the stability, to such a model independent signature.

Additional corollary investigations have been also pursued on the nature of the DM candidate particle. This latter corollary investigation is instead model-dependent and due to the large uncertainties on the astrophysical, nuclear and particle physics assumptions and on related parameters, it has no general meaning (as well as e.g. exclusion plots
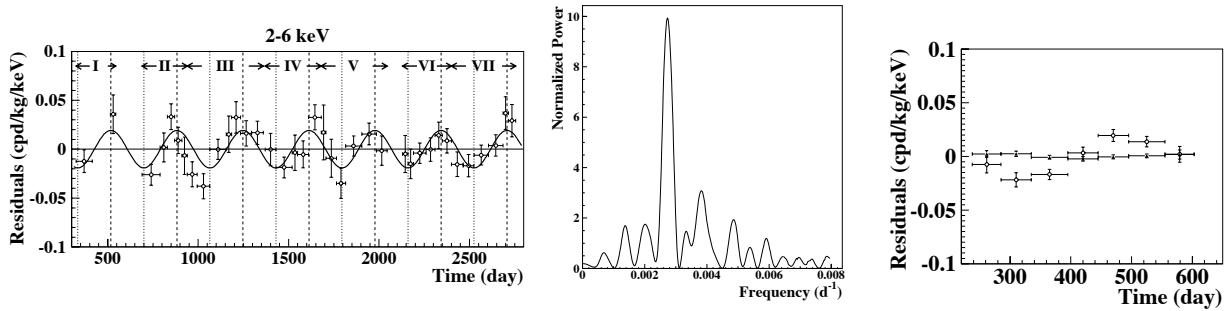
Figure 1: On the left: experimental residual rate for *single-hit* events in the cumulative (2–6) keV energy interval as a function of the time over 7 annual cycles, end of data taking July 2002. The experimental points present the errors as vertical bars and the associated time bin width as horizontal bars. The superimposed curve represents the cosinusoidal function behaviour expected for a Dark Matter particle signal with a period equal to 1 year and phase exactly at 2nd June; the modulation amplitude has been obtained by best fit.[3]. Center: power spectrum of the measured *single-hit* residuals for the cumulative (2–6) keV energy interval calculated including also the treatment of the experimental errors and of the time binning. As it can be seen, the principal mode corresponds to a frequency of $2.737 \cdot 10^{-3}$ d^{-1}, that is to a period of $\simeq 1$ year. On the right: experimental residual rates over seven annual cycles for *single-hit* events (open circles) – class of events to which DM events belong – and over the last two annual cycles for *multiple-hits* events (filled triangles) – class of events to which DM events do not belong – in the (2–6) keV cumulative energy interval. They have been obtained by considering for each class of events the data as collected in a single annual cycle and using in both cases the same identical hardware and the same identical software procedures. The initial time is taken on August 7th.

in direct and indirect detection experiments). Thus, it should be handled in the most general way ([3] and 2005 publication list).

DAMA/NaI, having both a light (the ^{23}Na) and a heavy (the ^{127}I) target-nucleus, is intrinsically sensitive to Dark Matter particle both of low and high mass. Moreover, it is fully sensitive not only to spin independent (SI) coupling, but also to spin dependent (SD) one, to the SI and SD mixed case, to the preferred inelastic coupling and it is favoured for some other candidates.

In the framework of DAMA investigation several corollary quests for a candidate particle have been carried out on the class of DM candidate particles named WIMPs [3]; in literature several candidates for WIMPs have been considered, all foreseen in theories beyond the Standard Model of particle Physics. In particular in case of a candidate with dominant SI interaction, in the framework of models considered in ref. [3], a comparison with the expectations for a neutralino, in MSSM can be found in ref. [20].

Other possibilities exist with a phenomenology similar as for the WIMP cases: the mirror Dark Matter particles [21], the self-interacting dark matter particles [22], etc. and in principle even whatever particle with suitable characteristics, even not yet foreseen by theories, can be a good candidate as DM in the galactic halo.

Moreover, other candidates have been widely considered in literature such as e.g.

axion-like particles, of $\sim$ keV mass[1], either with the pseudoscalar or scalar coupling, non-relativistic since they should be trapped in the galactic halo. The detection principle of such particles does not involve nuclear recoils.

1.1.2 Other corollary investigations: the axion-like particles at keV scale

In 2005 the DAMA collaboration has also considered this class of candidates in some of the possible scenarios.

The full analysis of the 107731 kg $\cdot$ day exposure from DAMA/NaI in this framework has been given in a devoted publication (see 2005 publication list).

Axion-like particles can be considered particles having similar phenomenology with ordinary matter like the axion, but with coupling constants and mass significantly different than those foreseen in the DFSZ and KSVZ models: for example, the axion itself in the Kaluza-Klein theories [23], where it would have similar couplings as in the DFSZ and KSVZ models, but much higher mass states or the "exotic" axion models proposed by [24]. Other candidates are pseudo-Nambu-Goldstone bosons related to spontaneous global symmetry breaking different from the $U(1)_{PQ}$ hypothesised by Peccei-Quinn, such as the pseudoscalar familon in the case of the family symmetry or the Majoron for the lepton number symmetry [25].

It is worth to note that some indirect astrophysical observations: i) the Solar corona problem; ii) the X-rays flux detected by ROSAT in the direction of the dark side of the Moon; iii) the X-rays background radiation in the 2-8 keV region measured by CHANDRA (XRB); iv) the excess of X-rays from clusters of galaxies; have recently been analysed in a model of axion-like particles with mass in the keV range and coupling to photons $g_{a\gamma\gamma}$ of the order of $10^{-13} GeV^{-1}$ [26], that is requiring a model with expectations for the coupling constants and masses well different compared to those expected in the DFSZ and KSVZ models. It has also been argued that the existence of axion-like particles may account for the high energy cosmic rays [27]. Finally, a keV Majoron has been suggested as DM particle [28] and a $\sim$ keV DM pseudoscalar candidate has also been taken into account in ref. [24, 29].

Several mechanisms can be advocated for the production of these particles in the early Universe (see e.g. ref. [24, 28, 29]) demonstrating that they can be of cosmological interest.

It is worth to note that the direct detection process for light bosonic DM candidates is based on the total conversion in NaI(Tl) crystal of the mass of the absorbed bosonic particle into electromagnetic radiation. Thus, in these processes the target nuclei recoil is negligible and is not involved in the detection process; therefore, signals from these light bosonic DM candidates are lost in all the experiments based on rejection procedures of the electromagnetic contribution to the counting rate.

The main processes involved in the detection of a DM light bosonic particle (here generically named a for the pseudoscalar case) both in the pseudoscalar and in the scalar interaction types are "Compton - like" effect, "Axioelectric" or "photoelectric-like" effect and Primakoff effect (see Fig.2).

---

[1]In fact, considering the phenomenology of this candidate a keV-scale bosonic candidate naturally arises as an additional solution to the observed model-independent DAMA/NaI annual modulation signal.
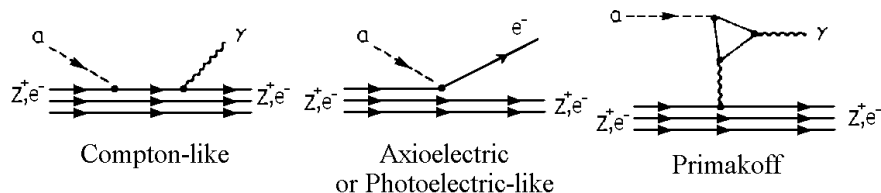
Figure 2: Possible diagrams for the direct detection processes of a light boson particle. On the left: "Compton - like" effect; on the center: "Axioelectric" or photoelectric-like effect; on the right: Primakoff effect. See text.

In all these processes the total (including the secondary processes: X-rays and Auger electrons) energy release, E_{rel}, in the detector (providing that its detection efficiency is $\simeq 1$ for low-energy electrons and low-energy photons) matches the total energy of the a particle, $E_a \simeq m_a$ since the a velocity is of the order of $10^{-3}c$. In terms of annual modulation investigation all the interactions considered above for the pseudoscalar candidate contribute to the costant part of the signal, while the Compton-like interaction does not contribute to the modulation part of the signal. Moreover, as it can be easily demonstrated, for the pseudoscalar case the axioelectric contribution to the total expected counting rate is largely dominant with the respect to the contributions of Primakoff and Compton-like on nuclei at least in all the "natural" cases, where $g_{a\bar{e}e}/m_e$ is not lower than a factor $\sim 10^{-3}$ the coupling constant to mass ratios of the other charged fermions; in addition, it still remains at least one order of magnitude larger than the one due to the Compton-like effect on electrons, for a particle mass below $\simeq 6$ keV.

Obviously, these results are not exhaustive of the many scenarios (still possible at present level of knowledge) for these and for other classes of candidates (such as the WIMPs we have already investigated at some extent [3] and references therein).

First of all, as already mentioned, the axioelectric contribution is dominant with the respect to the Compton-like and Primakoff effects in all the "natural" cases; thus, the results can be presented in terms of only two variables $g_{a\bar{e}e}$ and m_a (see Fig. 3). The allowed region in the plane defined by these two variables has been calculated considering the DAMA/NaI results on the model independent annual modulation signature. This allowed region is almost independent on the adopted $g_{a\bar{u}u}$ and $g_{a\bar{d}d}$ coupling constants.

The allowed region reported in Fig. 3 can only marginally be affected by the results already presented at low energy by low-background ionization detectors; in fact, due e.g. to their energy resolution and to their quoted counting rate at low energy, their results do not rule out a particles with $m_a \lesssim 3$ keV and, for $m_a \gtrsim 3$ keV, a particles with $g_{a\bar{e}e} \lesssim 2 \times 10^{-10}$. Some strongly model dependent astrophysical limits on the $g_{a\bar{e}e}$ can be found in literature (see e.g. [30]) by studying the globular cluster stars; however, these constraints only apply to particles with masses much below few keV, which is the typical core temperature of the stars. Moreover these constraints can also be avoided by following an approach similar to that of ref.[31].
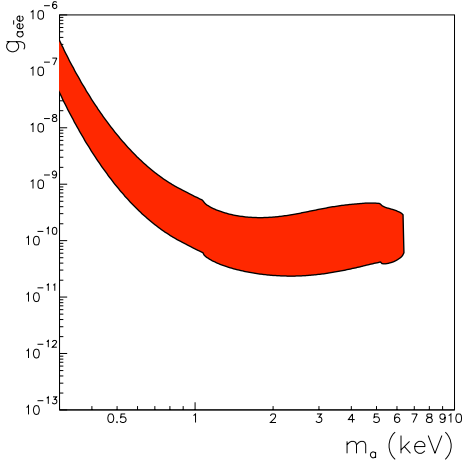
Figure 3: DAMA/NaI allowed region at 3σ C.L. in the plane $g_{a\bar{e}e}$ vs m_a for a pseudoscalar candidate; see devoted paper.
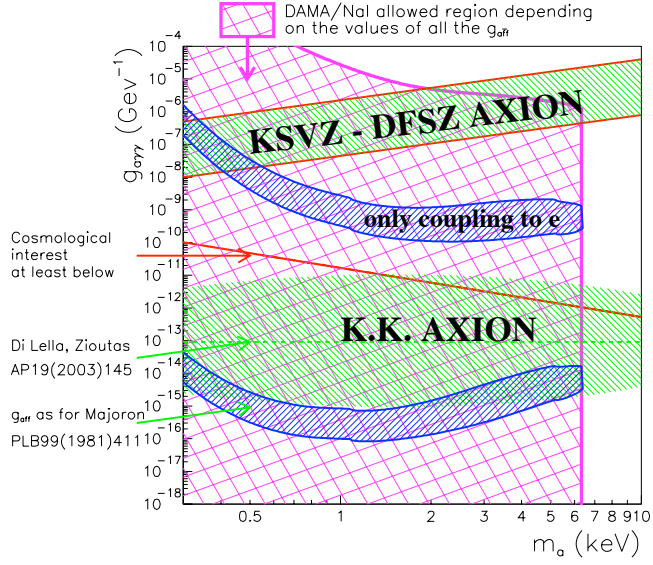
Figure 4: DAMA/NaI allowed region at 3σ C.L. in the plane $g_{a\gamma\gamma}$ vs m_a(*crossed hatched region*) for a pseudoscalar candidate. All the configurations in this region can be allowed depending on the values of all the $g_{a\bar{f}f}$; see devoted paper.

In addition the pseudoscalar boson particle can decay into two photons but its lifetime can be also of cosmological interest as shown in Fig. 4, where the allowed region in the plane $g_{a\gamma\gamma}$ vs m_a is reported. The upper bound on $g_{a\gamma\gamma}$ is given when the Primakoff effect is largely dominant (that is, if $g_{a\bar{e}e} = g_{a\bar{u}u} = g_{a\bar{d}d} = 0$ and only contributions from other charged fermions are present). All the other values of $g_{a\gamma\gamma}$ below this upper bound are allowed depending on the values of all the $g_{a\bar{f}f}$.

In case of a scalar candidate all the interactions already discussed for the pseudoscalar case also hold (see Fig.2 changing a with h). In terms of annual modulation all of them contribute to the constant part of the signal, while the photoelectric-like interaction does not contribute to the modulation part of the signal. However, the photoelectric-like interaction gives a dominant contribution compared to the Compton-like process on the electrons and to the other effects. Thus the coupling to the electrons can not produce any significant time variation of the signal. Moreover, the upper limit on $g_{h\bar{e}e}$, which can be easily derived from the energy distribution measured by DAMA/NaI (given elsewhere), ranges from $\simeq 3 \times 10^{-16}$ to $\simeq 10^{-14}$ for m_h between $\simeq 0.5$ and 10 keV. Therefore, it is worth to investigate the case of a scalar h particle coupled only to the hadronic matter ($g_{h\bar{e}e} << g_{h\bar{u}u}, g_{h\bar{d}d}$). In this case, non-zero modulation term of the signal is expected by the contributions of the Compton-like effect on nuclei and of the Primakoff effect. According to the scenarios described in the devoted paper, we report in Fig. 5 the region allowed by the DAMA/NaI data in the plane $g_{h\bar{N}N}$ vs m_h.

This allowed region can only marginally be affected by the results already presented at low energy by low-background ionization detectors, which do not rule out h particles with $m_h \lesssim 3$ keV and, for $m_h \gtrsim 3$ keV, h particles with $g_{h\bar{N}N} \lesssim 8 \times 10^{-7}$. Moreover,
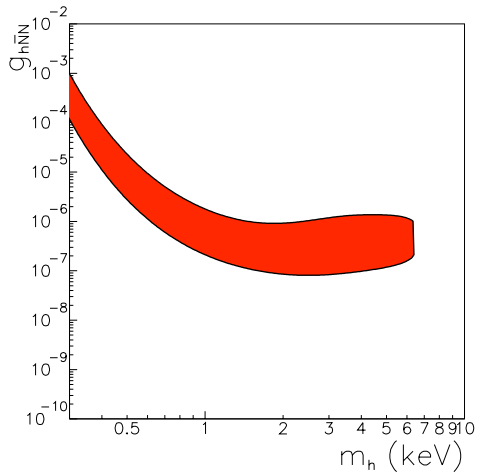
Figure 5: DAMA/NaI allowed region at 3σ C.L. in the plane $g_{h\bar{N}N}$ vs m_h for a scalar candidate. See devoted paper.
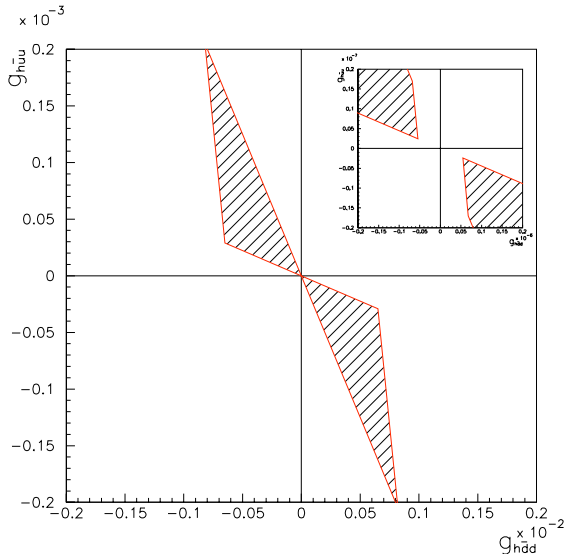
Figure 6: DAMA/NaI allowed configurations of cosmological interest in the $g_{h\bar{u}u}$ vs $g_{h\bar{d}d}$ plane. In the inset: a magnification of the regions around (0,0). See devoted paper.

we note that the strongly model dependent globular cluster constraints [32] only apply to particles with masses much below few keV. The region in Fig. 5 does not allow a direct information on the h lifetime; however, the large number of free coupling constants allows to expect the existence of a large number of h configurations of cosmological interest as it has been calculated for some model frameworks in the devoted paper (see Fig. 6).

In conclusion, a pseudoscalar DM candidate as well as a scalar one can also account for the DAMA/NaI model independent result as well as the WIMP solution we extensively discussed elsewhere [3] and references therein.

Further analyses are in progress considering [33] that contributions to the Dark Matter particles in the galactic halo should be expected from tidal streams from the Sagittarius Dwarf elliptical galaxy. Since this galaxy was undiscovered until 1994 and from galaxy formation theories, one has to expect that also other satellite galaxies do exist and contribute as well. In particular, the Canis Major satellite galaxy has been pointed out as reported in 2003 in ref. [34]; it can, in principle, play a very significant role being close to our galactic plane, role that we plan to investigate in future. A preliminary work on the investigation of Sagittarius Dwarf streams on DAMA/NaI data has been carried out during part of 2005 for the WIMP candidates.

1.1.3 Few arguments on comparisons with some model dependent results

As regards some claimed model-dependent comparisons by experiments insensitive to the annual modulation signature, often an incorrect/partial/not updated quotation of the DAMA/NaI result is performed, the exposures are orders of magnitude lower than the one by DAMA/NaI, different target nuclei are used etc., specific discussions can be found e.g. in ref.[3] and in the 2005 publication list.

Moreover, generally they neglect for example the uncertainties on: i) the nature of the

candidate particle(s); ii) the real coupling with ordinary matter; iii) the spin-dependent and spin-independent form factors and related parameters for each nucleus; iv) the spin factor used for each nucleus; v) the real scaling laws for nuclear cross sections among different target materials; vi) experimental and theoretical parameters; vii) the effect of different halo models and related parameters on different target materials, etc. Moreover, large differences are expected in the counting rate for instance among nuclei fully sensitive to the SD interaction (as ^{23}Na and ^{127}I) with the respect to nuclei largely insensitive to such a coupling (as e.g ^{nat}Ge, ^{nat}Si, ^{nat}Ar, ^{nat}Ca, ^{nat}W, ^{nat}O) and also when nuclei in principle all sensitive to this coupling but having different unpaired nucleon (e.g. neutron in case of the odd spin nuclei, such as ^{129}Xe, ^{131}Xe, ^{125}Te, ^{73}Ge, ^{29}Si, ^{183}W and proton in the ^{23}Na and ^{127}I). Moreover, in case the detection of the CDM particles would involve electromagnetic signals (see, for example, the case of the light bosons discussed above), all the experiments, such as e.g. CDMS, EDELWEISS, CREST, ZEPLIN, WARP and their extensions, do lose this signal in the rejection procedures of the e.m. contribution to the counting rate. For completeness, it is also worth to note that no results obtained with different target nuclei can intrinsecally be directly compared even for the same kind of coupling. In fact, this requires – among others – the knowledge of the scaling laws among the DM particle-nuclear cross sections, situation even worse than that in the field of double beta decay experiments when different materials are used. As regards the indirect searches, a comparison would always require the calculation and the consideration of all the possible CDM particle configurations in the given particle model, since it does not exist a biunivocal correspondence between the observables in the two kinds of experiments: CDM particle-nucleus elastic scattering cross section (direct detection case) and flux of either muons from secondary neutrinos or antimatter or photons following CDM annihilations (indirect detection cases).

1.2 A search for spontaneous emission of heavy cluster in the ^{127}I nuclide

During year 2005 an exposure of $33834 \, \mathrm{kg} \cdot \mathrm{day}$ collected by DAMA/NaI has been analysed in order to search for spontaneous cluster decay in ^{127}I (see 2005 publication list). New lower limits on the lifetime of $^{24}_{10}$Ne, $^{28}_{12}$Mg, $^{30}_{12}$Mg, $^{32}_{14}$Si, $^{34}_{14}$Si, $^{48}_{20}$Ca, $^{49}_{21}$Sc cluster radioactivity in ^{127}I have been achieved.

The spontaneous emission of nuclear fragments heavier than α particles and lighter than the most probable fission fragments, named cluster decay, was theoretically predicted in 1980 [35] and experimentally observed for the first time in 1984 [36, 37]. Up to date, spontaneous emission of clusters ranging from ^{14}C to ^{34}Si from near twenty translead nuclei (from ^{221}Fr to ^{242}Cm) have been observed with branching ratios relative to α decay from 10^{-9} down to 10^{-16} and partial half-lives from 3.2×10^3 y up to 1.2×10^{20} y [38, 39]. In all these decays double magic nucleus ^{208}Pb, or nuclei close to ^{208}Pb, are produced; for this reason this effect has been cited in literature as "lead radioactivity" [39]. For about ten cases, only the half-life limits are known with the highest value of $T_{1/2} > 5.0 \times 10^{21}$ y for decay ^{232}Th $\rightarrow$ $^{24-26}$Ne + $^{208-206}$Hg [38, 40].

A new region of parent nuclei, for which cluster radioactivity can be observed experimentally, was predicted recently in ref. [41]: these are the nuclei with $Z = 56 - 64$ and

$N = 58 - 72$; daughter nuclei are close to double magic $^{100}_{50}$Sn. First searches in this domain were performed resulting only in limit $T_{1/2} > 3.5$ h for ^{114}Ba $\rightarrow ^{12}$C $+ ^{102}$Sn [42].

Using new table of atomic masses [43], one can find that 215 different decay modes are possible for ^{127}I with positive energy release Q. However, probably the most interesting ones are those with emission of double magic nucleus $^{48}_{20}$Ca and its neighbour $^{49}_{21}$Sc: they have the highest Q values of 28.9 and 29.4 MeV, respectively [43]. Other examples, investigated in this work, lie in the region close to $^{100}_{50}$Sn.

Theoretical calculations for ^{127}I cluster decay, based on analytical superasymmetric fission model [44], were pessimistic: estimated half-lives were greater than 10^{43} y. Recently, several semiempirical formulae for calculation of $T_{1/2}$ in cluster decays were proposed [45, 46, 47] with numerical parameters determined by fitting the known experimental data. However, despite these formulae work nicely in the region of the so-called "lead radioactivity" [39], they give very discrepant results when applied to cluster decay of ^{127}I: calculated $T_{1/2}$ differ by orders of magnitude. In case of $^{48}_{20}$Ca and $^{49}_{21}$Sc emission, the model [46] gives unrealistically low ^{127}I half-lives of 1.6×10^6 y and 2.1 h, respectively. Such a discrepancy gives us additional motivation for experimental investigation of the ^{127}I cluster decay.

The most widely used technique in experiments on cluster radioactivity is based on solid state nuclear track detectors which are able to register the tracks of the heavy clusters emitted from thin samples while rejecting much more numerous low-energy α particles with great efficiency [38]. In few first measurements also Si detector telescopes were applied [36]. Ge detectors were used in two experiments looking for γ rays created in cluster decay nuclear residuals: ^{24}Na in decay of ^{233}U (where the limit $T_{1/2} > 1.7 \times 10^{17}$ y was established) [48], and various clusters in decays of Hg isotopes (with $T_{1/2}$ limits up to few by 10^{21} y) [49]. In our research the ^{127}I parent nuclei are incorporated in the NaI detector itself (natural abundance of ^{127}I is 100%) and the initial energy release and the subsequent decay of the created clusters (which usually are radioactive) are searched for. The processes investigated in the present experimental search are: i) $^{127}_{53}$I $\rightarrow ^{30}_{12}$Mg $+ ^{97}_{41}$Nb; ii) $^{127}_{53}$I $\rightarrow ^{34}_{14}$Si $+ ^{93}_{39}$Y; iii) $^{127}_{53}$I $\rightarrow ^{24}_{10}$Ne $+ ^{103}_{43}$Tc; iv) $^{127}_{53}$I $\rightarrow ^{28}_{12}$Mg $+ ^{99}_{41}$Nb; v) $^{127}_{53}$I $\rightarrow ^{32}_{14}$Si $+ ^{95}_{39}$Y; vi) $^{127}_{53}$I $\rightarrow ^{49}_{21}$Sc $+ ^{78}_{32}$Ge; vii) $^{127}_{53}$I $\rightarrow ^{48}_{20}$Ca $+ ^{79}_{33}$As. The deep experimental site, the large exposure, the effective shielding of the detectors and the detectors' radiopurity have allowed to investigate these possible processes by using NaI(Tl) crystals.

Such possible decays have been investigated by searching for the energy released in the initial decay (detected energy depends on the Q value and on the light yields of the nuclear fragments) and subsequent decays of radioactive daughter nuclei. In those cases when the initial or intermediate decay has too long lifetime, only subsequent decays of radioactive daughter nuclei have been looked for. In particular, in order to reduce at most the background contribution, very selective event patterns have been considered; consequently, they select small fractions of the total ^{127}I cluster decay in the studied channels. However, limits of the same orders of magnitude as those presented here (see Table 1) can be achieved when considering some other peculiar components of the decays. For details on the analysis see the devoted paper (2005 publication list).

Table 1: Limits on lifetimes of some of the possible cluster decay modes of ^{127}I measured in the present experiment.

Process	Lower limit of the lifetime (90% C.L.) [y]
$^{127}_{53}I \rightarrow ^{30}_{12}Mg + ^{97}_{41}Nb$	2.1×10^{24}
$^{127}_{53}I \rightarrow ^{34}_{14}Si + ^{93}_{39}Y$	5.5×10^{22}
$^{127}_{53}I \rightarrow ^{24}_{10}Ne + ^{103}_{43}Tc$	1.4×10^{23}
$^{127}_{53}I \rightarrow ^{28}_{12}Mg + ^{99}_{41}Nb$	2.0×10^{22}
$^{127}_{53}I \rightarrow ^{32}_{14}Si + ^{95}_{39}Y$	3.0×10^{21}
$^{127}_{53}I \rightarrow ^{49}_{21}Sc + ^{78}_{32}Ge$	2.8×10^{21}
$^{127}_{53}I \rightarrow ^{48}_{20}Ca + ^{79}_{33}As$	6.8×10^{21}

Further experimental efforts are foreseen on the basis of the new DAMA/LIBRA set-up; moreover, other nuclides are also under considerations.

2 DAMA/LIBRA

In 1996 DAMA proposed to realise a ton set-up [50] and a new R&D project for highly radiopure NaI(Tl) detectors was funded at that time and carried out for several years in order to realise as an intermediate step the second generation experiment, successor of DAMA/NaI, with an exposed mass of about 250 kg.

As a consequence of the results of this second generation R&D, the new experimental set-up DAMA/LIBRA (Large sodium Iodide Bulk for RAre processes), $\simeq$250 kg highly radiopure NaI(Tl) crystal scintillators (matrix of twenty-five $\simeq$ 9.70 kg NaI(Tl) crystals), was funded at end 1999 and realised. The experimental site as well as many components of the installation itself have been implemented (environment, shield of the photomultipliers, wiring, High-Purity Nitrogen system, cooling water of air conditioner, electronics and data acquisition system, etc.). In particular, all the Copper parts have been chemically etched before their installation following a new devoted protocol and all the procedures performed during the dismounting of DAMA/NaI and the installation of DAMA/LIBRA detectors have been carried out in High-Purity Nitrogen atmosphere (see 2005 publication list).

DAMA/LIBRA is taking data since March 2003. Just as an example of the quality of the data taking, Fig. 7 — *right panels* show the stability of the calibration factor and of the ratio of the peaks' positions of the ^{241}Am source during about one year of data taking.

Fig. 7 – *left panel* shows the energy distribution of the ^{241}Am source as measured by one of the new DAMA/LIBRA detectors (σ/E = 6.7% at 59.5 keV).

The highly radiopure DAMA/LIBRA set-up is a powerful tool that will further investigate the model independent evidence pointed out by DAMA/NaI with increased sensitivity and some interesting physical and astrophysical aspects.

As an example, we recall the effects induced on the Dark Matter particles distribution by the contributions from tidal streams [33] of satellite galaxies, by possible caustics and
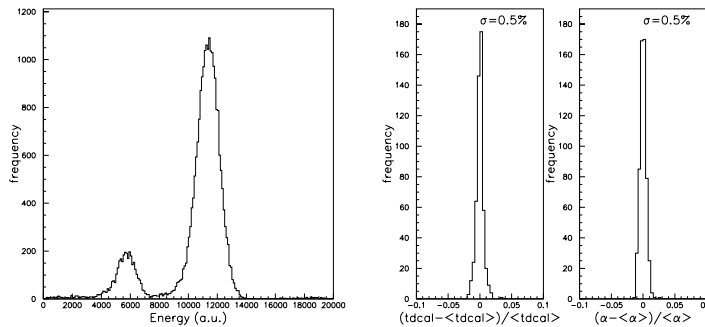
Figure 7: *Left panel*: energy distribution of the ^{241}Am source as measured by one of the new highly radiopure DAMA/LIBRA NaI(Tl) detectors ($\sigma/E = 6.7\%$ at 59.5 keV). *Right panels*: examples of the stability of the calibration factor (*tdcal*) and of the ratio of the peaks' positions (α) of the measured energy distribution of the ^{241}Am source during about one year of data taking.

by possible "solar wakes" [51]. In particular, it will possible to further investigate contributions to the Dark Matter particles in the galactic halo expected from tidal streams (from the Sagittarius Dwarf elliptical galaxy and from the Canis Major satellite galaxy). At present, the best way to investigate the presence of a stream contribution is to determine more accurately the phase of the annual modulation, t_0, as a function of the energy; in fact, for a given halo model — in presence of streams — t_0 would be expected to be (slightly) different from $\simeq 152.5$ d of the year (i.e. $\simeq$ June, 2nd) and to vary with energy.

Moreover, other topics will be further addressed by the highly radiopure DAMA/LIBRA, such as the study (i) on the velocity and spatial distribution of the Dark Matter particles in the galactic halo (for details see the discussions in ref. [3] and in the 2005 reference list); (ii) on possible structures as clumpiness with small scale size; (iii) on the coupling(s) of the Dark Matter particle with the ^{23}Na and ^{127}I target-nuclei; (iv) on the nature of the Dark Matter particles (susy particles in various scenarios, a neutrino of a fourth family, particles from multi-dimensional Kaluza-Klein like theories, Mirror Dark Matter, self-interacting dark matter, axion-like particles, ...); (v) on scaling laws and cross sections that, even for the neutralino candidate, the usually adopted scaling laws could not hold); etc. A large work will be faced by the new DAMA/LIBRA, which will also further investigate with higher sensitivity several other rare processes. The first data release is foreseen at end of 2008.

3   R&D-III and beyond

A third generation R&D effort towards a possible NaI(Tl) ton set-up has been funded by I.N.F.N. and related works on selection of materials for detectors and photomultipliers have already been started.

The low background DAMA/1ton will also act as a "general purpose" set-up (as the previous ones) allowing to investigate not only other approaches for Dark Matter, but also many other interesting topics in underground Physics having the following main advantages:

- well known technology;

- high radiopurity by selections, chem./phys. purifications, protocols;

- high duty cycle with the respect to all the experiments available so far;

- high light response and routine calibrations feasible down to keV range in the same production run conditions;

- well controlled operational condition feasible;

- No need re-purification procedures (reproducibility ...);

- absence of microphonic noise;

- no cryogenic complexities;

- effective investigation of the annual modulation signature feasible;

- sensitivity to all the CDM particle candidates, including those having interaction not involving nuclear recoils;

- safe and ecological clean set-up;

- sensitivity to several rare processes;

- the cheapest;

- etc.

At present measures on several materials have been done with ICP-MS and DAMA/Ge. Some protocols have been set in order to further reduce some contaminants and it is starting the production of first prototypes.

4 DAMA/LXe

As regard the LXe experiment, following the former Xelidon experiment on R&D developments of liquid Xenon detectors in latest 80's, DAMA considered many years ago (see e.g. ref. [52]) the use of the liquid Xenon as target-detector material for particle dark matter investigations and realised several LXe prototype detectors using natural Xenon. Then, it preliminarily put in measurement the set-up employed in the data taking of ref. [53, 54] by using Kr-free Xenon enriched in ^{129}Xe at 99.5%. This set-up was significantly upgraded at fall 1995 and again – deeply – in summer 2000, when the handling of Kr-free Xenon enriched in ^{136}Xe at 68.8% and in ^{134}Xe at 17.1% was also introduced. Main features of the set-up are described in ref. [55]. Investigations on several rare processes have been carried out with time passing in the various configurations [53, 54, 55, 56, 57, 58, 59, 60, 61, 62, 63, 64, 65]. On the contrary of the NaI(Tl) case, plans for enlarging its exposed mass have never been considered because of the technical

reasons (specific of liquid xenon detectors) pointed out several times in the past (see e.g. [66]).

After the stop of using cryogenic liquids in the underground laboratories, the set-up has taken data for some months until December 2004. After such a period, it has been again stopped waiting for the restart of LNGS cooling water plant operation, in order to avoid the overload of the chiller that works for all the DAMA/set-ups.

After the analysis of the already available data, collected above the threshold of 550 keV during 8823.54 h with the set-up filled with the Xenon enriched in ^{136}Xe at 68.8%, new experimental limits have been set on the investigation of possible tri-nucleon (NNN) decays into invisible channels for the ^{136}Xe isotope: disappearance or decay to neutrinos, Majorons, etc. [67] and in 2005 they have been published (see 2005 publication list).

5   DAMA/R&D

The DAMA/R&D set-up has been upgraded several times (see Fig. 8) and is used for tests on prototype PMTs and/or detectors and for small scale experiments mainly devoted to the search for double beta decay processes in various isotopes, such as ^{40}Ca, ^{46}Ca, ^{48}Ca, ^{106}Cd, ^{130}Ba, ^{136}Ce, ^{138}Ce, ^{142}Ce (see refs. [68, 69, 70, 71, 72, 73, 74] and in 2005 publication list). Both the active and the passive source techniques have been exploited as well as – sometimes – the coincidence technique.

Figure 8: Shield of the DAMA/R&D set-up and the automatic system to close it.

In 2005 the results on measurements taken with a LaCl$_3$:Ce crystal have been published (see 2005 publication list). In particular results on detector properties and experimental limits on some channels of cluster decays of ^{138}La and of ^{139}La have been studied, see later; other processes are under investigation. In 2005 also data taking with a very radiopure CaF$_2$(Eu) crystal has been performed; other rare processes are under investigation and other measurements on small scale experiments have been scheduled and some already prepared.

5.1 Performances and potentialities of a LaCl$_3$:Ce scintillator

The used detector is a commercial crystal LaCl$_3$:(8.5±1.0%)Ce[75] and no particular selection of crystal materials has been pursued; in fact, one of the goal of this work was the identification of the starting levels of residual contaminations in such a detector. The crystal scintillator has been viewed by a low background photomultiplier (PMT) EMI9265-B53/FL ($\simeq$ 30% quantum efficiency at 380 nm) through a Tetrasil-B light guide (7.6 cm diameter 10 cm long) to even further reduce the residual contribution from the low background PMT. In order to reduce further the environmental radioactivity, the voltage divider has directly been mounted on the flying leads of the PMT over a teflon disk by using miniaturised SMD capacitors and resistors, which are soldered by low radioactive lead and special resin. In particular, three charge ADC channels are acquired (with a 120 ns gate) to collect energy information in different energy ranges; moreover, the signals from the PMT are also recorded by a 160 MSa/s Transient Digitizer, TD, over a time window of 3125 ns.

The light response, the linearity, the energy resolution, the α/β ratio and the α/β discrimination capability have been studied. The main radioactive contaminations in the background have been quantified. The data have been then used to investigate some possible cluster decays in La isotopes.

The collected light is reduced by about 33% when using that light guide on LaCl$_3$:Ce. By comparing the measured energy calibration spectra with those obtained by a devoted MonteCarlo full simulation, the number of photoelectrons/keV has been derived: 7.2±1.0 for the case without light guide and and 4.8±1.0 for the case with light guide, respectively.

The pulse shape discrimination capability between α and $\gamma(\beta)$ particles has been investigated by studying the pulses recorded by Transient Digitizer. Various analysis approaches can be pursued, in particular the optimal digital filter method [76] has been used.

To obtain the numerical characteristic of the LaCl$_3$:Ce scintillation signal, namely the shape indicator (SI), the following formula has been applied for each pulse: $SI = \sum_k f(t_k) \times P(t_k)$, where k identifies the TD time channel in the time interval 44—200 ns. Moreover, $f(t)$ is the digitized amplitude of a given signal normalised to its area. The weight function $P(t)$ is defined as: $P(t) = f_\alpha(t) - f_\gamma(t)$, where $f_\alpha(t)$ and $f_\gamma(t)$ are the reference pulse shapes for α particles and γ quanta, respectively. In particular, $f_\alpha(t)$ has been obtained by averaging about 40000 individual events in the energy range 1800 – 2400 keV, where the analysis of the behaviour of the measured background assures the presence of only α particles' events from U and Th chains. To obtain instead $f_\gamma(t)$ about 40000 individual events of energy around 1500 keV have been averaged; in fact, the events below 1600 keV can be mainly ascribed to β and EC decays of ^{138}La (natural abundance: 0.0902%), see the devoted paper for details (2005 publication list).

The scatter plot of the shape indicator versus energy for the deep underground background measurements with the used LaCl$_3$:Ce crystal is depicted in Fig. 9.

The population of the α events is slightly shifted relatively to that of the $\gamma(\beta)$ events. As it is visible in the inset of Fig. 9, the distributions of the shape indicator for $\gamma(\beta)$ and α events are well described by gaussian functions.

The results of this analysis are in substantial agreement with the possibility of statis-
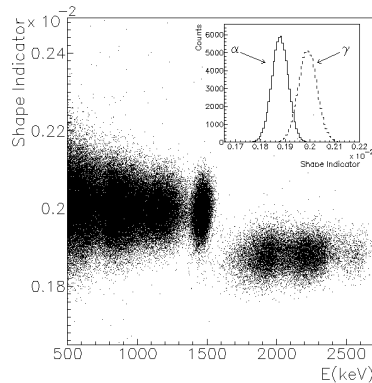
Figure 9: Scatter plot of the shape indicator SI (see text) versus energy for the deep underground background measurements with the LaCl$_3$:Ce scintillation detector. The α events are in the region above $\simeq 1600$ keV, while the γ (β) events are below this energy. In the inset: the distributions of the shape indicator measured for γ quanta (corresponding to energies around 1500 keV) and for α events (corresponding to the $1800 - 2400$ keV energy interval). See devoted paper.

tical pulse shape discrimination in LaCl$_3$:Ce as already suggested in ref. [77].

An analysis of the events time correlated in the TD time window – for the data collected deep underground during 70.2 h – has been carried out.

As first, we have investigated α–α time correlated events in the TD time window. They can be produced in particular by α decay of ^{219}Rn into ^{215}Po followed by ^{215}Po α decay ($T_{1/2} \sim 1.781$ ms) into ^{211}Pb (isotopes of the ^{235}U chain) and can be identified by applying the shape indicator method. Note that when considering only α particles the mean rate measured by the detector is $\simeq 0.37$ Hz, i.e. – considering an effective TD time window of 2400 ns – the expected α–α random coincidences are 0.03 events/day to be compared with the measured rate of (6.2 ± 1.4) events/day.

From the α–α events it is possible to derive the α/β ratio by comparing the detected α energy on the energy scale calibrated with γ sources and the real α energy. In our detector $\alpha/\beta = 0.328\pm0.004$ for the ^{219}Rn peak and 0.343 ± 0.003 for the ^{215}Po peak; these values are largely consistent with the value of (0.33 ± 0.01) for the ^{214}Po α of 7.686 MeV given in ref. [78]. Moreover, from the analysis of these events, the contamination of ^{235}U in the detector can be quantified: an activity of $(66\pm16)\times10^2$ dec/day has been estimated, that is when assuming the ^{235}U chain in equilibrium: (19 ± 5) ppb of ^{235}U.

We have also analysed the class of the so-called Bi-Po events. Also these events can be identified by studying the pulse information recorded by the TD: however, considering also in this case an effective TD time window of 2400 ns, Bi-Po events from ^{232}Th chain are mostly recorded; in this case the α/β ratio is $\simeq0.37$, suggesting an energy dependence of this quantity.

From the Bi-Po events it is also possible to estimate the ^{238}U and ^{232}Th contamination inside the LaCl$_3$:Ce detector. Considering the chains in equilibrium, it results in ^{232}Th and ^{238}U contaminations,

$$C_{^{232}Th} \quad < \quad 88 \quad \text{ppt} \quad (90\% \text{ C.L.}), \tag{1}$$

53

$$C_{238U} \quad < \quad 2.8 \quad \text{ppb} \quad (90\% \text{ C.L.}) \tag{2}$$

Let us comment the contaminations of ^{238}U with the respect to ^{235}U in the LaCl$_3$:Ce crystal. Typically, considering the halflife and the natural abundance of these two isotopes, the activity of ^{238}U should be about 20 times larger than that of ^{235}U. This is not the case in LaCl$_3$:Ce as obtained here and by other authors [79, 78, 80] and also later.

The measured background is fully dominated by the internal residual contaminants; in particular, as already mentioned, the events below $\simeq$1600 keV are mainly due to the radioactive decays of ^{138}La present in the natural La, while the events above $\simeq$1600 keV are due to α particles mainly from ^{235}U decay chain as suggested also from the previous analysis on the $\alpha - \alpha$ events. A further analysis of events due to α contaminations has been performed by realising a MonteCarlo simulation of the α decays of ^{227}Th, ^{223}Ra, ^{219}Rn, ^{215}Po and ^{211}Bi (because of the absence of ^{231}Pa). In particular, for the α particles the α/β ratio has been written as: $\alpha/\beta = a_0 + a_1 \times E_\alpha$, explicating its linear dependence on the α deposited energy, E_α. The expected energy distribution, $S_{a_0,a_1,c_1,c_2,N_1,N_2}(E)$, is a linear combination of the energy distribution obtained by the previous simulations and is function of 6 parameters. The a_0 and a_1 parameters are related to the α/β ratio; the c_1 and c_2 are related to the energy resolution: $\sigma/E = c_1 + c_2/\sqrt{E}$. The parameter N_1 represents the number of decays due to ^{227}Th (and, therefore, to its daughters: ^{223}Ra, ^{219}Rn and ^{211}Bi, which are considered at equilibrium) and N_2 is the number of decays due to ^{215}Po acquired by the DAQ system; we expect $N_2 << N_1$ because of the DAQ dead time. Form the best fit it was obtained the ratio:

$$\alpha/\beta = 0.187 + 0.0216 \times E_\alpha[MeV] \tag{3}$$

that is valid for α particles with energy E_α between 6 and 7.5 MeV and is well in agreement with estimates given above. In addition it follows that, in our case the ^{227}Ac ($T_{1/2} = 21.8$ y) can be considered as father isotope of the decay chain, while there are no traces of decays due to the first isotopes of the ^{235}U chain.

Let us now put forward some other considerations about this fact. At first [79] the chemistry of Lanthanides and Actinides is similar, so the U and Th content in Lanthanide minerals can be high: as example the Australian monazite, from which Lantanium can be derived, contains 6.7% of Th. Moreover, even if the decay chains would originally be in equilibrium, U and Th would be removed during the Lanthanide purification, but this procedure is not so efficient for some of the daughters; thus, a trace of U and Th can be kept in form of ^{227}Th, ^{223}Ra and daughters with a similar activity [79].

By using the value of the activity obtained by the α contamination analysis, we obtain for the ^{227}Ac: $C_{227Ac} = (6.7 \pm 0.3) \times 10^{-4}$ ppt.

As already mentioned, the energy distribution measured by the LaCl$_3$:Ce detector below 1600 keV is dominated by the ^{138}La decays ($T_{1/2} = (1.05 \pm 0.03) \times 10^{11}$ y [81]). Our crystal, (49.7 ± 1.3) g mass with a Ce concentration of (8.5 ± 1.0)%, contains $(1.01 \pm 0.04) \times 10^{20}$ nuclei of ^{138}La; thus, an activity of (21.1 ± 1.4) Bq can be derived.

The peak at $\simeq$ 38 keV (see Fig. 10–*Left*) can also be used to evaluate the ^{138}La activity in the detector; the resulting activity of ^{138}La is: $a_{138La} = \frac{N_{peak}}{\epsilon_{peak} \times T} = (20.5 \pm 0.4)$ Bq. This result is well in agreement with the previous estimation. Another determination of the ^{138}La activity can be obtained analysing the whole experimental energy spectrum below

1600 keV, it results in activity for ^{138}La: $a_{^{138}La} = \frac{N}{T} = (20.7 \pm 0.4)$ Bq, also in agreement with the previous estimates.

Finally, our evaluation of the $T_{1/2}$ of ^{138}La can be derived from the measured activity: $a_{^{138}La} = \ln 2 \times \frac{N_{^{138}La}}{T_{1/2}}$, thus, considering the number of ^{138}La nuclei in the detector it follows: $T_{1/2} = \ln 2 \times \frac{N_{^{138}La}}{a_{^{138}La}} = (1.07 \pm 0.06) \times 10^{11}$ y, well compatible with previous experimental estimation: $T_{1/2} = (1.05 \pm 0.03) \times 10^{11}$ y [81].

Fig. 10–*Right* shows the comparison between the experimental energy spectrum (continuous histogram) and the full simulation contributions (dashed line). A good agreement has been obtained.
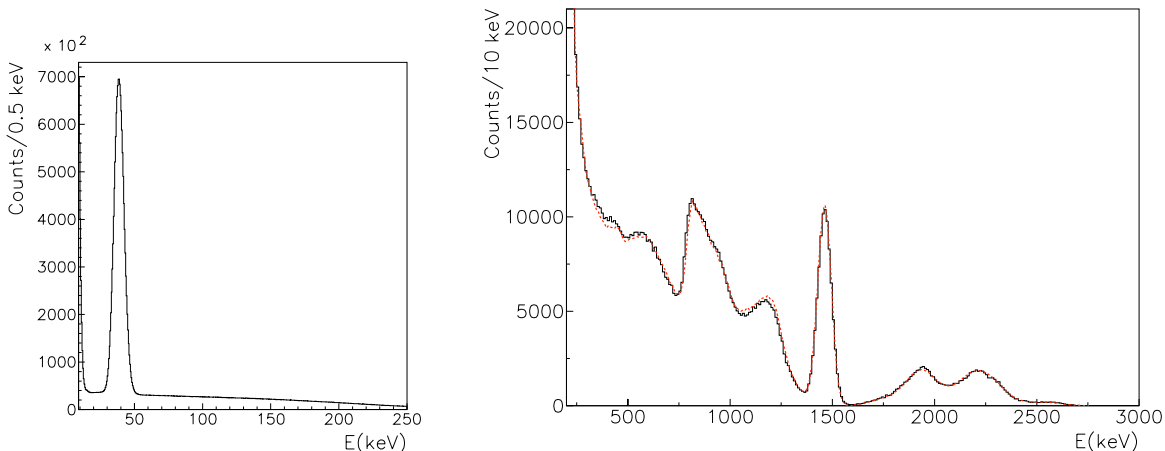
Figure 10: *Left*: energy distribution measured by the LaCl$_3$:Ce detector at low energy. *Right*: comparison between the experimental energy distribution at higher energy (continuous histogram) and simulation (dashed line). See text.

We have used the exposure collected deep underground with this commercial LaCl$_3$:Ce detector in order to investigate some of the possible cluster decay modes in ^{138}La and ^{139}La, as already done for ^{127}I (see above).

The ^{138}La and ^{139}La parent nuclei are incorporated in the LaCl$_3$:Ce detector itself (natural abundance of ^{138}La and ^{139}La are 0.0902% and 99.9098%, respectively) and the subsequent decays of the created clusters (which are usually radioactive) are searched for. Thus, for each considered decay channel, the data analysis has been realised by searching for the signals produced in the subsequent decay chain of the nuclides in the cluster. The obtained limits are given in Table 2.

In conclusion, the features of a LaCl$_3$:Ce detector have been investigated deep underground for the first time. An investigation of time correlated events, such as α-α and Bi-Po events, and a study of the experimental energy distribution have been carried out and have allowed e.g.: i) to determine the α/β light ratio in the used detector; ii) to investigate the α/β pulse shape discrimination capability; iii) to quantify the main radioactive contaminants of the detector. As an example of possible application a search for some possible cluster decays modes in La isotopes has been carried out setting new experimental limits. Other processes are under analysis.

However, due to the high ^{138}La content in natural La and to the presence of daughters from the broken ^{235}U chain, an extensive application of LaCl$_3$:Ce in the search for rare pro-

Table 2: New experimental lower limits (90% C.L.) on $T_{1/2}$ obtained for the quoted cluster decays of ^{138}La and ^{139}La. Still significant part of the expected energy distributions remains above 2.83 MeV, that is in the region where zero counts have been measured; thus, we focus our attention on the energy region above 2.83 MeV. The η values are the number of events (per 1 decay) detected above 2.83 MeV for each cluster decay; it is worth to note that one cluster decay can give rise to more than a single detected event. Moreover, $N_d < 2.3/\eta$ are the upper limits (90% C.L.) on the number of cluster decays searched for; see text.

Decay	η	N_d (90% C.L.)	$T_{1/2}$ (y) (90% C.L.)
^{138}La $\rightarrow$ ^{48}Ca $+^{90}$Rb	0.286	< 8.0	> 7.0×10^{16}
^{139}La $\rightarrow$ ^{48}Ca $+^{91}$Rb	0.187	< 12.3	> 5.0×10^{19}
^{139}La $\rightarrow$ ^{51}Sc $+^{88}$Kr	0.461	< 5.0	> 1.2×10^{20}

cesses appears at present difficult, remaining however this kind of scintillator potentially very competitive for some sea level applications.

6   DAMA/Ge

Various R&D developments to improve low background set-ups and scintillators as well as new developments for higher radiopure PMTs are regularly carried out. The related measurements on samples are usually performed by means of the DAMA low background Ge detector, specially realised with a low Z window. It is operative deep underground in the low background facility of the Gran Sasso Laboratory. Some selected materials are in addition measured with high sensitivity ICP-IP and mass spectrometers.

During year 2005 a significant improvement of the DAMA/Ge installation has been performed: a new sealing system, a new system for neutron shielding, an automatic Marinelli and shield opening/closure system have been realised, see Fig.11.

Figure 11: New shield and Marinelli system of the DAMA/Ge set-up.

7 List of Publications during 2005

1. R. Bernabei, P. Belli, F. Cappella, F. Montecchia, F. Nozzoli, A. Incicchitti, D. Prosperi, R. Cerulli, C.J. Dai, H.H. Kuang, J.M. Ma, Z.P. Ye, *Further results on the WIMP annual modulation signature by DAMA/NaI*, Nucl. Phys. B (Proc. Suppl.) 138 (2005) 45.

2. R. Bernabei, P. Belli, F. Cappella, F. Montecchia, F. Nozzoli, A. d'Angelo, A. Incicchitti, D. Prosperi, R. Cerulli, C.J. Dai, H.H. Kuang, J.M. Ma, Z.P. Ye, *Prospects for DAMA/LIBRA and beyond*, Nucl. Phys. B (Proc. Suppl.) 138 (2005) 48.

3. R. Bernabei, P. Belli, F. Cappella, F. Montecchia, F. Nozzoli, A. Incicchitti, D. Prosperi, R. Cerulli, C.J. Dai, H.H. Kuang, J.M. Ma, Z.P. Ye, *Very low background scintillators in DAMA project: results and perspectives*, in the volume "Calorimetry in particle Physics", World Sc. pub. (2005) 477.

4. R. Bernabei, P. Belli, F. Cappella, F. Montecchia, F. Nozzoli, A. d'Angelo, A. Incicchitti, D. Prosperi, R. Cerulli, C.J. Dai, H.H. Kuang, J.M. Ma, Z.P. Ye, *Search for spontaneous transition of nuclei to a superdense state*, Eur. Phys. J. A23 (2005) 7-10.

5. R. Bernabei, P. Belli, F. Cappella, F. Montecchia, F. Nozzoli, A. d'Angelo, A. Incicchitti, D. Prosperi, R. Cerulli, C.J. Dai, H.L. He, H.H. Kuang, J.M. Ma, Z.P. Ye, V.I. Tretyak, A search for spontaneous emission of heavy cluster in the ^{127}I nuclide, Eur. Phys. J. A 24 (2005) 51-56.

6. R. Bernabei for DAMA coll., *Particle Dark Matter*, in publication on the Proceed. of the Conf. "Results and perspectives in particle Physics", La Thuile, Feb.- March 2005.

7. P. Belli, R. Bernabei, F. Montecchia, F. Nozzoli, F. Cappella, A. d'Angelo, A. Incicchitti, D. Prosperi, R. Cerulli, C.J. Dai, H.L. He, H.H. Kuang, J.M. Ma, Z.P. Ye, *Particle Dark Matter in the Galactic Halo: Results from DAMA/NaI and Perspectives for DAMA/LIBRA at Gran Sasso*, in publication on the Proceed. of the Baksan 05 Int. School, Baksan Valley (Russia), April 2005.

8. R. Bernabei, P. Belli, F. Nozzoli, F. Montecchia, F. Cappella, A. Incicchitti, D. Prosperi, R. Cerulli, C.J. Dai, V.Yu. Denisov, V.I. Tretyak, *Search for rare processes with DAMA/LXe experiment at Gran Sasso* , in publication on the Proceed. of the Baksan 05 Int. School, Baksan Valley (Russia), April 2005.

9. R. Bernabei, P. Belli, F. Cappella, F. Montecchia, F. Nozzoli, A. Incicchitti, D. Prosperi, R. Cerulli, C.J. Dai, H.H. Kuang, J.M. Ma, Z.P. Ye, *Signature for signals from the Dark Universe*, in the volume Vulcano Workshop 2004 "Frontier Objects in Astrophysics and Particle Physics", Societá Italiana di Fisica (2005) 201.

10. R. Bernabei, P. Belli, F. Cappella, F. Montecchia, F. Nozzoli, A. d'Angelo, A. Incicchitti, D. Prosperi, R. Cerulli, C.J. Dai, H.H. Kuang, J.M. Ma, Z.P. Ye, *The*

new DAMA/LIBRA and beyond, in the volume Vulcano Workshop 2004 "Frontier Objects in Astrophysics and Particle Physics", Societá Italiana di Fisica (2005) 581.

11. R. Bernabei, P. Belli, F. Montecchia, F. Nozzoli, F. Cappella, A. Incicchitti, D. Prosperi, R. Cerulli, C.J. Dai, V.Yu. Denisov, V.I. Tretyak, *Search for rare processes with DAMA/LXe experiment at Gran Sasso*, in publication on EPJA (NPA 2005).

12. R. Bernabei, P. Belli, F. Montecchia, F. Nozzoli, F. Cappella, A. d'Angelo, A. Incicchitti, D. Prosperi, R. Cerulli, C.J. Dai, H.L. He, H.H. Kuang, J.M. Ma, Z.P. Ye, *From DAMA/NaI to DAMA/LIBRA at LNGS*, in publication on EPJA (NPA 2005).

13. R. Bernabei, P. Belli, F. Montecchia, F. Nozzoli, F. Cappella, A. d'Angelo, A. Incicchitti, D. Prosperi, R. Cerulli, C.J. Dai, H.L. He, H.H. Kuang, J.M. Ma, Z.P. Ye, *Particle Dark Matter: from DAMA/NaI to DAMA/LIBRA*, in publication on the Proceed. of the NANP05 Int. Conf., Dubna (Russia), June 2005.

14. R. Bernabei, P. Belli, F. Montecchia, F. Nozzoli, A. d'Angelo, F. Cappella, A. Incicchitti, D. Prosperi, S. Castellano, R. Cerulli, C.J. Dai, V.I. Tretyak, *Performances and potentialities of a LaCl$_3$:Ce scintillator*, Nucl. Inst. and Meth. A555 (2005) 270-281.

15. R. Bernabei, P. Belli, F. Montecchia, F. Nozzoli, F. Cappella, A. d'Angelo, A. Incicchitti, D. Prosperi, R. Cerulli, C.J. Dai, H.L. He, H.H. Kuang, J.M. Ma, Z.P. Ye, *Highlights of DAMA*, to appear on Journal of Physics: Conference Series TAUP 2005.

16. R. Bernabei, P. Belli, F. Montecchia, F. Nozzoli, F. Cappella, A. d'Angelo, A. Incicchitti, D. Prosperi, R. Cerulli, C.J. Dai, H.L. He, H.H. Kuang, J.M. Ma, Z.P. Ye, *Physics and astrophysics with dark Matter particles*, to appear on Journal of Physics: Conference Series TAUP 2005.

17. R. Bernabei, P. Belli, F. Montecchia, F. Nozzoli, F. Cappella, A. Incicchitti, D. Prosperi, R. Cerulli, C.J. Dai, H.L. He, H.H. Kuang, J.M. Ma, Z.P. Ye, *Investigating pseudoscalar and scalar dark matter*, Int. J. Mod. Phys. A in press (ROM2F/2005/19 & astro-ph/0511262).

18. R. Bernabei, P. Belli, F. Montecchia, F. Nozzoli, F. Cappella, A. d'Angelo, A. Incicchitti, D. Prosperi, R. Cerulli, C.J. Dai, H.L. He, H.H. Kuang, J.M. Ma, Z.P. Ye, *Recent DAMA results*, in publication on the Proceed. of the ICATPP05 Int. Conf., Como (Italy), October 2005.

References

[1] R. Bernabei et al., Il Nuovo Cimento A112 (1999) 545.

[2] R. Bernabei et al., Eur. Phys. J. C18 (2000) 283.

[3] R. Bernabei et al., La Rivista del Nuovo Cimento 26 n.1 (2003) 1-73, R. Bernabei et al., Int. J. Mod. Phys. D 13 (2004) 2127.

[4] R. Bernabei et al., Phys. Lett. B424 (1998) 195.

[5] R. Bernabei et al., Phys. Lett. B450 (1999) 448.

[6] P. Belli et al., Phys. Rev. D61 (1999) 023512.

[7] R. Bernabei et al., Phys. Lett. B480 (2000) 23.

[8] R. Bernabei et al., Phys. Lett. B509 (2001) 197.

[9] R. Bernabei el al., Eur. Phys. J. C23 (2002) 61.

[10] P. Belli et al., Phys. Rev. D66 (2002) 043503.

[11] R. Bernabei et al., Phys. Lett. B389 (1996) 757.

[12] R. Bernabei et al., Il Nuovo Cimento A112 (1999) 1541.

[13] R. Bernabei et al., Phys. Rev. Lett. 83 (1999) 4918.

[14] F. Cappella et al., Eur. Phys. J.-direct C14 (2002) 1.

[15] R. Bernabei et al., Phys. Lett. B515 (2001) 6.

[16] R. Bernabei et al., Phys. Lett. B408 (1997) 439.

[17] P. Belli et al., Phys. Rev. C60 (1999) 065501.

[18] P. Belli et al., Phys. Lett. B460 (1999) 236.

[19] R. Bernabei et al., Nucl. Phys. B (Proc. Suppl.) 70 (1999) 79.

[20] A. Bottino et al., Phys. Rev. D69 (2004) 037302, Phys. Rev. D68 (2003) 043506.

[21] R. Foot, Phys. Rev. D 69 (2004) 036001.

[22] S. Mitra, Phys. Rev. D 71 (2005) 121302.

[23] L. Di Lella et al., Phys. Rev. D62 (2000) 125011.

[24] D. B. Kaplan and K. M. Zurek, hep-ph/0507236

[25] G. B. Gelmini and M. Roncadelli, Phys. Lett. B99 (1981) 411, E. Masso, Nucl. Phys. B (Proc. Suppl.) 114 (2003) 67.

[26] L. Di Lella and K. Zioutas, Astropart. Phys. 19 (2003) 145.

[27] D. S. Gorbunov, G. G. Raffelt and D. V. Semikoz, Phys. Rev. D 64 (2001) 096005.

[28] V. Berezinsky and J. W. F. Valle, Phys. Lett. B 318 (1993) 360, V. Berezinsky, A. Bottino and G. Mignola, Nucl. Phys. B (Proc. Suppl.) 48 (1996) 22.

[29] E. Masso and R. Toldra, Phys. Rev. D 52 (1995) 1755.

[30] G.G. Raffelt and A. Weiss, Phys. Rev. D 51 (1995) 1495.

[31] P. Jain and S. Mandal, astro-ph/0512155.

[32] S. Eidelman et al., Phys. Lett. B 592 (2004) 1.

[33] K. Freese, P. Gondolo and H. J. Newberg, Phys. Rev. D 71 (2005) 043516, K. Freese et al., Phys. Rev. Lett. 92 (2004) 111301.

[34] N. F. Martin et al., Mon. Not. Roy. Astr. Soc. 348 (2004) 12.

[35] A. Sandulescu et al., Sov. J. Part. Nucl. 11 (1980) 528.

[36] H.J. Rose and G.A. Jones, Nature 307 (1984) 245.

[37] D.V. Aleksandrov et al., JETP Lett. 40 (1984) 909.

[38] R. Bonetti and A. Guglielmetti, in "Heavy elements and related new phenomena", ed. by W. Greiner and R.K. Gupta, vol. 2, World Sci. (1999) p. 643.

[39] S.P. Tretyakova et al., Progr. Theor. Phys. Suppl. 146 (2002) 530.

[40] R. Bonetti et al., Phys. Rev. C 51 (1995) 2530.

[41] D.N. Poenaru et al., Phys. Rev. C 47 (1993) 2030.

[42] A. Guglielmetti et al., Phys. Rev. C 56 (1997) 2912.

[43] G. Audi et al., Nucl. Phys. A 729 (2003) 337.

[44] D.N. Poenaru et al., At. Data Nucl. Data Tables 34 (1986) 423.

[45] D.N. Poenaru et al., Phys. Rev. C 65 (2002) 054308.

[46] M. Balasubramaniam et al., Phys. Rev. C 70 (2004) 017301.

[47] Z.Z. Ren et al., Phys. Rev. C 70 (2004) 034304.

[48] A.Ya. Balysh et al., Sov. Phys. JETP 64 (1986) 21.

[49] E. Bukhner et al., Sov. J. Nucl. Phys. 52 (1990) 193.

[50] R. Bernabei et al., Astrop. Phys. 4 (1995) 45; R. Bernabei, "Competitiveness of a very low radioactive ton scintillator for particle Dark Matter search", in the volume *The identification of Dark Matter*, World Sc. pub. (1997) 574.

[51] F.S. Ling, P. Sikivie and S. Wick, Phys. Rev. D 70 (2004) 123503.

[52] P. Belli et al., Il Nuovo Cimento A103 (1990) 767.

[53] P. Belli et al., Il Nuovo Cimento C19 (1996) 537.

[54] P. Belli et al., Astrop. Phys. 5 (1996) 217.

[55] R. Bernabei et al., Nucl. Instr. & Meth. A482 (2002) 728.

[56] P. Belli et al., Phys. Lett. B387 (1996) 222 and Phys. Lett. B389 (1996) 783 (erratum).

[57] R. Bernabei et al., Phys. Lett. B436 (1998) 379.

[58] R. Bernabei et al., Eur. Phys. J.-direct C11 (2001) 1.

[59] R. Bernabei et al., New Journal of Physics 2 (2000) 15.1.

[60] P. Belli et al., Phys. Rev. D61 (2000) 117301.

[61] P. Belli et al., Phys. Lett. B465 (1999) 315.

[62] R. Bernabei et al., Phys. Lett. B493 (2000) 12.

[63] R. Bernabei et al., Phys. Lett. B527 (2002) 182.

[64] R. Bernabei et al., Phys. Lett. B546 (2002) 23.

[65] R. Bernabei et al., in the volume "Beyond the Desert 2003", Springer (2003), 365-374.

[66] R. Bernabei et al., in the volume "Cosmology and particle Physics", AIP ed. (2001) 189.

[67] F. Cappella, PhD thesis, Univ. Roma "Tor Vergata" (2005).

[68] R. Bernabei et al., Il Nuovo Cimento A110 (1997) 189.

[69] R. Bernabei et al., Astrop. Phys. 7 (1997) 73.

[70] P. Belli et al., Nucl. Phys. B563 (1999) 97.

[71] P. Belli et al., Astrop. Phys. 10 (1999) 115.

[72] R. Bernabei et al., Nucl. Phys. A705 (2002) 29.

[73] P. Belli et al., Nucl. Instr. & Meth. A498 (2003) 352.

[74] R. Cerulli et al., Nucl. Instr. & Meth. A525 (2004) 535.

[75] Saint Gobain crystals & detectors, private communication.

[76] E. Gatti and F. De Martini, Nuclear Electronics, Vol. 2, IAEA, Vienna, (1962) p.265.

[77] C. Hoel et al., Nucl. Instr. & Meth. A540 (2005) 205.

[78] M. Balcerzyk et al., Nucl. Instr. & Meth. A537 (2005) 50.

[79] G. Gautier et al., presented at IEEE conf. (2005).

[80] J.K. Hartwell and R. J. Gehrke, Applied Rad. and Isotopes 63 (2005) 223.

[81] J.K. Tuli, Nucl. Data Sheets 74 (1995) 349.

The ICARUS T600 Experiment at GranSasso Laboratory

A. Ankowski[o], M. Antonello[c], P. Aprili[d], F. Arneodo[d], A. Badertscher[e], B. Baiboussinov[a], M. Baldo Ceolin[a], G. Battistoni[f], P. Benetti[h], M. Bischofberger[e], A. Borio di Tigliole[h], R. Brunetti[h], G. Bucciarelli[d], A. Bueno[e,i], E. Calligarich[h], F. Carbonara[b], M.C. Carmona[e,i], F. Cavanna[c], P. Cennini[j], S. Centro[a], A. Cesana[k,f], D.B. Cline[m], K. Cieślik[n], A.G. Cocco[b], Z. Dai[e], C. De Vecchi[h], A. Dąbrowska[n], A. Di Cicco[b], R. Dolfini[h], A. Ereditato[b], A. Ferella[c], A. Ferrari[j,f], F. Ferri[c], G. Fiorillo[b], S. Galli[c], D. Garcia Gamez[i], Y. Gel[e], D. Gibin[a], A. Gigli Berzolari[h], I. Gil-Botella[e], K. Graczyk[o], L. Grandi[h], A. Guglielmi[a], J. Holeczek[g], C. Juszczak[o], D. Kiełczewska[p,q], J. Kisiel[g], T. Kozłowski[p], M. Laffranchi[e], J. Łagoda[q], B. Lisowski[m], J. Lozano[e,i], M. Markiewicz[n], A. Martinez de la Ossa[i], C. Matthey[m], F. Mauri[h], A.J. Melgarejo[i], A. Menegolli[h], G. Meng[a], M. Messina[e], C. Montanari[h], S. Muraro[f], S. Navas-Concha[e,i], J. Nowak[o], S. Otwinowski[m], O. Palamara[d], L. Periale[s,t], G. Piano Mortari[c], A. Piazzoli[h], P. Picchi[u,t,s], F. Pietropaolo[a], W. Półchłopek[v], M. Prata[h], M.C. Prata[h], P. Przewłocki[p], A. Rappoldi[h], G.L. Raselli[h], E. Rondio[p], M. Rossella[h], A. Rubbia[e], C. Rubbia[h], P. Sala[f], R. Santorelli[b], D. Scannicchio[h], E. Segreto[c], Y. Seo[m], F. Sergiampietri[m,w], J. Sobczyk[o], S. Stach[g], J. Stepaniak[p], R. Sulej[x], M. Szeptycka[p], M. Szarska[n], A. Szelc[n], M. Terrani[k,f], F. Varanini[a], S. Ventura[a], C. Vignoli[h], H. Wang[m], X. Yang[m], A. Zalewska[n]

[a]Università di Padova e INFN, Padova, Italy

[b]Università Federico II di Napoli e INFN, Napoli, Italy

[c]Università dell'Aquila e INFN, L'Aquila, Italy

[d]INFN - Laboratori Nazionali del Gran Sasso, Assergi, Italy

[e]Institute for Particle Physics, ETH Hönggerberg, Zürich, Switzerland

[f]Università di Milano e INFN, Milano, Italy

[g]Institute of Physics, University of Silesia, Katowice, Poland

[h]Università di Pavia e INFN, Pavia, Italy

[i]Dpto de Física Teórica y del Cosmos & C.A.F.P.E., Universidad de Granada, Granada, Spain

[j]CERN, Geneva, Switzerland

[k]Politecnico di Milano (CESNEF), Milano, Italy

[m]Department of Physics, UCLA, Los Angeles, USA

[n]H.Niewodniczański Institute of Nuclear Physics, Kraków, Poland

[o]Institute of Theoretical Physics, Wrocław University, Wrocław, Poland

[p]A.Sołtan Institute for Nuclear Studies, Warszawa, Poland

[q]Institute of Experimental Physics, Warsaw University, Warszawa, Poland

[r]Institute of Mechanics and Machine Design, Cracow University of Technology, Kraków, Poland

[s]IFSI, Torino, Italy

[t]INFN Laboratori Nazionali di Frascati, Frascati, Italy

[u]Università di Torino, Torino, Italy

[v]University of Mining and Metallurgy, Kraków, Poland

[w]INFN, Pisa, Italy

[x]Warsaw University of Technology, Warszawa, Poland

Abstract

The ICARUS T600 detector is the largest liquid Argon TPC ever built, with a size of about 600 tons of fully imaging mass. The design and assembly of the detector relied on industrial support and represents the application of concepts matured in laboratory tests to the kton-scale.

The detector was developed to act as an observatory for astroparticle and neutrino physics at the Gran Sasso Underground Laboratory and a second generation nucleon decay experiment.

The ICARUS T600 was commissioned in 2001 for a technical run performed at surface in the Pavia INFN site. During this period all the detector features were extensively tested with an exposure to cosmic–rays. During 2004 the detector was moved from Pavia to the LNGS underground site. In 2005 remounting of the detector and of the cryogenic system has been performed. This phase is still under way and is expected to be completed by the end of 2006.

In this report some results from analysis and studies based on the experimental data collected during the technical run are summarized.

1   Introduction

The technology of the Liquid Argon Time Projection Chamber (LAr TPC), first proposed by C. Rubbia in 1977 [1], was conceived as a tool for a completely uniform imaging with high accuracy of massive volumes. The operational principle of the LAr TPC is based on the fact that in highly purified LAr ionization tracks can be transported practically undistorted by a uniform electric field over macroscopic distances. Imaging is provided by a suitable set of electrodes (wires) placed at the end of the drift path continuously sensing and recording the signals induced by the drifting electrons.

Non–destructive read–out of ionization electrons by charge induction allows to detect the signal of electrons crossing subsequent wire planes with different orientation. This provides several projective views of the same event, hence allowing space point reconstruction and precise calorimetric measurement.

The LAr TPC was developed in the context of the ICARUS programme and currently finds its application in studies concerning some of the major issues of particle and astroparticle physics:

- the study of solar and atmospheric neutrino interactions;

- the study of nucleon decay for some channels predicted by GUTs;

- the detection of neutrinos following a Supernova explosion;

- the study of neutrino oscillations with beams from particle accelerators.

After the original proposal, the feasibility of the technology has been first demonstrated by an extensive R&D programme, which included ten years of studies on small LAr volumes and five years of studies with several prototypes of increasing mass[2, 3, 4, 5, 6, 7, 8, 9, 10, 11, 12, 13, 14, 15, 16].

The second step was represented by the construction of the T600 module[17]: a detector employing about 600 tons of liquid Argon to be operated at LNGS. This step–wise

strategy allowed to progressively develop the necessary know–how to build a multi–kton liquid Argon detector.

The realization of the T600 detector (from design to construction) lasted about four years and culminated with the full test of the experimental set–up, carried out at surface during 2001. This test demonstrated the maturity of the project. All technical aspects of the system, namely cryogenics, LAr purification, read–out chambers, detection of LAr scintillation light, electronics and DAQ had been tested and performed as expected. Statistically significant samples of cosmic–ray events (long muon tracks, spectacular high–multiplicity muon bundles, electromagnetic and hadronic showers, low energy events) were recorded. The subsequent analysis of these events, carried out in 2002-03, has allowed the development and fine tuning of the off–line tools for the event reconstruction and the extraction of physical quantities. It has also demonstrated the performance of the detector in a quantitative way, issuing in a number of papers published in 2003-04:

- Analysis of the liquid Argon purity in the T600 detector [18];

- Observation of very long ionizing tracks [19];

- Measurement of the muon decay spectrum [20];

- Study of ionization quenching in liquid Argon [21];

A detailed description of the T600 detector and of its technical performance as obtained from the acceptance tests has been reported in a dedicated milestone paper [22] published in 2004.

More recently, in 2005, a paper dedicated to the characterization tests at cryogenic temperature of the photomultipliers adopted in ICARUS for the detection of the LAr scintillation light has been published [23] and will be here shortly summarized. Additional results from current studies on optimization of methods for particle identification and event reconstruction are here also reported.

2 Characterization of the ETL 9357FLA Photomultipliers

Extracted from [23] "Characterization of ETL 9357 FLA Photomultiplier Tubes for cryogenic temperature applications", ICARUS Collaboration, Nucl. Inst. and Meth. A. **556** (2005), 146.

In the ICARUS T600 apparatus a system based on 74 photomultiplier tubes (PMTs) is used to detect the light coming from the liquid argon scintillation for T_0 and trigger purposes.

The adopted PMT model, Electron Tubes Ltd (ETL) 9357FLA, is a 12-stage LF-dynode PMT with an hemispherical glass window of 200 mm (8-in.) diameter. The bialkali photocathode (K_2CsSb) is deposited on a Pt under-layer in order to extend the device operating temperature range.

Each PMT was extensively tested and characterized before the final installation inside the detector. A lot of data was collected during the tests which assumes statistical significance of the operating performances at cryogenic temperature of these devices and certifies the PMT system assembled in the ICARUS T600 apparatus for the direct measurement of light coming from liquid argon scintillation.
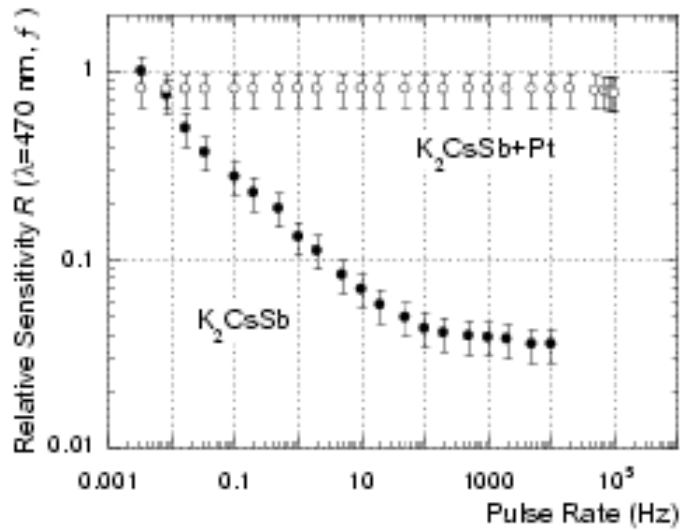
Figure 1: Relative sensitivity vs. light pulse rate for K₂CsSb and K₂CsSb+Pt photocathodes and $\lambda = 470$ nm light source. The vertical bars indicate the statistical spread (sigma) of each measurement.

The main PMT parameters and the spread of the distinctive features over different samples are:

- good capability to withstand thermal shocks from room to cryogenic temperature;

- good suitability of the bialkali photocathode on Pt under-layer to work and detect the light both at room and at cryogenic temperature, with a sensitivity decrease of about 20% ($\lambda = 470$ nm) at T=77 K with respect to room temperature;

- rise time (3.9±1.1 ns) and FWHM (7.3±1.4 ns) in good agreement with the nominal values;

- SER charge resolution characterized by a P/V ratio of 1.86 ± 0.54, a worsening of about 22% with respect to room temperature;

- good linearity up to about 300 photoelectrons both at room and at cryogenic temperature;

- wide variation of gain losses, ranging from -15% to -80%, from room to cryogenic temperature;

- dark noise rate of 1142 ± 235 Hz, an increase of about 70% relative to room temperature;

- transit time jitter of about 1.2 ns, a factor two better than that measured at room temperature;

- a slight decrease of afterpulse rate from room to cryogenic temperature.

Detailed investigations were carried out about the parameters which presented remarkable differences from room and cryogenic temperature, such as the photocathode sensitivity, the the gain losses and the dark count rate.

The adopted PMT model uses a bialkali photocathode deposited at manufacture on a Pt under-layer ($K_2CsSb+Pt$) which avoids the drawbacks due to the photocathode resistivity increase at cryogenic temperature.

The suitability of this photocathode to detect light at cryogenic temperature was demonstrated by measuring the relative sensitivities R, i.e. the ratio between the cathode signal at cryogenic and at room temperature using the same light stimulation. As shown in Figure 1 the ratio R of a standard bialkali (K_2CsSb) photocathode rapidly decreases as the pulse rate f increases, meaning that its sensitivity is affected by a resistivity problem at cryogenic temperature; on the contrary the $K_2CsSb+Pt$ photocathode shows a quite flat behaviour with a slight sensitivity reduction at cryogenic temperature which depends on the light wavelength adopted in the test.

Further investigations about the behaviour of the $K_2CsSb+Pt$ photocathode as a function of the light wavelength λ showed that the maximum sensitivity values at cryogenic temperature are attained in the blue region ($\lambda = 470$ nm) with about a 20% reduction with respect to room temperature.
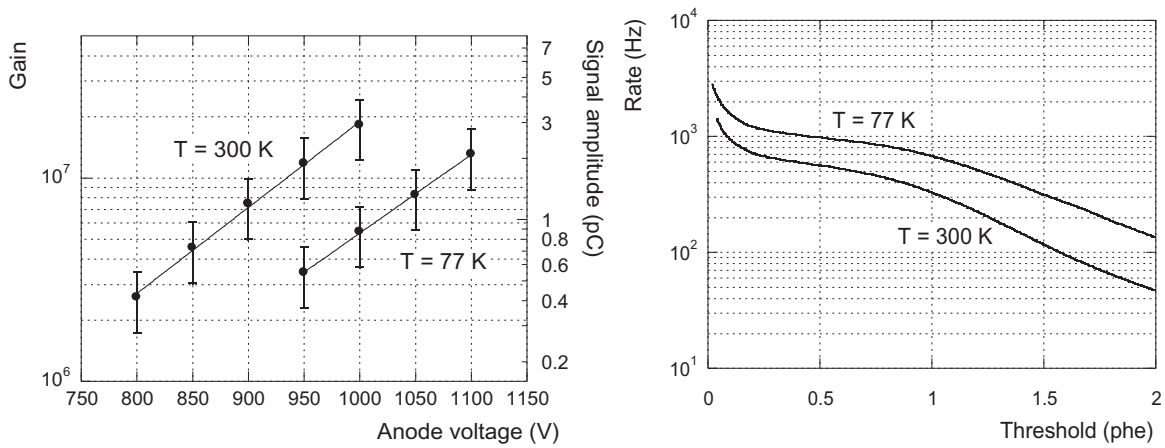
Figure 2: [Left] Signal amplitude as a function of the anode voltage at room and at cryogenic temperature. For each measurement the peak position (dots) and the SER distribution width (vertical bars) coming from a best-fit procedure are shown. [Right] PMT dark count rate as a function of the discrimination threshold at room and at cryogenic temperature. The threshold value is normalized to fraction of photoelectron (phe).

The study of the gain dependence on the operating temperature was carried out by measuring the PMT response to single electron excitation (SER) for different dynode-chain voltages at room and at cryogenic temperature.

SER data were fitted using an analytical expression and the value of the peak position was assumed as the operating gain value. In Figure 2 [Left] the results obtained at room and at cryogenic temperature, using the same PMT sample, are plotted. The signal amplitude is well represented by an exponential trend as a function of the anode voltage for both operating temperatures, with an appreciable reduction of the multiplier gain at 77 K with respect to room temperature.

Similar behaviours were observed for all the tested PMTs. The samples showed wide variations of gain losses from room to cryogenic temperature, ranging from -15% to -80%. Anyway, an increase of about 100 V of the anode voltage is enough to recover the original

gain values.

The measurements of the PMT dark count rate at room temperature and at cryogenic temperature were carried out with the device under test operating in complete darkness condition.

The spectrum structure as a function of the discrimination threshold, as shown in Figure 2 [Right], is characterized by a clear bump profile centered in the region around one photoelectron, that is caused mainly by the cathode dark noise. An increase of the counting rate at cryogenic temperature was experienced for all the tested PMTs.

The measurement distributions over the tested samples operating at 10^7 nominal gain give very low counting rates at room temperature (mean=700 Hz, RMS=175 Hz at 0.2 phe threshold) with a sensible rise when operating at 77 K (mean=1142 Hz , RMS=235 Hz at 0.2 phe threshold).

3 Kalman Filter method for μ-momentum measurement

The analysis of any kind of event occurring in ICARUS requires a good knowledge of the event kinematics, and this includes not only the track positions along its path but also the momentum information, fundamental to select and classify the interesting events.

While low energy muons may stop inside the liquid Argon and its momentum easily measured by calorimetry, a substantial fraction of atmospheric muons with energies of the order and above 1 GeV will generally escape the active volume. In such cases, the multiple scattering technique (MS) appeared as the best solution to estimate the particle momentum provided the track extends over a relatively long (few meters) path (see for instance [1] and references therein). We will refer to the MS technique as the *classical method* hereafter. As shown in [2], in case of short escaping tracks, other techniques based on the use of the most probable energy lost by the muon can be exploited to estimate the muon momentum.

The momentum measurement for partially contained particles has been revisited using Kalman Filter (KF) techniques. We have previously shown [3] that the use of a KF [4] to process the information provided by multiple coulomb scattering, offers the best resolution over a broad range of momenta. Our results were obtained using a sample of Monte-Carlo muons fully simulated in a T300-like detector. The method was validated and the KF behavior studied when applied to real data [5]. To this purpose, we use a large fraction of the total sample of stopping muons collected during the 2001 Pavia technical run, namely those having a decaying electron [6]. Those contained muons are useful to check the validity of the proposed method since their momenta can be measured from calorimetry, and therefore be directly compared with the values provided by the KF algorithm.

---

[1] A. Bueno, A.J. Melgarejo and S. Navas-Concha, "Multiple Scattering and Muon Momentum Measurement", ICARUS-TM/2004-8

[2] S. Navas-Concha, A. Rubbia and F. Pietropaolo, "On the use of Δ_{mp} to estimate Muon Momentum", ICARUS-TM/2002-11

[3] A. Bueno, A.J. Melgarejo, S. Navas-Concha, "Application of the Kalman Filter Algorithm to the Problem of Momentum Measurement for Through-Going Particles", ICARUS-TM/04-15

[4] R.E. Kalman, Trans. ASME, J. Bas. Eng. 82D (1960). R. Fruhwirth, Nucl. Instrum. Meth. A **262** (1987) 444.

[5] A. Bueno, A.J. Melgarejo and S. Navas-Concha, "Momentum Measurement of the T600 Stopping Muon Sample Using a Kalman Filter", ICARUS-TM/2005-3.

[6] J. Rico, Ph.D. Thesis, Diss. ETH No. 14906. Swiss Institute of Technology. Nov 2002., [20]

The analysis procedure is similar for Monte Carlo and real data events. We summarize here the main steps:

- Individual 2D reconstruction of each muon track;

- Removal of hits associated to δ-rays and electrons resulting from muon decay;

- Momentum measuring using both calorimetry and Kalman Filter algorithms.

When computing momentum by means of calorimetry, recombination effects should be taken into account. Equation 1 relates measured and deposited charges, being R the electron recombination factor in liquid Argon and τ stands for the mean life of the electrons [18].

$$Q_{meas} = R \cdot Q_{dep} \cdot e^{\frac{t-t_0}{\tau}} \tag{1}$$
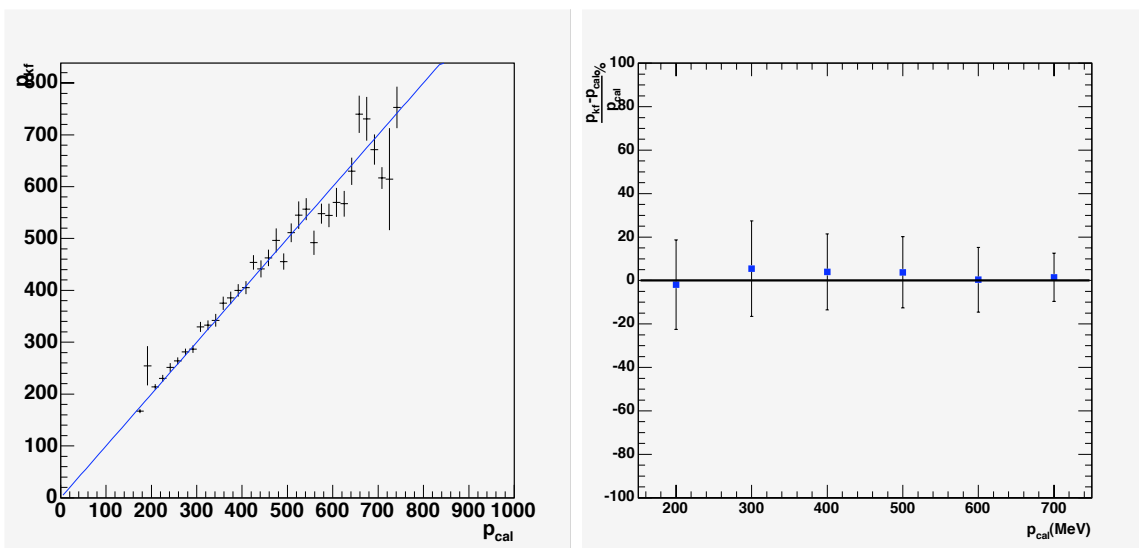
Figure 3: [Left] Profile plot of the correlation between the momentum measured by calorimetry p_{cal} and the one obtained by means of a Kalman Filter, p_{kf}. [Right] Dispersion of the Kalman Filter measurements with respect to the momentum measured by calorimetry, p_{cal}. The filled squares represent the mean value of the dispersion distribution. The error bars correspond to the RMS.

We have used for this study 1000 stopping muons. Given the characteristics of the selected muons, the range of considered momenta spans from about 200 MeV up to 800 MeV (being the mean value 400 MeV). For higher momenta, the sample of recorded muons is not statistically significant. The Monte-Carlo tells us that the Kalman Filter performance for the lower momentum range is not as good as the one expected for muons above 1 GeV. However a demonstration that the method performs reasonably well in the low momentum range, will give us confidence on the fact that the algorithm can be also applied at higher momenta.

In our approach we take the momentum measured by calorimetry, p_{cal}, as the *true* momentum value. On a track by track basis, we compare the momentum obtained with

101

the Kalman Filter, p_{kf}, to p_{cal}. To visualize the linear correlation among p_{kf} and p_{cal}, we plot the profile of the analyzed data in Figure 3 [Left]. It shows that, on average, our measurements tend to cluster around the solid line, which depicts the ideal condition where $p_{kf} = p_{cal}$. In the high momentum region, the decrease of statistics results in bigger fluctuations around the central line.

We also plot the dispersion of the Kalman Filter measurements with respect to p_{cal} in Figure 3 [Right]. For each of the six momentum bins into which we group the data, the mean dispersion is very close to zero. The error bars correspond to the RMS of each individual distribution. For the lowest momenta, the error is around 20%. As the momentum increases, the error bar diminishes reaching a minimum value of about 12%. These results are in very good agreement with the resolutions obtained, for the low momentum range, in our Monte-Carlo simulation.

In view of these results, we conclude that real data confirm the fact that the Kalman Filter algorithm, when combined with multiple Coulomb scattering information, is an optimal method to obtain an accurate measurement of partially contained track momenta. The Kalman Filter approach is an excellent tool to get precise kinematics information of the set of partially contained atmospheric neutrino events that we expect to record at the Gran Sasso underground laboratory.

4 Particle Id. with Neural Net and Random Forest techniques

One of the standard tasks that will have to be fulfilled in ICARUS is to determine the *identity* of the particles. In the works presented in [7] a set of criteria to distinguish muons, pions, kaons and protons with the highest efficiency and purity, based on a realistic simulation of the detector, have been defined.

In order to have an efficient identification, we have exploited the information provided by the particle *before* and *after* it loses all its energy and decays. It is the combination of the analyses in both regions which gives the final results:

- On one hand, the study of the hits recorded before (and close) to the mother particle decay vertex is essential. Because of the mass difference and for energies below the minimum ionizing value, each particle exhibits a distinct $< dE/dx >$ curve as a function of the kinetic energy which is, in most cases, sufficiently pronounced to separate them. The "$< dE/dx >$ vs. Energy" analysis can be combined with a "Energy vs. Range" analysis, trying to exploit the distinct penetration power of the particles.

- On the other hand, the study of the activity after the mother particle decay vertex can be very helpful to disentangle harder (kaons) from softer (pions and muons) decaying particles. In the case of protons, the absence of decaying particles gives an even more clear signature.

The analysis of the data is made of several steps:

1. Spatial track reconstruction (hit finding and views matching, delta ray tagging, decay vertex identification, etc.) and track segmentation;

---

[7]A. Bueno and S. Navas-Concha, "Particle identification in ICARUS", ICARUS-TM/2004-09. A. Bueno and S. Navas-Concha, "Random Forest and Neural Network Classification Algorithms Applied to Particle Identification", ICARUS-TM/2005-01.

2. χ^2 particle hypothesis test;

3. Particle mass calculation (from fit to particle hypothesis);

4. Decaying particles analysis.

We have tried and compared three different methods to separate particles: one based on *sequential cuts*, one on a Multi-layer perceptron *Neural Network* (NN) and the last based on a *Random Forest* classification.

The basic point that makes the NN interesting is their capability to adapt themselves

Neural Network result for Particle identification analysis
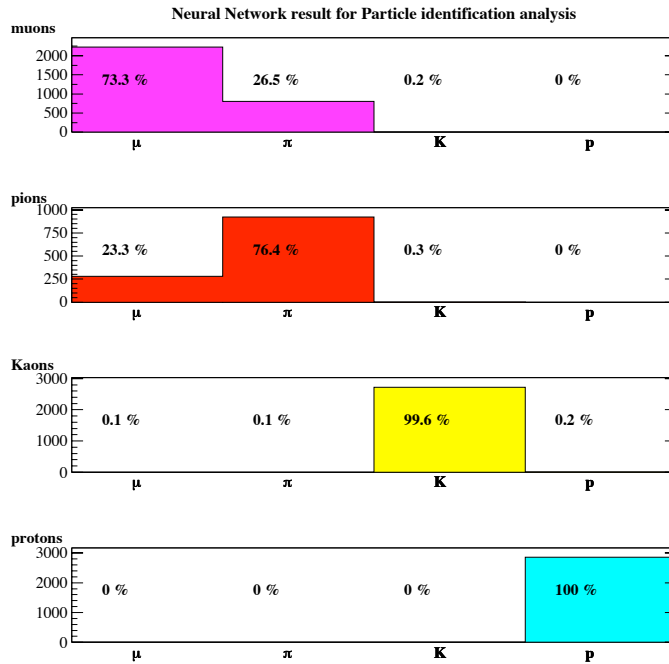
Figure 4: Multi-layer perceptron Neural Network analysis results on Particle Identification. The histograms (from top to bottom) show how each type of particle gets classified in different categories (bins from left to right).

to the data by means of non-linear functions. For more details see for instance [8]. We have built a simple Multi-layer perceptron (MLP) function with 1 input layer (10 nodes), 1 hidden layer (5 nodes) and 1 output layer (4 nodes), making a 10–5–4 architecture. To feed the MLP we have used the χ^2_{anal} and the fitted masses under each hypothesis plus the energy from the decaying particles computed from the 2D and 3D reconstructed tracks. The MLP is such that gives four outputs (neurons nn_i) accounting for each of the four particle types: the neuron i will be 1 for hypothesis i and 0 otherwise. For instance, when analyzing the muon sample, the first neuron would be *signal* ($nn_1 = 1$) and the rest *background* ($nn_i = 0$, $i = 2, 3, 4$). The events were divided into independent samples in order to properly *learn*, *test* and *validate* the net.

----

[8]S. Haykin, *"Neural Networks: A comprehensive foundation"*. Prentice Hall, 1999. C.M. Bishop, *"Neural Networks for Pattern Recognition"*. Oxford University Press, 1995.

On the other hand, a Random Forest is a classifier consisting in a collection of single classification trees [9]. Each tree gives a classification ("cast a vote"). The forest labels the event as a member of the class that have received the most votes. In our case events will be classified in four different classes: muons, pions, kaons and protons. It can be demonstrated that Random Forests do not over-fit. There is also no need for cross-validation or a separate test set to get an unbiased estimate of the test set error, since the fraction of the original training data, not used for building a particular tree, is used as the test set. In addition, Random Forests automatically provide a list of the variable importance. This allows to run again the classification algorithm using only the most important variables.

The best results are provided by the most complete Neural Net (`NN: 10-5-4`): purities above 99 % and muon-pion misidentification of the order of 25 % (see also Figure 4).

As an example, the final distributions in the Multi-layer perceptron discriminating variables for the (`NN:10-5-4`) case are shown in Figure 5. Plots are made in logarithmic scale in order to enhance the tails of the distributions. We remind here that for each single event the NN gives four numbers, the states of the four output layer neurons. The decision of which particle type we assign to a particular event is dictated by these values: a track will be of type j if nn_j is the maximum of all nn_i ($i = 1, ..., 4$). The results of
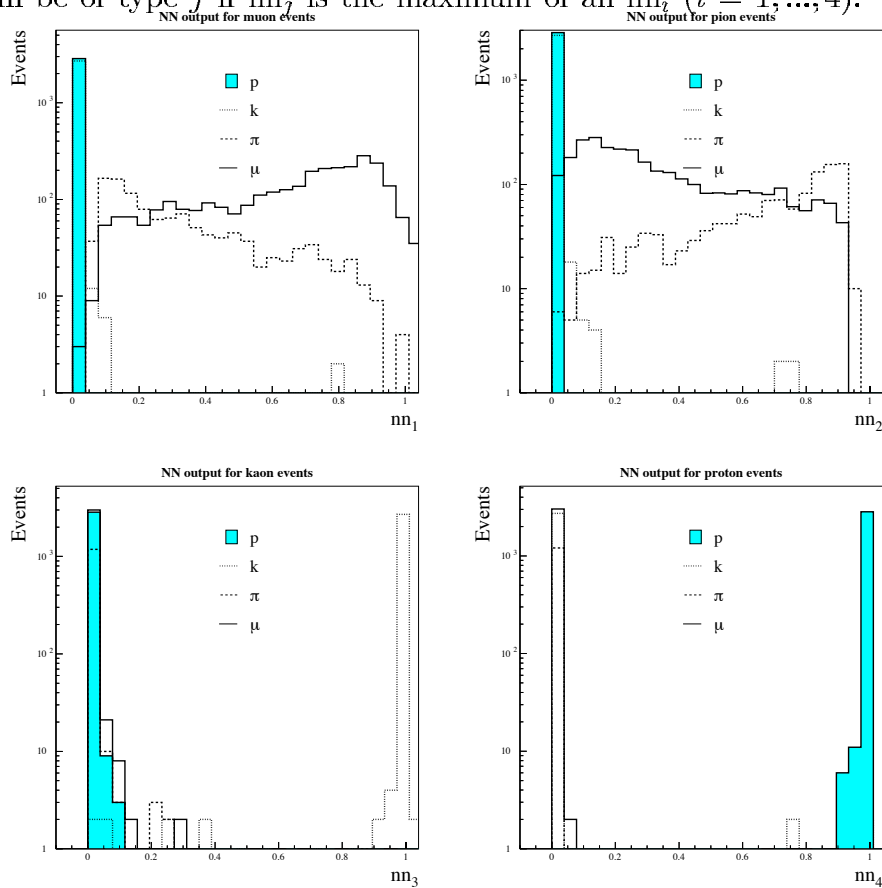
Figure 5: Multi-layer perceptron output for muons (nn_1), pions (nn_2), kaons (nn_3) and protons (nn_4). We see how, in all cases, *signal* events accumulate around 1 and *background* peaks at 0.

---

[9]L. Breiman, Machine Learning 45 (2001) 5.
http://stat-www.berkeley.edu/users/breiman/RandomForests/cc_home.htm.

the different parallel analyses carried out are computed in terms of *efficiency* and *contamination* of each type of particle. The NN based analysis exhibits a better performance compared to sequential cuts. It is able to distinguish muons (pions) from pions (muons) with 81% (91%) efficiency. On the other hand, the pion sample has a low contamination from kaons (0.6%) whereas the contamination on the kaon sample from pions is below 0.5% and negligible from muons. After visual scan of a fraction of the wrongly tagged events, we conclude that misclassification can be explained in terms of reconstruction problems, inefficiencies on the decay vertex tagging and events with overlapping particles. The protons are very well tagged and very few contaminate the kaon sample (0.25%).

When comparing the performances of two independent classification methods based on pattern recognition techniques (*Random Forest* and a Multi-layer perceptron *Neural Network*) we conclude that both exhibit similar capabilities for particle identification. The results obtained with both methods when using different groups of variables or all of them are compatible within statistical errors.

Considering muons and pions as the same sort of particle, we quote identification efficiencies above 99% for kaons, protons and muons-pions, whereas the contaminations between the three groups remains below 1%. On the other hand, concerning pions and muons, both the Random Forest and the NN analysis succeed to separate them with a ~75% probability. In other words, according to this result only one out of four muons or pions will be misidentified.

5 An improved study of TPC wire signal discrimination

An algorithm to treat ICARUS wire signals and improve the efficiency in the identification of physical ionization events was studied, in view of the development of a software filter able to select low energy events. This algorithm ("double rebinning") is based on the difference between the estimation of the signal over a short interval (of the order of the physical peak width) and over a longer one. The purpose of this treatment is to cut away both the baseline oscillations and the high frequency noise in the wire signals while preserving the peak height, thus improving the peak identification efficiency and reducing the probability of fake hits.

Both the average and the median estimators have been used and tested. The median is indeed less sensitive to the presence of the peak on the long rebinning interval, therefore giving a better estimation of the wire baseline and a higher efficiency on hit identification. The Figure 6 shows the effect of the treatment on a typical wire signal: the analysis has also been performed on the sum of 32 adjacent wires (AWS), which is expected to be implemented in a possible trigger system.

This algorithm has been tested on a sample of T600 stopping muon tracks recorded during the test run in Pavia. A full single hit detection efficiency for single wire was obtained with both versions of the algorithm even for low threshold (≈ 4 ADC counts). Considering the AWS case the use of the median leads to an improvement in the efficiency (93% with respect to 90% for a threshold of 35 ADC counts); however, the fake hit frequency is higher, i.e. 29% for AWS at a threshold of 35 ADC counts, with respect to 10% in the average case. The dependency of the algorithm performance on the track direction, and therefore on the height and width of the physical signal peak, has also been analyzed.
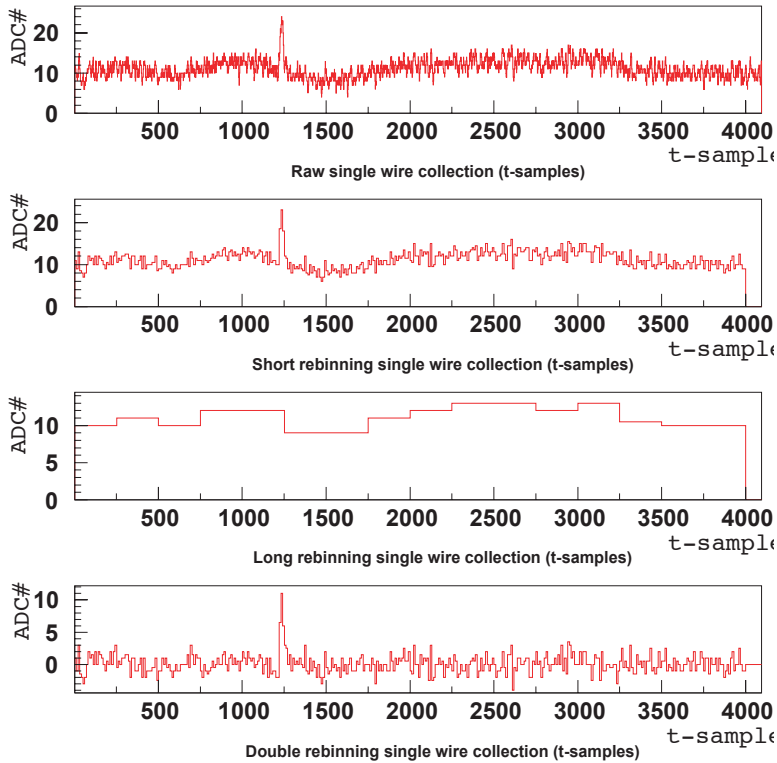
Figure 6: Effect of the median algorithm on a typical single wire signals (1 t-sample=400 ns).

6 Analysis of ν-events with the 50 l LAr prototype

In 1997 a liquid Ar TPC was operated for the first time in conjunction with a multi-GeV neutrino beam. The chamber had a volume of 50 liters and was placed between the NOMAD and CHORUS experiments at CERN. The TPC was irradiated with the high-energy broad-band CERN West Area Neutrino Beam. Due to reduced chamber size, NOMAD was used as a magnetic spectrometer during this test. The readout was performed by two orthogonal planes of wires. Each plane consisted of 128 wires, with a 2.54 mm wire pitch and a total drift distance of about 47 cm.

The accumulated data (81000 triggers) offer an unique possibility to evaluate the reconstruction and identification capabilities of liquid Ar TPCs operated at an accelerator neutrino beam. Given that this sort of detector is an excellent candidate for next-generation super-beam or neutrino-factory experiments, it was important to analyze these data using the reconstruction tools developed during these last years by the ICARUS[1, 24, 25] collaboration.

In particular low multiplicity events (quasi-elastic (QE) interactions) were studied in detail. About 10% of the 81000 triggers were identified as a neutrino charged current interaction with a primary vertex inside the 50 liter chamber. A sub-sample of golden quasi-elastic muon neutrino interactions was obtained by imposing very strict requirements: the event should have a fully contained proton with measured kinetic energy in excess of 50 MeV/c plus an exiting primary charged track matching the direction of a reconstructed muon in the NOMAD detector. After a careful visual scanning of the whole data sample, 71 events were identified as golden QE candidates. The QE event selection

106

efficiency has been evaluated with a Monte-Carlo simulation based on FLUKA[10]. According to the Monte-Carlo 73.5 events are expected, while 71 candidates were identified in real data.
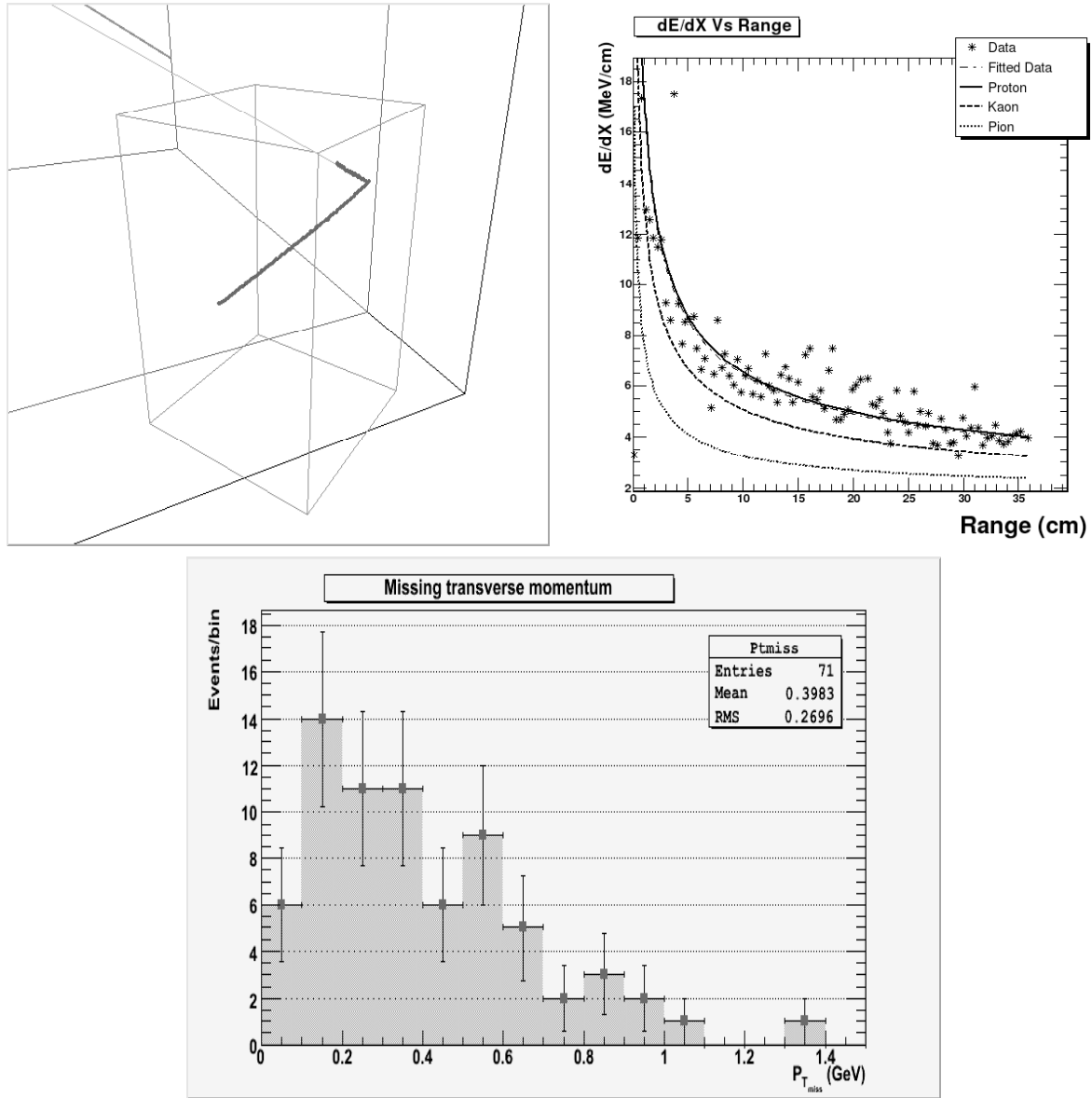
Figure 7: Top left: Three-dimensional reconstruction of a muon neutrino quasi-elastic interaction. Top right: Proton identification: dE/dX vs. range. Bottom: Missing transverse momentum distribution for a golden sample of real-data quasi-elastic interactions.

After the selection, the golden events were reconstructed using the techniques developed by the ICARUS collaboration for the analysis of the T600 data. We briefly describe the

[10] A. Ferrari, P.R. Sala, A. Fassò, J. Ranft, FLUKA: a multi-particle transport code (program version 2005) CERN-2005-010, INFN/TC_05/11 (2005). A. Ferrari, P.R. Sala, A. Fassò, J. Ranft, The physics models of FLUKA: status and recent developments. Proc. of CHEP2003, eConf C0303241 , arXiv:hep-ph/0306267 (2003).

different steps that allow to go from single hit identification to three dimensional track reconstruction.

The basic energy deposition unit is the hit, defined as the segment of track whose energy is read by a given wire of the read-out planes. Therefore, the spatial and calorimetric information of the track segment is contained in the associated hit, and the sensitivity of the detector entirely depends on the hit spatial and calorimetric resolutions. The hits are independently searched for in every wire (disregarding, at this stage, the information provided by adjacent wires). Hits are identified as signal regions of a certain width with signal values above the baseline. Each time a signal is found to be above the baseline by more than a given number of ADC counts, a hit candidate is flagged. All subsequent output samples above threshold are added to the hit and the information about its width, *i.e.* the distance (in drift samples) between the hit initial and final points, is stored. The parameters defining the hit (position, height, area) contain the relevant physical information of the original track segment. They are extracted through a fit to the identified hits by means of a function that reproduces the hit shape.

In a second step clusters are identified. A cluster is defined as a group of adjacent hits within the wire/drift coordinate plane. The goal of the cluster reconstruction program is to perform a first grouping of hits belonging to common charge deposition distributions, such as tracks or showers. Clusters are split into two-dimensional tracks and primary and secondary interactions vertexes are defined as the crossing points of 2D tracks.

Finally a three-dimensional (3D) reconstruction is performed. Each wire plane constrains two spatial degrees of freedom of the hits, one common to all wire planes (the drift coordinate) and one specific for each plane (the wire coordinate). The redundancy on the drift coordinate is the key for 3D reconstruction, since it allows the association of hits from the two wire planes to a common energy deposition. The devised 3D hit reconstruction algorithm performs efficiently on events of low track multiplicity as can be seen in the top left panel of Figure 7. This shows a real-data 3D reconstructed QE neutrino interaction inside the 50 liter fiducial volume (represented as a parallelepiped in the drawing). The longest track corresponds to a fully contained proton. The shortest one is the muon that is matched to a track reconstructed in NOMAD (thin line in the figure).

The superb 3D reconstruction capabilities shown by the liquid Ar TPC allows to extract very accurate Physics information from the recorded events. In particular, the particle identification capabilities are excellent. As an example the dE/dX versus range plot for the reconstructed proton of Figure 7 in shown in top right panel. A fit to the data (asterisks in the figure) is compatible with the proton hypothesis as given by the Bethe-Block formula, while the kaon and pion hypothesis are ruled out at a high confidence level.

The reconstructed missing transverse momentum (P_t) for the golden sub-sample of QE events has a mean value is 400 MeV/c (see the bottom of Figure 7). Taking into account that Fermi motion contribution to P_t is on average 250 MeV/c and that nuclear effects have a sizable contribution as well, it can be concluded that the liquid Ar TPC reconstructs with very high accuracy both transverse and longitudinal kinematic variables. This is a key issue when looking for neutrino oscillations.

This analysis has shown the excellent performance a liquid Ar TPC offers for the study of low multiplicity neutrino interactions. Nuclear effects and their influence on quasi-elastic events are presently being studied with the help of a FLUKA-based simulation.

7 Conclusions

We have presented a brief description of the ICARUS T600 detector, a large–mass Liquid Argon TPC meant as the basic unit for a multi-kton astroparticle observatory and neutrino detector to be installed in the underground Gran Sasso Laboratory.

An extended technical run with the T600 detector has been performed at surface in the Pavia INFN site during 2001. The design, the description of the basic components, assembly, start–up and test-run procedures of the detector have been recently published, as well as the demonstration of the off–line event reconstruction capabilities. The detector space and energy resolution, particle identification and full events reconstruction have been also the subjects of several analyses published during the last two years. Additional results from more recent studies are here briefly reported and will be soon matter of dedicated publications.

The main conclusion from the test is that the measurements and the experimental results demonstrate that it is feasible to master all technical issues related to the construction and operation of a large size LAr TPC, within and sometimes beyond the design specifications.

The T600 detector has been transported from Pavia to the INFN Gran Sasso Underground Laboratory in 2004. The installation of the ancillary infrastructures in the LNGS Hall B represented the main hardware activity in 2005 and is presently still under way. The re-assembly of the detector components will be the main goal of the activity during 2006.

References

[1] C. Rubbia, *The Liquid-Argon Time Projection Chamber: A New Concept For Neutrino Detector*, CERN–EP/77–08, (1977).

[2] P. Benetti *et al.* [ICARUS Collaboration], *A 3 Ton Liquid Argon Time Projection Chamber*, Nucl. Instrum. Meth. A **332**, (1993) 395.

[3] P. Cennini *et al.* [ICARUS Collaboration], *Performance Of A 3 Ton Liquid Argon Time Projection Chamber*, Nucl. Instrum. Meth. A **345**, (1994) 230.

[4] F. Arneodo *et al.* [ICARUS Collaboration], *The ICARUS 50 l LAr TPC in the CERN neutrino beam*, arXiv:hep-ex/9812006.

[5] F. Arneodo *et al.* [ICARUS Collaboration], *First Observation Of 140-Cm Drift Ionizing Tracks In The Icarus Liquid-Argon Tpc*, Nucl. Instrum. Meth. A **449**, (2000) 36.

[6] F. Arneodo *et al.* [ICARUS Collaboration], *Determination Of Through-Going Tracks' Direction By Means Of Delta-Rays In The Icarus Liquid Argon Time Projection Chamber*, Nucl. Instrum. Meth. A **449**, (2000) 42.

[7] P. Cennini *et al.* [ICARUS Collaboration], *Detection Of Scintillation Light In Coincidence With Ionizing Tracks In A Liquid Argon Time Projection Chamber*, Nucl. Instrum. Meth. A **432**, (1999) 240.

[8] F. Arneodo *et al.* [ICARUS Collaboration], *Performance Evaluation Of A Hit Finding Algorithm For The Icarus Detector*, Nucl. Instrum. Meth. A **412**, (1998) 440.

[9] P. Cennini *et al.* [ICARUS Collaboration], *A Neural Network Approach For The Tpc Signal Processing*, Nucl. Instrum. Meth. A **356**, (1995) 507.

[10] P. Cennini *et al.* [ICARUS Collaboration], *Improving The Performance Of The Liquid Argon Tpc By Doping With Tetramethyl Germanium*, Nucl. Instrum. Meth. A **355**, (1995) 660.

[11] P. Benetti *et al.* [ICARUS Collaboration], *A 3D Image Chamber For The Lar Tpc On Multilayer Printed Circuit Board*, Nucl. Instrum. Meth. A **346**, (1994) 550.

[12] P. Benetti *et al.* [ICARUS Collaboration], *Argon Purification In The Liquid Phase*, Nucl. Instrum. Meth. A **333**, (1993) 567.

[13] A. Bettini *et al.* [ICARUS Collaboration], *A Study Of The Factors Affecting The Electron Lifetime In Ultrapure Liquid Argon*, Nucl. Instrum. Meth. A **305**, (1991) 177.

[14] S. Bonetti *et al.* [ICARUS Collaboration], *A Study Of The Electron Image Due To Ionizing Events In A Two-Dimensional Liquid Argon Tpc With A 24-Cm Drift Gap*, Nucl. Instrum. Meth. A **286**, (1990) 135.

[15] F. Arneodo *et al.* [ICARUS Collaboration], *Performance Of The 10 m^3 Icarus Liquid Argon Prototype*, Nucl. Instrum. Meth. A **498**, (2003) 293.

[16] F. Arneodo *et al.* [ICARUS Collaboration], *Detection Of Cerenkov Light Emission In Liquid Argon*, Nucl. Instrum. Meth. A **516** (2004), 348.

[17] ICARUS Collaboration, *A First 600 Ton ICARUS Detector Installed At The Gran Sasso Laboratory*, Addendum to Proposal by the ICARUS Collaboration, LNGS–95/10, (1995).

[18] S. Amoruso *et al.* [ICARUS Collaboration], *Analysis Of The Liquid Argon Purity In The ICARUS T600 TPC*, Nucl. Inst. Meth., A **516**, (2004) 68.

[19] F. Arneodo *et al.* [ICARUS Collaboration], *Observation Of Long Ionizing Tracks With The ICARUS T600 First Half–Module*, Nucl. Inst. Meth., A **508**, (2003) 287.

[20] S. Amoruso *et al.* [ICARUS Collaboration], *Measurement Of The Muon Decay Spectrum With The ICARUS T600 Liquid Argon TPC*, Eur. Phys. J., C 33 (2004) 233.

[21] S. Amoruso *et al.* [ICARUS Collaboration], *Study Of The Electron Recombination In Liquid Argon With The ICARUS TPC*, Nucl. Inst. Meth., A 523 (2004) 275.

[22] S. Amerio *et al.* [ICARUS Collaboration], *"Design, construction and tests of the ICARUS T600 detector"*, Nucl. Inst. Meth., A 527 (2004) 329.

[23] A. Ankowski *et al.*, [ICARUS Collaboration], *Characterization of ETL 9357 FLA Photomultiplier Tubes for cryogenic temperature applications*, Nucl. Inst. and Meth. A 556 (2005) 146.

[24] F.Arneodo *et al.*, [ICARUS Collaboration], *The ICARUS Experiment: a Second Generation Proton Decay and Neutrino Observatory at The Gran Sasso Laboratory*, LNGS-P28, 2001, LNGS-EXP13/89 add. 1/01.

[25] P.Aprili *et al.*, [ICARUS Collaboration], *Cloning of the T600 modules to reach the design sensitive mass*, CERN/SPSC 2002-027 (SPS-P-323),updated from LNGS-EXP 13/89 add. 2/01.

LVD. Large Volume Detector

N.Y.Agafonova[9], M.Aglietta[14], E.D.Alyea[7], P.Antonioli[1], G.Badino[14], G.Bari[1],
M.Basile[1], V.S.Berezinsky[9], M.Bertaina[14], R.Bertoni[14], G.Bruni[1], G.Bruno[14], G.Cara
Romeo[1], C.Castagnoli[14], A.Chiavassa[14], J.A.Chinellato[3], L.Cifarelli[1], F.Cindolo[1],
A.Contin[1], V.L.Dadykin[9], E.A. Dobrynina[9], L.G.Dos Santos[3], R.I.Enikeev[9],
W.Fulgione[14], P.Galeotti[14], M.Garbini[1], P.L.Ghia[5,14], G.Giuliani[5,14], P.Giusti[1],
F.Gomez[14], F.Grianti[4], G.Iacobucci[1], E.Kemp[3], E.V.Korolkova[9], V.B.Korchaguin[9],
V.V.Kuznetsov[9], M.Luvisetto[1], A.A.Machado[15], A.S.Malguin[9], H.Menghetti[1],
N.Mengotti Silva[3], C.Morello[14], R.Nania[1], G.Navarra[14], K.Okei[10], L.Periale[14], A.Pesci[1],
P.Picchi[14], I.A.Pless[8], A.Porta[14], A.Romero[14], V.G.Ryasny[9], O.G.Ryazhskaya[9],
O.Saavedra[14], K.Saitoh[13], G.Sartorelli[1], M.Selvi[1], N.Taborgna[5], N.Takahashi[12],
V.P.Talochkin[9], G.C.Trinchero[14], S.Tsuji[11], A.Turtelli[3], P.Vallania[14], S.Vernetto[14],
C.Vigorito[14], L.Votano[4], T.Wada[10], R.Weinstein[6], M.Widgoff[2], V.F.Yakushev[9],
G.T.Zatsepin[9], A.Zichichi[1]

[1] *University of Bologna and INFN-Bologna, Italy*
[2] *Brown University, Providence, USA*
[3] *University of Campinas, Campinas, Brazil*
[4] *INFN-LNF, Frascati, Italy*
[5] *INFN-LNGS, Assergi, Italy*
[6] *University of Houston, Houston, USA*
[7] *Indiana University, Bloomington, USA*
[8] *Massachusetts Institute of Technology, Cambridge, USA*
[9] *Institute for Nuclear Research, Russian Academy of Sciences, Moscow, Russia*
[10] *Okayama University, Okayama, Japan*
[11] *Kawasaki Medical School, Kurashiki, Japan*
[12] *Hirosaki University, Hirosaki, Japan*
[13] *Ashikaga Institute of Technology, Ashikaga, Japan*
[14] *IFSI-INAF, Torino; University of Torino and INFN-Torino, Italy*
[15] *Centro Brasileiro de Pesquisas Fisicas, Rio de Janeiro, Brasil*

Abstract

The Large Volume Detector (LVD) in the INFN Gran Sasso National Laboratory, Italy, is a ν observatory mainly designed to study low energy neutrinos from the gravitational collapse of galactic objects.

The experiment has been monitoring the Galaxy since June 1992, under increasing larger configurations: in January 2001 it has reached its final active mass $M = 1$ kt. LVD is one of the largest liquid scintillator apparatus for the detection of stellar collapses and, besides SNO, SuperKamiokande and Amanda, it is a charter member of the SNEWS network, that has become fully operational since July 1st, 2005.

1 The LVD experiment

1.1 Scientific ground

The Large Volume Detector (LVD), located in the hall A of the INFN Gran Sasso National Laboratory, Italy, is a multipurpose detector consisting of a large volume of liquid scintillator interleaved with limited streamer tubes in a compact geometry (a front view is shown in fig.1). The major purpose of the LVD experiment is the search for neutrinos from Gravitational Stellar Collapses (GSC) in our Galaxy [1].

Indeed, in spite of the lack of a "standard" model of the gravitational collapse of a massive star, the correlated neutrino emission appears to be well established. At the end of its burning phase a massive star ($M > 8M_\odot$) explodes into a supernova, originating a neutron star which cools emitting its binding energy $E_B \sim 3 \cdot 10^{53}$ erg mostly in neutrinos. The largest part of this energy, almost equipartitioned among neutrino and antineutrino species, is emitted in the cooling phase: $E_{\bar{\nu}_e} \sim E_{\nu_e} \sim E_{\nu_x} \sim E_B/6$ (where ν_x denotes generically $\nu_\mu, \bar{\nu}_\mu, \nu_\tau, \bar{\nu}_\tau$ flavors). The energy spectra are approximatively a Fermi-Dirac distribution, with different mean temperatures, since ν_e, $\bar{\nu}_e$ and ν_x have different couplings with the stellar matter: $T_{\nu_e} < T_{\bar{\nu}_e} < T_{\nu_x}$.
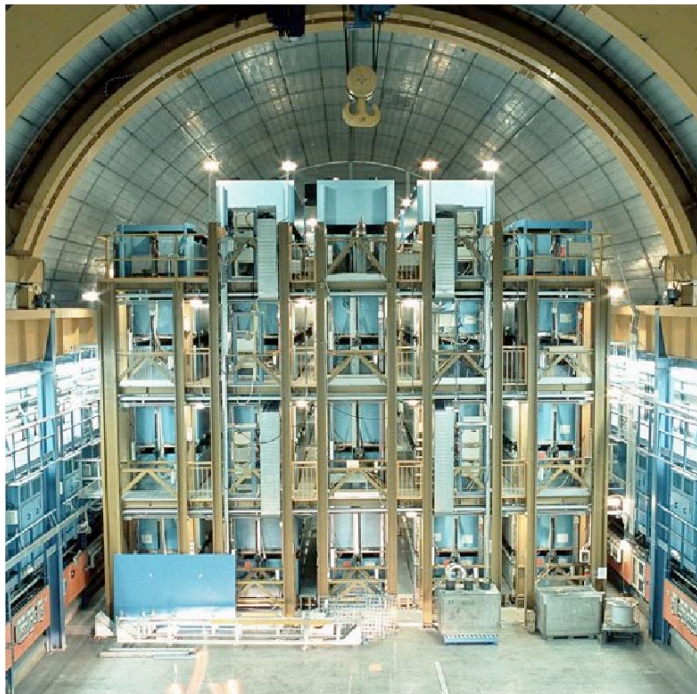
Figure 1: *Front view of the LVD detector in the hall A of the Gran Sasso National Laboratory, INFN.*

LVD is able to detect $\bar{\nu}_e$ interactions with protons in the scintillator, which give the main signal of supernova neutrinos, with a very good signature. Moreover, it can detect ν_e through the elastic scattering reactions with electrons, $(\nu_e + \bar{\nu}_e)$ through charged current

interactions with the carbon nuclei of the scintillator, and it is also sensitive to neutrinos of all flavors detectable through neutral currents reactions with the carbon nuclei. The iron support structure of the detector can also act as a target for electron neutrinos and antineutrinos. The products of the interaction can exit iron and be detected in the liquid scintillator. The amount of neutrino-iron interaction can be as high as about 20% of the total number of interactions. The signal observable in LVD, in different reactions and due to different kinds of neutrinos, besides providing astrophysical informations on the nature of the collapse, is sensitive to intrinsic ν properties, as oscillation of massive neutrinos and can give an important contribution to define some of the neutrino oscillation properties still missing.

1.2   The detector

The LVD experiment has been in operation since 1992, under different increasing configurations. During 2001 the final upgrade took place: LVD became fully operational, with an active scintillator mass $M = 1000$ t.

LVD consists of an array of 840 scintillator counters, 1.5 m^3 each, arranged in a compact and modular geometry; each of them is viewed on the top by three photomultipliers (visible in fig. 2). Up to 2004, before a re-calibration of the full detector, the counters were divided in two subsets: the external ones (43%), operated at energy threshold $\mathcal{E}_h \simeq 7$ MeV, and inner ones (57%), better shielded from rock radioactivity and operated at $\mathcal{E}_h \simeq 4$ MeV. After the re-calibration (which, started in 2004, ended during 2005) all the counters are operated at a common threshold, $\mathcal{E}_h \simeq 5$ MeV.
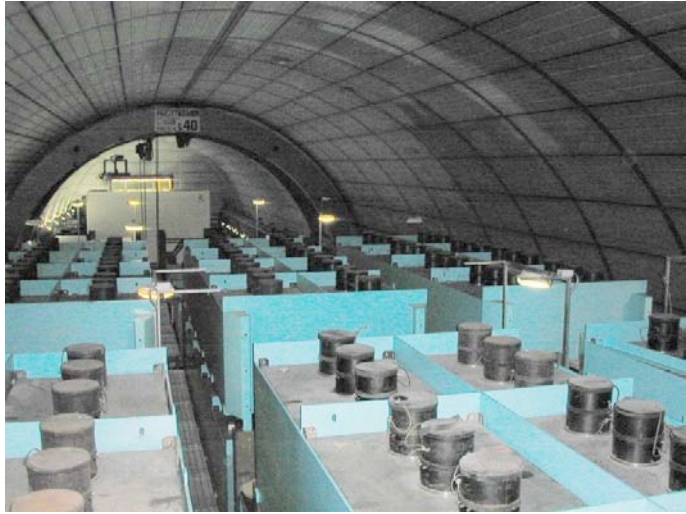
Figure 2: *Top view of the LVD detector in the hall A of the Gran Sasso National Laboratory, INFN.*

To tag the delayed γ pulse due to n-capture, all counters are equipped with an additional discrimination channel, set at a lower threshold, $\mathcal{E}_l \simeq 1$ MeV.

Other relevant features of the detector are: (i) good event localization and muon tagging; (ii) accurate absolute and relative timing: $\Delta t_{abs} = 1\,\mu s$, $\Delta t_{rel} = 12.5\,ns$; ($iii$) energy resolution: $\sigma_E/E = 0.07 + 0.23 \cdot (E/MeV)^{-0.5}$; ($iv$) very high duty cycle, i.e. $> 99.5\%$ in the last five years; (v) fast event recognition.

1.3   Supernova neutrino interactions in LVD

The observable neutrino reactions in the LVD scintillator are:

(1) $\bar{\nu}_e p, e^+ n$, (physical threshold $E_{\bar{\nu}_e} > 1.8\ MeV$) observed through a prompt signal from e^+ above threshold $\mathcal{E}_h$ (detectable energy $E_d \simeq E_{\bar{\nu}_e} - 1.8$ MeV $+2m_e c^2$), followed by the signal from the $np, d\gamma$ capture ($E_\gamma = 2.2$ MeV), above $\mathcal{E}_l$ and with a mean delay $\Delta t \simeq 180\ \mu s$.

(2) $\nu_e\ ^{12}C, ^{12}N\ e^-$, (physical threshold $E_{\nu_e} > 17.3\ MeV$) observed through two signals: the prompt one due to the e^- above $\mathcal{E}_h$ ($E_d \simeq E_{\nu_e} - 17.3$ MeV) followed by the signal, above $\mathcal{E}_h$, from the β^+ decay of ^{12}N (mean life $\tau = 15.9$ ms).

(3) $\bar{\nu}_e\ ^{12}C, ^{12}B\ e^+$, (physical threshold $E_{\bar{\nu}_e} > 14.4\ MeV$) observed through two signals: the prompt one due to the e^+ ($E_d \simeq E_{\bar{\nu}_e} - 14.4\,\text{MeV} + 2m_e c^2$) followed by the signal from the β^- decay of ^{12}B (mean life $\tau = 29.4$ ms). As for reaction *(2)*, the second signal is detected above the threshold $\mathcal{E}_h$.

(4) $\overset{(-)}{\nu_\ell}\ ^{12}C$, $\overset{(-)}{\nu_\ell}\ ^{12}C^*$ ($\ell = e, \mu, \tau$), (physical threshold $E_\nu > 15.1\ MeV$), whose signature is the monochromatic photon from carbon de-excitation ($E_\gamma = 15.1$ MeV), above $\mathcal{E}_h$.

Figure 3: *Cross section behavior for the different neutrino reactions observable in the LVD scintillator.*

(5) $\overset{(-)}{\nu_\ell}\ e^-$, $\overset{(-)}{\nu_\ell}\ e^-$, which yields a single signal, above $\mathcal{E}_h$, due to the recoil electron.

The LVD detector is supported by an iron structure made basically by two components: the tank (mean thickness: $0.4\ cm$), containing the scintillator, and the "portatank" (mean thickness: $1.5\ cm$) hosting a cluster of 8 tanks. The higher energy part of the ν flux can thus be detected also with the $\nu(\bar{\nu})$Fe interaction, resulting in an electron (positron) that may exit the iron and release energy in the scintillator. The reactions of interest are the following:

(6) $\nu_e\,^{56}Fe, ^{56}Co\ e^-$. The mass difference between the nuclei is $\Delta_{m_n} = m_n^{Co} - m_n^{Fe} = 4.055$ MeV, the first Co allowed state being at 3.589 MeV. Other higher energy allowed states are present in ^{56}Co: considering $E_{e^-}^{kin} = E_{\nu_e} - \Delta_{m_n} - E_{level} - m_e$ MeV, where E_{level} is the energy difference between the excitation level and the ground state level, this can take values: $3.589, 4.589, 7.589, 10.589\ MeV$. The efficiency for electron and gammas (also produced in the interaction) to reach the scintillator with energy higher than $\mathcal{E}_h$ is greater than 20% for $E_\nu > 30$ MeV and grows up to 70% for $E_\nu > 100$ MeV. On average, the detectable electron energy is $E_d \simeq 0.45 \times E_\nu$.

(7) $\bar{\nu}_e\,^{56}Fe, ^{56}Mn\ e^+$, the energy threshold and the efficiency are very similar to those of reaction *(6)*.

132

The number of all the possible targets present in the LVD detector is listed in table 1.

Table 1: Number of targets in the LVD detector.

Target Type	Contained in	Mass	Number of targets
Free protons	Liquid Scintillator	$1000\ t$	$9.34\ 10^{31}$
Electrons	LS	$1000\ t$	$3.47\ 10^{32}$
C Nuclei	LS	$1000\ t$	$4.23\ 10^{31}$
Fe Nuclei	Support Structure	$710\ t$	$7.63\ 10^{30}$

2 LVD and its experimental activity in 2005

2.1 Operation on the detector

2.1.1 Re-calibration and upgrade

Since April 2004 to July 2005, LVD has undergone an exceptional systematic program of maintenance, re-calibration and upgrade. Thanks to the high modularity of the detector (which consists of three large modules - named "towers"), this process has not influenced at all the duty cycle, and great attention has been given in limiting the reduction of the effective mass.

The re-calibration of the PMTs has been realized through the use of a ^{60}Co source moved from counter to counter: this operation was meant for changing the PMTs gains and equalizing them between internal and external counters; and also to recover the gain matching of the almost 2500 PMTs. On the other side, the upgrade concerned the electronics, tuned to get the threshold matching for all the counters, both internal and external ones. The result of the re-calibration and upgrade effort is a more uniform and sensitive detector as demonstrated by the analysis of the experimental energy thresholds, $\mathcal{E}_h{}^1$.

---

[1]The single counter spectrum, in the low-energy part, i.e. below 10 MeV, can be fitted by a function describing the natural radioactivity spectrum, folded with the detector response. The latter can be approximated by a gaussian integral function

$$\frac{1}{\sqrt{2\pi}} \int_{-\infty}^{x} exp(\frac{-y^2}{2}) dy$$

where

$$y = \frac{E - E_{th}}{\sigma_E}$$

being E_{th} the threshold and σ_E the energy resolution. With respect to the radioactivity spectrum shape, we adopt a power-law form, with exponent fixed to -4.5, which best describes the LVD counters spectra. E_{th} can thus be estimated, being a free parameter in the combined fit (power-law plus gaussian) to the spectrum of each counter.

We show in fig. 4 the distributions of the estimated new thresholds for internal (dashed histogram) and and external counters (dotted histograms): both have an average value around 5 MeV and almost the same distribution.

The re-calibration and upgrade has an outcome also on the response of the detector with respect to low energy thresholds, $\mathcal{E}_l$: indeed, we expect that counters similarly exposed to rock radioactivity have similar counting rates. This is visible in fig.5 where counting rates (Y-axis) are grouped by levels (from 1 - ground floor -, to 7) and by towers. Equal-exposed counters have similar rates independently of the tower: the lower counting rates in tower 2 are due to its better shielding, being located between tower 1 and 3.
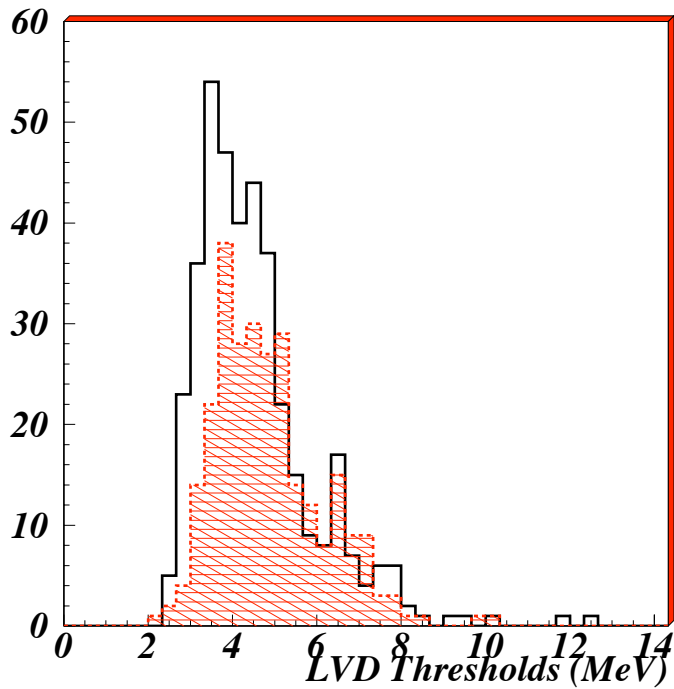
Figure 4: LVD thresholds: internal (full line) and external (dashed line) counters.

The highest counting rate of the top floor in tower 3 is well explained by its different upper shielding with respect to the other two towers.
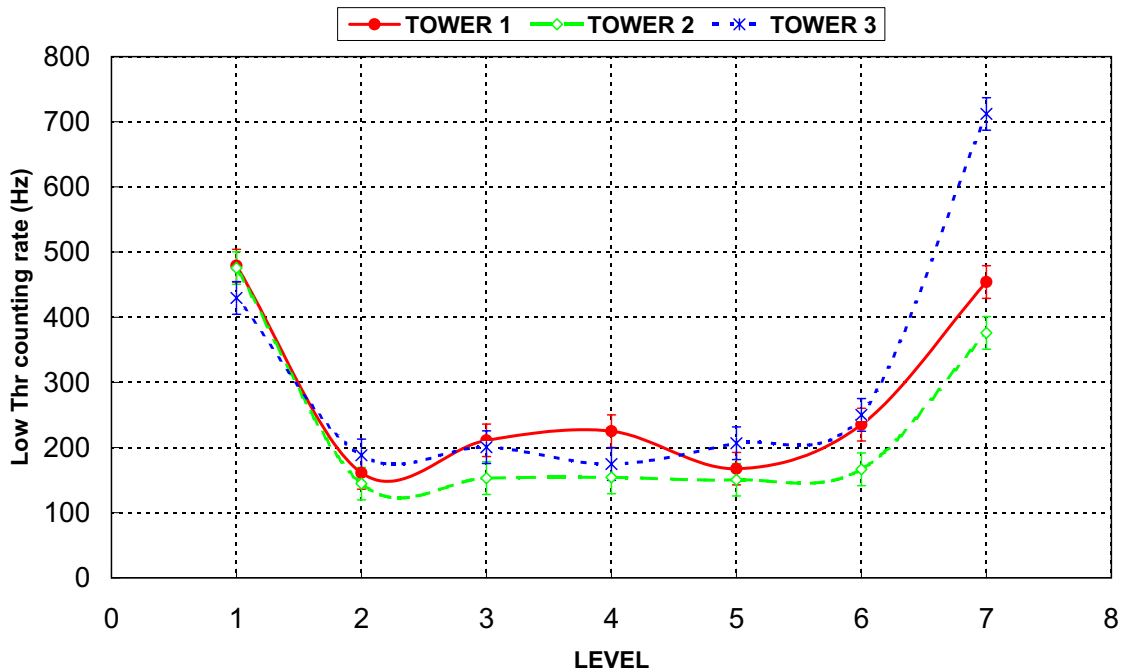
Figure 5: Low threshold counting rate behavior, grouped by levels and towers.

2.1.2 Test facility

The change of the PMTs gain, which is the result of the calibration and upgrade of LVD, allowed to accomplish a higher efficiency for the neutron capture detection (which is the signature for the main neutrino interaction in the scintillator). To make systematic measurements on this issue, we have set up a test facility in the mounting hall of the Gran Sasso National Laboratory. This facility includes several LVD counters, which are used for different kinds of test. One of them is dedicated to the measurement of the neutron detection from a neutron source (^{252}Cf): the efficiency is measured as a function of a tunable threshold in the counter electronics. The result of this study has been the subject of a PhD thesis [15] and is shown in fig.6. The use in parallel of a Montecarlo simulation allowed to interpret the experimental result, and to derive the efficiency for the detection of neutrons in the same counter where the originating inverse beta decay took place (see fig. 7).
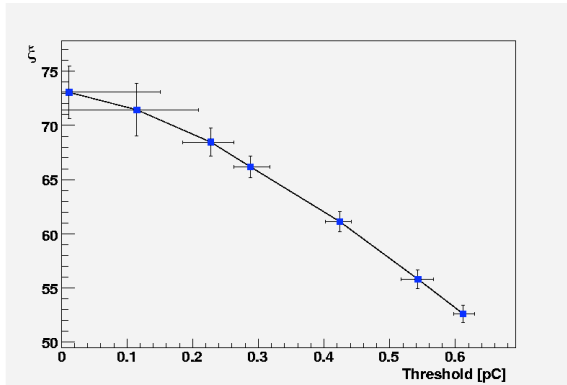
Figure 6:
Neutron detection efficiency (with experimental errors) as a function of the threshold in charge (pC).
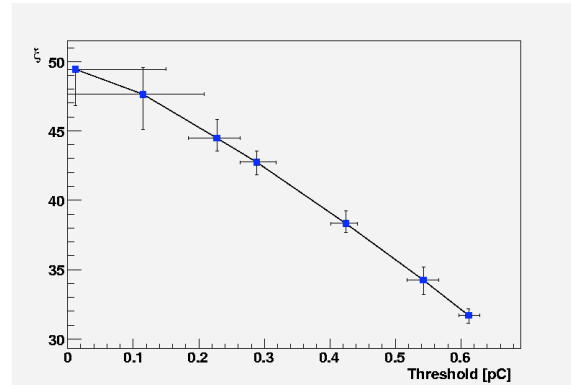
Figure 7:
Simulation results: detection efficiency of inverse beta decay induced neutrons as a function of the threshold in charge (pC).

Other two counters are dedicated to the study of Gadolinium-loaded scintillator, as part of a R&D program which is on-going in LVD.

2.2 Supernova physics

2.2.1 Monitoring the Galaxy

LVD has been continuously monitoring the Galaxy since 1992 in the search for neutrino bursts from GSC [2].

---

[2]The results of this search have been periodically updated and published[3, 4, 5, 6, 7, 8, 9]

Its active mass has been progressively increased from about 330 t in 1992 to 1000 t in 2001, always guaranteeing a sensitivity to gravitational stellar collapses up to distances $d = 20$ kpc from the Earth, even in the case of the lowest ν-sphere temperature.

The telescope duty cycle has been continuously improving since 1992. As it can be seen in Fig.8, in the last five years the average duty cycle was $> 99.5\%$.
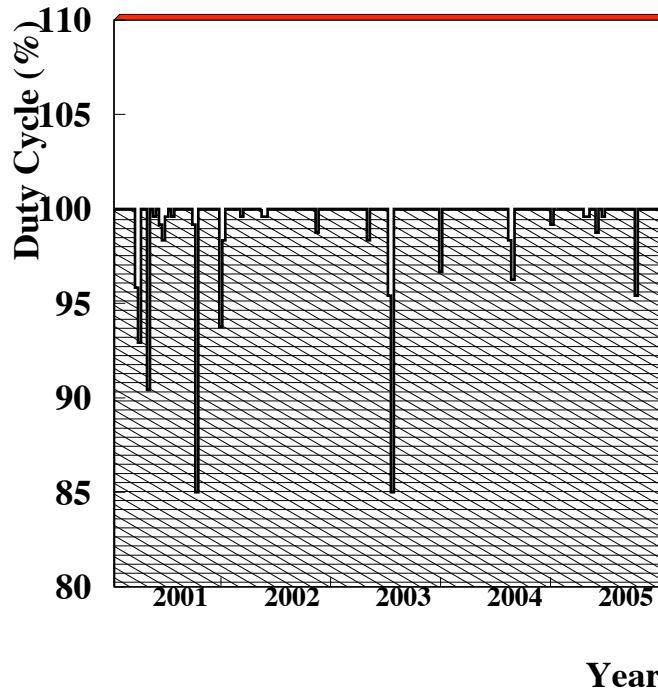
Figure 8: LVD duty cycle during year 2000-2005.

Since the LVD sensitivity is higher than expected from GSC models, even if the source is at a distance of 20 kpc and for soft neutrino energy spectra, we can conclude that no gravitational stellar collapse has occurred in the Galaxy in the whole period of observation: the resulting upper limit to the rate of GSC at 90% c.l. is 0.2 event/yr.

2.2.2 SNEWS

The SNEWS (SuperNova Early Warning System)[13, 14] project is an international collaboration including several experiments sensitive to a core-collpase supernova neutrino signal in the Galaxy and neighbour. The goal of SNEWS is to provide the astronomical community with a prompt and confident alert of the occurrence of a Galactic supernova event, generated by the coincidence of two or more active detectors. In addition the collaboration is engaged in cooperative work, such as the downtime coordination and inter-experiment timing verification, designed to optimize the global sensitivity to a supernova signal.

In July 2005, after a few years of tuning, the charter members of SNEWS (i.e., LVD, Super-K and SNO) together with the newly joined Amanda/IceCube, started the effective operation of the network.

There is currently a single coincidence server, hosted by Brookhaven National Laboratory. The BNL computer continuously runs a coincidence server process, which waits for alarm datagrams from the experiments' clients, and provides an alert if there is a coincidence within a specified time window (10 seconds for normal running). A scheme of "GOLD" and "SILVER" alerts has been implemented: GOLD alerts are automatically disseminated to the community; SILVER alerts are disseminated only after human checking.

Up to now, no inter-experiment coincidence, real or accidental, has ever occurred (except

during a special high rate test mode), nor any core collapse event been detected within the lifetimes of the currently active experiments.

2.2.3 Effects of neutrino oscillations

Neutrino conversion among flavors has been discovered and firmly established in the recent few years studying atmospheric, solar, reactor and accelerator neutrinos. The interpretation of all these phenomena in terms of neutrino oscillations is very robust, because it is able to include all the experimental data (except the "not yet confirmed" LSND signal). In the standard three flavor scenario, six parameters must be determined by oscillation experiments: 3 mixing angles (θ_{sol}, θ_{13}, θ_{atm}), 2 squared mass differences (Δm_{sol}^2 and Δm_{atm}^2) and 1 CP-violation phase δ. A recent analysis of all the available experimental data constrains the "atmospheric" and "solar" parameters to be in the following 99% $C.L.$ ranges:

Δm_{sol}^2 $(7.2 \div 8.9) \, 10^{-5} \, eV^2$
$|\Delta m_{atm}^2|$ $(1.7 \div 3.3) \, 10^{-3} \, eV^2$
θ_{sol} $30° < \theta_{sol} < 38°$
θ_{atm} $36° < \theta_{atm} < 54°$

However the other parameters are not completely determined: the θ_{13} mixing angle is only upper limited, mainly by the Chooz experiment data ($sin^2 \theta_{13} < 3. \, 10^{-2}$ at the 99% $C.L.$), the sign of Δm_{atm}^2 (that fixes the so–called mass hierarchy) is completely unknown, as well as the CP–violation phase δ.

Because of the wide range of matter density in the stellar envelope, a supernova explosion represents a unique scenario for further study of the neutrino oscillation mixing matrix. Indeed neutrinos can cross two resonance density layers and therefore the resulting possible mixing scenarios are different from the solar ones. The emerging neutrino spectra are sensitive to the sign of Δm_{atm}^2 and to the value of θ_{13}.

We will show how neutrino oscillations affect the signal detected by LVD and also evaluate the impact on the signal of the astrophysical parameters of the supernova explosion mechanism, such as the total energy emitted in neutrinos, the star distance, the neutrino–sphere temperatures and the partition of the energy among the neutrino flavors.

Preliminary results have been presented previously in [10] [11] [12].

For a normal mass hierarchy (NH) scheme, ν (not $\bar{\nu}$) cross two resonance layers: one at higher density (H), which corresponds to $\Delta m_{atm}^2, U_{e3}^2$, and the other at lower density (L), corresponding to $\Delta m_{sol}^2, U_{e2}^2$. For inverted mass hierarchy (IH), transitions at the higher density layer occur in the $\bar{\nu}$ sector. Given the energy range of SN ν (up to ~ 100 MeV) and considering a star density profile $\rho \propto 1/r^3$, the adiabaticity condition is always satisfied at the L resonance for any LMA solution, while at the H resonance, this depends on the value of U_{e3}^2. When $U_{e3}^2 \geq 5 \cdot 10^{-4}$ the conversion is completely adiabatic, meaning that the flip probability between two adjacent mass eigenstates is null ($P_h = 0$). In the adiabatic case and NH, the $\bar{\nu}_e$ produced in the SN core arrive at Earth as ν_1, and they have a high ($U_{e1}^2 \simeq cos^2 \theta_{12} \simeq 0.7$) probability to be detected as $\bar{\nu}_e$. On the other hand, the original $\bar{\nu}_x$ arrive at Earth as ν_2 and ν_3 and are detected as $\bar{\nu}_e$ with probability $U_{e2}^2 \simeq sin^2 \theta_{12}$.

The oscillations scheme can be summarized as:

$F_e = P_h U_{e2}^2 F_e^0 + (1 - P_h U_{e2}^2)F_x^0$ and

$F_{\bar{e}} = U_{e1}^2 F_{\bar{e}}^0 + U_{e2}^2 F_{\bar{x}}^0$ for normal hierarchy;

$F_e = U_{e2}^2 F_e^0 + U_{e1}^2 F_x^0$ and

$F_{\bar{e}} = P_h U_{e1}^2 F_{\bar{e}}^0 + (1 - P_h U_{e1}^2) F_{\bar{x}}^0$ for inverted hierarchy,

where F_{any}^0 are the original neutrino fluxes in the star and F_{any} are the observed ν fluxes. One can notice that, in the antineutrino channel, the non adiabatic ($P_h = 1$), IH case, is equivalent to the NH case (which does not depend on adiabaticity).

With respect to the astrophysical parameters, we assumed a galactic supernova explosion at a typical distance of $D = 10$ kpc, parametrized with a pure Fermi–Dirac energy spectrum ($\eta = 0$) with a total energy $E_b = 3 \cdot 10^{53}$ erg and perfect energy equipartition $f_{\nu_e} = f_{\bar{\nu}_e} = f_{\nu_x} = 1/6$; we fixed $T_{\nu_x}/T_{\bar{\nu}_e} = 1.5$, $T_{\nu_e}/T_{\bar{\nu}_e} = 0.8$ and $T_{\bar{\nu}_e} = 5$ MeV.

For the chosen supernova parameters, it results that the expected number of events and their energy spectrum depend on the unknown oscillation parameters: the mass hierarchy and the value of θ_{13}.

In particular, the inverse beta decay interactions ($\bar{\nu}_e p, e^+ n$) are highly sensitive to the mass hierarchy: for adiabatic transition, the number of events increases of $\sim 25\%$ in the IH case, with respect to the NH one, since the detected $\bar{\nu}_e$ completely come from the higher energy ν_x. The mean energy of the detected positrons is correspondingly increased. The total number of ($\nu_e + \bar{\nu}_e$) CC interaction with ^{12}C nuclei is highly increased taking into account neutrino oscillations, because of their high energy threshold. For adiabatic transition the expected number of events is higher than the non adiabatic one, because at least one specie (between ν_e or $\bar{\nu}_e$) comes significantly from the original and higher–energy ν_x in the star. However, if it is not possible to discriminate between ν_e and $\bar{\nu}_e$, the normal and inverted hierarchy cases present similar results. Indeed, in the NH (IH) case, the increase in ν_e ($\bar{\nu}_e$) is compensated by a decrease in $\bar{\nu}_e$ (ν_e).

The neutrino interactions with the iron of the support structure, which are studied in details in this work, are also incread by the oscillations. The efficiency for the detection of the produced charged leptons and gammas in the active part of the detector has been calculated with a full simulation of the apparatus. The contribution of ($\nu_e + \bar{\nu}_e$) Fe interactions can be as high as 15% of the total number of events (in the adiabatic NH case) and they contribute mostly to the high energy part of the spectrum.

With respect to the previous detection channels, the number of NC interactions with ^{12}C nuclei does not depend on oscillations. In principle they could be used as a reference to identify the ν_x–sphere temperature. However, this is partly limited by the unknowledge of the other astrophysical parameters.

In conclusion, for our choice of the astrophysical parameters, the expected signal of neutrinos in the LVD detector from a supernova core collapse greatly benefits of the neutrino oscillation mechanism, practically in all the possible detection channels, especially if the transition is adiabatic and the hierarchy inverted (since in LVD the most relevand signal is given by $\bar{\nu}_e$).

However, being aware of the fact that the astrophysical parameters of the supernova mechanism are up to now not well defined, we performed the same calculations using different values of them. The resulting differences are in fact important; they are mainly due to the poor theoretical knowledge of the physics of the gravitational collapse. This will be hopefully improved after the occurence and detection of the next galactic supernova, to which the LVD experiment can give a significant contribution.

2.3 Periodicities in the low energy threshold counting rate and Radon monitor

The LVD background, at the low energy threshold level, is mainly due to: nuclear decays of ^{238}U, ^{232}Th and ^{40}K present in the rock, to Radon present in the experimental hall and to secondary neutral particles generated in the interaction of high energy cosmic muons with the rock surrounding the detector or with the detector material itself.

In the LVD data-stream, the low energy threshold counting rate of each counter is recorded every 10 minutes, for 10 seconds: these data represent a powerful tool for monitoring the background in an energy range which is fundamental for the LVD physics aim.

The time variations of the low energy background has been studied, applying a spectral analysis to the counting rate. This shows a variation of the rate, possibly attributed to the variation of the concentration of the radioactivity due to the human activity in the hall A. To check this hypothesis, the LVD collaboration started a cooperation with the low radioactivity monitoring group of the Gran Sasso Laboratory, to compare the LVD data with those collected by a radon-meter (located between two towers of LVD), consisting in an ionization chamber measuring α particles with an air flow of $1\ l \cdot min^{-1}$.
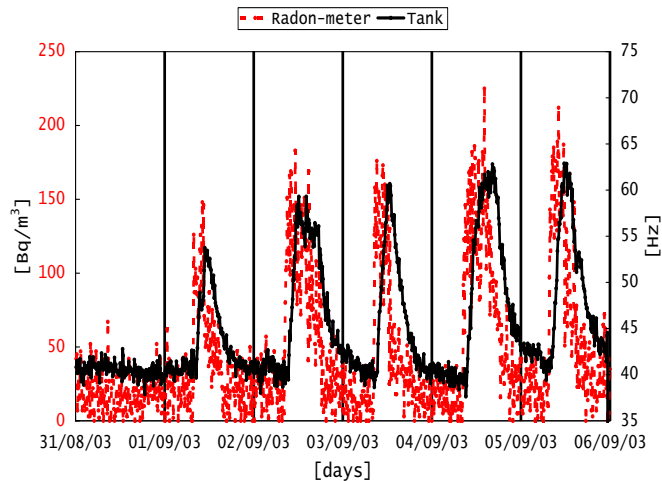
Figure 9: *Comparison between LVD low energy threshold counting rate (full black line, s^{-1}) and the radon-meter data (dashed red line, $Bq \cdot m^{-3}$)*

As shown in Figure 9, there is a strong correlation between the radon-meter data and the LVD ones; thus the observed modulations can be explained in terms of variations in the Radon concentration due to Radon injection into the hall atmosphere. The delay between the LVD data and the radon-meter data can be explained by considering that the radon-meter is sensitive to the α particle from the Rn and Po decays while the LVD counters are sensitive to betas and gammas from Pb and Bi decays. By this analysis we evaluated the LVD low threshold counting rate sensitivity in terms of Radon activity: the variation of $1\ counts \cdot s^{-1}$ in the LVD low threshold counting rate corresponds to an average variation in the Radon concentration of about $7\ Bq \cdot m^{-3}$.

3 List of publications in 2005

- *CNGS beam monitor with the LVD detector.*
  Nucl. Phys. B Proc. Suppl., **138** (2005) 424-426

- *Study of the effect of neutrino oscillation on the supernova neutrino signal with the LVD detector*

Nucl. Phys. Proc. Suppl., **138** (2005) 115-118

- *Study of muon-induced neutron background with the LVD detector at LNGS*
  Nucl. Phys. B Proc. Suppl. **143** (2005) 518

- *1992-2004: search for neutrino bursts from collapsing objects with LVD*
  Nucl. Phys. B Proc. Suppl. **143** (2005) 540

- *Study of muon-induced neutron background with the LVD detector at LNGS*
  IDM2004 conference proceeding (World Scientific Ltd.)

- *Update to 2005 of the results of the search for bursts from gravitational stellar collapses with LVD*
  Proc. 29th ICRC, Pune, India, ita-vigorito-C-abs1-og25-oral

- *Triggering on neutrino bursts in LVD*
  Proc. 29th ICRC, Pune, India, ita-fulgione-W-abs1-og27-oral

- *The muon decay and muon capture detection with LVD*
  Proc. 29th ICRC, Pune, India, rus-ryazhskaya-O-abs2-he11-poster

- *The measurement of the total specific muon-generated neutron yield using LVD*
  Proc. 29th ICRC, Pune, India, rus-ryazhskaya-O-abs1-he23-oral

- *Study of the muon-induced neutron production, propagation and energy spectrum with the LVD detector at LNGS*
  Proc. 29th ICRC, Pune, India, ita-garbini-M-abs1-he21-oral

References

[1] LVD Collaboration, Il Nuovo Cimento **A105** (1992) 1793

[2] A. Strumia, F. Vissani, `astro-ph/0302055.`

[3] LVD Collaboration, 23th ICRC Conf.Proc.,HE 5.1.1,Vol.4,468,1993

[4] LVD Collaboration, 24th ICRC Conf.Proc., HE 5.3.6,Vol.1,1035,1995

[5] LVD Collaboration, 25th ICRC Conf.Proc., HE 4.1.12,1997

[6] LVD Collaboration, 26th ICRC Conf.Proc., HE 4.2.08,Vol.2,223,1999

[7] LVD Collaboration, 27th ICRC Conf.Proc., HE230,1093,2001

[8] LVD Collaboration, 28th ICRC Conf.Proc., HE2.3,1333,2003

[9] LVD Collaboration, 29th ICRC Conf. Proc., OG2.5, 2005

[10] LVD Collaboration, Nucl. Phys. B Proc. Sup. 110 (2002) pp 410-413, astro-ph/0112312

[11] A. Zichichi, *The most powerful scintillator supernova neutrino detector*, talk presented at the symposium *LVD: the First Ten Years*, LNGS, 28-29 October, 2002).

[12] LVD Collaboration, 28th ICRC Conf.Proc., HE2.3,1297,2003

[13] http://hep.bu.edu/~snnet/

[14] P. Antonioli et al., New J. Phys., 6 (2004) 114

[15] A. Porta, "Energy measurement in LVD to reconstruct Supernova neutrino emission", PhD Thesis, University of Torino, Italy (2005)

LUNA. Laboratory for Underground Nuclear Astrophysics

D.Bemmerer[1], R.Bonetti[2], C.Broggini[1]*, F.Confortola[3], P.Corvisiero[3], H.Costantini[3], J.Cruz[4], A.Formicola[5], Z.Fülöp[6], G.Gervino[7], A.Guglielmetti[2], C.Gustavino[5], G.Gyürky[6], G.Imbriani[8], A.P.Jesus[4], M.Junker[5], A.Lemut[3], M.Marta[2], R.Menegazzo[1], A.Ordine[8], P.Prati[3], V.Roca[8], D.Rogalla[9], C.Rolfs[10], M.Romano[8], C.Rossi Alvarez[1], F.Schümann[10], E.Somorjai[6], O.Straniero[11], F.Strieder[10], F.Terrasi[9], H.P.Trautvetter[10]

[1] INFN, Padova, Italy
[2] Università di Milano, Dipartimento di Fisica and INFN, Milano, Italy
[3] Università di Genova, Dipartimento di Fisica and INFN, Genova, Italy
[4] Centro de Fisica Nuclear, Universidade de Lisboa, Portugal
[5] Laboratori Nazionali del Gran Sasso, Assergi, Italy
[6] ATOMKI, Debrecen, Hungary
[7] Politecnico di Torino, Dipartimento di Fisica and INFN, Torino, Italy
[8] Università di Napoli, Dipartimento di Fisica and INFN, Napoli, Italy
[9] Dipartimento di Scienze Ambientali, Seconda Università di Napoli, Caserta, Italy
[10] Institut für Experimentalphysik III, Ruhr-Universität Bochum, Germany
[11] Osservatorio Astronomico di Collurania, Teramo, and INFN, Napoli, Italy

Abstract

LUNA is measuring fusion cross sections down to the energy of the stellar nucleosynthesis. This year we completed the study of ^{14}N(p,γ)^{15}O, the key reaction of the CNO cycle, we started the measurement of ^{3}He(α, γ)^{7}Be and the preparation of the ^{25}Mg(p,γ)^{26}Al experiment.

---

*Spokesperson

Introduction

Nuclear reactions that generate energy and synthesize elements take place inside the stars in a relatively narrow energy window: the Gamow peak. In this region, far below the Coulomb energy, usually below 100 keV, the reaction cross-section $\sigma(E)$ drops almost exponentially with decreasing energy E:

$$\sigma(E) = \frac{S(E)}{E} \, exp(-2\,\pi\,\eta), \tag{1}$$

where $S(E)$ is the astrophysical factor and η is the Sommerfeld parameter, given by $2\,\pi\,\eta = 31.29\, Z_1\, Z_2 (\mu/E)^{1/2}$. Z_1 and Z_2 are the nuclear charges of the interacting particles in the entrance channel, μ is the reduced mass (in units of amu), and E is the center of mass energy (in units of keV).

The extremely low value of the cross-section inside the Gamow peak, from pico to femto-barn and even below, has always prevented its measurement in a laboratory at the Earth's surface, where the signal to background ratio would be too small because of cosmic ray interactions. In order to explore this new domain of nuclear astrophysics we have installed two electrostatic accelerators underground at LNGS: a 50 kV accelerator and a 400 kV one. The qualifying features of both the accelerators are a very small beam energy spread and a very high beam current even at low energy.

Outstanding results obtained up to now are the only existing cross-section measurements within the Gamow peak of the sun: $^3\mathrm{He}(^3\mathrm{He},2\mathrm{p})^4\mathrm{He}$[1] and $\mathrm{D}(\mathrm{p},\gamma)^3\mathrm{He}$ [2]. The former plays a big role in the proton-proton chain, largely affecting the calculated solar neutrino luminosity, whereas the latter is the reaction that rules the proto-star life during the pre-main sequence phase. With these measurements LUNA has shown that, by going underground and by using the typical techniques of low background physics, it is possible to measure nuclear cross sections down to the energy of the nucleosynthesis inside stars.

In the following we report on the activity during the year 2005, when we completed the study of $^{14}\mathrm{N}(\mathrm{p},\gamma)^{15}\mathrm{O}$, we started the measurement of $^3\mathrm{He}(^4\mathrm{He},\gamma)^7\mathrm{Be}$ and the preparation of the $^{25}\mathrm{Mg}(\mathrm{p},\gamma)^{26}\mathrm{Al}$ experiment.

1   The ^{14}N(p,γ)^{15}O reaction

$^{14}\mathrm{N}(\mathrm{p},\gamma)^{15}\mathrm{O}$ (Q=7.297 MeV) is the slowest reaction of the CNO cycle, the one which determines the rate of the cycle. The final analysis of the LUNA solid target data [3][4] includes all the transitions which contribute to the $^{14}\mathrm{N}(\mathrm{p},\gamma)^{15}\mathrm{O}$ cross section at low energy: ground state, 6.17 and 6.79 MeV, measured down to 119 keV, 5.18 and 5.24 MeV down to 157 keV. In addition, the astrophysical factor of the radiative capture into the 6.79 MeV state has been remeasured at 'high' energy (from 0.6 to 1.3 MeV proton energy) with the Bochum tandem accelerator. The resulting R-matrix fit, extrapolated to zero energy, gives a total astrophysical factor $S_{tot}(0) = 1.61 \pm 0.08$ keV·b, smaller than the value given in most recent compilations: $3.5^{+0.4}_{-1.6}\, keV \cdot b$ [5] and $3.2\pm0.8\, keV \cdot b$ [6].

In order to measure the $^{14}\mathrm{N}(\mathrm{p},\gamma)^{15}\mathrm{O}$ total cross section at very low energies, it is essential to have both γ ray detectors with very high efficiency to compensate for the rapidly decreasing cross section as well as a very pure and thin $^{14}\mathrm{N}$ target, to suppress
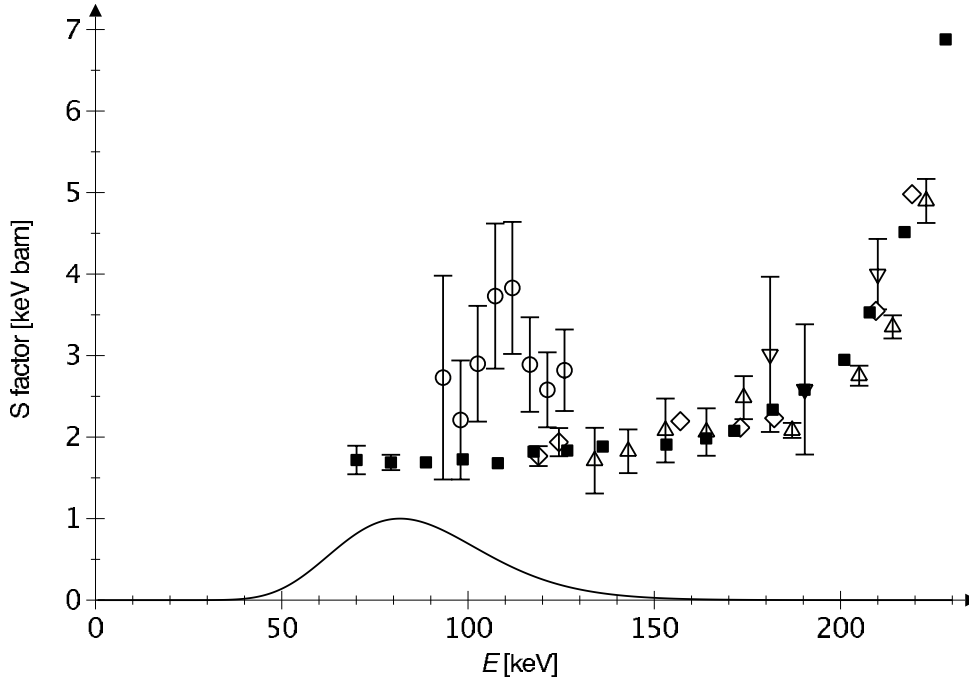
Figure 1: Astrophysical S-factor for the $^{14}N(p,\gamma)^{15}O$ reaction from the present work (filled squares) and from previous studies: circles [8], inverted triangles [9], diamonds [3, 4], triangles [10]. Error bars ($\pm 1\sigma$ statistical uncertainty) are only shown where they are larger than the symbols used. The Gamow peak for $T_6 = 80$ is also shown.

the ion beam induced background and to minimize the straggling on the energy loss. In addition, the target must be stable for the long time required by the low energy measurements. All this has been achieved in the second phase of the LUNA study with a large 4π BGO summing detector (about 70% efficiency and 8% resolution in the energy region between 6 and 8 MeV) and with a windowless gas target.

Figure 1 shows our results [7], corrected for the electron screening effect (10% and 3% effect at 70 and 150 keV, respectively). Typical errors are 3% (stat) and and 4.5% (syst). Only at the lowest energy, 70 keV, corresponding to a cross section of 0.24 pb, they increase to 10% (stat) and 7% (syst), with the latter one mainly due to beam energy calibration and detection efficiency.

The LUNA results account for more tha 90% (50%) of the area under the Gamow peak for T_6 >90 (60), where T_6 is the stellar temperature in 10^6 K units (the energy region covered by previous experiments corresponds to T_6 >170). This way, the $^{14}N(p,\gamma)^{15}O$ has been measured at energies where CNO burning takes place in important astrophysical scenarios as AGB stars (asymptotic giant branch, i.e. stars which burn hydrogen and helium, respectively, in two shells surrounding a degenerate carbon-oxigen core).

The astrophysical consequences of our results are significant: the CNO neutrino yield in the Sun is decreased by about a factor two [12][13][14], with respect to the current estimates, the age of the oldest Globular Clusters is increased by 0.7-1 Gyr [11][12] and the dredge-up of carbon to the surface of AGB stars is much more efficient [15].

115

2 The ^{3}He(^{4}He,γ)^{7}Be measurement

The ^{3}He(^{4}He,γ)^{7}Be reaction is a key parameter for the production of ^{7}Be and ^{8}B neutrinos in the Sun. The joint effort of all experiments on solar neutrinos and solar physics has finally cast light on the long-standing solar neutrino puzzle but detailed nuclear physics properties are required to study the solar interior from neutrino observations. The error on $S_{3,4}$ represents, at the moment, the main nuclear limitation to the extraction of physics from the ^{8}B neutrino flux measurements [16, 13]. The ^{3}He(^{4}He,γ)^{7}Be reaction is responsible for the production of ^{7}Li in a high baryon density universe. Its uncertainty dominates the prediction of the primordial ^{7}Li abundance [17].
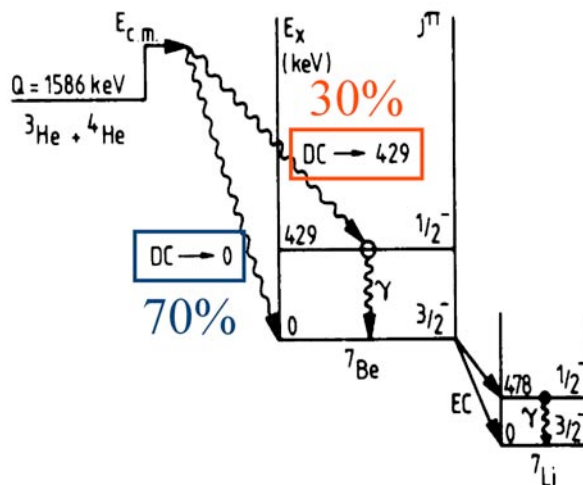
Figure 2: Level scheme of ^{7}Be near the ^{3}He+^{4}He threshold. The ^{3}He(^{4}He,γ)^{7}Be capture reaction, Q-value = 1.586 MeV, is expected to proceed predominantly via the direct capture (DC) mechanism into the ground state and the 429 keV excited state. The EC decay of the ^{7}Be ground state will populate the level at 478 keV in ^{7}Li with a branching ratio of 10.44 $\pm$ 0.04 %.

The capture reaction is dominated, at low energies (see Fig. 2), by the non-resonant direct capture mechanism to the ground state and the 429 keV first excited state of ^{7}Be. One expects to observe two primary γ-ray transitions, DC$\rightarrow$0 and DC$\rightarrow$429 keV with the latter followed by a 429 keV secondary transition. An independent determination of the number of ^{7}Be nuclei produced in the reaction requires the detection of the 478 keV γ-ray activity of the first excited state in the daughter nucleus ^{7}Li populated in the EC decay of the ^{7}Be ground state. Both methods have been used in the past to determine the absolute cross section σ(E) in the energy range $E_{c.m.} \geq 107$ keV (see [18], [19] and References therein) but the dispersion of the evaluated $S_{3,4}$ astrophysical factors produce a significant uncertainty on the adopted $S_{3,4}$ value. Moreover, the $S_{3,4}$ extracted from the measurements of the induced ^{7}Be activity are systematically higher [20] than the values obtained from the measurements of the prompt capture γ-rays transitions.

We decided to reinvestigate the ^{3}He(^{4}He,γ)^{7}Be reaction with high accuracy (relative error $\leq 5\%$) and measure at energies never reached before ($E_{c.m.} \simeq 70$ keV in-beam and 100 keV off-line counting) and crucial to extrapolate the S(E) factor at zero energy. The measurements include the detection of the prompt capture γ-ray transitions as well as the 478 keV γ-ray produced in the EC decay of the ^{7}Be residual in a common setup.

2.1 Experimental setup

The experiment is performed with the ^{4}He beam from the LUNA2 400 kV accelerator [21] at the LNGS underground laboratory in conjunction with a ^{3}He windowless gas target (a schematic diagram of the setup is shown in Fig. 3). Typical gas pressure inside the target chamber is around 1 mbar.

The beam enters the target chamber through a 7 mm diameter Copper collimator (A_1 in Fig. 3) and is stopped on a power calorimeter placed at 35 cm downstream. The combination of this collimator with other two apertures (A_3 and A_2 of 15 and 8 mm diameter), placed between different pumping stages, defines the beam direction. During the experiment the ^{3}He gas in the target is continuously recirculated: the gas is recovered from the first two pumping stages, cleaned through a heated getter gas purifier (Monotorr from SAES GETTER) and fed back into the target chamber. The target pressure is monitored by a Baratron capacitance manometer (MKS model 127) in two different positions inside the gas target with an uncertainty of 0.25 %. Local target densities without the beam
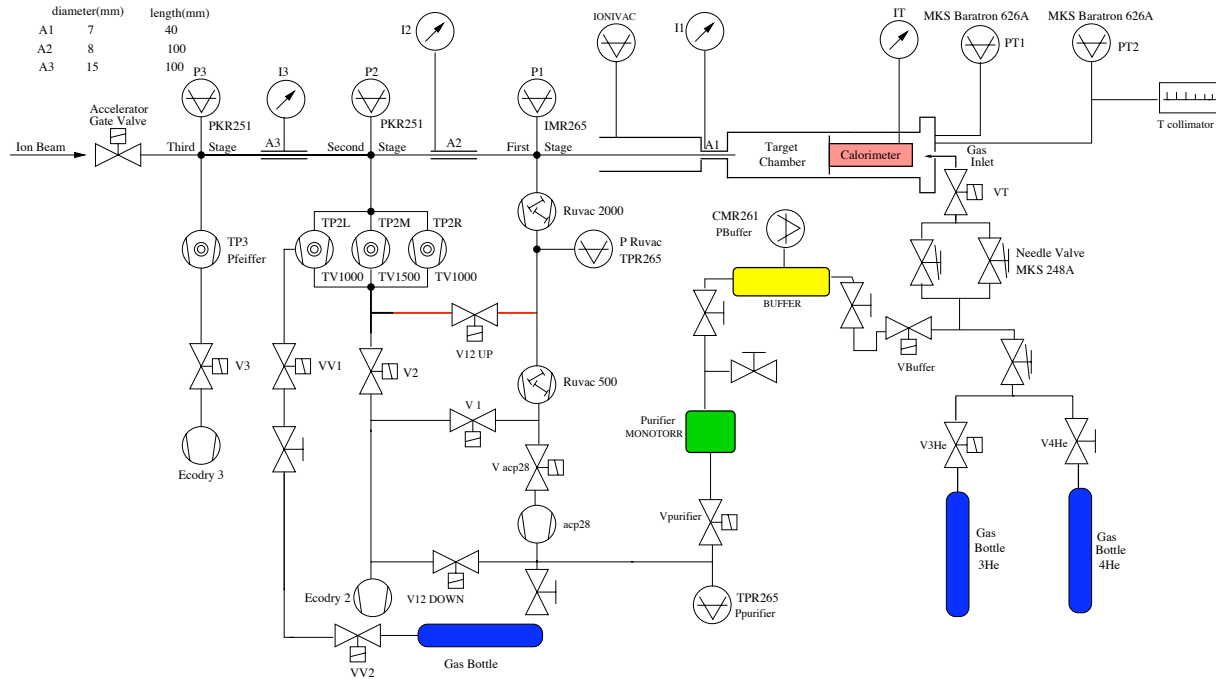
Figure 3: Schematic diagram of the windowless gas target system.

have been determined using a stainless steel test chamber equipped with flanges for the measurement of gas pressure and temperature. They are nearly constant along the beam

axis: small deviations are evident only close to the entrance collimator and around the hot calorimeter surface at the highest target pressures. The final target chamber, an exact copy of the test chamber without the flanges and entirely built with low activity OFHC Copper, has been mounted and is now fully operational. All measurements of gas pressure and temperature on specific positions allow to extend to this new chamber the results obtained with the test chamber. The intense beam current, $I \simeq 250\,\mu A$, modify local target characteristics lowering the target density along the beam path. This effect, known as beam heating, depends on the power per unit volume delivered by the beam on the gas target [22]. The solution adopted to monitor this effect, measuring the product of target density and beam current, will be discussed in the next Section. This system could also provide the real target density if combined to an independent beam current measurement and allows a continuous check on the gas purity.

For a gas target system the classical current measurement with a Faraday cup is not possible because of gas ionization. In our case, the beam current is measured through a power calorimeter used as beam stopper: the power delivered by the beam is calculated as the difference between heating power needed to keep a constant temperature gradient along the calorimeter, without and with ion beam. The calorimeter is periodically calibrated using the target chamber without gas as a Faraday cup with secondary electrons suppressed by the electrically isolated 7 mm diameter Copper collimator (A_1 in Fig. 3) operated at negative voltage.

2.2   Beam heating effects

In order to control all possible sources of systematical errors, a considerable effort was required to study beam heating effects and find a viable solution to determine the correct value of target density in presence of an intense beam. It was decided to use a Silicon detector to measure the elastic scattering of beam on target nuclei, since the counting rate is directly related to the product of beam intensity and target pressure by the well known Rutherford scattering cross section.

A quite complex mechanical system has been developed (see Fig. 4). The telescopic mounting, moving longitudinally inside the target chamber, allows to fully investigate the effective target length and see possible quasi-punctual density (pressure) variations.

To limit the number of particles impinging on the ion-implanted Silicon detector (Ortec, Ultra series) and increase its service life it was decided to use a double scattering process, the first scattering being that of ^{4}He beam on ^{3}He target particles and the second that of scattered ^{4}He particles on a very thin ^{12}C foil (15 μg/cm^2): the total rate is anyhow related to the pressure in the investigated target length. The extremely low final energy of double scattered alpha particles for 100-200 keV CM beam energy (i.e. the region in which ^{3}He(^{4}He,γ)^{7}Be will be studied) required particular care to reduce the electronic noise and keep multiple scattering processes, which make difficult the correct rate determination, as low as possible. A very low noise preamplifier was therefore developed by the electronic division of INFN Milano and different collimators were used to define, in the best possible way, the path of double scattered alphas reaching the Si detector while reducing the possibility of detection of multiple scattered ions. Moreover, the whole mechanical structure was manufactured in Delrin instead of Copper to reduce

118
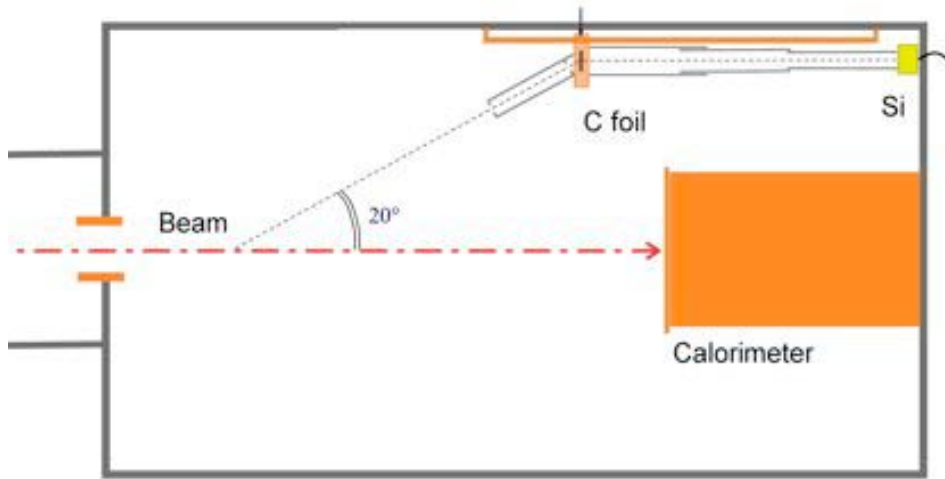
Figure 4: Schematic view of the gas target chamber: the calorimeter and Silicon detector mechanical system are visible. The beam direction is indicated by an arrow.

the probability of undesired scattering processes on the structure itself by keeping the Z of the material low.

During the optimization phase, two additional problems affecting the quality of rate determination in view of real pressure determination came out: namely the presence of small quantities of Nitrogen in the gas target due to small leaks and the instability of electronic noise conditions as testified by the pulser FWHM. The first problem was solved by subtracting from the peak ROI the fraction due to scattering of beam-like ^{4}He beam particles on Nitrogen while for the second a correction in the ROI definition was applied. After optimization, the device was used for a systematic beam-heating characterization using the stainless steel gas target chamber. Since the final geometrical efficiency of the Silicon detector is quite difficult to be calculated and is dependent on the beam focalization conditions, it was decided to proceed as follows: for a fixed position along the gas target chamber and for fixed beam energy and beam intensity, a set of rate determinations were performed changing only the target pressure. A reference pressure was selected (0.1 mbar) for which beam heating effects are negligible and ratios of rates were calculated referred to this low pressure measurement. In this way it was possible to eliminate unknown geometrical factors (including the scattering angle which is of 20° only for the central position of the investigated target portion) which keep constant during a set of measurements and obtain real pressures for each other value (>0.1 mbar). The beam heating effect (BH) was calculated as:

$$BH = \frac{\rho_{bar} - \rho_{scat}}{\rho_{bar}}$$

where ρ_{bar} is the target density as obtained from Baratron gauge pressure measurement and ρ_{scat} is the target density as obtained from double scattering rate. For each investi-

119
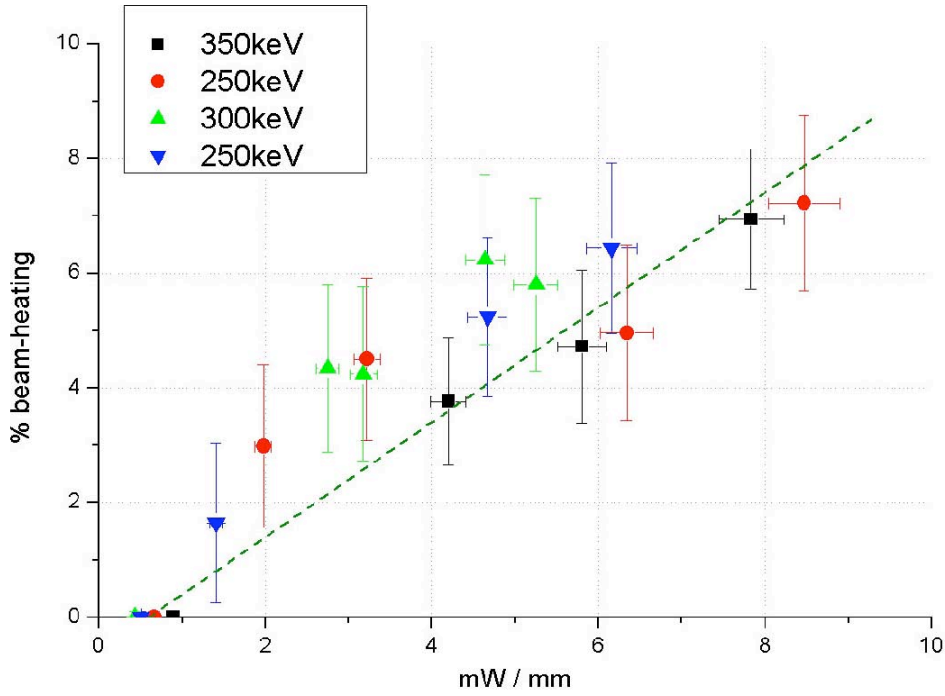
Figure 5: Beam heating effect as a function of transferred linear power for the position at 8 cm from the 7 mm diameter entrance collimator.

gated position, BH was studied as a function of transferred linear power (dW/dx) and a linear behavior was found. As an example the results for the position at 8 cm from the 7 mm diameter collimator are shown in Fig. 5.

Different transferred linear power conditions were obtained by changing beam energy and/or beam intensity and target pressure but for a fixed dW/dx ρ_{scat} was always deduced from the ratios of rates at a given pressure and at 0.1 mbar. After mounting the Copper chamber, the beam heating characterization was re-measured for few positions along the target chamber and the obtained results are comparable with those for the stainless steel chamber. During the $^3\mathrm{He}(^4\mathrm{He},\gamma)^7\mathrm{Be}$ measurement phase, the real target pressure will be always monitored with the Silicon detector device at a fixed position and beam heating corrections calculated on the basis of the above described results.

2.3 Cross section measurement with activation method

An alternative way to measure the $^3\mathrm{He}(^4\mathrm{He},\gamma)^7\mathrm{Be}$ cross section is to determine the number of produced $^7\mathrm{Be}$ nuclei. $^7\mathrm{Be}$ decays by electron capture to $^7\mathrm{Li}$ populating the 478 keV first excited state with $10.44 \pm 0.04\,\%$ branching ratio [23]. The 478 keV excited state decays with 100% branching ratio to the ground state and the detection of the 478 keV γ-radiation is used to determine the number of produced $^7\mathrm{Be}$ nuclei and hence the $^3\mathrm{He}(^4\mathrm{He},\gamma)^7\mathrm{Be}$ cross section independently from the in-beam γ-detection. The relatively long half-life of $^7\mathrm{Be}$ ($\mathrm{T}_{1/2} = 53.22 \pm 0.06$ day [23]) allows to measure the activity by measuring the γ-activity off-line, after the irradiation has been finished. This way the γ-counting can be done with

a well-shielded detector far from the accelerator avoiding the beam induced background.

As discussed above, in the present LUNA experiment ^{7}Be residual nuclei are produced inside the ^{3}He gas target. Because of the kinematics and low lateral straggling (as has been checked by Monte Carlo simulation with GEANT4 [24]) the ^{7}Be nuclei are implanted into the beam stop i.e. the calorimeter surface. A removable calorimeter cap (7 cm diameter) made of oxygen free Copper has been fixed to the calorimeter surface to collect ^{7}Be. After the irradiation, this cap is removed and transported to the counting facility.

Since ^{7}Be decays with electron capture, its half life might depend on the host material. However, a recent study [26] shows that the half life of ^{7}Be at room temperature implanted into several different metals is consistent with the adopted half life value used in the analysis of the present experiment. The validity of the half life value is also checked in the present experiment following the decay of the produced ^{7}Be, albeit with inferior precision.

Two detectors are used to measure the collected ^{7}Be activity. Both are placed in the low level laboratory of LNGS [25]. The first detector is a 120 % relative efficiency HPGe detector with Lead + Copper shielding. The laboratory background in this detector at 478 keV is roughly 6 counts/keV/day. The second HPGe detector has similar efficiency but it is an ultra low background detector equipped with Lead shielding and Radon box. The relevant laboratory background here is 0.2 counts/keV/day.

The γ-ray detection efficiencies of the detectors used for the activation counting have been measured with calibrated ^{7}Be sources. Three weak ^{7}Be sources have been prepared at ATOMKI, Debrecen, Hungary especially for this study. Thin layers of LiF evaporated onto Al and Ta backings have been irradiated with 2.5 MeV protons. The ^{7}Be nuclei are produced by the ^{7}Li(p,n)^{7}Be reaction. The sources are protected by thin gold and lacquer layers. The absolute activity of the sources has been measured with three HPGe detectors at ATOMKI to the precision of 3 %. The known absolute efficiencies of the three detectors used for the activity measurement were checked with calibrated radioactive sources.

Two irradiations at the LUNA2 400 kV accelerator and the subsequent γ-countings have already been performed at ^{4}He energies of 300 and 350 keV. Typical spectra taken with the two HPGe detectors after the 350 keV irradiation are shown in Fig. 6. The preliminary analysis shows that it is feasible to measure the cross section with activation method down to $E_\alpha = 250$ keV which corresponds to $E_{c.m.} = 107$ keV. The lowest energy ever measured with activation is $E_{c.m.} = 420$ keV [19] so LUNA can go much lower in energy (i.e. much closer to the astrophysically relevant energy region) than previous experiments. Parasitic reactions such as ^{6}Li(d,n)^{7}Be and ^{10}B(p,α)^{7}Be induced by the d or p impurities of the beam on the Li or B impurities of the Cu calorimeter cap can lead to the undesired production of ^{7}Be. In order to investigate the impurities of the calorimeter cap material, the same Copper was irradiated with 700 keV protons and deuterons at ATOMKI. The samples were then measured with the low background HPGe detector at Gran Sasso. No induced ^{7}Be activity was found within the detection limit of the setup i.e. the concentration of both ^{6}Li and ^{10}B in the Copper is below 1 ppm. With an order-of-magnitude limit of 3×10^{-9} deuterons per α obtained in a rough test for the LUNA2 machine, a ^{6}Li concentration of 1 ppm leads to a rate of parasitic ^{7}Be production of much less than one atom per day which can be neglected when compared with the yield of ^{3}He(α,γ)^{7}Be.
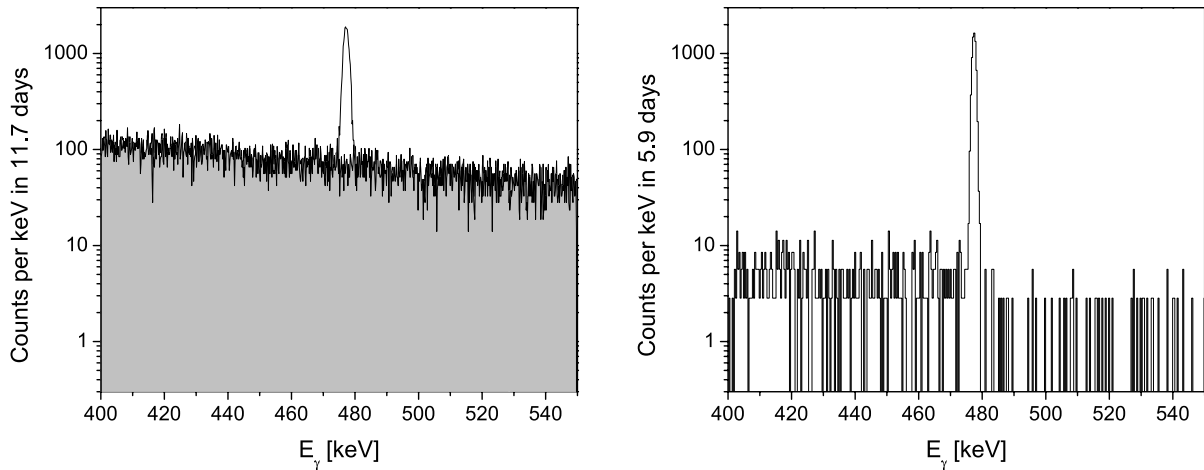
Figure 6: Gamma-spectra of the calorimeter cap taken with the two HPGe detectors. The cap has been irradiated with a 350 keV ^{4}He beam of roughly 200 μA intensity for 9 days. Note the different counting times for the two detectors. The better background condition of the second detector is clearly visible. In the first spectrum the gray shaded area shows the laboratory background rescaled for the same counting time.

3 The ^{25}Mg(p,γ)^{26}Al reaction

The ^{25}Mg(p,γ)^{26}Al is the slowest reaction of the Mg-Al cycle. The β^+ decay of ^{26}Al$_{\rm gs}$ [1] (half life: $7 \cdot 10^5$ year) to the excited state of ^{26}Mg gives rise to a 1.8 MeV γ-ray, one of the most important line for γ astronomy. Indeed, the presence of ^{26}Al in the interstellar medium has been determined on the basis of direct observations of this γ-ray line from the GRO [27, 28] and INTEGRAL [29, 30] satellites and from the observation of ^{26}Mg isotopic enrichments (extinct ^{26}Al) in carbonaceous meteorites [31]. While the observations from COMPTEL and INTEGRAL provide evidence that ^{26}Al nucleosynthesis is still active on a large scale, the Mg isotopic variations show that ^{26}Al must have also been produced not later than 4.6 billion years ago (time of the condensation of solar-system material). Any astrophysical scenario for ^{26}Al nucleosynthesis must be concordant with both observations.

The most important site for the activation of this reaction is the hydrogen-burning shell (HBS), which may be active in off main sequence stars of any mass. In particular, the Mg-Al cycle is at work in the hottest region of the HBS, close to the point of the maximum nuclear energy release. In addition, the ^{25}Mg(p,γ)^{26}Al may be also active within the carbon-burning regions in massive stars.

Concerning the HBS, the ^{25}Mg(p,γ)^{26}Al reaction starts when the temperature exceeds about $30 \cdot 10^6$ K. Then, between $40 < T/10^6 K < 60$ almost all the original ^{25}Mg is converted into ^{26}Al (but only $\simeq$ 80% into its long lived ground state). At larger temperature, the destruction by ^{26}Al$_{\rm gs}$(p,γ)^{27}Si and the refurbishment of ^{25}Mg by ^{24}Mg(p,γ)^{25}Al(β^+)^{25}Mg begins to play a relevant role. Once the HBS advances in mass, the ^{26}Al$_{\rm gs}$ is accumulated within the H-depleted core. A convective dredge up cou-

---

[1]About 80% of the released ^{26}Al is in the ground state ($\tau_{1/2} = 7 \cdot 10^5$ year), the remaining 20% goes into the 228 keV isomeric state ($\tau_{1/2} = 6$s).

122

pled to a huge stellar wind or an explosive ejection of the freshly synthesized material are needed in order to make the $^{26}Al_{gs}$ an "observable". Everything must occur before its decay could take place, of course. Since the existence of an active HBS is a common feature, very different class of stars can have these characteristics: low mass AGB, massive AGB, Novae, Core Collapse Supernovae and Wolf-Rayet stars. An additional very important constraint is that the material so enriched in $^{26}Al_{gs}$ cannot be exposed to a neutron flux, because of its large neutron capture cross section. This is a major problem for AGB stars.

Stellar nucleosynthesis studies have not yet identified which one of the possible ^{26}Al sources could explain the observed evidences. Extant stellar models predict that 30%-50% of the production of ^{26}Al comes from the HBS of massive stars (core collapse supernovae or WR-stars). The remaining should be searched elsewhere.

Note, however, that the effective ^{26}Al production and, more in general, the Mg-Al yields are extremely sensitive to the temperature at which the H burning occurs. Thus, a variety of very different situations may be encountered, simply changing the original mass of the star or its initial composition.

In summary, the quantitative evaluation of the amount of ^{26}Al in the ashes of stars having an active HBS is a quite complicated task, due to the simultaneous actions of many variables. For sure, a more firm evaluations of the relevant reaction rates could help in reducing the free parameters. This is the reason why we decided to measure the $^{25}Mg(p,\gamma)^{26}Al$ cross section. The presence of many states in the ^{26}Al isotope makes
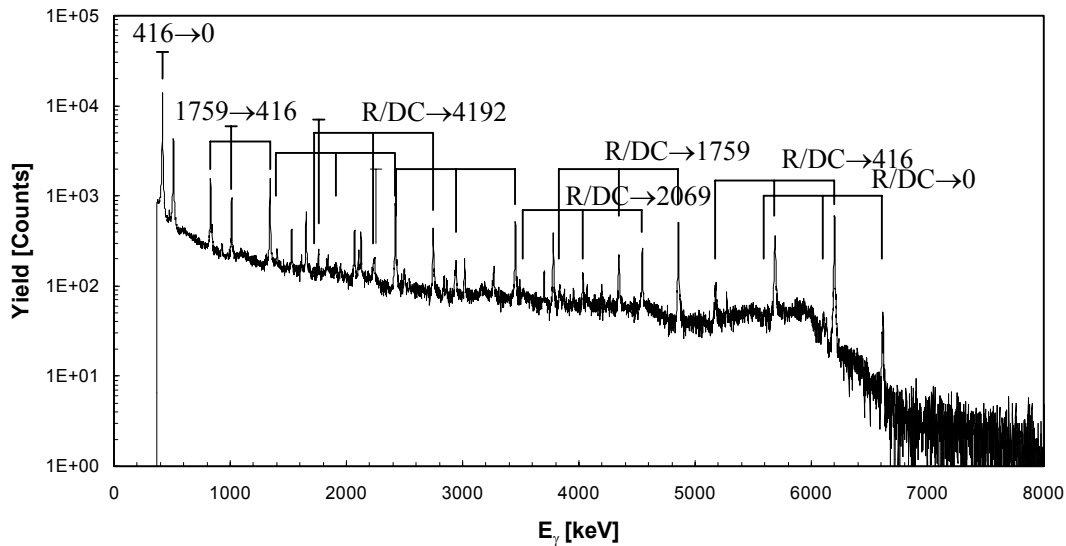
Figure 7: γ-ray spectrum for the $^{25}Mg(p,\gamma)^{26}Al$ reaction taken at 304 keV center of mass energy.

the study complicated (see Figure 7); in the past the states down to 6496 keV, which correspond to a center of mass energy of 189 keV in the $^{25}Mg+p$ channel (Q=6306 keV), have been directly and indirectly studied [32, 33, 34, 35, 36, 37, 38, 39, 40, 41]. The

123

E_{cm} (keV)	E_X (keV)	Reaction per day
37.5	6343.5	3.65E-08
58.0	6364.0	2.80E-01
92.6	6398.6	7.35E+01
108.5	6414.5	1.64E+01
130.4	6436.4	6.80E+01
189.9	6495.9	2.68E+05
244.3	6550.3	1.53E+06
292.3	6598.3	1.32E+07
304.4	6610.4	8.55E+12
374.5	6680.5	1.62E+13
418.2	6724.2	2.78E+13

Table 1: Estimated number of reactions per day for selected resonances of the ^{25}Mg$(p, \gamma)^{26}$Al reaction.

most used set up was a proton beam impinging in a ^{25}Mg target with a HP Ge placed at 55° degree, which gave the possibility to recognize all the cascade peaks. For the five lower energy states just upper limits have been indirectly deduced by the study of the ^{25}Mg$(^3$He, d$)^{26}$Al. The peculiarity of the 400 kV LUNA facility [21] are particularly well suited for the study, where reaction γ-ray lines up to $\simeq$ 6.5 MeV have to be measured with very low intensities. High beam intensities and high detection resolutions or efficiencies have to be coupled to high target stability and purity, which allow low beam-induced background; cosmic background is strongly suppressed by the mountain shielding and low intrinsic activity detectors are employed [42]. In Table 1 we report the expected number of reactions per day for the ^{25}Mg$(p, \gamma)^{26}$Al, using for the resonance strength the data from the NACRE compilation and a beam of 500 μA with a target of pure ^{25}Mg. The resonance at 190 keV has a high enough rate to be studied with a Ge detector in order to improve the accuracy of the strength determination and to assess the structure of the γ-ray cascade. Then, the measurement of the strength of the resonances at 130 and 93 keV will be performed using a high efficiency detector, in particular a summing crystal based on a 4π BGO. The summing efficiency will be calculated by a Montecarlo code which will be tuned using the detailed knowledge of the cascades for the resonance at 190 keV.

Last year we have started the production and the study of the ^{25}Mg enriched target. We prepared targets using tantalum backings (0.3mm) and magnesium oxide enriched in the mass 25 isotope (99.2%). To reduce the magnesium oxide we mixed it with tantalum powder and we evaporated the ^{25}Mg by using an electron gun. We produced $\simeq 65\mu g/cm^2$ and $\simeq 45\mu g/cm^2$ thickness targets, which correspond to a thickness of 30 keV and 20 keV, calculated by using the energy loss table of Zigler [43] at 100 keV. Finally, a thin layer of gold has been added to some of the targets, to prevent possible oxidation. In the next months we will test the targets using the LUNA accelerator.

References

[1] R. Bonetti et al. (LUNA Coll.), Phys. Rev. Lett. 82(1999)5205

[2] C. Casella et al. (LUNA Coll.), Nucl. Phys. A 706(2002)203

[3] A. Formicola et al. (LUNA Coll.) Phys. Lett. B 591(2004)61

[4] G. Imbriani et al. (LUNA Coll.) Eur. Phys. J A 25(2005)455A

[5] E.G. Adelberger et al., Rev. Mod. Phys. 70(1998)1265

[6] C. Angulo et al. (NACRE Coll.), Nucl. Phys. A 656(1999)3

[7] A. Lemut et al. (LUNA Coll.), nucl-ex/0602012

[8] W. Lamb and R. Hester, Phys. Rev. 108(1957)1304

[9] U. Schroeder et al., Nucl. Phys. A 467(1987)240

[10] R.C. Runkle et al., Phys. Rev. Lett. 94(2005)082503

[11] G. Imbriani et al. (LUNA Coll.), Astronomy and Astrophysics 420(2004)625

[12] S. Degl'Innocenti et al., Phys. Lett. B 590(2004)13

[13] J.N. Bahcall and M. Pinsonneault, Phys. Rev Lett. 92(2004)121301

[14] J.N. Bahcall et al., astro-ph/0412440

[15] F. Herwig and S.M. Austin, Astrophys. J 613(2004)L73

[16] G. Fiorentini *et al.*, astro-ph/0310753

[17] R. Cyburt, Phys. Rev. D 70(2005)023505

[18] M.Hilgemeier *et al.*, Z. Phys. A 329(1988)243

[19] B.S. Nara Singh *et al.*, Phys. Rev. Lett. 93(2004)262503

[20] E.G. Adelberger *et al.*, Rev. Mod. Phys. 70(1998)1265

[21] A. Formicola *et al.* (LUNA Coll.), Nucl. Inst. Meth. A 507(2003)609

[22] J. Görres *et al.*, Nucl. Inst. Meth. 177(1980)295

[23] D.R. Tilley *et al.*, Nucl. Phys. A 708(2002)3

[24] S. Agostinelli *et al.*, Nucl. Inst. Meth. A 506(2003)250

[25] C. Arpesella, Appl. Rad. and Isot. 47(1996)991

[26] B. Limata *et al.*, Eur. Phys. J. A *in press*

[27] Diehl, R., Dupraz, C., Bennett, K., et al. A&A, 298(1995)445.

[28] Knödlseder, J., Dixon, D., Bennett, K., et al. A&A 345(1999)813.

[29] Winkler, C., Courvoisier, T.C., Di Cocco, G., et al. A&A, 411(2003)L1.

[30] Diehl, R. et al. A&A 411(2003)L451L455.

[31] Wasserburg, G.J., in Protostars and planet II, edited by D.C. Black and M.S. Matthews (Universirty of Arizona Press, Tucson, 1985), p.703

[32] A. E. Champagne, A. J. Howard and P. D. Parker. Nucl. Phys.A 402(1983)159

[33] A. E. Champagne, A. J. Howard and P. D. Parker. Nucl. Phys.A 402(1983)179

[34] P. M. Endt, P. de Wit and C. Alderliesten. Nucl. Phys.A 459(1986)61

[35] A. E. Champagne et al., Nucl. Phys.A 451(1986)498

[36] P. M. Endt and C. Rolfs. Nucl. Phys.A 467(1987)261

[37] A. E. Champagne et al., Nucl. Phys.A 505(1989)384

[38] Ch. Iliadis et al., Nucl. Phys.A 512(1990)509

[39] P. M. Endt. Nucl. Phys.A 521(1990)1

[40] C. Iliadis et al., Phys. Rev.C 53(1986)475

[41] D.C.Powel et al., Nucl. Phys.A 644(1998)263

[42] D. Bemmerer et al, Eur. Phys. J A 24(2005)313

[43] J. F. Ziegler et al, SRIM program, version 2003-20, srim-org 2003 (www.srim.org).

4 Publications and Conferences

1. D. Bemmerer et al. (LUNA Coll.), "Feasibility of low energy radiative capture experiments at the LUNA underground accelerator facility", Eur. Phys. J A 24(2005)313

2. G. Imbriani et al. (LUNA Coll.), "S-factor of ^{14}N(p, γ)^{15}O at astrophysical energies", EpJA 25(2005)455A

3. D. Bemmerer, Nuclear Physics in Astrophysics II, Debrecen

4. C. Broggini, International School of Nuclear Physics, 27th Course, Erice

5. F. Confortola, TAUP 2005, Zaragoza

6. F. Confortola, XIC Congresso della Soc. Italiana di Fisica, Catania

7. F. Confortola, XLIII International Winter meeting on Nuclear Physics, Bormio

8. H. Costantini, 3rd European Summer School on Experimental Nuclear Astrophysics, S.Tecla

9. A. Formicola, XIC Congresso della Soc. Italiana di Fisica, Catania

10. A. Guglielmetti, XIC Congresso della Soc. Italiana di Fisica, Catania

11. A. Guglielmetti, Highlights in Physics 2005, Milano

12. G. Imbriani, 3rd European Summer School on Experimental Nuclear Astrophysics, S.Tecla

13. R. Menegazzo, 1st CARINA Workshop on "Perspectives in European Nuclear Astrophysics", Girona

14. R. Menegazzo, 22nd Meeting between Astrophysicists and Nuclear Physicists, Brussels

15. P. Prati, NUSTAR05, Guilford

16. P. Prati, V Riunione Nazionale di Astrofisica Nucleare, Teramo

THEORY GROUP

Members of the group: R. Aloisio, Z. Berezhiani, V. Berezinsky, P. Ciarcelluti, M.L. Co-stantini, G. Di Carlo, A. Galante, L. Gianfagna, A.F. Grillo, F. Mendez, F. Nesti, N. Rossi, A. Sakharov, F. Vissani.

The activity of the group in year 2005 has concerned research in the fields covered by four Iniziative Specifiche (IS): Astroparticle Physics (mainly in IS FA51), Particle Phenomenology (mainly in IS PI21), Planck Scale Phenomenology (IS GS51) and Computer simulations of Lattice Gauge Theory (in IS PI12). The activities are more specifically described below.

1   Astroparticle Physics

The Astroparticle group of LNGS in 2005 included R.Aloisio, V.Berezinsky, M.L.Costantini, F.Vissani and visitors V.Dokuchaev (Institute for Nuclear Research, Moscow), Yu.Eroshenko (Institute for Nuclear Research, Moscow), B.Hnatyk (Lviv University, Ukraine), S.Grigorieva (Institute for Nuclear Research, Moscow) and A.Gazizov (DESY, Germany). The group worked in close collaboration with A.Vilenkin (Tufts University, USA), M.Kachelriess (MPI, Munich), P.Blasi (Arcetri Observatory, Firenze), G.Senjanović (ICTP, Trieste), A.Strumia (Pisa University) and others.

Scientific work

The main field of the work is astroparticle physics, including neutrino oscillations, neutrinos from DM annihilation, massive neutrinos, ultra high energy cosmic rays, and high energy neutrino astrophysics. We work also in particle physics, including the fermion masses in supersymetric and non-supersymmetric SO(10).

Conferences, seminars and other activities

R.Aloisio works as the scientific secretary of the LNGS scientific committee.

V.Berezinsky works as an editor of Int. Journal "Astroparticle Physics".

F.Vissani works (together with C.Cattadori) as the organizer of the LNGS seminar.

R.Alosio presented the talk at TAUP-05 conference in Zaragoza and at 17th Conf. on HE Physics in Catania.

V.Berezinsky presented the invited talks at 11th Int. Workshop "Neutrino Telescopes"(Venice), at Aspen Workshop "Physics at the end of the galactic cosmic rays" (Aspen, USA), at ISAPP Int. Doct. School (Belgirate, Italy), at 59th Yamada Int. Conf. "Astrophysics and Cosmology" (Tokyo), at Int. Workshop " Highest Energy QCD" (Scopelous, Greece),

12th Lomonosov Conference (Moscow).

V.Berezinsky worked as the organizer of Summer Institute "Underground Physics" in Seattle (USA) and as member of Organizing Committee TAUP-05.

F.Vissani presented the talks at "Neutrino telescopes 2005", "Lepton and quark masses in SO(10)", IFAE 2005 . and at the Meeting of COMM.II, INFN at Villa Mondragone.

Journal and Proceedings publications in 2005

[1] R. Aloisio and V. Berezinsky
ANTI-GZK EFFECT IN ULTRA HIGH ENERGY COSMIC RAYS DIFFUSIVE PROPAGATION
Astrophys.J. 625 (2005) 249-255

[2] V.S.Berezinsky, A. Z. Gazizov, S. I. Grigorieva
DIP IN UHECR SPECTRUM AS SIGNATURE OF PROTON INTERACTION WITH CMB
Phys. Lett. B612 (2005) 147-153

[3] V.Berezinsky,
SUPER-GZK NEUTRINOS
Proc. of 11th Int. Workshop NEUTRINO TELESCOPES (ed. Milla Baldo Ceolin) p.339, 2005

[4] V.Berezinsky, M.Narayan, F.Vissani
LOW SCALE GRAVITY AS THE SOURCE OF NEUTRINO MASSES?
JHEP 0504 (2005) 009

[5] M.Cirelli, N.Fornengo, T.Montaruli, I.Sokalski, A.Strumia, F.Vissani
SPECTRA OF NEUTRINOS FROM DARK MATTER ANNIHILATIONS
Nucl. Phys. B 727 (2005) 99-138

[6] M.L.Costantini, F.Vissani
EXPECTED NEUTRINO SIGNAL FROM SUPERNOVA REMNANT RX J1713.7-3946 AND FLAVOR OSCILLATIONS
Astropart. Phys. 23 (2005) 477-485

[7] M.L.Costantini, A.Ianni, F.Vissani
SN1987A AND THE PROPERTIES OF NEUTRINO BURST
Phys. Rev. D 70 (2004) 043006

[8] M.Cirelli, G.Marandella, A.Strumia, F.Vissani
PROBING OSCILLATIONS INTO STERILE NEUTRINOS WITH COSMOLOGY, ASTROPHYSICS AND EXPERIMENTS
Nucl. Phys. B 708 (2005) 215-267

[1] R.Aloisio, V.Berezinsky
ANTI-GZK EFFECT IN UHECR SPECTRUM
astro-ph/0507325

[2] V.Berezinsky, A.Z.Gazizov
DIFFUSION OF COSMIC RAYS IN EXPANDING UNIVERSE. (I)
astro-ph/0512090

[3] V.Berezinsky, V.Dokuchaev, Y.Eroshenko
DESTRUCTION OF SMALL-SCALE DARK MATTER CLUMPS IN THE HIERAR-
CHICAL STRUCTURES AND GALAXIES
astro-ph/0511494

[4] V.Berezinsky
DIP IN UHECR AND TRANSITION FROM GALACTIC TO EXTRAGALACTIC COS-
MIC RAYS
astro-ph/0509069

[5] V.Berezinsky
ULTRA HIGH ENERGY NEUTRINO ASTRONOMY
astro-ph/0505220

[6] B.Bajc, A.Melfo, G.Senjanovic, F.Vissani
FERMION MASS RELATIONS IN A SUPERSYMMETRIC SO(10) THEORY
hep-ph/0511352

[7] B.Bajc, A.Melfo, G.Senjanovic, F.Vissani
YUKAWA SECTOR IN NON-SUPERSYMMETRIC RENORMALIZABLE SO(10)
hep-ph/0510139

2   Particle Phenomenology

During this year the activity of the group, which included Z. Berezhiani, P. Ciarcellutti, F. Nesti, L. Pilo, N. Rossi and A. Sakharov, was mainly devoted to different problems of particle phenomenology and its applications to astrophysics and cosmology. The following results can be mentioned.

Z. Berezhiani and P. Ciarcelluti in collaboration with D. Comelli and F. Villante (Ferrara), and P. Ciarcelluti in subsequent publications, have studied cosmological implications of the mirror world, an identical copy of the observed particle world which interacts with the latter only gravitationally. The mirror baryons, being invisible for ordinary observer, could constitute dark matter of the universe, with specific implications for for the large scale structure (LSS) of the Universe and the cosmic microwave background (CMB). It was given a complete numerical calculations by a special computational code for the LSS power spectrum and the CMB angular anisotropies in the cases of dark matter

entirely constituted by mirror baryons, and for the case of mixed cold dark matter and mirror dark matter model.

Z. Berezhiani in collaboration with L. Bento (Lisbon) discussed the phenomenological implications of the neutron (n) oscillation into the mirror neutron (n'), a hypothetical particle from a parallel mirror world, exactly degenerate in mass with the neutron but sterile to normal matter. It was shown that the present experimental data allow a maximal $n - n'$ oscillation in vacuum with a characteristic time τ much shorter than the neutron lifetime, in fact as small as 1 sec, which corresponds to a mass mixing $\delta m = \tau^{-1} \sim 10^{-15}$ eV between n and n' states. This phenomenon may manifest in neutron disappearance and regeneration experiments perfectly accessible to present experimental capabilities and may also have interesting astrophysical consequences, in particular it could help the propagation of ultra high energy cosmic rays at cosmological distances without substantial energy loses.

Z. Berezhiani in collaboration with P. Chankowski, A. Falkowski and S. Pokorski (Warsaw) suggested a mechanism for the Higgs potential stability against the "little hierarchy" problem. In this model the potential of the MSSM Higgs doublets is doubly protected: by supersymmetry and by an accidental global symmetry, as far as the Higgses appear as pseudo-Goldstone modes of the spontaneoulsy broken extra global symmetry.

Z. Berezhiani and F. Nesti suggested a supersymmetric SO(10) model with a flavour symmetry $SU(3)$. The mass matrices of all fermion types (up and down quarks, charged leptons and neutrinos) appear in the form of combinations of three symmetric rank-1 matrices common for all types of fermions, with different coefficients that are successive powers of small parameters related to each-other by SO(10) symmetry properties. The model perfectly describes the mass and mixing patterns for the quarks and leptons, dangerous D=5 operators for the proton decay are naturally suppressed and flavour-changing supersymmetric effects are under control.

Participation in conferences and schools

1st ENTApP Meeting on Astroparticle Physics, Valencia, Spain, 11-16 Apr 2005: invited talk of Z. Berezhiani "Unified origin of the visible matter, dark matter and UHECR"

Int. Conf. Planck'05, Trieste, Italy, 23-28 May 2005: invited talk di Z. Berezhiani "Neutron-mirror neutron oscillation and ultra-high-energy cosmic rays"

Int. Conf. Planck'05, Trieste, Italy, 23-28 May 2005: talk of F. Nesti "Supersymmetric SO(10) model for fermion masses"

10th Gran Sasso Summer Institute, Assergi, Italy, 29 Aug - 16 Sept 2005: Lectures of Z. Berezhiani "Neutron - mirror neutron oscillation: how fast might it be?", F. Nesti "Supersymmetric SO(10) and flavour structures", L. Pilo "Higgsless models: gauge symmetry breaking through boundary conditions", and A. Sakharov "Time structures of the Gamma Ray Bursts"

Int. ISPM Conf. "Selected Topics in Theoretical Physics", Tbilisi, Georgia, 18-25 Sept. 2005, invited talk of Z. Berezhiani "How fast the neutron oscillations might be?"

Papers published in 2005

[1] Z. Berezhiani, P. Ciarcelluti, D. Comelli, F.L. Villante, STRUCTURE FORMATION WITH MIRROR DARK MATTER: CMB AND LSS, Int.J.Mod.Phys. D14, 107-120 (2005)

[2] P. Ciarcelluti, COSMOLOGY WITH MIRROR DARK MATTER 1: LINEAR EVOLUTION OF PERTURBATIONS, Int.J.Mod.Phys. D14, 187-222 (2005)

[3] P. Ciarcelluti, COSMOLOGY WITH MIRROR DARK MATTER 2: COSMIC MICROWAVE BACKGROUND AND LARGE SCALE STRUCTURE, Int.J.Mod.Phys. D14, 223-256 (2005)

[4] G. von Gersdorff, L. Pilo, M. Quiros, A. Riotto, V. Sanz, SUPERSYMMETRY FROM BOUNDARY CONDITIONS, Nucl. Phys. B712, 3-19 (2005)

[5] M. Giannotti, F. Nesti, NUCLEON-NUCLEON BREMSSTRAHLUNG EMISSION OF MASSIVE AXION, Phys. Rev. D72:063005 (2005)

[6] F. Nesti, SO(10) FERMION MASSES FROM RANK-1 STRUCTURES OF FLAVOUR, Nucl.Phys. Proc.Suppl. 145, 258-262 (2005)

[7] M.Yu. Khlopov, S.G. Rubin, A.S. Sakharov, PRIMORDIAL STRUCTURE OF MASSIVE BLACK HOLE CLUSTERS, Astropart. Phys. 23, 265-277 (2005)

[8] Z. Berezhiani, THROUGH THE LOOKING-GLASS: ALICE'S ADVENTURES IN MIRROR WORLD, I. Kogan Memorial Volume "From Fields to Strings: Circumnavigating Theoretical Physics", Eds. M. Shifman et al., Vol. 3, 2147-2195 (2005), e-Print Archive: hep-ph/0508233

Papers submitted for publication in 2005

[1] A. Drago, G. Pagliara, Z. Berezhiani, SHORT GRAVITATIONAL WAVE BURSTS INDUCED BY R-MODE SPIN-DOWN OF HYBRID STARS, accepted in Astron. & Astrophys.

[2] Z. Berezhiani, L. Bento, NEUTRON - MIRROR NEUTRON OSCILLATIONS: HOW FAST MIGHT THEY BE?, July 2005, e-Print Archive: hep-ph/0507031, accepted in Phys. Rev. Lett.

[3] Z. Berezhiani, S. Cassisi, P. Ciarcelluti, A. Pietrinferni, EVOLUTIONARY AND STRUCTURAL PROPERTIES OF MIRROR STAR MACHOS, July 2005, e-Print Archive: astro-ph/0507153, accepted in Astropart. Phys.

[4] Z. Berezhiani, P.H. Chankowski, A. Falkowski, S. Pokorski, DOUBLE PROTECTION OF THE HIGGS POTENTIAL IN A SUPERSYMMETRIC LITTLE HIGGS MODEL, Sep 2005, e-Print Archive: hep-ph/0509311, accepted in Phys. Rev. Lett.

[5] Z. Berezhiani, F. Nesti, SUPERSYMMETRIC SO(10) FOR FERMION MASSES AND MIXINGS: RANK-1 STRUCTURES OF FLAVOR, Oct 2005, e-Print Archive: hep-ph/0510011, accepted in JHEP

[6] Z. Berezhiani, L. Bento, FAST NEUTRON - MIRROR NEUTRON OSCILLATION AND ULTRA HIGH ENERGY COSMIC RAYS, Dec. 2005, accepted in Phys. Lett. B

3 Computer Simulations of Lattice Gauge theories

During year 2005 this activity was pursueded by: G. Di Carlo, A. Galante in collaboration with V. Azcoiti and V. Laliena (Zaragoza). The following items are to be noted:

3.1 Non-zero baryonic density QCD

We have introduced a new variant of the well known Hasenfraz-Karsch action that allows some step forward toward the determination of the critical line in the Temperature-Baryon density plane. A study in three dimensional Gross-Neveu model and a detailed analysis of 4 Flavours QCD has produced exciting results. A study of the deconfinig phase transition of 4 Flavours QCD, extended in the Temperature-Chemical potential plane up to values of the quark chemical potential as large as 270 MeV, has been carried out.[1]

3.2 Models with θ term in the action

Using the methods we have introduced in the last years we continue this study with the simulation of other models with topological terms, in particular SO(3) and in general $CP^{(n-1)}$ models and SU(2) gauge.

Journal and Proceedings publications in 2005

[1] Vicente Azcoiti, Giuseppe Di Carlo, Angelo Galante, Victor Laliena
PHASE DIAGRAM OF QCD WITH FOUR QUARK FLAVORS AT FINITE TEMPER-ATURE AND BARYON DENSITY
Nucl.Phys. B723 (2005) 77-90

[2] Vicente Azcoiti, Giuseppe Di Carlo, Angelo Galante, Victor Laliena
TESTING NEW STRATEGIES IN FINITE DENSITY
Nucl.Phys.Proc.Suppl.140 (2005) 502-504

[3] Vicente Azcoiti, Giuseppe Di Carlo, Angelo Galante, Victor Laliena
STRONG COUPLING ANALYSIS OF DIQUARK CONDENSATION
Nucl.Phys.Proc.Suppl.140 (2005) 523-525

[4] Vicente Azcoiti, Giuseppe Di Carlo, Angelo Galante, Victor Laliena
NEW IDEAS IN FINITE DENSITY QCD
Nucl.Phys.Proc.Suppl.140 (2005) 499-501

4   Planck Scale Kinematics and Phenomenology

This activity during 2005 concerned the possible origin and the analysys of phenomenological consequences, in particular in Ultra High Energy Cosmic Ray Physics, of possible departures from (special) relativistic invariance at energy-momentum scales near the Planck Mass. The persons involved are R. Aloisio (partly, main activity in FA51), A. Galante (partly), A. Grillo and F. Mendez.

The activities in 2005 mainly involved the analysis of the so-called Doubly (or Deformed) Special Relativity-DSR models which are momentum space relativistic theories where, apart from the (low energy) speed of light, there exist a second invariant qantity chosen to be the Planck mass. These theories are expected to incorporate some aspects of Quantum Gravity. The research performed mainly concerned the possible emergence of DSR as a semi-classical measurement theory in a fluctuating space-time as expected from Quantum Gravity.

In May, 2005, an informal workshop was held in Gran Sasso with the partecipation of the other groups of the IS GS51 (Rome and Sissa) and of the foreign collaborators: J.L. Cortes, J. Gamboa, F. Girelli and J. Kowalsky.

Journal and Proceedings publications in 2004

[1] R.Aloisio, A.Galante, A.F.Grillo, E.Luzio, F.Mendez
A NOTE ON DSR-LIKE APPROACH TO SPACE-TIME
Phys. Lett. B 610 (2005) 101-106

[2] R.Aloisio, P.Blasi, A.Galante, P.L.Ghia, A.F.Grillo, F.Mendez
PHENOMENOLOGICAL QUANTUM GRAVITY: THE BIRTH OF A NEW FRONTIER?
Nuovo Cim. B 120 (2005) 859-866

[3] R.Aloisio, A.Galante, A.Grillo, S.Liberati, E.Luzio, F.Mendez
DEFORMED SPECIAL RELATIVITY AS AN EFFECTIVE THEORY OF MEASUREMENTS ON QUANTUM GRAVITATIONAL BACKGROUNDS
Phys. Rev. D73 (2006) 045020

UNDERSEIS - Underground Seismic Array

C. Fischione[a], M. Martini[a], G. Saccorotti[a], R. Scarpa[b], F. Tronca[a]

[a] Osservatorio Vesuviano, INGV - Napoli, Italy
[b] Dipartimento di Fisica, Università di Salerno - Italy

Abstract

This report describes a geophysical instrument under installation in the underground physics laboratories of Gran Sasso (LNGS-INFN), located in the seismic zone of central Apennines, Italy. This instrument is aimed to monitor seismic radiation with very high sensitivity; it is a small aperture seismic array composed by 20 three-components short period seismomenters (Mark L4C-3D).

1   Introduction

The physics of earthquakes is based on the measurements of radiated seismic waves and ground displacement associated with this phenomena. The inertial pendulum is the oldest and most diffused instrument used to measure the main features of seismic waves. The advantages of this instrument are the simplicity of the theory, the high sensitivity, the robust design and the simple calibration methods, in spite of the quite reduced frequency band and linearity (Wielandt, 1983). Other instruments based on different physical principles, such as strainmeters and gyroscopes, are only partially used by seismologists (Benioff, 1935; Farrell, 1969, Aki and Richards, 1980). Networks of short period seismometers are as far the most diffused system to monitor local and regional seismicity (Lee and Stewart, 1981). Broad-band instruments make up a powerful system to study the details of seismic sources and also to study large earthquakes at global scale (Lee and Wallace, 1995). Moreover arrays of seismometers and accelerometers are used to study the details of sources and radiation patterns of earthquakes, nuclear underground explosions and volcanic activity (Bolt, 1976; Chouet, 1996). Strainmeters and tiltmeters (Agnew, 1986) are used to study the lower frequencies radiated from seismic sources and allow to detect slow earthquakes and strain steps (i.e. anelastic deformations around seismic sources). At present, the seismic activity of central Apennines, and in particular of the Gran Sasso massif, is relatively low, as compared to other seismically active areas of Europe such as Turkey or central Greece. Three seismic swarms were monitored in August 1992, June 1994 and October 1996, with the largest earthquake having $M_L = 4.2$. These swarms

are the largest events occurred since 1985 in this region. However, this area experienced destructive earthquakes in the past: a magnitude 7 event occurred in 1703. Close to this region, the 1915 Avezzano earthquake ($M_S = 6.8$) occurred, causing more than 15,000 victims. On average, about 1 microearthquake per day above $M_L = 1$ occurs, within 20 Km radius from LNGS-INFN. The facilities existing in the laboratories, and the seismo-tectonics features of the Gran Sasso massif, make them an excellent site for studies related to the physics of earthquake source, wave propagation in a complex medium and seismic monitoring.

2 The Underground Seismic Array

A seismic array is a set of seismographs distributed over an area of the Earth's surface at spacing narrow enough so that the signal waveform may be correlated between adjacent seismometers (Aki and Richards, 1980).
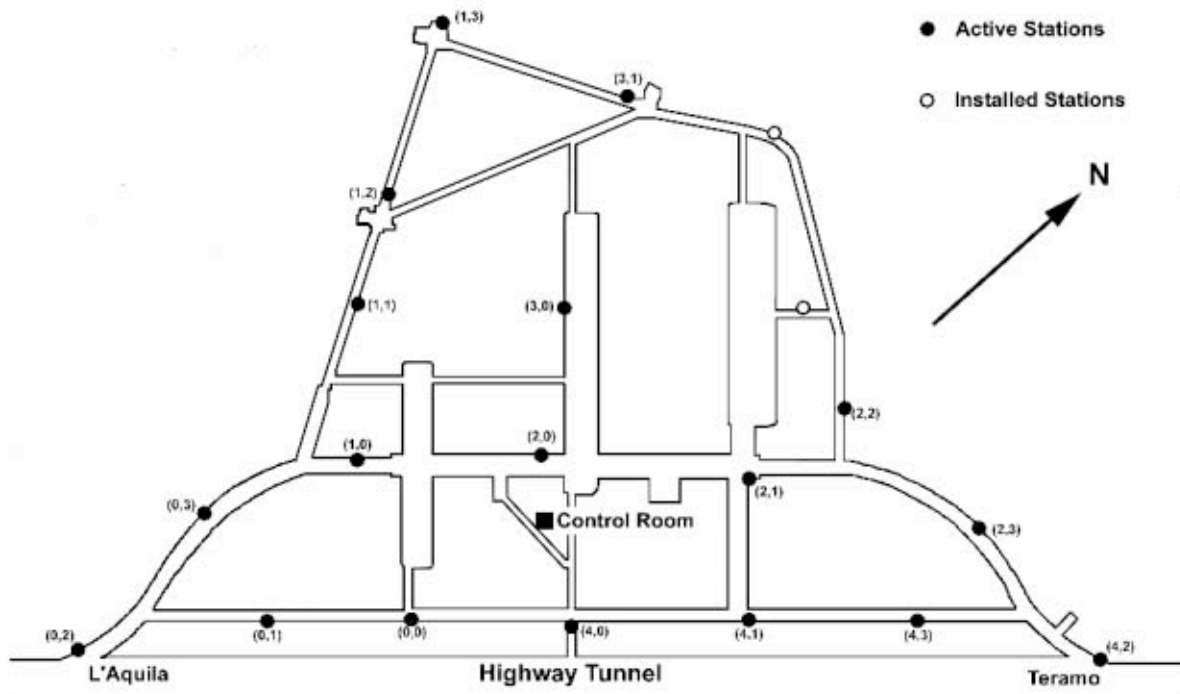
Figure 1: Map of the Underground Seismic Array. The notation (n,m) shows the line number (n) and the station number (m).

The main advantages of such geometrical configurations are the improvement of signal-to-noise ratio and the possibility to perform a detailed analysis of wave propagation and composition. The development of large aperture seismic arrays such as LASA in Montana, USA (Green et al., 1965) and NORSAR in Norway (Kedrov and Ovtchinnikov, 1990) led to many improvements in the knowledge of Earth's structure (Aki et al., 1977) other than to monitor underground nuclear explosions. More recent developments of these arrays

194

make use of low number of sensors and smaller apertures in order to reduce the effects of lateral inhomogeneities (Mykkeltveit, 1985). The need to monitor local seismicity in the very large underground physics laboratories of LNGS-INFN led to some preliminary experiments to understand the site response; a L-shaped array along the way to access the LNGS, having spatial extension of 10.5 km, was deployed in 1993. This array was formed by 17 three component short period digital seismic stations spaced 600 m (De Luca et al., 1997). In the same region, from 1992 to 2001, a digital seismic network equipped with a maximum of 18 3D short period seismic stations was installed.
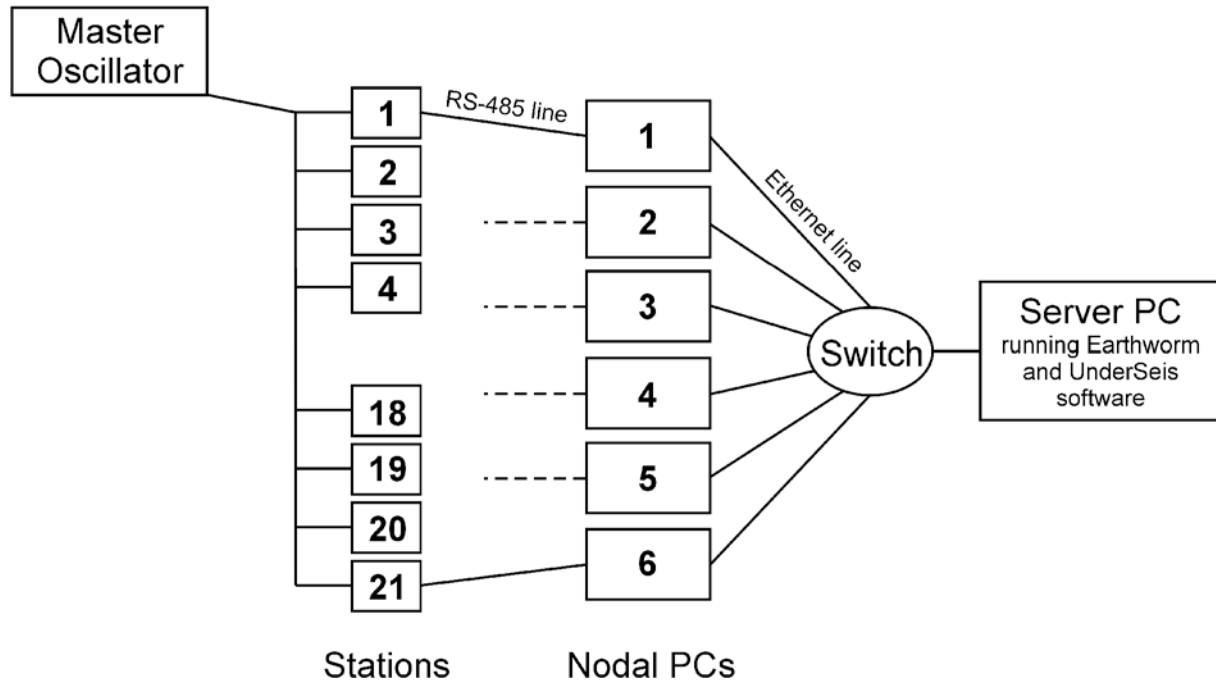
Figure 2: Block scheme of the Underground Seismic Array.

Two important features of seismic response in the region have been observed: a substantial homogeneity of spectral response from underground linear array and, for S waves, an average decrease of amplitudes with respect to the data recorded at the surface, in the band 1-8 Hz. In particular the horizontal components are reduced by a factor 4, while the vertical one is reduced by a factor 2. Strain monitoring, in the same region, through GPS, EDM, levellings and microgravimetry has been also carried out. The optimal array configuration is generally obtained through a compromise between the need of sampling coherent portions of wavefield and the need for adequate azimuthal resolution, which requires a large antenna aperture. However we were limited by the geometry of the underground laboratories, so we decided to start with 20 receivers. In consequence, the underground seismic array has a small aperture (400 m x 600 m) and the average spacing between the short period seismographs is about 90 m (Fig. 1), thus allowing to resolve wavelenghts in the range $180 - 500m$ which correspond to phase velocity $0.2 - 10\frac{km}{sec}$ (the frequency response is in the range $1 - 20Hz$). At present, we have completely developed the electronics and the data acquisition system, which constitute an original project. Each

seismometer is linked, through a 24 bits A/D board, to an industrial PC which is, in its turn, connected to a serial communication line via a RS-485 standard. The PCs placed at the head of each serial line (nodal PCs) transmit data to a server through an ethernet network. Time syncronization is provided by a Master Oscillator controlled by an atomic clock (Fig. 4). Earthworm package is used for real time data processing and transmission. High quality data have been recorded since May 2002, including local and regional earthquakes. In particular the 31 October, 2002, Molise ($M_W = 5.8$ earthquake) and its aftershocks have been recorded at this array. Array techniques such as polarization and frequency-slowness analyses with the ZLCC algorithm indicate the high performance of this array, as compared to the national seismic network, for analyzing the main source parameters of earthquakes located up to distances of few hundreds of km.

Figure 3: Underground Seismic Array components and control room.

Figure 4: The Underground Array seismic stations acquire data simultaneously. The time syncronization is controlled by a Master Oscillator: it takes a 1 pps input signal from an atomic clock located in the labs and generates codified time signals which are send to the single stations in order to provide simultaneous data acquisition.

3 Preliminary data analysis and results

3.1 Background noise features

Spectral analysis was done using Matlab. Spectrograms were calculated, over a 20 day time window (from jday 046 to jday 065, february 15 to march 6, 2005), on the motion vertical component, using 200 s sliding windows with 50% overlapping and a 0.2 Hz spectral smoothing. Spectra were then stacked on all the active stations. Following you can see a typical 24 hour (feb 22, 2005) spectrogram plot.
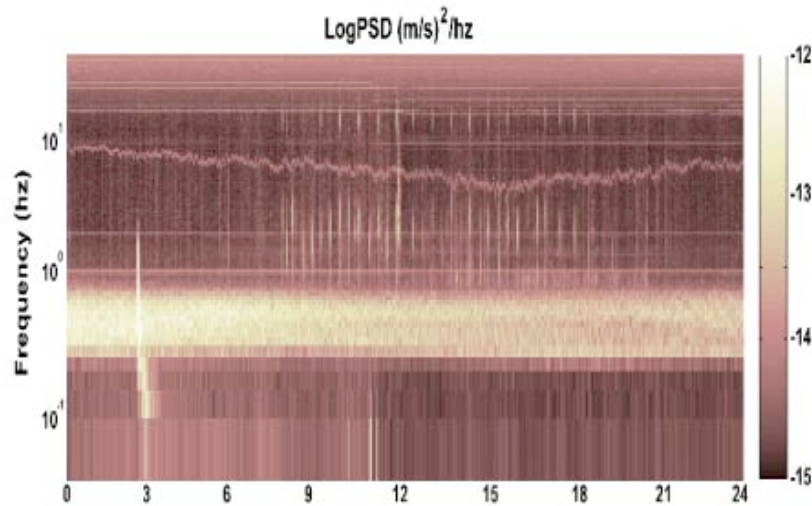
Figure 5: 24 hour (feb 22, 2005) spectrogram plot.

A spectrogram peak can be noted in the 0.4 - 1 Hz. The amplitude of this peak shows periodical variations: they are reasonably due to the sea action. With a quick look to the daily spectrogram plot (Fig. 5), an event can be observed at 02.30 (it is a magnitude 3.5 event). The 2 Hz events, occurring during the daily hours about every 20 minutes, are due to the LNGS shuttle service vehicles.

3.2   Noise spatial correlations at various frequency bands and at various spatial distances

Array background noise correlation calculus was performed, at various frequencies, using Matlab. The script reads files in Sac format, selects a 5 minutes time window for the computation, filters on a known frequency band and computes the correlation coefficient matrix using the *Corrcoef* matlab function. Then it iterates on all the frequency bands (included between 0 an 20 Hz) an on all the pairs of active stations. The analyzed frequency bands are 0.5 Hz wide and they slide with a 50% overlap every next iteration. Following, results obtained from the correlation analysis of a daily window (jday 047, february 15 2005, 10.10 GMT) and of a night window (jday 047, february 15 2005, 23.10 GMT) are showed. A strong noise correlation can be noted on frequencies up to about 2 Hz.
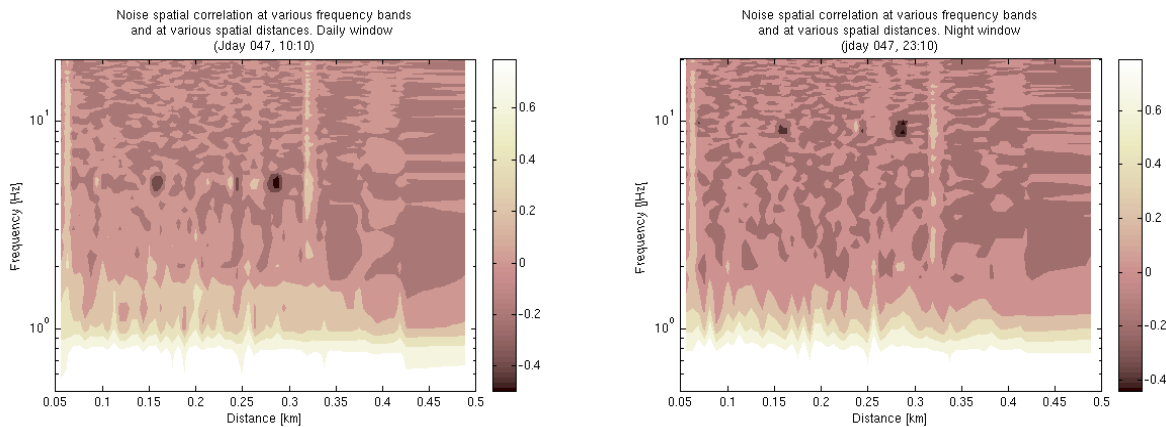
Figure 6: Noise spatial correlations at various frequency bands and at various spatial distances.

After the background noise spectral analysis (spectrograms) and the background noise correlation analysis at various frequencies and spatial distances, we decided to analyse the data (for an automatic selection of the earthqukes) in the 2 - 8 Hz frequency band.

3.3   Magnitude extimation

In order to obtain a correct magnitude extimation of the earthquakes recorded by the seismic array, we decided to use the following relation: $M = B \cdot LOG(d) + A$. The A and B parameters were computed using about 50 events of known magnitude between a minimum value of 1 and a maximum value of 5 (data from INGV bulletin) recorded by the array. The d parameter (event duration) was measured with SAC. These events were then plotted on a duration/magnitude picture and fitted with a logarithmic function (linear regression) in order to obtain a reasonable extimate of the A and B parameters. The results are showed in figure 7.
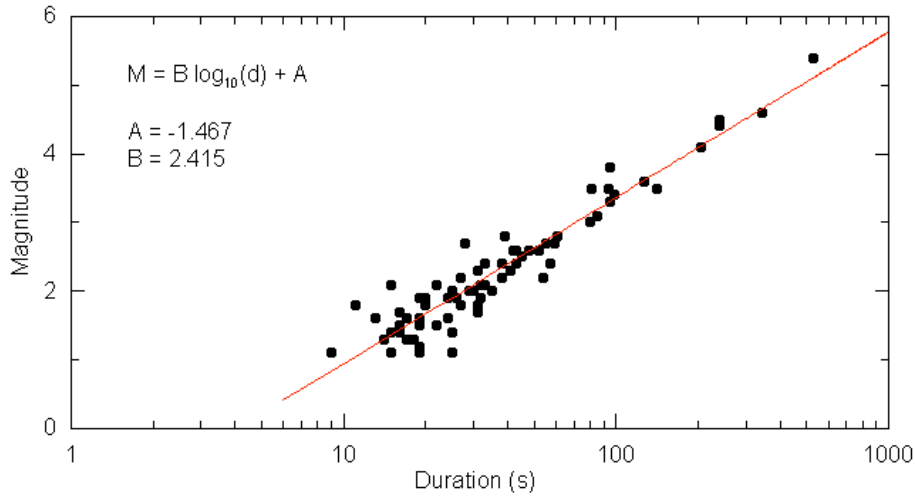
Figure 7: magnitude extimation with linear regression.

3.4   Array records

The following picture show magnitude/distance (from LNGS)/number of recorded events plot, for the Gran Sasso Underground Array, for the January-November 2005 period. Regarding the seismic array, about 460 events were recorded, and the best recording performances occur for events with magnitude between 1.7 and 2 at an epicentral distance between 20 and 30 km. Good performance occurs also for nearer (10 - 20 km) and low magnitude (1 - 1.5) earthquakes.
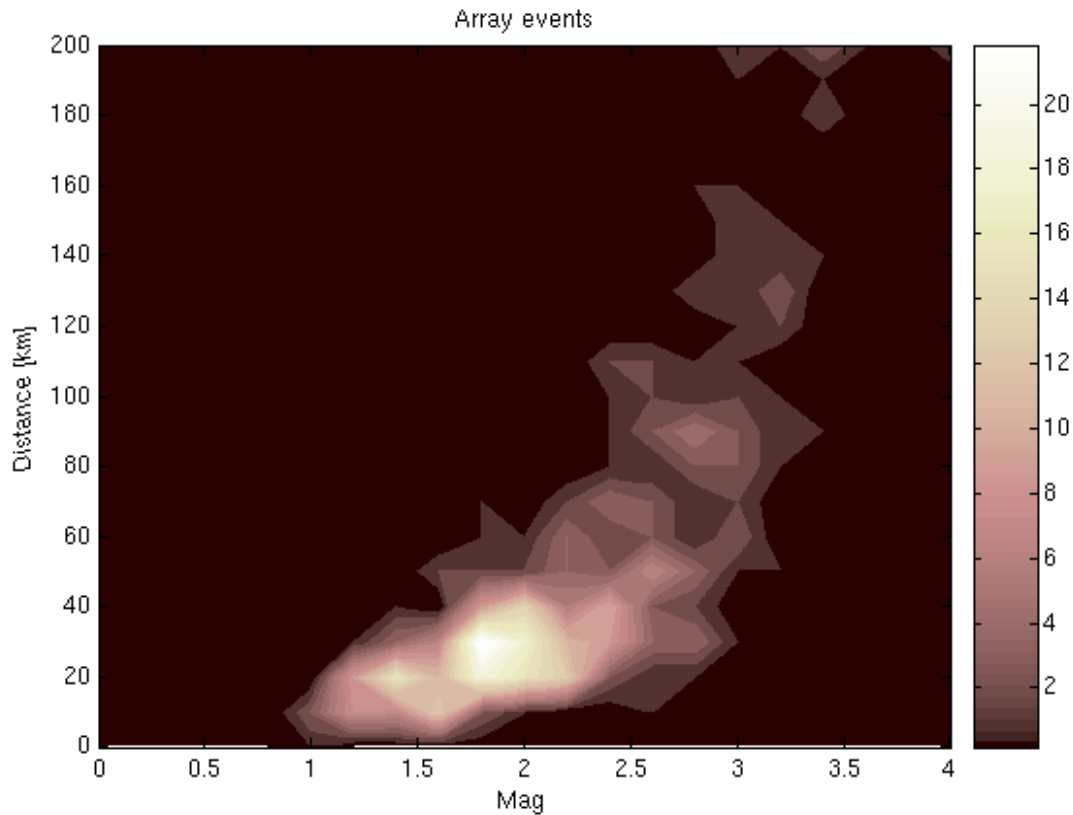
Figure 8: magnitude/distance (from LNGS)/number of recorded events plot.

4 Conclusions

The dense small-aperture seismic array is a powerful high-sensitivity instrument designed and presently under realization and installation. The underground location beneath Gran Sasso has been proved to be an ideal site, in spite of the local noise sources due to human activity, to record seismic waves from regional and local microearthquakes. Its location is rather unique in the world, due to the close distance from active fault segments of the seismogenetic zone of central Apennines. The scientific goals of this multichannel seismic observational system are an improvement of the seismotectonical knowledge of a high potential seismogenetic region of Italy, and a very detailed study of the physical processes leading to seismic ruptures in the area. Moreover the installation of this underground seismic array will allow an experimental study of wave propagation phenomena within a complex medium, leading to results of relevant interest for seismic hazard evaluation in areas of complex geology, for physics of earthquake process, with particular reference to the study of rupture preparation and for all relevant precursory phenomena, seismic radiation and earthquake waveform modeling for hazard reduction.

5 List of Publications

1. R. Scarpa, R. Muscente, F. Tronca, C. Fischione, P. Rotella, M. Abril, G. Alguacil, W. De Cesare, M. Martini. *Underseis: The Underground Seismic Array.* Seismological Research Letters. Vol. 75, number 4, July/August 1994.

References

[1] Agnew D. C., 1986. *Strainmeters and tiltmeters.* Rev. Geophys. 24, 579-624.

[2] Aki K. and Richards P., 1980. *Quantitative seismology: Theory and methods.* Freeman, San Francisco, California, 932 pp.

[3] Aki K., Christoffersson A. and Husebye E. S., 1977. *Determination of the three dimensional seismic structure of the lithosphere.* J. Geophys. Res. 82, 277-296.

[4] Benioff H., 1935. *A linear strain seismographs.* Bull. Seism. Soc. Am. 25, 283-309.

[5] Bolt B. A., 1976. *Nuclear explosions and earthquakes. The parted veil.* Freeman, San Francisco.

[6] Capon J., 1969. *High resolution frequency-wavenumber spectrum analysis.* Proc. IEEE 57, 1408-1418.

[7] Chouet B., 1996. *New methods and future trends in seismological volcano monitoring.* In "Monitoring and mitigation of volcano hazards", R. Scarpa and R. Tilling (Eds.), Springer-Verlag, New York.

[8] Chouet B., G. Saccorotti, M. Martini, P. Dawson, G. De Luca, G. Milana and R. Scarpa (1997). *Source and path effects in the wavefields of tremar and explosions at Stromboli Volcano, Italy.* J. Geophys. Res., 102, 15,129-15,150.

[9] De Luca G., Scarpa R., Del Pezzo E. and Simini M., 1997. *Shallow structure of Mt. Vesuvius volcano, Italy, from seismic array analysis.* Geophys. Res. Lett. 24,481-484.

[10] De Luca G., Del Pezzo E., Di Luccio F., Margheriti L., Milana G. and Scarpa R., 1998. *Site response study in Abruzzo (centraI Italy): underground array versus surface stations.* J. Seismol., 2, 223-226.

[11] Farrell W. E., 1969. *A gyroscopic seismometer: measurements during the Borrego earthquake.* Bull. Seism. Soc. Am. 59, 1239-1245.

[12] Green Jr., Frosh B. A. and Romney C. F., 1965. *Principles of an experimental large aperture seismic array.* Proc. IEEE 53, 1821-1833.

[13] Kedrov O. K. and V. M. Ovtchinnikov, 1990. *An on-line analysis system for three component seismic data: method and preliminary results.* Bull. Seism. Soc. Am. 80, 2053-2071.

[14] Lee W. H. K. and Stewart S. W., 1981. *Principles and applications of microearthquake networks.* Academic Press, New York, 293 pp.

[15] Lay T. and Wallace T. C., 1995. *Modern Global Seismology.* Academic Press, New York, 517 pp.

[16] Mikkeltveit S., 1985. *A new regional array in Norway: design, work and results from analysis of data from a provisional installation, in The Vela Program.* A twenty- Five Review of Basic Research, edited by U. A. Kerr (Defence Advanced Research Project Agency), 546-553.

[17] Milana G., Barba S., Del Pezzo E. and Zambonelli E., 1996. *Site response from ambient noise measurements: new perspectives from an array study in CentraI Italy.* Bull. Seism. Soc. Am. 86, 1-9.

[18] Schmidt R. O., 1986. *Multiple emitter location and signal parameter estimation.* IEEE Trans Antennas Propagation 34, 276-280.

[19] Wielandt E., 1983. *Design principles of electronic inertial seismometers.* In H. Kanamori and E. Boschi (Eds.) ”Earthquakes: Observation, Theory and Interpretation”. Proc. Int. School of Phys. ”E. Fermi”, North Holland, Amsterdam.

First Monte Carlo Simulation of Double Beta Decay Tracks in a Ge Detector and their Dependence on Particle and Nuclear Physics Parameters

H.V. Klapdor-Kleingrothaus[a,d], I.V. Krivosheina[a,b], I.V. Titkova[a,c]

[a] Max-Planck Institut für Kernphysik, Heidelberg, Germany
[b] Institute of Radiophysical Research, Nishnij Novgorod, Russia
[c] Joint Institute of Nuclear Research, Dubna, Russia
[d] Spokesman of the Collaboration; E-mail: H.Klapdor@mpi-hd.mpg.de
Home-page: http://www.mpi-hd.mpg.de.non_acc/

Abstract

The sizes of tracks of events of neutrinoless double beta decay in a Germanium detector depend on particle physics and nuclear physics parameters such as neutrino mass, right-handed current parameters, etc., and nuclear matrix elements. The knowledge of this dependence is of importance, since the key to probe the existence of $0\nu\beta\beta$ decay *beyond* observation of a signal at the Q value of the process, $Q_{\beta\beta}$, is the discrimination of $\beta\beta$ events from background γ events (or other events), in almost *any* double beta decay experiment (see [3]). We have performed (see [1, 2]) for the first time Monte Carlo simulations of neutrino-accompanied ($2\nu\beta\beta$) and neutrinoless double beta decay ($0\nu\beta\beta$) events, and of various kinds of background processes such as multiple and other γ interactions for a Ge detector. The time history of the evolution of the individual events is followed and a systematic study has been performed of the sizes of the events (volumes in the detector inside which the energy of the event is released which determine the observed signals). Effects of the angular correlations of the two electrons in $\beta\beta$ decay, which again depend on the above nuclear and (for $0\nu\beta\beta$ decay) particle physics parameters, are taken into account and have been calculated for this purpose for ^{76}Ge for the first time on basis of the experimental half-life and of realistic nuclear matrix elements. The potential of future experiments with respect to determination of the particle physics parameters $\langle m_\nu \rangle, \langle \lambda \rangle, \langle \eta \rangle$ is briefly discussed.

1 Introduction

The question whether neutrinos are massive or massless has become one of the most important topics of particle physics and astrophysics. For massive neutrinos there arises

the even more fundamental question whether they are Dirac or Majorana particles. In *models* like SO(10), and most other GUT models, neutrinos *are* Majorana particles. The $\beta\beta$ decay is probably the only process which can decide directly the Dirac or Majorana nature of the neutrinos. The main two decay modes are: the neutrino accompanied - mode ($2\nu\beta\beta$), allowed in the Standard Model,

$$N_A(A, Z) \rightarrow N_B(A, Z+2) + 2e^- + 2\tilde{\nu}_e, \tag{1}$$

and the neutrinoless mode ($0\nu\beta\beta$), which cannot occur in the Standard Model, since it violates total lepton number by $\Delta L = 2$,

$$N_A(A, Z) \rightarrow N_B(A, Z+2) + 2e^-. \tag{2}$$

The $0\nu\beta\beta$ mode can occur only when neutrinos are Majorana particles and have a non-vanishing mass (see, e.g. [25, 21, 24, 19]).

The most sensitive double beta decay experiment over the last 13 years already, is the HEIDELBERG-MOSCOW experiment [5] using High Purity Ge detectors enriched in the double beta emitter ^{76}Ge to 86%. This experiment has reported evidence for this decay mode on a 4.2σ level [3, 4].

The first proof for observation of this rare process in a $\beta\beta$ experiment is *to find a line at the right energy* - $Q_{\beta\beta}$. A *further* proof is to show that this line is mostly consisting of $e^- e^-$ events and *not* of γ events, to rule out that one just has found a new γ -line. For this proof one has to discriminate single-site events (SSE) against multiple-site events (MSE) in the germanium crystal (see [3]). Double beta events are overwhelmingly SSE, i.e, events confined to a few mm region in the detector. SSE can *also* be produced by γ -rays in *single*-Compton scattering, photoelectric interactions, or multiple-site interactions within a small distinct region. MSE result from multiple-Compton scattering, and single-Compton scattering plus photoelectric absorption of photons taking place at some distance from the single-Compton scattering.

The discrimination of SSE and MSE events seems to be the *key to* prove the existence of neutrinoless $\beta\beta$ decay, since experiments looking for the *tracks* of the electrons unfortunately are not feasible like EXO with *liquid xenon* [7], or not sensitive enough like (Super)NEMO (see [6, 8]). Other experiments like CUORICINO/CUORE [9] have *in general* unfortunately no way to distinguish between β and γ events by pulse shape, however, may benefit from detector modularity to reject part of the Compton γ background.

We present here for the *first time* (see [1, 2]), a systematic Monte Carlo study of the sizes of events in Ge detectors (i.e. the partial volume in the detector, in which the energy is released) for double beta events (2ν and 0ν processes) including effects of the angular correlations of the two emitted electrons which again depend on particle (for $0\nu\beta\beta$) and nuclear structure parameters of these processes, and also of various types of γ -events. The knowledge of the distribution of sizes of events is of central importance for a calculation of the pulse shapes produced by the events in the detectors, and subsequent pulse shape analysis of measured $\beta\beta$ spectra, aiming at discrimination of $\beta\beta$ and γ events and determination of the spatial locations of individual events in the detectors (see [3, 10]).

The results obtained for the spectral-angular distributions for the neutrino-accompanied and neutrinoless $\beta\beta$ decay are given in Section 2. In Section 3 the results of the

Monte Carlo simulations of event sizes are given for $\beta\beta$ events, γ -Compton-scattering, single escape, double escape events and events with full energy, deposited in the detector. Some conclusions are presented in Section 4.

2 Spectral-Angular Correlations for the $2\nu\beta\beta$ and $0\nu\beta\beta$ decay for the $0^+ \to 0^+$ transition

2.1 $2\nu\beta\beta$ Decay

Formalism: In the $0^+ \to 0^+$ transition the emitted electrons are in the S-wave state and P-wave state with j=1/2. The half-life of the $0^+ \to 0^+$ transition in the $2\nu\beta\beta$ mode is expressed as [18, 17, 22, 19]

$$[T_{2\nu}(0^+ \to 0^+)]^{-1} = \left| \frac{M_{GT}^{2\nu}}{\mu_0} \right|^2 G_{GT}, \tag{3}$$

where G_{GT} is the phase space factor:

$$G_{GT} = g_0 \int d\Omega_{2\nu} a(\epsilon_1\epsilon_2)[\langle\mu_a\rangle(\langle K_a\rangle + \langle L_a\rangle)/2]^2. \tag{4}$$

The first factor in equation (3) is related to the reduced nuclear matrix elements of the double Gamow-Teller (nuclear spin flip) transitions by the following definition:

$$\left(\frac{M_{GT}^{2\nu}}{\mu_0} \right) = \sum_a \left(\frac{M_{GTa}^{2\nu}}{\mu_a} \right), \tag{5}$$

where $\sum_a$ means the sum over nuclear states E_a in the intermediate nucleus and

$$\mu_a m_e = E_a - \frac{M_i + M_f}{2}, \tag{6}$$

m_e, M_i and M_f denote masses of electron, parent and daughter nuclei, respectively. In the factor G_{GT} in eq. (4), $g_0 = 3.78 \cdot 10^{-24} \cdot g_A^4 \ yr^{-1}$ (we take $g_A = 1.254$).

The $\langle K_a \rangle$ and $\langle L_a \rangle$ in eq. (4) come from the intermediate energy denominators due to the second-order perturbation, and are defined as

$$\langle K_a \rangle = \frac{2\langle\mu_a\rangle}{\langle\mu_a\rangle^2 - K_D^2}, \qquad \langle L_a \rangle = \frac{2\langle\mu_a\rangle}{\langle\mu_a\rangle^2 - L_D^2}, \tag{7}$$

where $\langle\mu_a\rangle$ is some average of μ_a in eq. (5) and

$$K_D = \frac{\epsilon_1 + w_1 - \epsilon_2 - w_2}{2m_e}, \qquad L_D = \frac{\epsilon_1 - w_1 - \epsilon_2 + w_2}{2m_e}. \tag{8}$$

The replacement of μ_a by $\langle\mu_a\rangle$ means to introduce an approximation into the exact formula. The reliability of this approximation is discussed in [18].

Including explicitly the angular correlation between the emitted electrons, it is found (see [16, 17, 18, 22]), that $\frac{d^3\Gamma}{dT_1 dT_2 dcos\theta} = A \cdot (1 + T_1)^2(1 + T_2)^2(T - T_1 - T_2)^5 \times$

$$\times \ h_{2\nu}(T_1, T_2) d_0(T_1) d_0(T_2) \left[1 - \frac{\sqrt{T_1 T_2(T_1 + 2)(T_2 + 2)}}{(T_1 + 1)(T_2 + 1)} \cdot cos\theta \right], \tag{9}$$

$$A = \left| \frac{M_{GT}}{\mu_0} \right|^2 g_0 (2\pi\alpha Z)^2, \qquad d_0(T_i) = \left[1 - exp(-\frac{2\pi\alpha Z(T_i+1)}{\sqrt{T_i(T_i+2)}}) \right],$$

where $T_j m_e = \epsilon_j - m_e$ is the kinetic energy of the j-th electron, T stands for the maximum kinetic energy release, $T m_e = M_i - M_f - 2m_e$ and α is the fine structure constant. The factor $h_{2\nu}(T_1, T_2)$ related to the energy denominator is defined as

$$h_{2\nu}(T_1, T_2) = \frac{30}{4} \cdot \frac{\langle \mu_a \rangle^2}{w^5} \int_0^w dw_1 w_1^2 (w - w_1)^2 H_1, \qquad (10)$$

where $w = (T - T_1 - T_2) \cdot m_e$. The constant factor comes from the normalization $\lim_{\langle \mu_a \rangle \to \infty} h_{2\nu}(T_1, T_2) = 1$. The factor H_1 is $H_1 = [\frac{\langle K_a \rangle + \langle L_a \rangle}{2}]^2$, where $\langle K_a \rangle, \langle L_a \rangle$ are defined in eq. (7). In eq. (8) K_D and L_D are expressed as

$$K_D = [2T_1 - T + 2w_1/m_e]/2, \qquad L_D = -[2T_2 - T + 2w_1/m_e]/2. \qquad (11)$$

The nuclear *matrix element* $|\frac{M_{GT}^{2\nu}}{\mu_0}|$ *is taken* in this paper *from the experimentally determined half-life for* ^{76}Ge *of* $T_{2\nu} = 1.74 \cdot 10^{21} yr$ [11, 12]. The phase-space factor was taken from [23], $G_{GT} = 1.317 \times 10^{-19}$. Then the first factor in eq. (3) is $|\frac{M_{GT}^{2\nu}}{\mu_0}| = 0.0661$. According to [17], for ^{76}Ge $\langle \mu_a \rangle = 18.42$.

Results: The angular correlations for the single electron spectrum calculated for the above parameters for ^{76}Ge is presented in Fig. 1. The electrons are predominantly emitted in back to back direction.
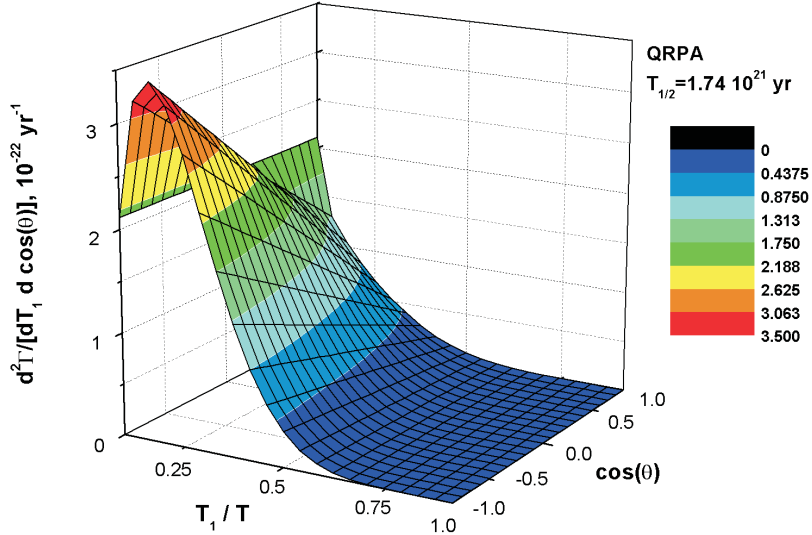
Figure 1: Calculated angular correlations of the single electron spectrum for the $0^+ \to 0^+$ transition for the $2\nu\beta\beta$ mode for ^{76}Ge.

Formalism: The half-life formula is [17, 19, 22]

$$[T_{0\nu}]^{-1} = C_{mm}\left(\frac{\langle m_\nu\rangle}{m_e}\right)^2 + C_{m\lambda}\left(\frac{\langle m_\nu\rangle}{m_e}\right)\langle\lambda\rangle + C_{m\eta}\left(\frac{\langle m_\nu\rangle}{m_e}\right)\langle\eta\rangle + \tag{12}$$

$$+C_{\lambda\lambda}\langle\lambda\rangle^2 + C_{\eta\eta}\langle\eta\rangle^2 + C_{\lambda\eta}\langle\lambda\rangle\langle\eta\rangle,$$

where the C_{ij} are products of matrix elements and phase space integrals for the terms coming from the effective neutrino mass $\langle m\rangle = \sum_j m_j U_{ej}^2$, and from effective right-handed current parameters $\langle\eta\rangle = \eta\sum_j U_{ej}V_{ij}$ and $\langle\lambda\rangle = \lambda\sum_j U_{ej}V_{ij}$.

For the matrix elements see below. For the phase space integrals G_i we calculated, following [19, 23]:

$$G_1 = 6.895\cdot 10^{-15}, \quad G_2 = 1.110\cdot 10^{-14}, \quad G_3 = 3.823\cdot 10^{-15}, \quad G_4 = 1.337\cdot 10^{-15},$$

$$G_5 = 2.082\cdot 10^{-13}, \quad G_6 = 1.592\cdot 10^{-12}, \quad G_7 = 9.839\cdot 10^{-11}, \quad G_8 = 6.470\cdot 10^{-12},$$

$$G_9 = 3.586\cdot 10^{-10}. \tag{13}$$

Since the 0ν mode contains various contributions from the neutrino mass part and V+A part, the single electron kinetic energy spectrum and the angular correlations are rather complicated. The differential decay rate can be written as [18, 17, 22, 16]:

$$\frac{d^2\Gamma_{0\nu}}{dT_1 d\cos\theta} = |M_{GT}|^2 N_{0\nu}(A_{0\nu}(0) + B_{0\nu}(0)\cos\theta), \quad \begin{pmatrix}A_{0\nu}(0)\\B_{0\nu}(0)\end{pmatrix} = (T_1+1)^{2\gamma_1}(T_2+1)^{2\gamma_1} d_{00}\begin{pmatrix}A_0'\\B_0'\end{pmatrix},$$

$$A_0' = C_1\left(\frac{\langle m_\nu\rangle}{m_e}\right)^2 + C_2\langle\lambda\rangle\frac{\langle m_\nu\rangle}{m_e}\cos\Psi_1 + C_3\langle\eta\rangle\frac{\langle m_\nu\rangle}{m_e}\cos\Psi_2 + C_4\langle\lambda\rangle^2 + C_5\langle\eta\rangle^2 + \tag{14}$$

$$+C_6\langle\lambda\rangle\langle\eta\rangle\cos(\Psi_1 - \Psi_2), \qquad B_0' = \frac{p_1 p_2}{\epsilon_1 \epsilon_2}[C_1'\left(\frac{\langle m_\nu\rangle}{m_e}\right)^2 + C_2'\langle\lambda\rangle\frac{\langle m_\nu\rangle}{m_e}\cos\Psi_1 +$$

$$+C_3'\langle\eta\rangle\frac{\langle m_\nu\rangle}{m_e}\cos\Psi_2 + C_4'\langle\lambda\rangle^2 + C_5'\langle\eta\rangle^2 + C_6'\langle\lambda\rangle\langle\eta\rangle\cos(\Psi_1 - \Psi_2)]$$

In eq. (14) $T_2 = T - T_1$, and Ψ_1, Ψ_2 are the CP phases. As we assumed CP conservation, $\Psi_1 = \Psi_2 = 0$ or π. The structure of the coefficients C_i of the spectrum part and the C_i' of the angular part of the expression (14) can be found in [18, 16, 17, 22]. Some general discussion of the shapes of the spectra and angular correlations for the $\langle m_\nu\rangle^2, \langle\lambda\rangle^2, \langle\eta\rangle^2$ parts in expression (14) is already given in [16, 17, 22, 15].

In the next subsection we investigate in detail the case of ^{76}Ge decay exploiting *the present knowledge of the experimental half-life and using realistic matrix elements.*

Spectral angular distributions for the $0\nu\beta\beta$ decay of ^{76}Ge: The angular correlations of the electrons in $0\nu\beta\beta$ decay of ^{76}Ge required for the Monte Carlo calculation of the tracks in the detector are calculated here using the values of the matrix elements from the proton-neutron quasiparticle random phase approximation (QRPA) [20, 28]. The nine matrix elements required for the calculations are shown in Table 1. They enter into the factors C, C' in eqs. (12,14).

Table 1: Nuclear matrix elements of the neutrinoless double-beta decay of ^{76}Ge calculated by QRPA [28]. Here $\chi_\alpha = \frac{M_\alpha}{M_{GT}}$.

M_{GT}	χ_F	χ_{GTW}	χ_{FW}	χ_{GTq}	χ_{Fq}	χ_T	χ_P	χ_R
3.01	-0.39	0.97	-0.34	0.65	-0.35	-0.20	-0.18	1.19

The QRPA calculation [28] yields the best *prediction* of the matrix element of $2\nu\beta\beta$ decay of ^{76}Ge *which was not yet measured at the time of that calculation* (deviation from the later experiment [11, 12] *only* 29%).

With the matrix elements of Table 1 we find from the experimental half-life $T_{1/2} = 1.19 \cdot 10^{25}$ yr [3] the constraints on the effective neutrino mass and on the two parameters of the right-handed current contributions shown in Fig. 2. The allowed ranges lie *inside* the curves. Under the purely phenomenological condition that only one of the terms contributes (this assumption is often made in analysis of $\beta\beta$ experiments), we find,

$$\langle m_\nu \rangle = 0.4264 \, eV, \qquad \langle \lambda \rangle = 0, \qquad \langle \eta \rangle = 0 \ ;$$

$$\langle m_\nu \rangle = 0 \, eV, \qquad \langle \lambda \rangle = 9.509 \cdot 10^{-7}, \qquad \langle \eta \rangle = 0 \ ; \qquad (15)$$

$$\langle m_\nu \rangle = 0 \, eV, \qquad \langle \lambda \rangle = 0, \qquad \langle \eta \rangle = 4.187 \cdot 10^{-9}.$$
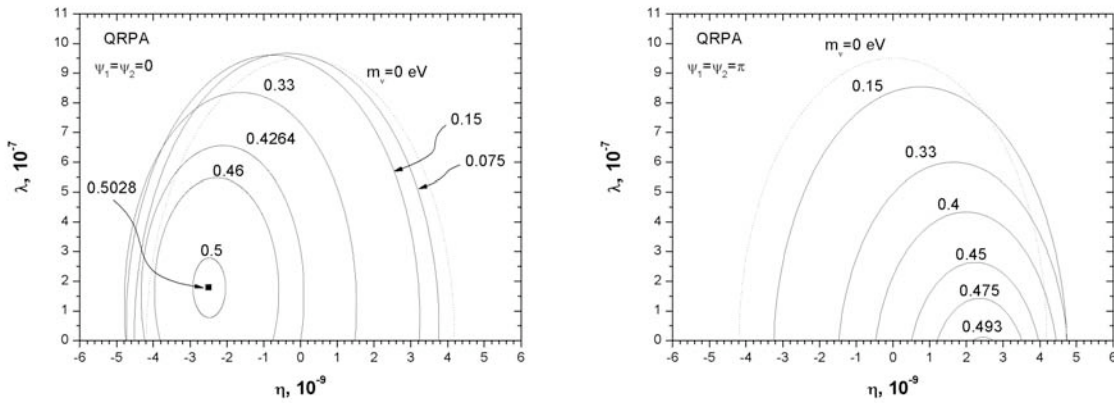
Figure 2: Allowed parameters for $\langle m_\nu \rangle$, $\langle \lambda \rangle$, $\langle \eta \rangle$ from the measured half-life of $0\nu\beta\beta$ decay of ^{76}Ge [3] according to analysis with QRPA [28] (Table 1) for CP parities $\psi_1 = \psi_2 = 0$ (left) and $\psi_1 = \psi_2 = \pi$ (right).

In the frame of Grand Unified Models the terms are *not* independent, and a right-handed current contribution can occur *only*, when the neutrino has a *finite* (Majorana) mass (see [31, 32, 21]).

The maximum value of $\langle m_\nu \rangle$ is obtained to be (see Fig. 2)

$$\langle m_\nu \rangle = 0.5028 \, eV, \quad with \quad \langle \lambda \rangle = 1.793 \cdot 10^{-7}, \quad \langle \eta \rangle = -2.495 \cdot 10^{-9}. \qquad (16)$$

The corresponding values for the half-lives $T_{1/2}^{0\nu} = 0.69$ and $4.18 \cdot 10^{25}$ yr (3σ allowed range according to [3]) are

$$\langle m_\nu \rangle = 0.66\,eV, \qquad \langle \lambda \rangle = 2.36 \cdot 10^{-7}, \qquad \langle \eta \rangle = -3.28 \cdot 10^{-9}$$

$$\langle m_\nu \rangle = 0.23\,eV, \qquad \langle \lambda \rangle = 9.59 \cdot 10^{-8}, \qquad \langle \eta \rangle = -1.33 \cdot 10^{-9}. \qquad (17)$$

The values for $\langle m_\nu \rangle$ could be somewhat, up to $\sim 30\%$, *lower* then deduced above, when considering that the $0\nu\beta\beta$ matrix element may be slightly underestimated, as the $2\nu\beta\beta$ matrix element (see above). As obvious from Fig. 2, the experiment gives *very sharp limits* for the right-handed current contributions η, λ in addition to the effective neutrino mass.

The spectral-angular distributions for the sets of parameters eqs. (15,16) are shown in Figs. 3,4.
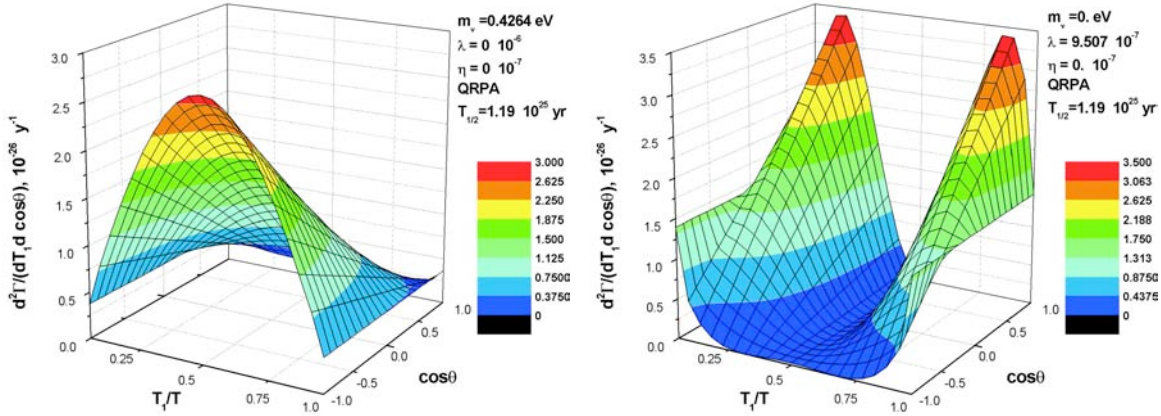
Figure 3: Calculated spectral angular correlation for the neutrino mass term for $0\nu\beta\beta$ decay of ^{76}Ge (left), and for the $\langle \lambda \rangle^2$ - term (right).

When *only* the neutrino mass term is considered, both electrons are emitted from the V-A vertex, so that their main helicities are the same. Due to the angular momentum conservation in the plane made of two electrons, two S-wave electrons should be emitted predominantly in the *back to back* configuration for the $0^+ \rightarrow 0^+$ transition (Fig. 3-left). For the V+A part, one electron is emitted from the V-A vertex and the other is from the V+A vertex, and thus their main helicities are opposite. Therefore, two electrons with $j = 1/2$ are emitted mostly in the same directions (Figs. 3-right and 4-left). When all three parameters are nonzero the situation may be different. For a 'large' neutrino mass the mass term plays the main role, the electrons are emitted in opposite directions (Fig. 4-right). But, for example, for the values $\langle m_\nu \rangle = 0.33$ eV, $\langle \lambda \rangle = 4.953 \cdot 10^{-7}$, $\langle \eta \rangle = 0$, which are *also* consistent with the experiment (see Fig. 2), the role of the mass term and the roles of right-handed parameters are approximately equal (Fig. 5). In this case the electrons can be emitted in opposite directions with energies equalling to half of the total kinetic energy or in the same directions with energies 15%/85% of the total kinetic energy. This shows that the shapes of the angular correlations can vary considerably within the 3σ-allowed range of parameters fixed by experiment.
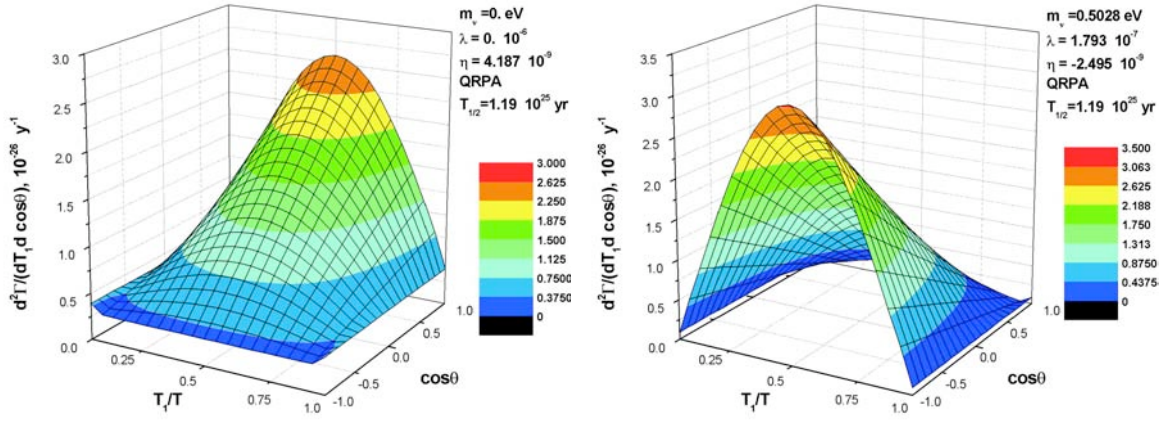
Figure 4: Calculated spectral angular distribution for the $\langle\eta\rangle^2$ -term for $0\nu\beta\beta$ decay of ^{76}Ge (left), and for the values $\langle m_\nu\rangle = 0.5028\,\mathrm{eV}$, $\langle\lambda\rangle = 1.793 \cdot 10^{-7}$, $\langle\eta\rangle$ = -2.495 $\cdot$ 10^{-9} (right).

We considered also other models of QRPA. Taking into account only the mass term from eq. (12), the kinematical factor G_1 eq. (13) and recent results for matrix elements published in [29] for different expansions of the QRPA nuclear model we calculated the effective neutrino mass, again starting from the experimental half-life $T^{0\nu}_{1/2} = 1.19 \cdot 10^{25}\,\mathrm{y}$ [3]. The deduced values are very close to the ones given above (see [14, 29]).

For some demonstration of the sensitivity of the calculated angular correlations to the chosen nuclear model also calculations for the very simple shell model (SM) [27], and for the VAMPIR approach [26] have been performed [14]. The results obtained in these models are very similar to the QRPA results.

3 Monte-Carlo Simulations of Tracks and Sizes of $\beta\beta$ and Gamma Events in the Ge Detector

The $\beta\beta$ decay, and photon interactions in a Ge detector, including photoelectric absorption, Compton scattering and pair-production result in fast electrons that lose energy via Compton interactions in the germanium crystal and via bremstrahlung. The produced free electrons and holes drift in opposite directions along the electric field created by the reverse bias voltage applied to p-type Ge detector. This charge separation and drift induces an image current on the electrodes. When these charge carriers reach the electrodes, they are collected and no longer contribute to the current. The total energy deposited is proportional to the charge obtained by integrating this current over time. The shape of the induced current pulse depends only on the electric field inside the detector, the position and *size* (i.e distribution of the energy depositions) and the effects of external electronics.

Calculations were made for 2ν and $0\nu\beta\beta$ events from the decay of ^{76}Ge, and for photon events from nuclear transitions 2614 keV, 2204 keV and 1620 keV, for the size of single- and double-escape (SE and DE) events for the lines 2614 keV and 2204 keV, respectively,
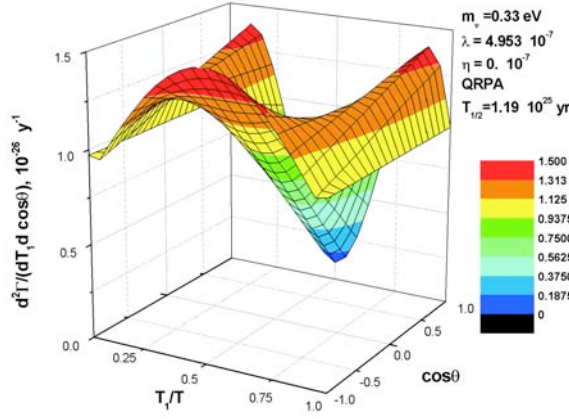
Figure 5: Calculated spectral angular distribution for the parameters $\langle m_\nu \rangle = 0.33\,\text{eV}$, $\langle \lambda \rangle = 4.953 \cdot 10^{-7}$, $\langle \eta \rangle = 0$, for $0\nu\beta\beta$ decay of ^{76}Ge.

and for the size of events in the energy range 2035-2043 keV ($Q_{\beta\beta}$= 2039 keV) resulting by Compton scattering from transitions 2614 keV and 2204 keV, for one of the enriched detectors of the HEIDELBERG-MOSCOW experiment, which is a coaxial p-type HP Ge detector of about 2.7 kg active mass.

The γ -events were started from an imaginary source *outside* the detector. The geometry of the detector was taken from [12]. While the location and energy depositions for photon events are determined by a standard Monte-Carlo photon routine (GEANT 4 [13]), both modes of $\beta\beta$ decay could not be simulated in the GEANT 4 code directly. For the simulation the following model has been used: the two electrons were started at a defined point *in* the detector, the energy, and the angle between the directions of their impulses were defined according to the *spectral-angular distributions of the emitted electrons* calculated in the previous section. Then the history of the events was determined by the Monte-Carlo procedure.

3.1 Calculation of $2\nu\beta\beta$ and $0\nu\beta\beta$ Event Histories:

For the calculation of the neutrino-accompanied mode of $\beta\beta$ decay we choose two cases for the total kinetic energy release from the spectrum: a point with energy 700 keV (near maximum of the spectrum at 673 keV) and the point with 2000 keV (near $Q_{\beta\beta}$). The energy distribution and angle between the two electrons were chosen according to the results shown in Fig. 1 (approximately 0.1T for one electron and 0.9T for another, the angle between the directions of their impulses was 180°). For the calculation of the $0\nu\beta\beta$ events the three cases in eq. (15) were considered according to the main features of the calculated angular distributions:

1. At first two electrons with energy 1020 keV each, were started at a given point in the detector. The angle between the directions of their impulses was 180° (only the neutrino mass part for the spectral-angular distribution was taken into account, see Fig. 3-left, but also Fig. 4-right).

87

2. Then the calculations were made for the case when the $\langle\lambda\rangle$ parameter is nonzero. The directions of the electrons were the same and the energy distribution according to the results shown in Fig. 3-right (approximately 0.15 T for one electron and 0.85 T for the other).

3. For the case when only the η term is nonzero (Fig. 4-left), the electrons were emitted to the same direction with half of the total kinetic energy each.

Then the time history of subsequent scattering or absorption events were calculated. The values of the energy depositions and coordinates of each interaction in the decay processes were written in data files. For the neutrino-accompanied mode in total 99606 events were calculated with full energy of 700 keV, and 95818 events for 2000 keV. For the $0\nu\beta\beta$ mode, in the first case, when only the mass term is taken into account, in
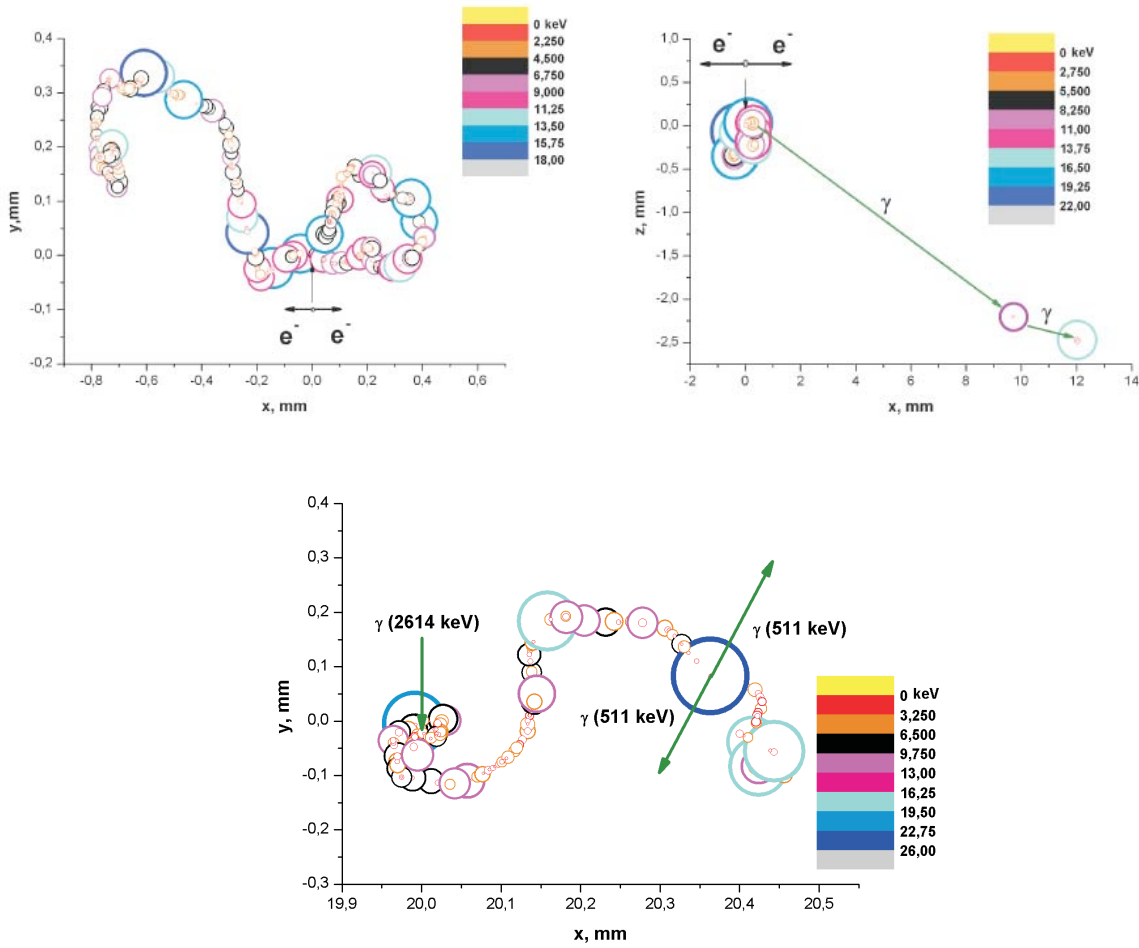
Figure 6: Upper part: Typical calculated event for $0\nu\beta\beta$ decay without photon emission (bremsstrahlung) (left), and with photon emission (bremsstrahlung) (right). Low part: Calculated photon event (the energy of the initial photon is 2614 keV) for the double escape case (leading to a line in the detector at 1592 keV) (see text).

total 96820 $\beta\beta$ events were calculated. For the second and third cases of spectral-angular distributions in total 95902 and 97768 events were considered, respectively.

Some examples of calculated tracks are presented in Fig. 6. The places of the energy depositions in germanium are indicated as circles. The sizes and colours of these circles indicate the amount of energy released at these points. Green lines denote γ -events (bremsstrahlung) in case of $\beta\beta$ decay, annihilation gammas in case of absorption of a γ by pair creation, all other events are electron (positron)-electron scattering.

Fig. 7 shows the calculated energy spectrum of $0\nu\beta\beta$ decay for the first case of $\beta\beta$ - events (mass term non-zero, right-handed current parameters zero). The sum energy of the electrons is shown on the x-axis. Most events lie in the sharp main peak at $Q_{\beta\beta}$ (2039 keV). The broad peak around 1850 keV corresponds to events with bremstrahlung emission. In total 94% of the $0\nu\beta\beta$ events are seen in the peak at $Q_{\beta\beta}$.
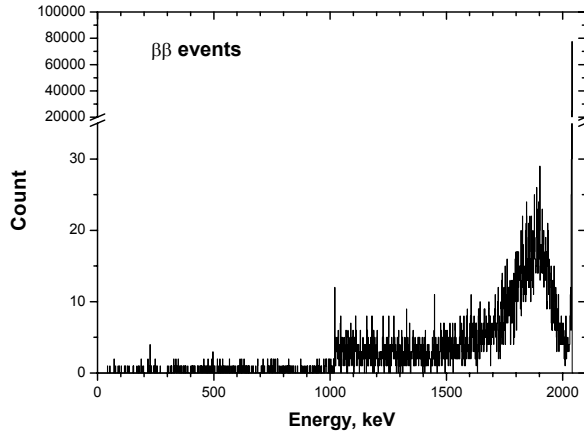
Figure 7: The Monte Carlo calculated energy spectrum of $0\nu\beta\beta$ decay of ^{76}Ge as seen in an enriched ^{76}Ge detector. The sum of the energies of the emitted electrons is shown on the x-axis.

3.2 Calculation of Photon Events:

For the calculations of photon events the imaginary point source of the photons with energy 2614 keV/2204 keV/1620 keV was put on the top part of the detector at a radius of 20 mm. The distance between top part of detector and source of the photons was 100 mm (the thickness of the lead collimator). The diameter of the hole in the collimator was 2 mm. For our investigations only events were considered which passed through the collimator without scattering in the lead. For the photon events the statistics was the following: 299365 photon events with initial energy 2614 keV, 298427 events with energy 2204 keV and 104193 events with 1620 keV were calculated. Fig. 6-(bottom) shows an example of a photon event in the detector. In the spectrum seen in the detector according to the Monte Carlo simulation of the 2614 keV γ -transition, besides the full energy peak at 2614 keV the single escape (SE) and double escape (DE) peaks occur (at 2103 and

1592 keV, respectively), resulting from absorption of the 2614 keV γ -quant by e^+e^- pair creation and subsequent annihilation of the positron with an electron and emission of two 511 keV γ -quanta, of which one (SE) or both (DE) escape from the detector (see for example Fig.7 in [3] from [30]).

3.3 Sizes of Events:

The sizes of individual events such as shown in Fig. 6 were defined in two different ways The *linear size* was calculated as the maximum distance between places of energy depositions without paying attention to the values of the latter:

$$R_l = max[\sqrt{(x_i - x_j)^2 + (y_i - y_j)^2 + (z_i - z_j)^2}]. \tag{18}$$

In the definition of the 'weighted' size the values of energy deposited in each point of interaction were taken into account:

$$R_W = \frac{\sum_{i,j} \epsilon_i \epsilon_j \sqrt{(x_i - x_j)^2 + (y_i - y_j)^2 + (z_i - z_j)^2}}{\epsilon^2_{total}}, \tag{19}$$

where ϵ_{total} is the full energy, deposited for this event in the detector. While naturally in the first case in a range of diameter R_l 100% of the released energy is contained, in the 'weighted' case a volume with diameter R_w contains typically about 60% of the total released energy.

In the analysis of sizes of events the cases 1-3 of subsection 3.1 were considered for $0\nu\beta\beta$ decay. For $2\nu\beta\beta$ decay two energies were considered (700 and 2000 keV). For photon events four energy regions were considered: Compton scattering in the energy region (2035-2043 keV), double escape (DE) region, single escape (SE) region and the main line (full energy peak). In our calculations for these energy regions the following statistics was obtained:

a) For 2614 keV: for Compton-scattering in the energy range 2035 - 2043 keV - 921 events, for the SE line - 5382 events, for the DE line - 1249 events, for the main line - 66024 events.

b) For 2204 keV: for Compton-scattering in energy range 2035 - 2043 keV - 1167 events, for the SE line - 3389 events, for the DE line - 816 events, for the main line - 72466 events.

c) For 1620 keV: for the main line - 28651 events.

The results of the calculations for 'linear' and 'weighted' event sizes are presented in Fig. 8. It is clear that 95% of $0\nu\beta\beta$ events lie within a distance of 2 mm for calculations of the 'weighted' size eq. (19) and 85% events for calculations of the 'linear' events size eq. (18). For the Compton-scattering region around $Q_{\beta\beta}$ (2035 - 2043 keV) for 'weighted' and 'linear' sizes definition only 50% and 25% of events, respectively, lie within this distance (and only 10% within $R_l = 1.4$ mm in contrast to 80% of the $0\nu\beta\beta$ events). The parts of the SE and the main line within R = 2 mm are only 20% and 25% for the 'weighted' sizes and a few percent for the 'linear' sizes. All these latter three types of events are mainly MSE. The $\beta\beta$ events are mostly SSE and we can clearly distinguish them by size. The

90

situation with DE gamma events is different. Since the DE events are SSE, their size is very similar to the $0\nu\beta\beta$ events but systematically slightly *smaller* in size. About 85/75% ('weighted'/'linear') of the DE events are lying within a distance of 2 mm.
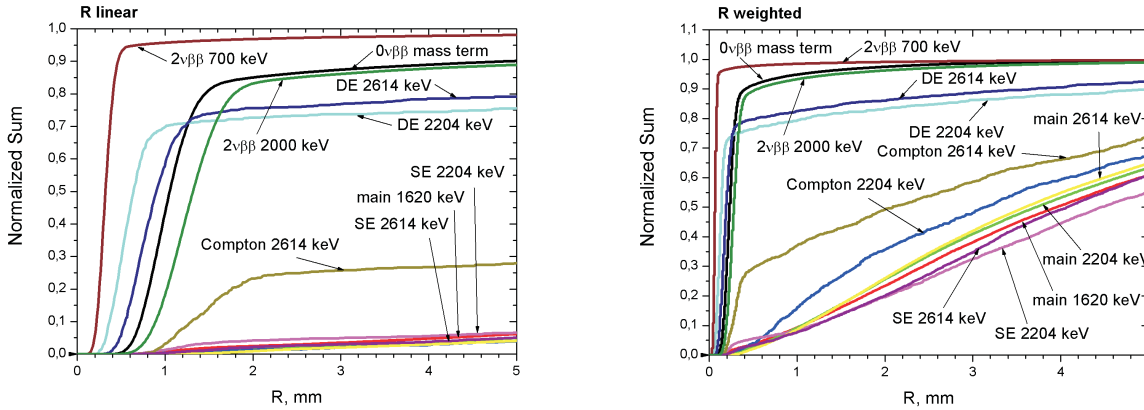
Figure 8: Calculated event sizes of $\beta\beta$ events (only mass term considered), and of γ - transitions 2614, 2204 and 1620 keV. For the first two in addition to the main line (full energy peak), also shown are the sizes of the double escape (DE) and single escape (SE) peaks, and of Compton events in the range 2035 - 2043 keV.
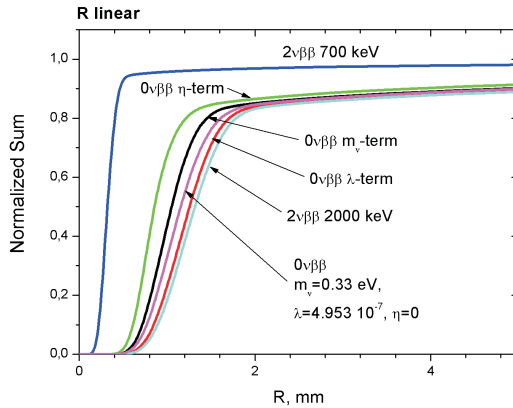
Figure 9: Calculated event sizes of $0\nu\beta\beta$ events for the $\langle m_\nu \rangle$, $\langle \eta \rangle$, $\langle \lambda \rangle$ parameter sets of eq. (15) and for $\langle m_\nu \rangle = 0.33$, $\langle \lambda \rangle = 4.95 \times 10^{-7}$, $\langle \eta \rangle = 0$.

Also the $2\nu\beta\beta$ events at 2000 keV are very close to the $0\nu\beta\beta$ events, while the $2\nu\beta\beta$ events at 700 keV - around the maximum of the 2ν continuous spectrum - have much smaller size. For the photon events of the 2204 keV γ -transition and the 1620 keV γ -transition the situation is similar to that of the 2614 keV transition

Then we compared $0\nu\beta\beta$ events sizes for our three cases (see eq. (15) and section 3.1) of spectral-angular distribution (Fig. 9). It is obvious from Fig. 9 that it *would be extremely difficult*, with the typical spatial resolution of Ge detectors of a few mm (linear), to distinguish the different particle physics cases by size of the corresponding

91

events. This has the advantage that for the parameters in the experimentally allowed 3σ range the sizes of the $0\nu\beta\beta$ events will be *practically* the same (compare also the curves for mass-term in Fig. 8, and for $\langle m_\nu \rangle = 0.33\,$eV in Fig. 9).

On the other hand Fig. 8 shows, that we can distinguish to some extent Compton events in the energy range around $Q_{\beta\beta}$, and $0\nu\beta\beta$ -events by event size. Since the DE events are mainly SSE similar to the $\beta\beta$ -events, this gives the possibility to use the DE events of the 2614 keV line from ^{228}Th for some pulse shape 'calibration' of the detector (see [3]). Of course a double escape γ -line *at* $Q_{\beta\beta}$ could *hardly* be separated from $0\nu\beta\beta$ events. However, such line should always have a corresponding *much* stronger full energy line at energy $Q_{\beta\beta}+$ 1022 keV (see Fig. 7 in [3] as example). Also some differentiation of the main part of $2\nu\beta\beta$ events from gamma events should be possible (Figs. 8,9).

4 Summary and Conclusions - Potential of Future $\beta\beta$ Experiments to Determine Neutrino Mass and Right-handed Current Parameters

A first systematic study has been performed of the sizes of double beta and γ -events in a Ge detector, which finally largely determine, together with the location of the events in the detector, the shapes of the pulses seen in the detector. For this purpose, time history and tracks of individual events have been calculated by a Monte Carlo procedure based on GEANT 4, for $0\nu\beta\beta$ and $2\nu\beta\beta$ decay, including the main effects of the simulated angular correlations between the two emitted electrons, and for different kinds of photon interactions which contribute to the background in measured $0\nu\beta\beta$ and $2\nu\beta\beta$ spectra. The $\beta\beta$ angular correlations which depend on the effective neutrino mass and the right-handed coupling parameters η and λ, have been calculated for this purpose for the first time starting from the experimental $\beta\beta$ half-lives and with realistic matrix elements. It is found that the 'sizes' of the events (partial volumes in the detector in which the energy is released) *show strong differences* for $0\nu\beta\beta$ and $2\nu\beta\beta$ events at $\sim 2000\,$keV on one side, and most of the Compton scattered gamma events in the energy range of $Q_{\beta\beta}$ on the other side. Further, events from the full energy γ -lines and the corresponding single escape peaks *differ strongly* in size from the $0\nu\beta\beta$ events. Therefore, $0\nu\beta\beta$ events in a ^{76}Ge detector should be selectable with by rejecting large size (high multiplicity) γ events. The events in the DE peaks of the γ -lines come - in size - close to the behaviour of $0\nu\beta\beta$ events. They were therefore of interest for pulse shape 'calibration' of a $0\nu\beta\beta$ decay detector [3].

The differences in sizes of $0\nu\beta\beta$ events for different choice of particle physics parameters $\langle m_\nu \rangle, \langle \lambda \rangle, \langle \eta \rangle$ are too small to be realized with the position resolution of a large Ge detector. This has the advantage, that the deduced possibility to distinguish $\beta\beta$ events from γ -events is essentially independent of the particle physics parameters of the $0\nu\beta\beta$ process.

Finally let us have a look into the potential of *future* $0\nu\beta\beta$ experiments with respect to the determination of the particle physics parameters $\langle m_\nu \rangle, \langle \lambda \rangle, \langle \eta \rangle$.

It has been mentioned in the Introduction that *none* of the future double beta ex-

periments like EXO, (Super-)NEMO or CUORE etc., will ever be able to identify *tracks* of neutrinoless double beta decay. But *even if* in some kind of future experiment the tracks *could* be clearly differentiated, then according to Figs. 3,4,5 (see this report) and Figs. 7,8,9 and 11 (from [2]) there would be *never a chance* to get information about the particle physics parameters dominating the $0\nu\beta\beta$ process, particularly in a low-statistics experiment. Only upper limits could be obtained for $\langle m_\nu \rangle, \langle \lambda \rangle, \langle \eta \rangle$.

This means that *no future single* double beta $0^+ \to 0^+$ $\beta^-\beta^-$ experiment will be able to obtain more information then a ^{76}Ge experiment. No confirmation by *another* $0^+ \to 0^+$ $\beta^-\beta^-$ experiment would yield any new additional information. It has been pointed out earlier [33] that *also several* simultaneous experiments looking for $\beta^-\beta^-$ *decay* cannot yield more information. E.g., if to the result of the ^{76}Ge (HEIDELBERG-MOSCOW) experiment the result of a high-sensitivity ^{136}Xe experiment would be added, *no fundamental new* information would be obtained (see Fig. 3a in [33]). The *only realistic way* we see to obtain information on the individual mass and right-handed weak current parameters $\langle m_\nu \rangle, \langle \lambda \rangle, \langle \eta \rangle$, is [33] from a simultaneous analysis of a high-sensitive $\beta^-\beta^-$ experiment, which has *observed* $0\nu\beta\beta$ decay, as ^{76}Ge), *and* a suitable *very high-sensitive mixed-mode experiment* looking for $0\nu\beta^+EC$ decay (e.g. ^{124}Xe) on a half-life level of 10^{27} years.

Another theoretical possibility is to look for the $0\nu\beta\beta$ half-life for the $0^+ \to 2^+$ transition, e.g. in ^{76}Ge, for which the mass mechanism vanishes in first order and the transition is driven mainly by the λ and η mechanism. Since the half-life to be expected [33, 34] for these modes would lie, however, with $\sim 10^{30}$ and $\sim 5 \times 10^{32}$ years almost in the range of that of proton decay, such experiment may be only of academic interest.

Therefore, the strategy in future $\beta\beta$ research should be, to *combine* confirmation of the HEIDELBERG-MOSCOW result with determination of the mechanism dominating the decay, instead of repeating earlier experiments or ideas. The future experiment thus should *not* use ^{76}Ge or ^{136}Xe, but instead of those ^{124}Xe.

Acknowledgements

References

[1] H.V. Klapdor-Kleingrothaus, I.V. Krivosheina and I.V. Titkova,
Phys. Lett. **B 632** (2006) 623-631.

[2] H.V. Klapdor-Kleingrothaus, I.V. Krivosheina and I.V. Titkova,
Phys. Rev. **D 73** (2006) 013010.

[3] H.V. Klapdor-Kleingrothaus, I.V. Krivosheina, A. Dietz et al., *Phys. Lett.* **B 586** (2004) 198-212. H.V. Klapdor-Kleingrothaus, A. Dietz, I.V. Krivosheina et al., *Nuclear Instr. and Methods* **A 522** (2004) 371-406.

[4] H.V. Klapdor-Kleingrothaus et al. *Mod. Phys. Lett.* **A 16** (2001) 2409-2420,
and *Foundation of Physics* **31** (2002) 1181-1223 and Corrigenda, 2003, and
Part. and Nucl. **110** (2002) 57, and
H.V. Klapdor-Kleingrothaus, In Proc. of International Conf. "Neutrinos and Impli-
cations for Physics Beyond the Standard Model", Stony Brook, USA, 11-13 October,
2002, ed. R. Shrock, World Scientific, 2003, 367-382 and hep-ph/0303217;
H.V. Klapdor-Kleingrothaus, *Nucl. Phys. B (Proc. Suppl.)* **143** (2005) 229-232, Proc.
of International Conf. "Neutrino 2004", 14-19 June, 2004, Paris, France.

[5] H.V. Klapdor-Kleingrothaus, **Proposal, MPI-1987-V17**, September 1987.

[6] H.V. Klapdor-Kleingrothaus, In Proc. of International Conf. "Neutrino Telescopes",
Venezia, Italy, February 2005, ed. M. Baldo-Ceolin., p. 215

[7] J. Vuilleumier for the EXO collaboration, in Proc. of Int. Workshop on Identification
of Dark Matter, Edinburg, Scotland, 2004 (World Scientific, Singapore, 2005), p.635.

[8] X. Sarazin et al., in Proc. of International Conf. "Neutrino 2004", 14-19 June, 2004,
Paris, France *Nucl. Phys. B Proc. Suppl.* **143** (2005) 221.

[9] E. Fiorini, in Proc. of International Conf. "Neutrino 2004", 14-19 June, 2004, Paris,
France, *Nucl. Phys. B Proc. Suppl.* **143** (2005) 225 and C. Brofferio et al., In Proc.
of International Conf. "Neutrino Telescopes", Venezia, Italy, February 2005, ed. M.
Baldo-Ceolin., p. 239.

[10] J. Hellmig, H.V. Klapdor-Kleingrothaus, *Nucl. Instr. Meth.* **A 455** (2000) 638-644;
J. Hellmig, F. Petry, H.V. Klapdor-Kleingrothaus, **Patent DE19721323A**.
B. Majorovits, H.V. Klapdor-Kleingrothaus. *Eur. Phys. J.* **A6** (1999) 463.

[11] M. Günther et al., HEIDELBERG-MOSCOW Coll., *Phys. Rev.* **D55** (1997) 54.

[12] Ch. Dörr, H.V. Klapdor-Kleingrothaus, *Nucl. Instr. Meth.* **A 513** (2003) 596-621.

[13] The GEANT4 collaboration, http://geant4.web.cern.ch/geant4/.

[14] H.V. Klapdor-Kleingrothaus et al., to be publ. (2006)

[15] M. Doi, T. Kotani, H. Nishiura, et al., *Prog. Theor. Phys.* **67** (1982) 281.

[16] M. Doi, T. Kotani, H. Nishiura, E. Takasugi, *Prog. Theor. Phys.* **70** (1983) 1353.

[17] M. Doi, T. Kotani, E. Takasugi, *Prog. Theor. Phys. Suppl.* **83** (1985) 1.

[18] M. Doi, T. Kotani, E. Takasugi, *Phys. Rev.* **C 37** (1988) 2104.

[19] K. Muto, H.V. Klapdor, in "Neutrinos", Graduate Texts in Contemporary Physics", ed.
H.V. Klapdor, Berlin, Germany: Springer (1988) 183-238.

[20] A. Staudt, K. Muto, H.V. Klapdor-Kleingrothaus, *Eur. Lett.* **13** (1990) 31.

[21] K. Grotz, H.V. Klapdor, "The Weak Interaction in Nuclear, Particle and Astrophysics", IOP Bristol (1990).

[22] T. Tomoda, *Rep. Prog. Phys.* **54** (1991) 53.

[23] J. Suhonen, O. Civitarese, *Phys. Rep.* **300** (1998) 123-214.

[24] H.V. Klapdor-Kleingrothaus, "60 Years of Double Beta Decay - From Nuclear Physics to Beyond the Standard Model", World Scientific (2001), 1281 pages.

[25] J. Schechter, J.W.F. Valle, *Phys. Rev.* **D 25** (1982) 2951-2954.

[26] T. Tomoda, et al., *Nucl. Phys.* **A 452** (1986) 591.

[27] W.C. Haxton, G.J. Stephenson, *Prog. Part. Nucl. Phys.* **12** (1984) 409.

[28] K. Muto, E. Bender, H.V. Klapdor, *Z. Phys.* **A 334** (1989) 187 and 177 pp.

[29] S. Stoica, H.V. Klapdor-Kleingrothaus, *Nucl. Phys.* **A 694** (2001) 269, Phys. Rev. C 63 (2001) 064304.

[30] B. Maier, Dissertation Nov. 1995, Univ. of Heidelberg.

[31] R.N. Mohapatra, 'Unification and Supersymmetry', Springer(Heidelberg) (1986).

[32] S.P. Rosen, *Comments Nucl. Part. Phys.* **18** (1988) 31.

[33] M. Hirsch, K. Muto, T. Oda, H.V. Klapdor-Kleingrothaus, *Z. Phys.* **A 347** (1994) 151.

[34] T. Tomoda, Nucl. Phys. A 484 (1998) 635.

List of Edited Proceedings (2005)

1. H.V. Klapdor-Kleingrothaus and D. Arnowitt (eds.), **Dark Matter in Astro- and Particle Physics.**, Proc. of 5th Heidelberg Dark Matter International Conference - DARK2004, Texas, USA, 3 - 9 October, 2004, Springer, Heidelberg, Germany (2005) 655 pp.

List of Publications and Conference Contributions (2005)

1. H.V. Klapdor-Kleingrothaus, *"First Evidence for Neutrinoless Double Beta Decay - and World Status of Double Beta Experiments"*, In Proc. of International Conf. "Neutrino Telescopes", Venezia, Italy, 22-25 February 2005, ed. M. Baldo-Ceolin., p. 215-237.

2. H.V. Klapdor-Kleingrothaus, *"First Evidence for Lepton Number Violation and of the Majorana Character of Neutrinos"*, in Proc. of Intern. Workshop "Neutrino oscillation - NOW 2004" Bary, Italy, September 2005, eds. G. Fogli, *Nucl. Phys. Proc. Suppl.* **145** (2005) 219-224, and in Proc. of Int. Workshop on Identification of Dark Matter, Edinburg, Scotland, 2004 (World Scientific, Singapore, 2005) 633-646.

3. H.V. Klapdor-Kleingrothaus, *"First Evidence for Neutrinoless Double Beta Decay, with Enriched ^{76}Ge in Gran Sasso 1990-2003."*, in Proc. of 21st International Conference on Neutrino Physics and Astrophysics (Neutrino 2004), Paris, France, 14-19 Jun 2004, *Nucl. Phys. Proc. Suppl.* **143** (2005) 229-232.

4. H.V. Klapdor-Kleingrothaus, *"First Evidence for Lepton Number Violation: the ^{76}Ge Double Beta Experiment in Gran Sasso 1990-2003"*, In Proc. of 10th International Symposium on "Particle, Strings and Cosmology" (PASCOS'04), Nath Fest, 16 - 22 August 2004, Boston, USA, June 2004, eds. P. Nath, 174-191.

5. H.V. Klapdor-Kleingrothaus, *"From Nuclear Physics to Physics Beyond the Standard Model: First Evidence for Lepton Number Violation and the Majorana Character of Neutrinos."* *Int. J. Mod. Phys.* **D 13** (2004) 2107-2126.

6. H.V. Klapdor-Kleingrothaus, in Proc. of Fifth International Heidelberg Conference on "Dark Matter in Astro and Particle Physics", DARK 2004, 3 - 9 October 2004, College Station, TX, USA: Springer, Heidelberg (2005), eds: H.V. Klapdor-Kleingrothaus and D. Arnowitt, *"Neutrinoless Double Beta Decay - and Hot Dark Matter"*, 93-115.

7. H.V. Klapdor-Kleingrothaus, International Workshop "Physics of High Energy Density in Matter", Hirschegg, Austria, 1-6 February 2005, *"New Results from the Search for Neutrinoless Double Beta Decay - and World Status of the Absolute Neutrino Mass."*

List of Colloquium Talks (2005)

1. H.V. Klapdor-Kleingrothaus, Kolloquium at University of München, München, Germany, March 2004, *"News from the Search for Neutrinoless Double Beta Decay."*

List of Seminars at Heidelberg University by Prof. H.V. Klapdor-Kleingrothaus (2004-2005)

1. Seminar für Mittlere Semester (WS 2004-2005): "Masse und Natur des Neutrinos"

The GENIUS Test Facility II and III in GRAN SASSO.

H.V. Klapdor-Kleingrothaus[a,d], I.V. Krivosheina[a,b],
V. Mironov[a,c], H. Strecker[a]

[a] Max-Planck Institut für Kernphysik, Heidelberg, Germany
[b] Institute of Radiophysical Research, Nishnij Novgorod, Russia
[c] Laboratory of Nuclear Problems, JINR, Dubna, Russia
[d] Spokesman of the Collaboration; E-mail: H.Klapdor@mpi-hd.mpg.de
Home-page: http://www.mpi-hd.mpg.de.non_acc/

Abstract

GENIUS-TF-II is an improved setup of now *six* naked high purity
Ge detectors (15 kg) in liquid nitrogen in Gran Sasso. It has been
installed in October, 2004 - after the first four naked Ge detectors
had been installed on May 5, 2003 (GENIUS-TF-I). The GENIUS-
Test-Facility (GENIUS-TF) is **the first** and up to now **only** setup
ever testing this novel technique aiming at extreme background re-
duction in search for rare decays in particular underground. The goal
of GENIUS-TF is to test some key operational parameters of the full
GENIUS project proposal in 1997 [1, 3, 4, 5, 6, 7]. Simultaneous phys-
ical goal is to search for the annual modulation of the Dark Matter
signal [18, 20].

In this report we describe the status of the background spectrum
measured with the GENIUS-Test-Facility-II and -III setup and in par-
ticular we consider the long-term stability of the naked detectors in
liquid nitrogen. Operational parameters are presented.

The results of the measurements show some reduction of the Ra
contamination in the 'new-old' room of the double beta experiment.
The effect of microphonics from bubbling in the liquid nitrogen and
from the noisy laboratory, traffic and construction is as far as it can be

seen now, small for high energies, but is very high, and has to be discriminated by pulse shape analysis for low energies. A corresponding method is under development.

The results obtained so far from GENIUS-TF, in particular for the long-term stability, are of decisive importance for any future GENIUS-like experiment aiming at use of the technique of naked detectors in liquid nitrogen (or other liquids).

1 Introduction

Some years ago, the status of cold dark matter search, of investigation of neutrinoless double beta decay and of low-energy solar neutrinos all required new techniques of *drastic* reduction of background in the experiments. For this purpose we proposed the GENIUS (GErmanium in liquid NItrogen Underground Setup) project in 1997 [1, 3, 4, 5, 6, 7].

After the success of the HEIDELBERG-MOSCOW experiment in $0\nu\beta\beta$ decay [11, 12, 13] this is no more needed for $\beta\beta$ decay experiments with ^{76}Ge, but it is still required for dark matter and solar neutrino experiments using Ge as target [17]. Therefore, we continued the research on the GENIUS Test Facility. *Monte Carlo simulations* for the GENIUS project, (and for GENIUS-TF) and investigation of the *new physics potential* of the project **have been performed in great detail**, and have been published elsewhere [1, 3, 7, 8, 14, 18]. We were **the first** to show (in our HEIDELBERG low-level facility already **in 1997**) that such device can be used for spectroscopy [1, 6].

A small scale version of GENIUS, the GENIUS-Test-Facility has the goal to test the long-term stability of the detectors under liquid nitrogen conditions and other operational parameters. A detailed description of the GENIUS-TF project is given in [18, 10]. The idea of GENIUS (and GENIUS-TF) is to operate 'naked' Ge detectors in liquid nitrogen (as applied **routinely already for more than 20 years by the CANBERRA Company** for technical functions tests [2]), and thus, by removing all materials from the immediate vicinity of the Ge crystals, to reduce the background considerably with respect to conventionally operated detectors. The liquid nitrogen acts both as a cooling medium and as a shield against external radiactivity.

That the removal of material close to the detectors is the crucial point

64

for improvement of the background, we know from our experience with the HEIDELBERG-MOSCOW double beta decay experiment, which is the most sensitive double beta experiment for more than 10 years now [11, 12].

The GENIUS-Test-Facility has been approved by the Gran Sasso Scientific Committee in March 2001.

Figure 1: Location of GENIUS-TF-I was the building on the right (car in front), opposite to the HEIDELBERG-MOSCOW experiment building (left side). Location of GENIUS-TF-II is the building of the HEIDELBERG-MOSCOW experiment (left).

Additionally to investigation of some key operational parameters of GENIUS the GENIUS-TF will extend our work on WIMP-nucleon cross sections with the HEIDELBERG-MOSCOW and HDMS experiments [21, 22], and aims at testing of the claimed evidence for WIMP dark matter from the DAMA experiment [23, 24]. The relatively large mass of Ge in the full scale GENIUS-TF compared to existing experiments would permit to search directly for a WIMP signature in form of the predicted seasonal modulation of the event rate [20]. Introducing the strongly 'cooled down' enriched detectors of the HEIDELBERG-MOSCOW $\beta\beta$-experiment into the GENIUS-TF setup, could in principle allow, to improve the present accuracy of the effective Majorana neutrino mass determined recently [11, 12, 13, 15, 16].

2   The GENIUS-TF-II Setup

After installation of the GENIUS-TF setup between halls A and B in Gran Sasso, opposite to the buildings of the HEIDELBERG-MOSCOW double

Figure 2: <u>Upper part - left and right:</u> Taking out the crystals from the transport dewars and fixing the electrical contacts in the clean room of the GENIUS-TF-I building - from left to right: H. Strecker, I. Krivosheina, H.V. Klapdor-Kleingrothaus. <u>Middle:</u> **The first four contacted naked Ge detectors** before installation into the GENIUS-TF-I setup. <u>Bottom part - left and right:</u> View from the top on the new GENIUS-TF-II setup during installation in October 2004. <u>Middle:</u> **The six contacted naked Ge detectors.**

beta decay experiment and of the DAMA experiment (Fig. 1), the first four detectors had been installed in liquid nitrogen on May, 5 2003 and had started operation. This has been reported in Cern Courier [7] and in [10] (see also Fig. 2, upper part).

In October 2004 we have installed a new setup GENIUS-TF-II (see Fig 2-lower part, and Fig. 3), containing in contrast to the earlier setup now **six naked** Ge detectors, and, as technical improvement **a second copper vessel**, for further shielding of the Radon. That ^{222}Ra diffusing into the setup has been a problem for GENIUS-TF-I, has been described in detail in [9]. Each detector has a weight of 2.5 kg. The depth of the core of the detectors was reduced to guarantee a very low threshold. The inner shielding by bricks of (5-10) cm polycristalline Germanium ($\sim$300 kg) was used also in this setup forming the inner highly efficient shield of the Ge detectors (see

Fig. 3).
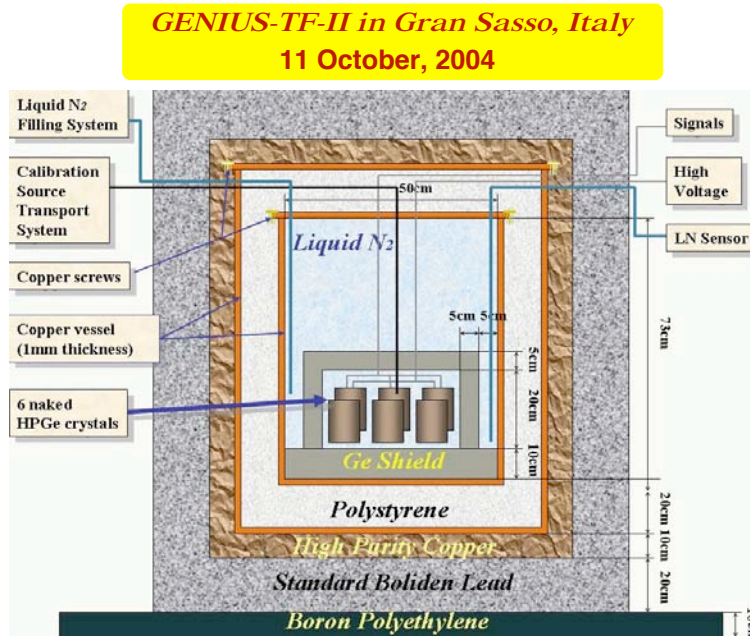
Figure 3: Cross section of the new setup GENIUS-TF-II.

The thin wall (1 mm) inner copper box containing the liquid nitrogen is made of high-purity electrolytic copper and is thermally shielded by 20 cm of special low-level styropor, the outer copper box (also made of electrolytic copper) is followed by a shield of 10 cm of electrolytic copper (15 tons) and 20 cm of low-level (Boliden) lead (>35 tons).

The high-purity liquid nitrogen used, is produced by the BOREXINO nitrogen plant, which has been extended for increase of the production capacity to be able to provide enough nitrogen also for GENIUS-TF. Liquid nitrogen of standard quality (99.99% purity) is directly purified in the liquid phase by an adsorber column system, consisting of two independent columns (Low Temperature Adsorber - LTA) filled with about 2 kg of 'activated carbon' each. One of them we purchased to supplying GENIUS-TF. The system is designed to continuously produce about 150 l of liquid nitrogen per hour, respectively about 100 m^3/h gaseous nitrogen for both experiments. During the regeneration phase of one column the other one is in use.

From the production plant the liquid nitrogen is transported by 200 l vessels to the building of the experiment. Filling of the copper container

67

with liquid nitrogen is provided by connecting them to the filling system consisting of isolated teflon tubes (see [10]).

The nitrogen level in the detector chamber is measured by a capacitive sensor consisting of two 40 cm long isolated selected-material copper tubes, one inside the other. The change of the medium between the tubes by the entering liquid nitrogen leads to a change of the capacity, which is measured by subsequent electronics and indicated by LED's outside of the setup. We measure the nitrogen level in ten steps between 0 and 100%. GENIUS-TF has to be refilled every two days (with some reserve of one more day).

3   Development of Operational Parameters

3.1   Data acquisition

The data acquisition system we developped recently for GENIUS-TF and GENIUS is decribed in detail in [19].

It uses multichannel digital processing technology with FLASH ADC modules with high sampling rates of 100 MHz and resolution of 12 bits. It allows to capture the detailed shape of the preamplifier signal with high-speed ADC, and then to perform digitally all essential data processing functions, including precise energy measurement over a range of 1 keV - 3 MeV, rise time analysis, ballistic deficit correction and pulse shape analysis. Thus we obtain both the energy and the pulse shape information from one detector using one channel of the Flash ADC module.

3.2   Energy Resolution and Threshold

To allow for regular calibration of the detectors, a source of ^{133}Ba fixed on a wire can be introduced through a teflon tube into the center among the detectors. The source is transported via a magnetic system. The activity of the source is 401 kBq.

Fig. 4 shows a spectrum measured with a ^{133}Ba source. The resolution is about 3 keV for $E_\gamma \sim 300$ keV, the threshold is about 5 keV.

68
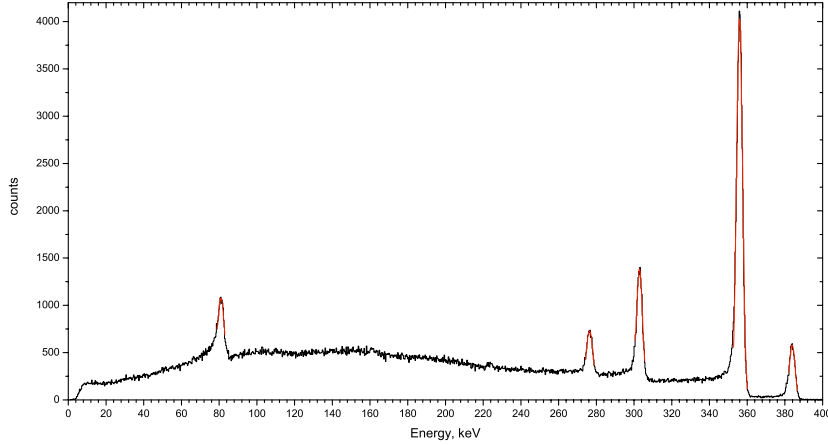
Figure 4: Calibration spectrum measured with detector 4 with the ^{133}Ba source inside the setup.

3.3 Microphonics

One of our major tasks is to try to reduce the noise from microphonics of the GENIUS-TF detectors.

The effect of microphonics from bubbling in the liquid nitrogen is as far as it can be seen now, negligible for high energies at present background level, but is very large (Fig. 6), and has to be discriminated by pulse shape analysis for low energies. This can be done by the new digital data acquisition system [19].

The main idea of the noise reduction method is to determine parameters setting limits on the shape of good signals. The procedure in short the following: From the raw data signal which is obtained from the flash-ADC, a compressed signal is produced summing up every 10 time channels. Then a differential filter with P/Z compensation is applied, to decrease low frequencies. Then, to decrease high frequencies, an n-pole integral filter is applied. The amplitude of this output signal is proportional to the energy of the input signal. The structure of the digital filter was taken from [19].

We look for location of extreme points of the signals, some ratios and

69

some other parameters. After applying this method we got a reduction of 99% of our raw data from 1.5-1. GB.

We formed a *preliminary* library of good and bad events - some examples are given in Fig. 5. Fig. 6 shows a spectrum measured over the full energy range without any pulse shape selection. A strong peak originating from microphonics is seen at $\sim 40\,\mathrm{keV}$.
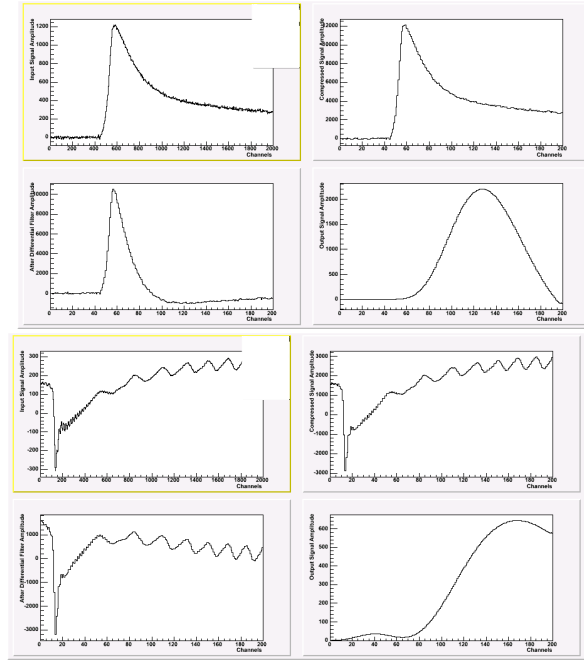
Figure 5: Examples of events: Top - a 'good' event, after our first preliminary analysis. Bottom - a 'bad' event, which was thrown away in our analysis. Shown are for both events the raw (list-file) signal (upper left), the compressed signal (upper right), the differentiated and integrated signal (lower left and right, respectively).

Applying this microphonics reduction method, it is found that the spectrum is, on the present background level, practically not affected by PSA for energies larger than 300 keV. At low energies the microphonics peak now, however, completely disappeared.

70
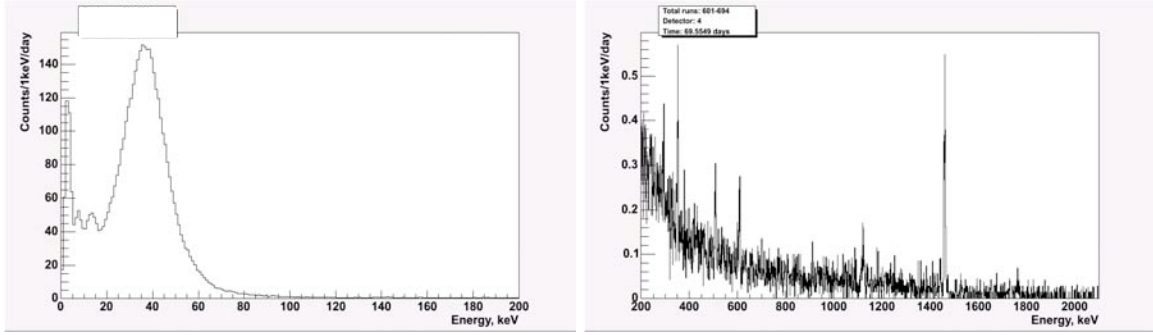
Figure 6: The first background spectrum measured with detector 4 and 6 over 69.6 days with the complete setup in different energy intervals.

3.4 Background from ^{222}Rn, and from other Experiments

The unexpected (according to our Monte Carlo simulations [18]) high background from ^{222}Rn in GENIUS-TF-I (see [9]) is reduced in GENIUS-TF-II by about a factor 2 according to preliminary analysis (simply compare Fig. 6, right of this paper with Fig.8 right of [9]). This means the contribution to the background in the range 0-50 keV of ^{222}Rn is about 5 counts/kg y keV. This corresponds to 1.4×10^{-2} counts/kg keV. This is about ~70% of the *total* background observed in this energy region. It should be stressed again – that this ^{222}Rn background is compatible with the goal of GENIUS-TF to search for dark matter, but will be a *serious problem* for any attempt to look for cold dark matter with full GENIUS-like experiments.

In addition to these internal problems we found a **strong** deterioration of our background starting with the operation of the WARP-experiment. This additional background vanished when the WARP experiment stops operation. This interference has to be solved before GENIUS-TF can continue its investigations.

3.5 Long-Term Stability

The long-term stability of the detector operation in liquid nitrogen is shown in Tables 1,2. In particular a very large sensitivity of the detector operability is found against opening of the setup, or more precisely, to taking detectors out of liquid nitrogen and installing them again. Such operation

has become necessary when GENIUS-TF-I was stopped and GENIUS-TF-II was constructed and put into operation, and a second time, when the inner shield of polycristalline Ge bricks was removed at end of February 2005, and GENIUS-TF-III started operation. Result in our case is that finally from initially six detectors at present only three are still working and of those still *only one* with the nominal high voltage (see Table 1). For the others the leakage current has increased.

Table 1: The high voltages applied to the detectors after installation in GENIUS-TF I, II and III as function of time, and the nominal voltages. At present (Jan. 2006) *only one* of the six detectors still runs with the nominal voltage.

Detectors	D1	D2	D3	D4	D5	D6
GENIUS-TF-I, from 10.12.2003, till 25.09.2004						
10.12.03	2404	2603	2879	2301	not inst.	not inst.
06.04.04	2600	2220	2879	2301	-	-
	incr. leak curr.					
04.05.04	2600	2220	3200	2500		
GENIUS-TF-II, from 18.11.2004, till 28.02.2005						
08.10.04	250	1296	261	954	1253	502
18.11.04	364	2200	347	2298	3501	1015
20.01.05						1000
GENIUS-TF-III, from 15.03.2005						
15.01.05	80	1802	20	2153	3501	980
16.04.05		1700				
18.04.05				1500		
	high test point voltage					
03.05.05	0	1700	0	1500	3501	980
15.12.05	-	1700	-	-	3500	911
Nominal	**3000**	**2600**	**3200**	**2500**	**3500**	**2000**

Table 2 shows that the resolution some time after locating the detectors back to liquid nitrogen improves almost to the original value, but on long terms seems to decrease systematically.

72

Table 2: Resolution (in keV) for all detectors of GENIUS-TF for the line 356 keV of ^{133}Ba and 344 keV from ^{152}Eu, respectively.

Detectors	D1	D2	D3	D4	D5	D6
GENIUS-TF-I, data taking from 10.12.2003, till 25.09.2004						
for line 356 keV ^{133}Ba						
07.03.04	2.98	1.87	1.86	1.86	not inst.	not inst.
for line 1173 keV ^{60}Co						
15.04.04	4.2	4.17	5.82	3.06		
GENIUS-TF-II, data taking from 18.11.2004, till 28.02.2005						
for line 356 keV ^{133}Ba						
08.10.04	11	8.2	-	8	11	9
10.10.04	13	10.4	-	9.2	8.7	8.31
26.10.04	-	5.4	-	4.96	5.68	5.27
30.10.04	-	3.94	-	2.86	3.06	3.08
22.11.04	-	3.46	-	3.39	3.55	3.59
06.12.04	-	3.37	-	3.19	3.53	3.85
31.01.05	-	3.31	-	3.1	3.4	3.9
07.02.05	-	3.3	-	2.56	3.18	3.76
GENIUS-TF-III, data taking from 15.03.2005						
15.03.05		5.34		2.9	7.37	6.14
for line 344 keV ^{152}Eu						
15.03.05		5.08		2.83	7.24	4.26
15.12.05		5.85			7.65	5.75

4   Perspectives

An important task is further to improve the presently used method of pulse shape analysis. In particular the efficiency of the method at low energies has to be carefully determined. The inner polycrystalline Ge shield which had to be removed according to contract with Kurchatov institute, at beginning of March 2005 should be replaced by a shield of monocrystalline Si, of which a sufficient amount is already available.

For the purpose of testing the modulation signal measured by DAMA the amount of detectors has to be increased to about 40 kg to reach a comfortable time scale of measurement of a few years.

5   Conclusions

A new GENIUS-TF-II setup has been installed in October, 2004 with additional shielding against radon and additional two Ge detectors in liquid nitrogen in the GRAN SASSO, increasing the total mass to 15 kg. This is the first time that this novel technique is applied under realistic background conditions of an underground laboratory. GENIUS-TF is the *only setup,* with naked Ge detectors *worldwide running underground or at the Earth's surface.*

This **pioneering experiment** gives important insight into the conditions of technical operation of a setup operating Ge detectors in liquid nitrogen. Among them is the observed very large sensitivity of detector operability against opening of the setup or more precisely, taking detectors out of the liquid nitrogen. Such operation *becomes necessary* for various reasons. In our case after two openings and taking out the detectors from liquid nitrogen, from 6 detectors only 3 are still working, and *only one* of them with the nominal high voltage. Such problem will have large influence particularly on the functionability of **much larger** experiments using the method of naked detectors in liquid nitrogen (or argon, etc.). *The information GENIUS-TF delivered after almost three years of operation on the possibility of long-term operation of such experiments, casts serious doubt on the possibility of such experiments in general.*

LNGS of this project.

References

[1] H.V. Klapdor-Kleingrothaus in Proceedings of BEYOND'97, First International Conference on Particle Physics Beyond the Standard Model, Castle Ringberg, Germany, 8-14 June 1997, edited by H.V. Klapdor-Kleingrothaus and H. Päs, *IOP Bristol* (1998) 485 - 531 and in *Int. J. Mod. Phys.* **A 13** (1998) 3953.

[2] J. Verplancke, **CANBERRA Company**, priv. commun. 5.03.2004.

[3] H.V. Klapdor-Kleingrothaus, J.Hellmig and M.Hirsch, *GENIUS-Proposal*, 20 Nov. 1997.

[4] J. Hellmig and H.V. Klapdor-Kleingrothaus, *Z. Phys.* **A 359** (1997) 351-359, and nucl-ex/9801004.

[5] H.V. Klapdor-Kleingrothaus, M. Hirsch, *Z. Phys.* **A359** (1997) 361-372.

[6] H.V. Klapdor-Kleingrothaus, J. Hellmig and M. Hirsch, *J. Phys.* **G 24** (1998) 483 - 516.

[7] H.V. Klapdor-Kleingrothaus, CERN Courier, Nov. 1997, 16 - 18.

[8] H.V. Klapdor-Kleingrothaus et al. **MPI-Report MPI-H-V26-1999**, and *Preprint: hep-ph/***9910205**, and in Proceedings of the 2nd Int. Conf. on Particle Physics Beyond the Standard Model BEYOND'99, Castle Ringberg, Germany, 6-12 June 1999, edited by H.V. Klapdor-Kleingrothaus and I.V. Krivosheina, *IOP Bristol* (2000) 915 - 1014.

[9] H.V. Klapdor-Kleingrothaus et al., *Nucl. In. Meth.* **A530** (2004) 410.

[10] H.V. Klapdor-Kleingrothaus et al., *Nucl. Instr. Meth.* **A511** (2003) 341; H.V. Klapdor-Kleingrothaus et al., Proc. of the 3nd Intern. Conf. on Particle Physics Beyond the Standard Model, BEYOND02, Castle Ringberg, Germany, 2002, IOP 2003, ed. H.V. Klapdor-Kleingrothaus, 499. H.V. Klapdor-Kleingrothaus et al., *Nucl. Instrum. Meth.* **A 530** (2004) 410-418; C.Tomei, A.Dietz, I.Krivosheina, H.V. Klapdor-Kleingrothaus, *Nucl. Instrum. Meth.* **A 508** (2003) 343-352; H.V. Klapdor-Kleingrothaus, CERN Courier, 2003.

[11] H.V. Klapdor-Kleingrothaus, I.V. Krivosheina, A. Dietz et al., *Phys. Lett.* **B 586** (2004) 198 - 212 and hep-ph/0404088, *"Search for neutrinoless double beta decay with enriched ^{76}Ge in Gran Sasso 1990-2003."*

[12] H.V. Klapdor-Kleingrothaus, A. Dietz, I.V. Krivosheina et al., , *Nucl. Instrum. Meth.* **A 522** (2004) 371-406 and hep-ph/0403018, *"Data Acquisition and Analysis of the ^{76}Ge Double Beta Experiment in Gran Sasso 1990-2003."*

[13] H.V. Klapdor-Kleingrothaus et al. hep-ph/0201231 and *Mod. Phys. Lett.* **A 16** (2001) 2409-2420.

[14] H.V. Klapdor-Kleingrothaus, "60 Years of Double Beta Decay - From Nuclear Physics to Beyond the Standard Model", WS (2001) 1281 p. H.V. Klapdor-Kleingrothaus, *Spring. Tr. Mod. Phys.* **163** (2000) 69.

[15] H.V. Klapdor-Kleingrothaus, A. Dietz and I.V. Krivosheina, *Part. and Nucl.* **110** (2002) 57-79.

[16] H.V. Klapdor-Kleingrothaus, A. Dietz and I.V. Krivosheina, *Foundations of Physics* **31** (2002) 1181-1223 and Corrigenda, 2003 home-page: http://www.mpi-hd.mpg.de/non_acc/main_results.html.

[17] H.V. Klapdor-Kleingrothaus, in Proc. of 2th Int. Workshop on Low Energy Solar Neutrino Detection, Tokyo, Japan, 4-5 Dec. 2000 (World Scientific, Singapore 2001) p.116.

[18] H.V. Klapdor-Kleingrothaus et al., *NIM* **A 481** (2002) 149-159.

[19] T. Kihm, V.F. Bobrakov and H.V. Klapdor-Kleingrothaus, *Nucl. Instrum. Meth.* **A 498** (2003) 334-339 and hep-ph/0302236.

[20] C.Tomei, A.Dietz, I.Krivosheina, H.V. Klapdor-Kleingrothaus, *Nucl. Instrum. Meth.* **A 508** (2003) 343-352.

[21] HEIDELBERG-MOSCOW collab., *Phys. Rev.* **D 59** (1998) 022001.

[22] H.V. Klapdor-Kleingrothaus, I.V. Krivosheina and C. Tomei, Phys. Lett. **B 609** (2005) 226-231.

[23] R. Bernabei et al., Phys. Lett. B **424** (1998) 195; Phys. Lett. B **450** (1999) 448; Phys. Lett. B **480** (2000) 23.

76

[24] R. Bernabei et al., Riv. Nuovo Cim. 26(2003) 1-73; Phys. Lett. B **424** (1998) 195; **450** (1999) 448; **480** (2000) 23.

List of Edited Proceedings (2005)

1. H.V. Klapdor-Kleingrothaus and D. Arnowitt (eds.), **Dark Matter in Astro- and Particle Physics.**, Proc. of 5th Heidelberg Dark Matter International Conference - DARK2004, Texas, USA, 3 - 9 October, 2004, Heidelberg, Germany: Springer (2005), pp. 655.

List of Publications and Conference Contributions (2005)

1. H.V. Klapdor-Kleingrothaus, *"First Evidence for Lepton Number Violation and of the Majorana Character of Neutrinos"*, in Proc. of Intern. Workshop "Neutrino oscillation - NOW 2004" Bary, Italy, September 2005, eds. G. Fogli, *Nucl. Phys. Proc. Suppl.* **145** (2005) 219-224, and in Proc. of Int. Workshop on Identification of Dark Matter, Edinburg, Scotland, 2004 (World Scientific, Singapore, 2005) 633-646.

2. H.V. Klapdor-Kleingrothaus and I.V. Krivosheina, in Proc. of Fifth International Heidelberg Conference on "Dark Matter in Astro and Particle Physics", DARK 2004, 3 - 9 October 2004, College Station, TX, USA: Springer (2005), eds: H.V. Klapdor-Kleingrothaus and D. Arnowitt, *"The GENIUS-Test-Facility and the HDMS Detector in GRAN SASSO"*, 149-162.

3. H.V. Klapdor-Kleingrothaus, International Workshop "Physics of High Energy Density in Matter", Hirschegg, Austria, 1-6 February 2005, *"New Results from the Search for Neutrinoless Double Beta Decay - and World Status of the Absolute Neutrino Mass."*

List of Colloquium Talks (2005)

1. H.V. Klapdor-Kleingrothaus, Kolloquium at University of München, München, Germany, March 2004, *"News from the Search for Neutrinoless Double Beta Decay."*

List of Seminars at Heidelberg University by Prof. H.V. Klapdor-Kleingrothaus (2004-2005)

1. Seminar für Mittlere Semester (WS 2004-2005): "Masse und Natur des Neutrinos"

GIGS. The Interferometric Station at LNGS

Antonella Amoruso[a,b], Luca Crescentini[a,b,c]

[a] Dip.to di Fisica Univ. di Salerno, Salerno - Italy
[b] INFN - LNGS, L'Aquila - Italy
[c] Spokeperson

Abstract

Since several years two Michelson-type laser interferometers, operating as geodetic extensometers, are working at LNGS. The two orthogonal baselines, striking N66E and N24W, are 90-m long. Nominal sensitivity is about 3×10^{-12} and recording rate is 5Hz.

The main result obtained during 2005 is the analysis of the free oscillations excited by the megathrust Sumatra-Andaman earthquake of 26 December 2004 (M_w from 9.15 to 9.3), and particularly of the gravest toroidal free oscillations $_0T_2$, $_0T_3$.

1 Introduction

Earth's free oscillations can be observed after most large earthquakes and are also detectable in seismic noise records, but the gravest oscillations with periods > 1000 s are observable only after the largest events. Spectra from both seismic and gravimeter data from the Sumatra-Andaman earthquake exhibit the gravest Earth oscillations with unprecedented signal-to-noise levels (e. g. Park et al., 2005). Because horizontal seismic records are often noisy and superconducting gravimeter data is sensitive primarily to vertical motion, measurements of horizontal strain offer an important data complement, especially for the detection and characterization of toroidal free oscillations $_nT_l$. Modal splitting and coupling effects, however, affect the oscillation envelope of all modes with angular degree $l \geq 1$. For the gravest modes Earth's steady rotation influences coupling and splitting most strongly, so a good estimate of likely coupling effects can be made without detailed knowledge of Earth's aspherical structure.

Uncertainty in estimatede seismic moment release, particularly between seismic and geodetic measurements, for the 2004 Sumatra-Andaman event could potentially reveal large "slow" coseismic motions on the fault system. Published estimates of the average fault area and slip of the 2004 Sumatra-Andaman earthquake do not agree about a possible slow slip component, so the observation of the gravest toroidal free oscillations $_0T_2$, $_0T_3$ etc. is very useful.

2   Data analysis and results

Raw data recorded during the great Sumatra-Andaman earthquake of December 26, 2004 are shown in Fig. 1. BC-BA is independent of laser frequency fluctuations, so S/N is the highest and we show results for this shear strain component.
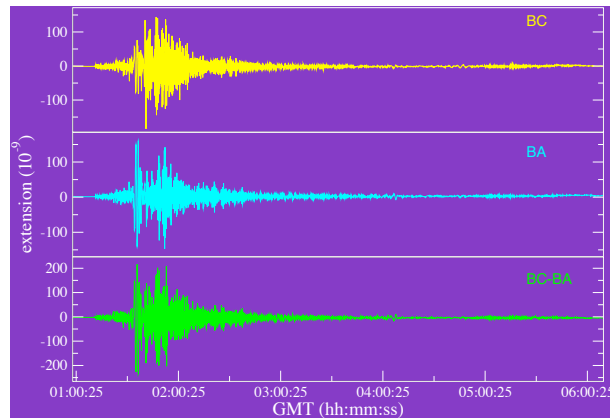
Figure 1. Raw strain data recorded during the Sumatra-Andaman earthquake of December 26, 2004. From top to bottom: extension of BC, extension of BA baseline, difference between BC and BA.

Spectral analysis evidences a very good S/N ratio for long-period (mainly toroidal) normal modes (Fig. 2), so it is possible to study the time history of multiplet envelopes (Fig. 3).
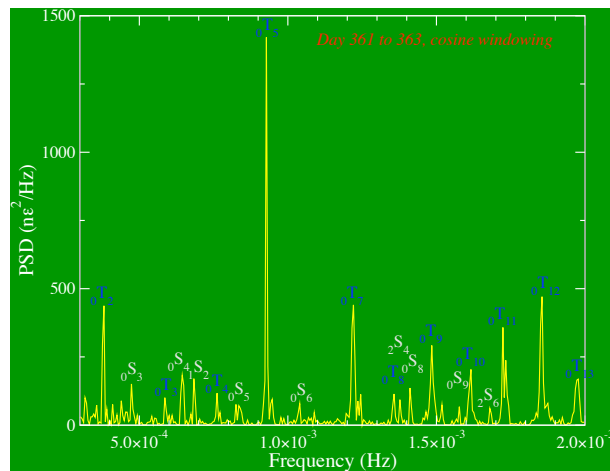
Figure 2. Power spectral density of BC-BA strain data, day 361 to 363 (cosine windowing).
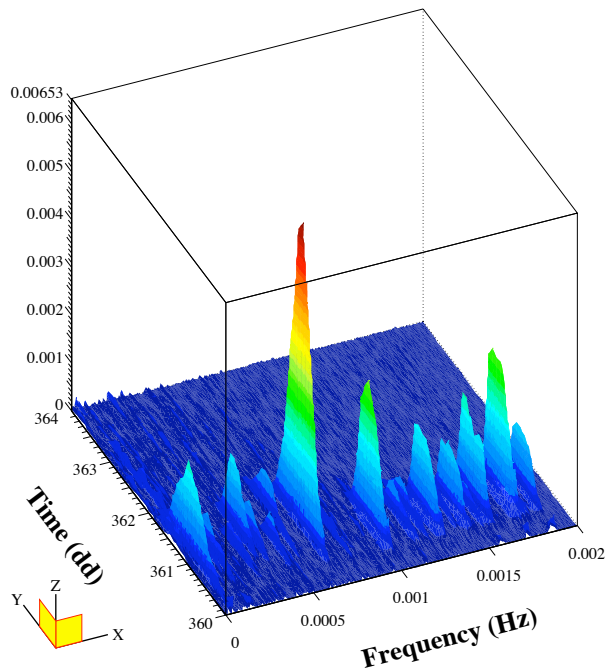
Figure 3. Time history of multiplet envelopes, DFT of 45hh-long moving windows (cosine tapering).

We have compared (Amoruso et al., 2005) the shapes of observed modal envelopes (Park, 1990) with those predicted by a synthetic seismogram computer code (Park and Yu, 1992). Each free-oscillation $_nS_l$ or $_nT_l$ is actually a multiplet of $2l+1$ distinct singlet oscillations with distinct geographic patterns. The singlet oscillations respond to Earth's rotation, ellipticity, and lateral structure in different ways, leading to the fine-splitting of frequencies and hybrid oscillation patterns. Rotational splitting within multiplets induces a beating pattern in the modal envelope that causes some to increase in amplitude over the first 20-40 hours after the Sumatra earthquake e.g., the mode $_0T_2$. Coriolis force deflects toroidal and spheroidal vibrations into hybrid vibrations in which a toroidal vibration pattern sprouts from an initially small amplitude at a spheroidal-mode frequency e.g., $_0S_3$. The synthetic strain records are computed for a rotating Earth that is elliptical, according to published coupling formulas. Despite the neglect of other lateral Earth structure and material anisotropy, simple rotation and ellipticity explains much of the complexities of the modal envelopes e.g.,the emergent oscillatory envelope of the mode $_1S_2$.

The choice of earthquake source mechanism is important, however. In Figs. 4 and 5 there are data (blue) plotted against synthetics computed for 1) the Mw=9.0 CMT double-couple source estimate made with hours of the Sumatra earthquake (red – see Lay et al 2005) and 2) for the Mw=9.3 five-subevent CMT solution published nine months later by Tsai et al (2005) (green). The Gran Sasso data is clearly fitted better by the larger earthquake source, but significant discrepancies persist, particularly the longest-period toroidal mode $_0T_2$. Overall, the match between predictions and data worsens for periods > 1000 s, which may indicate unmodelled slow rupture processes associated with the Sumatra-Andaman source.

179

Observed and Predicted Envelopes of Selected Free Oscillations
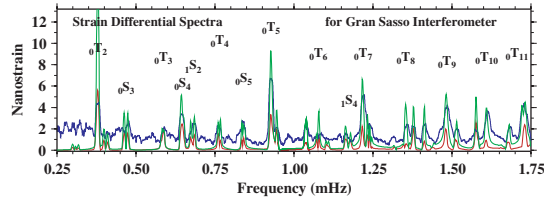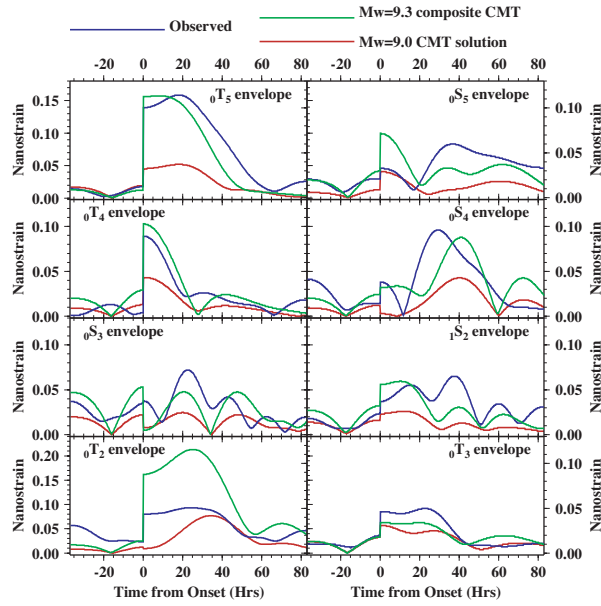
Figure 4.

Observed and Predicted Envelopes of Selected Free Oscillations
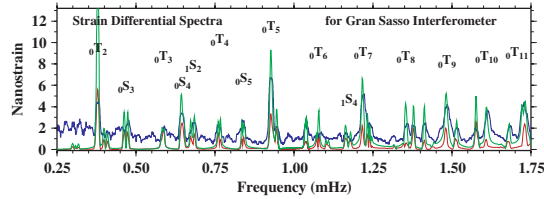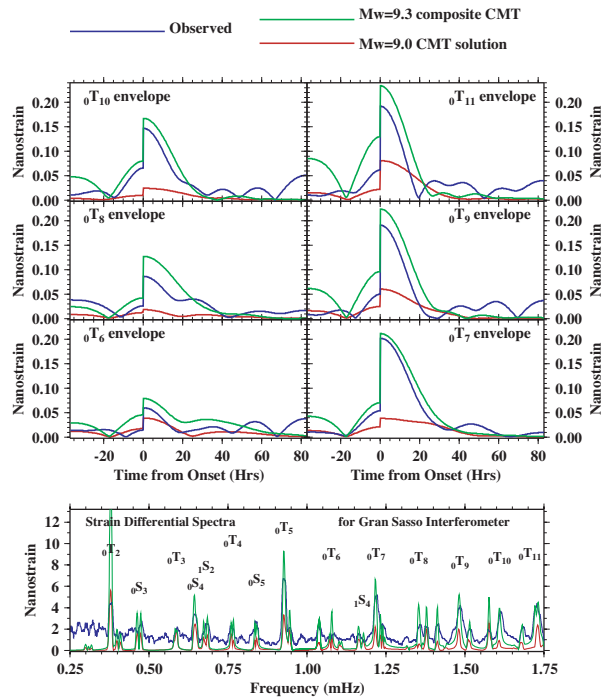
Figure 5.

Work is still in progress, but these data could represent a good opportunity to advance knowledge about the hypothetical "slow" part of the Sumatra-Andaman source.

This research is carried out in co-operation with Jeffrey Park, Department of Geology and Geophysics, Yale University, New Haven, Connecticut (USA).

Acknowledgement

References

[1] Amoruso, A., et al., EOS Trans. AGU, 86(52), Fall Meet. Suppl., 2005.

[2] Lay, T., et al., Science, **308**, 1127-1133, 2005.

[3] Park, J., Geophys. Res. Lett., **17**, 1489-1492, 1990.

[4] Park, J., and Y. Yu, Geophys. J. Int., **110**, 401-420, 1992.

[5] Park et al., Science, **308**, 1139-1144, 2005.

[6] Tsai, V.C., et al., Geophys. Res. Lett., **32**, L17304, doi:10.1029/2005GL023813, 2005.

OPERA

G. Van Beek[a], P. Vilain[a], G. Wilquet[a], M. Besnier[b], J. Damet[b], D. Duchesneau[b], J. Favier[b], H. Pessard[b], L. Arrabito[c], D. Autiero[c], Y. Caffari[c], L. Chaussard[c], Y. Dclais[c], O. Giarmana[c], L. Girard[c], I. Laktineh[c], J. Marteau[c], M. Dracos[d], J.P. Engel[d], C. Jollet[d], J.L. Guyonnet[d], J. Boucrot[e], J.E. Campagne[e], K. Winter[f], F.-W. Buesser[g], J. Ebert[g], C. Hagner[g], B. Koppitz[g], B. Naroska[g], W. Schmidt-Parzefall[g], J. Sewing[g], R. van Staa[g], R. Zimmermann[g], B. Mtterlein[h], H. Sohlbach[h], H. Dohmann[i], D. Frekers[i], M. Hierhoelzer[i], V. Pilipenko[i], J. Thies[i], M. Beyer[j], M. Braeuer[j], H. Schroeder[j], R. Waldi[j], A. Di Giovanni[k], N. Di Marco[k], P. Monacelli[k], N. Armenise[l], M. De Serio[l], M. Ieva[l], M.T. Muciaccia[l], A. Pastore[l], S. Simone[l], L. Consiglio[m], M. Cozzi[m], D. Di Ferdinando[m], G. Giacomelli[m], M. Giorgini[m], G. Mandrioli[m], L. Patrizii[m], M. Sioli[m], G. Sirri[m], F. Bersani Greggio[n], A. Cazes[n], V. Chiarella[n], C. Di Troia[n], B. Dulach[n], G. Felici[n], A. Franceschi[n], F. Grianti[n], T. Napolitano[n], A. Paoloni[n], M. Spinetti[n], F. Terranova[n], L. Votano[n], M. Ambrosio[o], S. Buontempo[o], N. D'Ambrosio[o], G. De Lellis[o], F. Di Capua[o], T. Ferraro[o], A. Marotta[o], P. Migliozzi[o], C. Pistillo[o], L. Scotto Lavina[o], G. Sorrentino[o], P. Strolin[o], V. Tioukov[o], D. Di Martino[p], L.S. Esposito[p], C. Gustavino[p], N. Ferrari[p], D. Orlandi[p], A. Bergnoli[q], R. Brugnera[q], E. Carrara[q], R. Ciesielski[q], F. Dal Corso[q], S. Dusini[q], C. Fanin[q], A. Garfagnini[q], A. Longhin[q], L. Stanco[q], A. Schembri[r], G. Rosa[r], C. Bozza[s], G. Grella[s], G. Romano[s], C. Sirignano[s], S. Ogawa[t], H. Shibuya[t], K. Kodama[u], N. Ushida[u], S. Aoki[v], T. Hara[v], K. Hoshino[w], M. Komatsu[w], M. Miyanishi[w], M. Nakamura[w], T. Nakano[w], K. Niwa[w], O. Sato[w], T. Toshito[w], Y. Sato[x], I. Tezuka[x], S. Gampert[y], I. Kreslo[y], U. Moser[y], K. Pretzl[y], N. Savvinov[y], T. Waelchli[y], M. Hauger[z], J. Janiscko[z], F. Juget[z], J-L. Vuilleumier[z].

[a] IIHE, Université Libre de Bruxelles, Brussels, Belgium
[b] LAPP, IN2P3-CNRS and Université de Savoie, Annecy, France
[c] IPNL, IN2P3-CNRS and Université Claude Bernard Lyon I, Villeurbanne, France
[d] IRES, IN2P3-CNRS and Université Louis Pasteur, Strasbourg, France
[e] LAL, IN2P3-CNRS and Université Paris-Sud, Orsay, France
[f] Humboldt University, Berlin, Germany
[g] Hamburg University, Hamburg, Germany
[h] Fachhochschule Südwestfalen, FB Naturwissenschaften und Informatik, Iserlohn, Germany
[i] Mnster University, Münster, Germany
[j] Fachbereich Physik der Universitaet Rostock, Rostock, Germany
[k] Universitá di L'Aquila and INFN, L'Aquila, Italy
[l] Universitá di Bari and INFN, Bari, Italy
[m] Universitá di Bologna and INFN, Bologna, Italy
[n] Laboratori Nazionali di Frascati, Frascati, Italy
[o] Universitá "Federico II" and INFN, Napoli, Italy
[p] Laboratori Nazionali del Gran Sasso, Assergi, Italy
[q] Universitá di Padova and INFN, Padova, Italy
[r] Universitá "La Sapienza" and INFN, Rome, Italy
[s] Universitá di Salerno and INFN, Salerno, Italy
[t] Toho University, Funabashi, Japan
[u] Aichi Educational University, Kariya, Japan
[v] Kobe University, Kobe, Japan
[w] Nagoya University, Nagoya, Japan
[x] Utsunomiya University, Utsunomiya, Japan
[y] Bern University, Bern, Switzerland
[z] Neuchatel University, Neuchatel, Switzerland

Abstract

The OPERA experiment has been designed for an appearance search of $\nu_\mu \to \nu_\tau$ oscillations in the parameter region indicated by Super-Kamiokande as the explanation of the zenith dependence of the atmospheric neutrino deficit. OPERA is a long baseline experiment being constructed at the Gran Sasso Laboratory in the CNGS neutrino beam from the CERN SPS. The detector design is based on a massive lead/nuclear emulsion target. Nuclear emulsions are used as high resolution tracking devices, for the direct observation of the decay of the τ leptons produced in ν_τ charged-current interactions. Electronic detectors are used to locate the event in the emulsions. Magnetized iron spectrometers measure charge and momentum of muons. The discovery potential of OPERA originates from the observation of a ν_τ signal with very low background level. The direct observation of $\nu_\mu \to \nu_\tau$ appearance will constitute a milestone in the study of neutrino oscillations. The OPERA experiment will also search for $\nu_\mu \to \nu_e$ with a sensitivity a factor two better than current limits from CHOOZ. During 2005 the OPERA collaboration made important progresses on the construction of the detector components and the installation in Hall C of LNGS.

144

1   Design Principles

The OPERA experiment [1] is designed for the direct observation of ν_τ appearance from $\nu_\mu \to \nu_\tau$ oscillations in the CNGS long-baseline beam from the CERN SPS to the Gran Sasso laboratory.

The measurements of atmospheric neutrino fluxes performed by the Super-Kamiokande experiment indicate a deficit of muon neutrinos with a zenith angle distribution consistent with $\nu_\mu \to \nu_\tau$ oscillations with $\Delta m_{23}^2 = 1.9 \div 3.0 \times 10^{-3} eV^2$ (90% C.L.) and full mixing.

MACRO, Soudan2 and K2K experiments also made observations compatible with this result. Therefore the primary goal of OPERA is to obtain direct evidence for ν_τ appearance, which would confirm the oscillation hypothesis and its nature. An important byproduct is the search for $\nu_\mu \to \nu_e$ oscillations which could lead to a first measurement of the mixing angle θ_{13}.

A long baseline of 732 km is used between the neutrino source (the CERN beam line) and the detector (located in the Gran Sasso underground laboratory), in order to be sensitive to the oscillation parameters indicated by the Super-Kamiokande data. The CNGS neutrino beam has been optimized for the detection of ν_τ charged current (CC) interactions and provides an average ν_μ energy of about 20 GeV. For the evaluation of the performance of the experiment an integrated fluence of 2.25×10^{20} protons on target is assumed, corresponding to 5 years SPS operation in shared mode. However, ongoing studies at CERN aim to obtain a beam intensity upgrade equivalent to a factor 1.5.

The main principle of the ν_τ search is the direct detection of the decay of the τ lepton produced by CC interactions. This is achieved by a massive (about 1.8 $kton$) neutrino target based on the Emulsion Cloud Chamber (ECC) design which combines, in a sandwich-like cell, the high-precision tracking capabilities of nuclear emulsions (two 40 μm layers on both sides of 200 μm plastic base) and the large target mass provided by the lead plates (1 mm thick). This technique has been recently demonstrated to be effective for τ detection by the DONUT Collaboration.
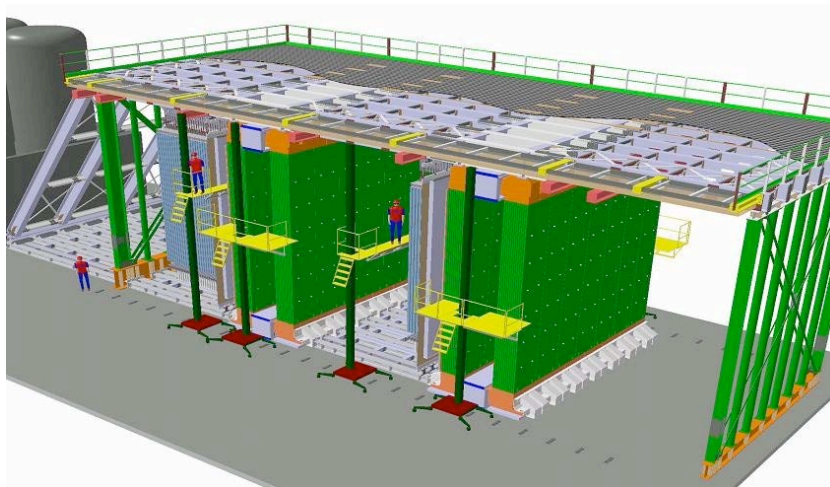
Figure 1: Schematic view of the OPERA detector during installation in Hall C.

145

The basic element of the target structure is the brick, made out of consecutive series of ECC cells with transverse dimensions of $10.2 \times 12.7~cm^2$. Bricks are arranged in planar structures (walls), which are interleaved with electronic tracker planes. These planes are built from vertical and horizontal strips of extruded plastic scintillator 2.6 cm wide, read out by wavelength-shifting fibers coupled with photodetectors at both ends. The main purposes of the target tracker are to provide a trigger for neutrino interactions, localize the particular brick in which the neutrino interacted and perform a first muon tracking within the target. The selected brick is then extracted from the target for the emulsion development and scanning in a quasi-online sequence. Large emulsion areas can be scanned with automatic microscopes equipped with fast track-recognition processors. This technique allows for the search of the tau decay topology and, at the same time, for the measurement of the event kinematic. Tracks momenta are measured from their multiple scattering in the brick and electron and gamma energies from showers development. The total number of bricks amounts to 206336 resulting in a target mass of 1766 ton.

Fig. 1 shows the side view of the OPERA detector, which is arranged in two independent super-modules. Each super-module includes a block of 31 walls+scintillator planes, followed downstream by a magnetized iron spectrometer. The spectrometers are used for the identification of muons and to measure their charge and momentum. Each spectrometer consists of a dipolar magnet made of two iron walls interleaved with pairs of precision trackers. Particle trajectories are measured by these trackers, consisting of vertical drift tube planes. Resistive Plate Chambers (RPC) with inclined strips, called XPC, are combined with the precision trackers to provide unambiguous track reconstruction in space. Moreover, planes of RPCs (Inner Tracker) are inserted between the magnet iron plates. They allow a coarse tracking inside the magnet to identify muons and ease track matching between the precision trackers. They also provide a measurement of the tail of the hadronic energy leaking from the target and of the range of muons which stop in the iron.

The OPERA design is optimized to achieve low background levels for the tau appearance search. The experiment aims at the analysis of all the single-prong tau decay modes (e,μ,h). Signal events are classified as long or short decays depending on whether the tau track traverses an emulsion sheet or not. The main background sources are charm production in CC interactions, hadronic interactions in lead and large-angle muon Coulombian scatterings. These events are rejected by the identification of the primary lepton in CC interactions and either by requiring the presence of a tau-like kink topology (long decays) or by an impact parameter method (short decays). In addition a kinematic analysis is used to enhance the signal-to-background ratio. Overall a total background of 0.7 events is expected. If $\nu_\mu \rightarrow \nu_\tau$ oscillations occur, the average number of detected signal events ranges from 8.0 (at $\Delta m^2 = 1.9 \times 10^{-3} eV^2$) to 19.9 (at $\Delta m^2 = 3.0 \times 10^{-3} eV^2$) and corresponds to 12.8 events for the Super-Kamiokande best fit value ($\Delta m^2 = 2.4 \times 10^{-3} eV^2$, full mixing).

For what concerns the search for $\nu_\mu \rightarrow \nu_e$ oscillations, still after a five years run, OPERA will be able to constrain the θ_{13} mixing angle at the level $\theta_{13} < 0.06$ at 90% C.L. (for $\Delta m^2 = 2.5 \times 10^{-3} eV^2$, $\sin^2 2\theta_{23} = 1$).

2 Detector construction progress in 2005

The OPERA experiment was approved in 2001. During 2002 the Collaboration completed the detector design, tests and optimization phase resulting in a two super-modules configuration. Important progresses were made in 2003, as foreseen by the construction schedule; in February 2003 the detector installation started in Hall C and has been going on with the assembly of the magnetic spectrometers and the RPC system (see Par. 3). After August 2004 most of the activities in the underground hall were halted to allow for the safety works in Hall C. These modifications of the LNGS infrastructures have been planned by the Commissioner appointed by the Italian government (July 2003) with the task of ensuring LNGS to be compliant with safety and environmental rules. The installation of the second magnet was resumed in autumn 2004 and completed in 2005. The target tracker modules (TT), assembled in Strasbourg (IRES), are being mounted in the underground detector. All the TT planes of the first super-module are mounted and cabled. The target walls have all been built and all the walls of the first super-module have been installed during 2004 and 2005. The installation of the walls of the second super-module will be completed in the first half of 2006. The two Brick Manipulator systems have been built in Annecy (LAAP)and the first manipulator system has been installed on one side of the detector. The mass production of the precision tracker for the spectrometers has started in Hamburg in January 2005. The first three planes have been mounted in the detector during 2005 (see Par. 4). The design of the Brick Assembly Machine (BAM) was completed, the tendering procedure has been accomplished, the industry has been selected and the construction has been finished and is ready to be assembled in Gran Sasso (see Par. 6). The mass production of nuclear emulsions started in April 2003. An underground facility for their refreshing (the erasure of the cosmic ray tracks accumulated during the production) was set up in the Tono mine in Japan. After production at Fuji Inc., the emulsion sheets are refreshed and then sent to Gran Sasso where an emulsion storage area, located in the hall B of LNGS, was built in summer 2003. The first set of refreshed emulsions (1.5 millions of emulsion sheets) have been shipped from Japan and has arrived in the underground laboratory on January 2005. During 2005 and beginning of 2006 all produced emulsions (78% of the required 12 Ml emulsion sheets) have arrived at Gran Sasso. The development of the scanning systems has improved significantly. A peak scanning power of 20 cm^2/h has been reached by the european laboratories. The development of the Japanese scanning system is also well in progress. In the external Laboratories of Gran Sasso a scanning station has been set up. At the end of 2005, 6 microscopes have been installed to be used for the automatic scanning of the Changeable Sheets. The OPERA installation will end in 2006/beginning of 2007, when the neutrinos from the CNGS beam are expected.

3 Status of the RPC system

During the year 2005 the project was fully set up in the underground area and provided the first tracks from cosmic events, so validating the correctness of installation procedures, electronic grounding and noise control. The RPC system in OPERA consists of the 22

147

detection layers which instrument each of the two Spectrometers. Each layer is read-out for a total of 560 digital channels, with a pitch of 2.6 cm in the bending coordinate and 3.5 cm in the other one. A big achievement was reached in March with the end of the installation of the 924 chambers, each of 3 m^2 of sensible region (see Fig. 2). Each detector underwent a strong series of laboratory tests before being considered for installation, for mechanical and electrical stresses and efficiency point of views. A total of 30% of tested detectors were put apart due essentially to high dark current performances. The selected ones own a reasonable expectation to well behave for all the OPERA data taking duration (10 years). During installation only a handful were replaced due to mechanical failures. Furthermore in May we succeeded to perform a measurement on the performances of 4 instrumented layers. The data taking lasted 2.5 days and the results were exceptionally good:

1. the 4×21 detectors showed to be fully operational;
2. the signal read-out was clearly recorded as expected;
3. the efficiency over the full area corresponded to the laboratory behavior, around 96% of the geometrical area (see Fig. 3);
4. comparison with detailed Monte Carlo predictions tested in previous experiments, showed an excellent agreement in term of total rate and angular distributions of the cosmic ray flux in the underground area of Gran Sasso (see Fig. 4).

Parallel works were developed and tested with concern to:

1. DAQ data taking, in the framework of the full OPERA system;
2. online monitoring system;
3. software reconstruction of single and multiple track events for either cosmic ray and CNGS beam fluxes.

Next steps in the project foresee the commissioning of

1. gas system distribution;
2. front-End cards, each of 64 channels;
3. operations with magnets on.

The schedule of the latter items are compatible with the foreseen start of the CNGS beam operations in June 2006. In particular switching on of the full system is scheduled in Spring 2006.

4   Status of Precision Tracker installation

Till end of December 2005 85 Precision Tracker modules (PT) are produced and wired. 84 modules of them are successfully tested. The wire tension, the dark current and the leakage rate is in an acceptable range. 49 of the produced modules are already installed in the OPERA detector as planes HPT 1, 2 and 5. Thus the half of the 1st spectrometer has been mechanically installed and successfully tested. All the HV boards for SM 1 and SM 2 are available and will be assembled and tested. The redesigned amplifier boards have excellent detection characteristics and minimized cross talk behavior and
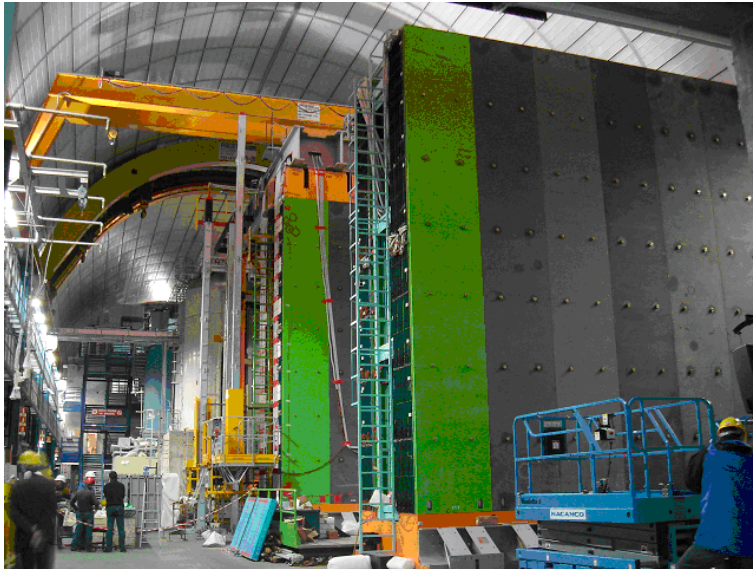
Figure 2: End of RPC installation on 2005, May 19th. The two magnets are visible from behind, each containing 22 layers of RPC chambers.
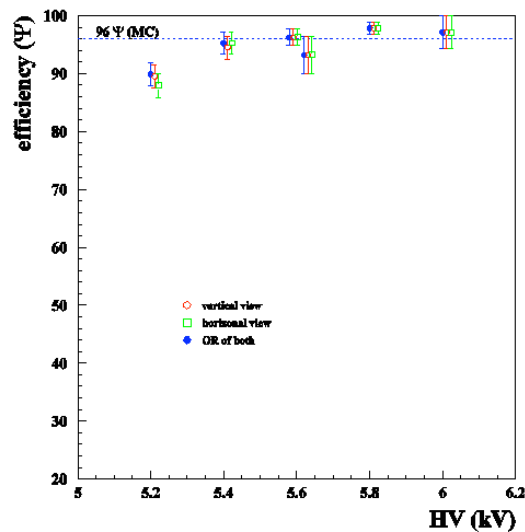
Figure 3: The efficiency of the 4 read-out layers for different HV working points. The three data sets correspond to vertical (red), horizontal (green) and both vertical and horizontal (blue) strips read-out. The dashed line corresponds to the Monte Carlo expectation from a simulation of the RPC signal read-out developed in laboratory tests. The working point of 5.6 kV corresponds to maximum efficiency and it corresponds to the same value used in the outside laboratory building.
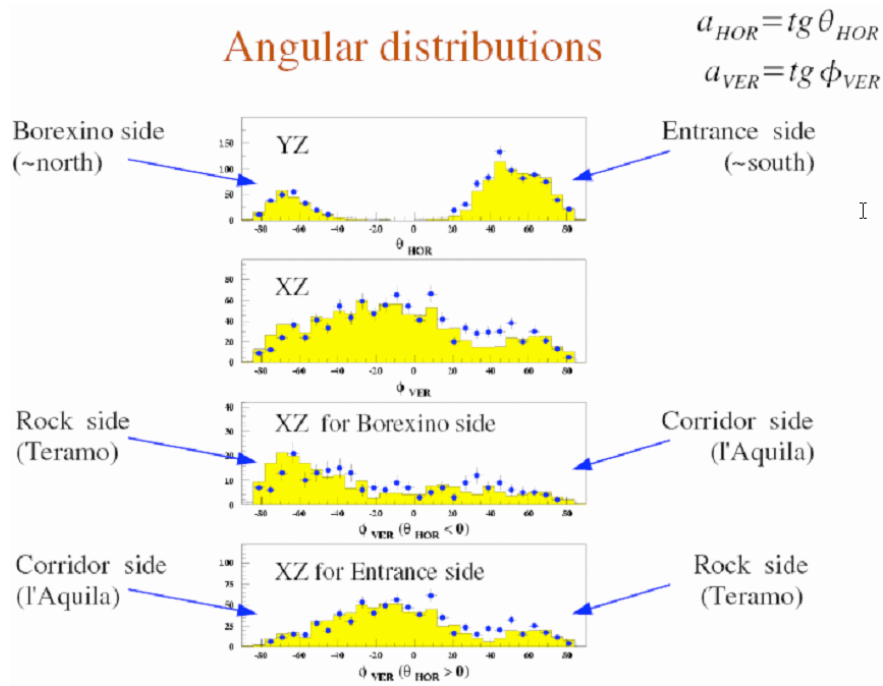
Figure 4: The angular distributions of the collected single track cosmic muons in 2.5 days of data taking. Z is the CNGS beam axis, Y the vertical axis and X the third component of the orthogonal system (positive X toward the corridor of HALL C). The blue dots are the measurements and the yellow histogram the Monte Carlo expectation from a MACRO parametrization of the cosmic flux in HALL B. Note that no relative normalization was applied, as well as no pre-alignment of the strips. The measured total rate is 15.6 ± 0.5/hour, to be compared with the expected Monte Carlo value 15.2 ± 0.3/hour.

are ready for mass production. The amplifier control boards for threshold settings and test pulse generation are successfully tested. The mass production has been started in December. The 1st TDC board (University of Rostock) has been successfully operated with the Mezzanine board (Lyon). All mass production TDC boards for SM1 and SM2 are delivered already in December and can be equipped with the mass produced Mezzanine. The slow control for the PT is under development. A new industrial standard system of the company Beckhoff will be used. It is possible to build the whole slow control for SM 1 and SM 2. The design of the gas system is ready for SM 1 and SM 2 and first prototypes are successfully tested. The system for SM 1 is being built. The construction of the gas system of SM 2 will be done in the next funding period 2006. The PT trigger board was designed and the first prototype will be build. During the installation of HPT 5 in November 2005 the commissioning of HPT 1, 2 and 5 has been started. The HV and LV cabling and the voltage and current tests were successfully done for the three planes. The HV current for one plane is less than 2 A and even better than the requirements. Furthermore the 1st part of the temperature monitoring was installed and successfully operated on the already installed modules with two different systems. One system will be used for normal temperature checking while the other system will be used for more accurate measurements on the modules and gas system. The first part of the gas system has been successfully tested as well. The whole plane HPT 2 and one module of HPT 1 was operated with pre-mixed gas and the designed distribution of our gas system. So there is the possibility to start data taking soon with two consecutive modules. The overall alignment of HPT 1 and 2 using the old reference system was better than 500 μm (within the requirement). HPT 5 was aligned using the new reference system better than 500 μm (overall alignment) too. Before May 2006 all the PT planes of the first super-module will be installed. PT planes of the second super-module are foreseen to be installed in the second half of 2006/beginning of 2007.

5   Target Tracker activity

The construction of the OPERA Target Tracker, responsible to indicate the right brick to extract from the detector target, is almost finished. The Target Tracker installation at LNGS is under way. During 2005, the whole first super-module has been installed.

The Target Tracker is composed by 62 walls, each one associated with one brick wall. Each Target Tracker wall contains four horizontal and for vertical modules defining a sensitive area of about $7 \times 7 \ m^2$. The Target Tracker modules enclose 64 scintillator strips readout by Wave Length Shifting fibres and multianode Hamamatsu photomultipliers. For the whole Target Tracker (496 modules), 992 photomultipliers, 31200 AMCRYS-H scintillator strips and about 300 km Kuraray WLS fiber have been used.

After construction at IReS-Strasbourg, each module is tested and calibrated before sending it to Gran Sasso for installation inside the detector.

For the Target Tracker wall mounting and detector insertion in LNGS underground laboratory, the strategy adopted by the experiment consists of mounting the Target Tracker walls outside the detector and inserting them one by one when needed. In this way, a brick-Target Tracker wall interference is limited and several teams can work in

parallel. For this purpose, the Target Tracker group has installed in Hall C a mounting platform and a wall storage arch. This operation way allowed to OPERA to double the installation speed of its target section.

The Target Tracker installation is expected to finish by May 2006. A partial commissioning of the detector has already started and it is expected to finished early after the whole installation is finished.

6 BAM project activity in 2005

The Brick Assembly Machine (BAM) is an automatic system whose aim is the mass production of about 207000 brick of the OPERA detector in about 220 working days. This will mean about 960 brick a day, meaning a production rate of about 1 brick each 30 seconds for 8 working hours a day. A brick is constituted by pile of 57 emulsion films interleaved with 56 lead sheets. The pile has to be performed within 50 μm piling precision and with no additional deformation to the lead sheets (10 μm flatness) and no distortion and chemical effects on the emulsion films while automatic handling occurs. The BAM project had in 2005 the beginning on the construction of the key parts of the machine for brick production and packaging, according to the mechanical method frozen and tested the year before. Three main parts of the machine have been started in parallel:

- the automatic system for the handling of the lead boxes;
- the piling/pressing station, to be produced in 5 samples;
- the wrapping station of the brick with Al tape.

The automatic system to handle lead transportation boxes (see Fig. 7) was conceived as a 25 m long double rolling carpet 1.7 m large on which the transportation boxes full of lead are coming in the BAM on the upper rolling carpet and are coming out on the rolling carpet below. The automatic handling system is capable to remove the cover of the boxes, take the lead cartridges one by one and position them on the shuttles that carry them in the BAM in dark. Moreover the same system takes the empty cartridges coming out from the BAM in ark ad positions them in the empty box. At the end of the cycle, the cover is positioned again on the box which is moved on the second rolling carpet below. All this system has been implemented and is being commissioned now.

The first piling/pressing station (see Fig. 8) has been constructed using two anthropomorphic robots and a custom pressing unit capable to close the brick Al case on top of the plastic components (cover and lateral protection). The piling operation demands the fast and clean handling of lead and emulsion sheets individually. To achieve that two custom pneumatic systems (for lead and emulsion respectively) have been produced. The first station was completed by the end of 2005 and 4 replicas have been implemented in last months. The piling precision of 50 μm in the lead/emulsion misalignment has been achieved and controlled with a video system which feeds back the piling operations. The 2 Al tape wrapping stations have been implemented in order to guarantee the complete light tightness of the brick. The first wrapping machine positions 2 covers on the top and bottom sides of the brick. The second wrapping machine positions the lateral ribbon of Al tape in order to guarantee the protection of all the 4 sides of the brick. All the

Figure 5: During commissioning of the Target Tracker walls in the first super-module.

Figure 6: Installation of the first Target Tracker wall in the second super-module end of 2005.

Figure 7: The automatic system to handle lead transportation boxes.

Figure 8: The top view of the first piling/pressing station.

brick movement from one station to the other has been implemented using a large size anthropomorphic robot capable to handle up to 25 kg weight. The wrapping cycle is well inside the specs both in terms of speed and precision.

Figure 9: The wrapping station of the brick with Al tape.

Figure 10: The BAM site in the LNGS underground laboratory.

On top of the above activities in the BAM project the design of the lead transportation box and transportation pallets were finalized. The final technical drawing and prototype of the box and pallet have been produced. 1000 boxes have been produced by an external firm and delivered to the lead firm. 18000 plastic pallets are being produced now (first 6000 already delivered to lead firm). At the LNGS the BAM site (see Fig. 10) has been completed in terms of air conditioning, electrical networking, safety and civil engineer infrastructures. The BAM site is now being commissioned in term of stability of performances of air conditioning and clean room.

7   Alignment

At the end of 2003 the OPERA collaboration decided to start a coherent and structured project for the alignment of the detector. This aspect is particularly relevant for the target, which is highly fragmented (bricks, modules of scintillator strips). The relative alignment of these components is important in order not to worsen the brick finding performance. The goal is to achieve better than 1 mm relative accuracy in the knowledge of the position of the bricks with respect to the strips. This level of accuracy has to be achieved on target elements (brick walls and target tracker biplanes), which have typically a front surface of about 50 m^2. In addition to the relative alignment of the target components, the alignment project covers also the positioning of all the sub-detectors (the target, the HPT precision tracker, the RPC strips and the brick manipulator) in a global reference frame of the experiment, extended to the two super-modules. Several techniques have

154

been tested implemented at Gran Sasso and largely exploited during 2005, which has been a crucial year for the construction of the detector.

The first technique, which was selected for the survey of the detector elements during and after the installation, was the "Close range targeted digital photogrammetry". This technique is commonly used at CERN for the metrology of LHC experiments. The technique is based on equipping the detector with various kinds of retro-reflective targets and on taking a large set of pictures with a high-resolution digital camera from many positions uniformly distributed on the front face of the detector. A specialized software allows for the reconstruction of the 3D image of the cloud of points measured on the detector by combining all the pictures and the 3D position of each point is determined with a global fit exploiting the all the triangulations. In collaboration with the CERN survey group, the expertise needed to apply this technique to the specific OPERA needs was quickly acquired. Two persons from LNGS: A.Lucente and L.Marrelli were trained in order to perform the measurements and contributed to all survey activities based on the photogrammetry. This technique was massively used since the fall of 2004 to the end of spring 2005 to perform a precise and extensive debugging of all the non-planarity and mechanical problems encountered during the installation of the first target detector elements (walls and target trackers). In February 2005 another technique was implemented based on the use of a Leica "Total Station System" TDA500. This instrument is capable of performing 3D measurements of a retro-reflective target (CCR) with an accuracy of about 0.2 mm on the typical distances of the OPERA installation (up to 20 m). The instrument is completely automatic, remote controllable and it is able to perform the target recognition (ATR), which replaces completely the human intervention in standard teodolites to align the target by looking through the optics of the instrument. Once the target is locked in, the TDA is able to track it automatically even if the target is moving up to a speed up of 3-4 m/s. The TDA technique has been used systematically during the construction of the target restarted in May 2005, and in order to obtain the final alignment data for the geometry database. The TDA was used successfully starting since June also for the survey of the first HPT (precision tracker) modules inserted in the first super-module. Given the need of starting the construction of the second target and of calibrating the brick manipulator movements over the two super-modules, in the fall 2005 it was the implementation of a global reference system in the experimental hall. The alignment activities will continue during 2006 with the construction of the second target, the HTP installation in the spectrometers, the calibration of the BMS, the measurement of the corrections to the target geometry during the loading with the bricks and the integration of all the data in the geometry database and their exploitation and validation with the analysis of the events recorded by the electronic detectors. In conclusion a variety of techniques have been developed to satisfy various alignment needs and have been largely exploited during the installation. OPERA is today disposing of the state of the art equipments for the alignment and survey. The OPERA collaboration acknowledges the cooperation and support obtained from LNGS both in terms of equipments and personnel for the alignment project.

8   The OPERA Data Acquisition System

IPNL (IN2P3, Lyon-France) has the entire responsibility of the OPERA DAQ system (Target Tracker, Spectrometer & VETO). The system relies on the concept of Ethernet capable "smart sensors" thanks to an embedded processor as close as possible to the front-end electronics. The processor is plugged with a sequencer (FPGA-type) on a daughter-board, called "mezzanine", which is common to all sub-detectors. More than 1200 such sensors, plugged on different motherboards (ADC for TT scintillator readout - 1042 boards also developed, produced and validated by IPNL -, TDC for drift tubes readout and Controller Board for RPCs) are connected through a standard Ethernet network to the event builders and general servers (NFS, DHCP, clock distribution servers etc.). The network is divided in different VLANs. The DAQ software has been developed in the CORBA general framework of distributed applications, implemented in C++, and validated on the sub-detectors already in commissioning. All the sensors are synchronized through a distributed 20 MHz clock, locked on the GPS signal delivered underground though the LNGS ESAT system. The clock distribution system was developed and validated by IPNL. The general system, in final configuration, except for the computing part, has been tested on a fraction of SM1 TT (up to 40% of SM1) which was equipped with complete electronics chain. Thousands of cosmic tracks have been recorded since September 2005. Various auto-triggering conditions have been tested and studies were performed on network load, servers CPU load etc.

9   List of Publications

1. M. De Serio *et al.*, "High precision measurements with nuclear emulsions using fast automated microscopes," Nucl. Instrum. Meth. A **554** (2005) 247.

2. N. Armenise *et al.*, "High-speed particle tracking in nuclear emulsion by last-generation automatic microscopes," Nucl. Instrum. Meth. A **551** (2005) 261.

References

[1] M. Guler *et al.*, OPERA proposal, CERN/SPSC 2000-028, SPSC/P318, LNGS P25/2000.

CRESST. Dark Matter Search

G. Angloher [a], C. Bucci [d], P. Christ [a], F. von Feilitzsch [c], D. Hauff [a],
S. Henry [b], Th. Jagemann [c], J. Jochum [e], H. Kraus [b], B. Majorovits [b],
J. Ninkovic [a], E. Pantic [a], F. Petricca [a], W. Potzel [c], F. Pröbst [a],
Y. Ramachers [b, *], M. Razeti [c], W. Rau [c], C. Rottler [e], W. Seidel [a, +],
M. Stark [c], L. Stodolsky [a], A. J. B. Tolhurst [b], W. Westphal [c],

[a] MPI für Physik, Föhringer Ring 6, 80805 Munich, Germany
[b] University of Oxford, Department of Physics, Oxford OX1 3RH, U.K.
[c] Technische Universität München, Physik Department, D-85747 Garching, Germany
[d] Laboratori Nazionali del Gran Sasso, I-67010 Assergi, Italy
[e] Eberhard-Karls-Universität Tübingen, D-72076 Tübingen, Germany
[+] Spokesperson E-mail address: seidel@mppmu.mpg.de
[*] present address: University of Warwick, Coventry CV4 7AL, U.K.

Abstract

The aim of CRESST (**C**ryogenic **R**are **E**vent **S**earch with **S**uperconducting **T**hermometers) is to search for particle Dark Matter and to contribute to the elucidation of its nature. The experiment is located at the 'Laboratori Nazionali del Gran Sasso' (LNGS), Italy, and it uses low background cryogenic detectors with superconducting phase transition thermometers for the direct detection of WIMP-nucleus scattering events.

1 The Dark Matter Problem

The search for Dark Matter and the understanding of its nature is of central interest for particle physics, astronomy and cosmology. There is strong evidence for its existence on all scales, ranging from dwarf galaxies, through spiral galaxies like our own, to large scale structures. The history of the universe is difficult to reconstruct without Dark Matter, be it Big Bang Nucleosynthesis or structure formation.

Particle physics provides a well motivated candidate with the lightest SUSY-particle, the "neutralino". Generically, such particles are called WIMPs (Weakly Interacting Massive Particles). WIMPs are expected to interact with ordinary matter by elastic scattering on nuclei. All direct detection schemes have focused on this possibility.

Conventional methods for direct detection rely on the ionization or scintillation caused by the recoiling nucleus. This leads to certain limitations connected with the low ionization or scintillation efficiency of the slow recoil

7

nuclei. The cryogenic detectors developed for the first phase of CRESST (CRESST-I) measure the deposited energy calorimetrically, independent of ionization, and allow a detection of much smaller recoil energies. When the cryogenic measurement of the deposited energy is combined with a measurement of scintillation light an extremely efficient discrimination of the nuclear recoil signals from radioactive background signals can be obtained. This type of detectors is beeing used in the upcoming phase CRESST-II.

2 Detection Principle

The low temperature calorimetric detectors consist of a target crystal, the so-called absorber, an extremely sensitive superconducting phase transition thermometer, and a weak thermal coupling to a heat bath to allow thermal relaxation of the system after an interaction. The thermometer is made of a tungsten film evaporated onto the absorber crystal. Its temperature is stabilized in the transition region from the superconducting to the normal conducting state, which occurs at termeratures of about 10 mK. A typical width of the transition region is about 1 mK. A small temperature rise (typically some μK), e.g. from a WIMP nucleus scattering event, leads to an increase of resistance, which is measured with a SQUID based readout. For the first phase of CRESST, which ended in Feb. 2001, 262 g sapphire detectors have been developed at the institute. These detectors provided an excellent energy resolution of 133 eV at 6 keV and a very low energy threshold of 600 eV.

In the upcoming second phase CRESST-II, we are using 300 g scintillating $CaWO_4$ crystals as absorbers. The scintillating crystal is equipped with a superconducting tungsten phase transition thermometer for the detection of the phonons created by particle interactions in the scintillating crystal. The scintillation light is measured in coincidence with a separate cryogenic detector, optimized for light detection. Fig. 1 schematically shows the setup of this composite detector. Starting with a proof of principle experiment in 1998, the technique of simultaneous measurement of phonons and scintillation light has been developed at the institue.

The important advantage of the simultaneous detection of phonons and scintillation light is that it offers an extremely efficient suppression of the radioactive background. The ratio of the energy in the phonon channel and the energy in the light channel depends on the type of interaction. Nuclear recoils, such as WIMP or neutron scattering events, emit substantially less scintillation light than fully ionizing interactions, e.g. γ or β interactions do. As the overwhelming part of the backgroud consists of β and γ interactions,

8
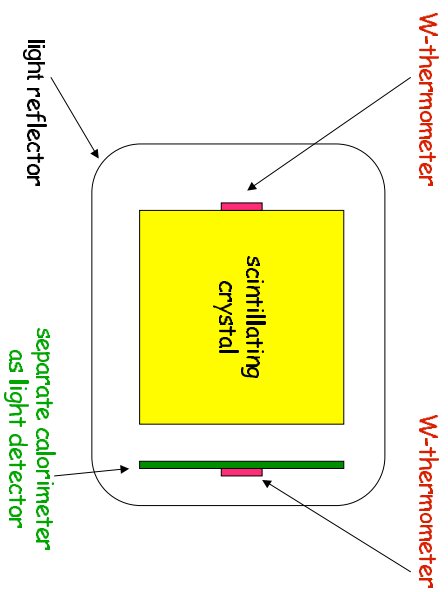
Figure 1: Sketch of the detector setup for the coincident detection of phonons and scintillation light. This novel concept will be used in CRESST-II. It allows to efficiently discriminate nuclear recoils signals from radioactive backgrounds.
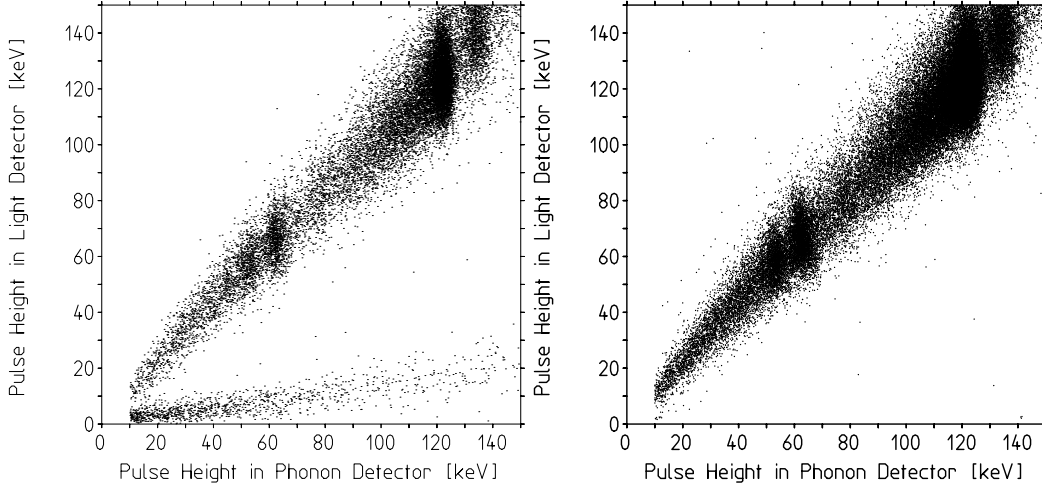
Figure 2: Coincident detection of phonons and scintillation light with a 6 g proof of principle CaWO$_4$ detector. Left fig.: The upper band of events is due to irradiation of the CaWO$_4$ crystal with electrons and gammas, whereas the lower band with lower light yield, is from nuclear recoils caused by a neutron source. Removing the neutron source (right fig.), confirms that there is no leakage of ionizing events into the nuclear recoil region.

this phonon/light technique provides a very effective method of background suppression. Fig. 2 illustrates this novel detection method. With this proof of principle device, a 99.7 % suppression of ionizing background in the energy range from 15 and 25 keV , and 99.9 % at energies above 25 keV has been demonstrted.

   Compared to the alternative approach of simultaneous measurement of phonons and charge in a semiconductor crystal, which is applied in the experiments CDMS and Edelweiss-II, the method developed for CRESST-II has the important advantage that it does not suffer from dead layers at the surface. A reduced charge collection for ionizing events occurring close to the surface in semiconducting crystals may lead to a false identification of low energetic γ's and β's as nuclear recoils. The result in Fig. 2, which was obtained with a gamma and beta source, confirms that the supression also works for low energy electrons impinging onto the crystal surface.

3   The CRESST Setup in Gran Sasso

The central part of the CRESST installation is the cryostat, sketched in figure 3. The low temperature generated in the mixing chamber of the di-
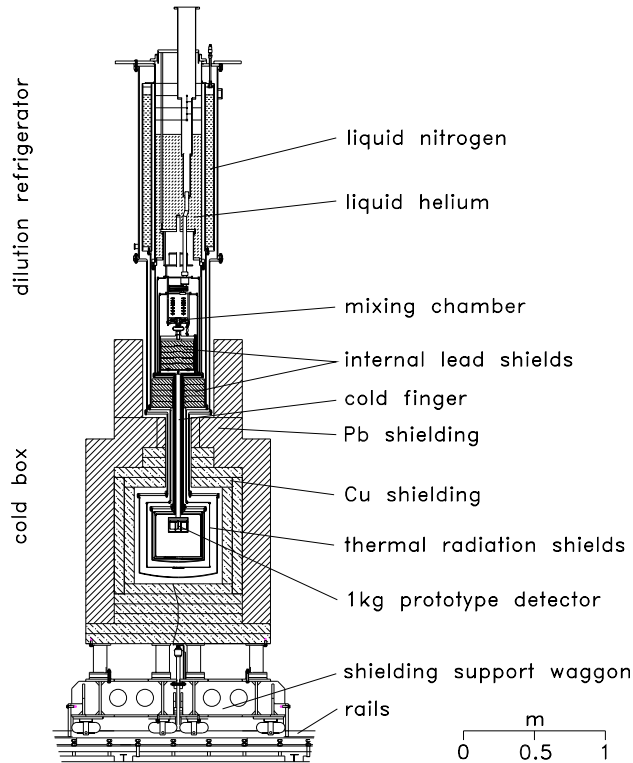
Figure 3: Layout of the CRESST ^{3}He/^{4}He dilution refrigerator and low background cold box with its shielding.

lution refrigerator is transferred into the radiopure cold box, which houses the detectors, via a 1.5 m long cold finger, protected by thermal radiation shields, all fabricated of low background copper. Two internal cold shields consisting of low level lead are attached to the mixing chamber and to a thermal radiation shield at liquid N_2 temperature, respectively, in order to block any line-of-sight from the non-radiopure parts of the dilution refrigerator to the detectors inside the cold box. The design completely avoids potentially contaminated cryogenic liquids inside the cold box.

An extensive passive shielding of low background copper and lead surrounds the cold box and serves to shield radioactivity from the surrounding rock. The entire shilding is inclosed inside a gas-tight radon box, that is flushed with boil of N_2 gas and maintained at a small overpressure. Special care has been taken to minimize above ground exposure of the construction materials of the cold box and the shielding to cosmic rays, in order to avoid activation.

Figure 4 schematically shows the CRESST experimental building. The cryostat is installed in a two level faraday cage to shield electromagnetic

11
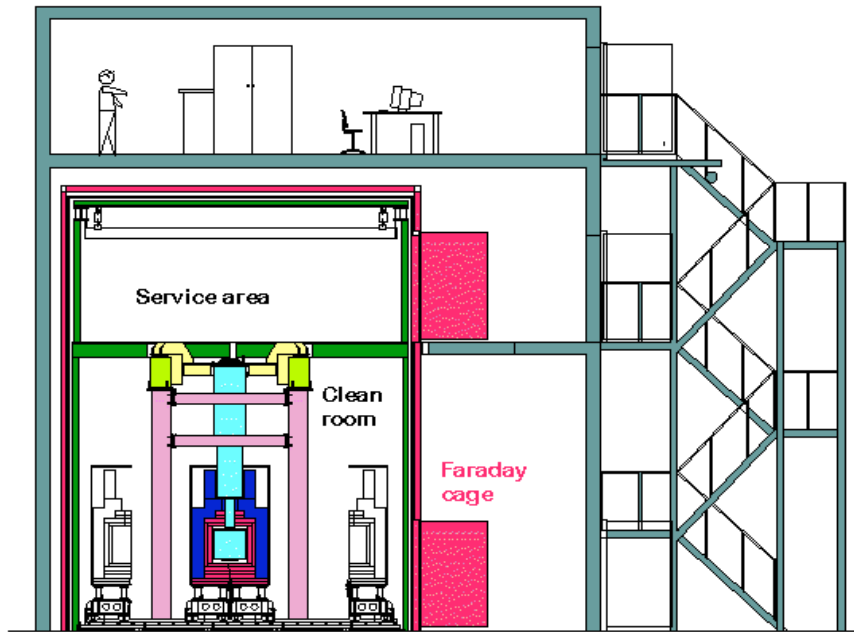
Figure 4: Schematic drawing of the three level CRESST building in hall B of the Gran Sasso Underground Laboratory.

interference. The ground level inside the faraday cage is equipped as a class-100 clean room, in order to minimize contamination of the detectors and cold box during mounting. The head of the cryostat extends into the first floor of the farady cage, which is outside the clean room to simplify servicing of the cryostat. The first floor also houses the sensitive analog electronics. The gas handling system of the cryostat and the DAQ is outside the faraday cage. In the top floor, of the experimantal building a laminar flow work place is installed which serves to assemble and rebond detectors under clean conditions.

The setup is now beeing upgraded for the experimental program of CRESST-II, which will use 33 of such 300 g phonon/light detector modules. The upgrade includes the installation of a 66 channel SQUID readout system in the existing cryostat, the installation of a neutron shield and a muon veto and a new multichannel electronics and DAQ. The cryostat with the upgraded shielding is shown schematically in fig. 5. The upgrade will be completed in 2006.
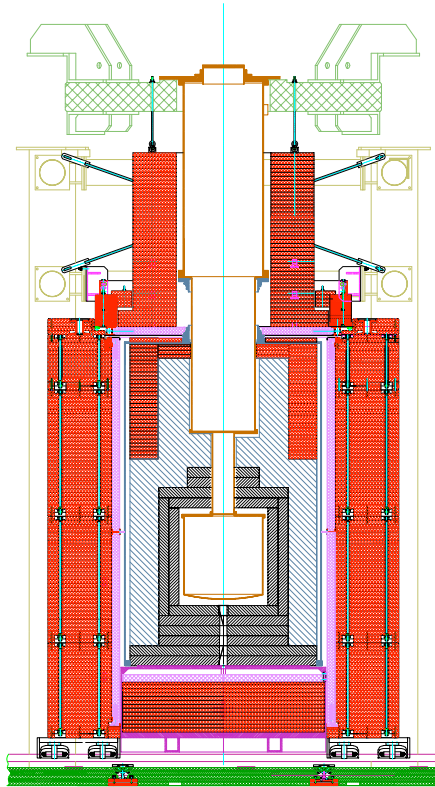
Figure 5: Dilution refrigerator and low background cold box with its shielding upgraded for CRESST-II. The gas tight radon box enclosing the Cu (shown in grey) and Pb (blue) shielding will be completely covered by a plastic scintillator μ-veto (pink) and 50 cm of polyethylen (red).

4 Preparations for CRESST-II

Starting in spring 2001, the CRESST set-up had to be moved from hall B to hall A within LNGS. After completion of this move the cryostat was still equipped with the four SQUID readout system of CRESST-I, which at most allows to run two detectors in parallel. In the beginning of 2002 operation started again with testing and optimization of $300\,\mathrm{g}$ $CaWO_4$ prototype detector modules for CRESST-II. In 2002 and 2003 a series of runs was made to optimize the performande of the detector modules. The mounting systems of the crystals again tuned out to be a very critical issue, and it introduced spurious events. In the last run at the end of 2003 the problem was solved. An additional run with two detectors was performed in 2004 with a net exposure of 20.5kg days. Form factor effects effectively limit the energy transfer to the heavy tungsten nuclei in elastic WIMP nucleus scattering to energies below 40 keV. We obtained 16 events in the nuclear recoil acceptance band in the relevant energy region between $12\,\mathrm{keV}$ and $40\,\mathrm{keV}$. The cryostat is still without neutron shield and this rate of 0.87 events per kg and day is consistent with the predicted neutron background. Moreover, most of this recoil events have a clear light signal associated with the phonon signal as expected for neutron generated recoils. Neutron events in this energy range are dominantly oxyxgen recoils, whereas WIMPs with spin independent interaction almost exclusively ($\sigma \propto A^2$) recoil off tungsten nuclei. We have measured a very large quenching factor of $Q \approx 40$ for W-recoils, whereas the quenching factor for oxygen recoils is $Q = 7.3$ at mK temperatures and $Q \approx 10$ at room temperature. If a similar quenching factor applies for the tungsten recoils at low temperature, there should be no light emission observed in the 12 to 40 keV region within the detection limit. The exclusion plot derived from this run is shown infig. 6.

The detector was calibrated with external ^{57}Co (122 keV γ's) and ^{60}Co (1.1 MeV and 1.3 MeV γ's) sources. With electric heater pulses the energy calibration is extended over the complete energy range of interrest. Periodically injected heater pulses also serve to confirm the stability of the calibration and to measure the trigger efficiency close to threshold. The phonon channel had a detection threshold for reoils of 3 keV at 100% efficiency and the threshold of the light channel was 8 keV for γ andβ interactions. As shown in fig. 7, the phonon channel exhibited an energy resolution of 1 keV at a 46.53 keV peak from an external ^{210}Pb contamination during the whole measuring period.

Since this detectors can clearly discriminate background from alpha particles and pgamma background one can obtain a background free alpa spectrum. In this spectrum we could unambigously detect the natural α-decay

WIMP-nucleon cross-section [pb]

WIMP mass [GeV/c²]

CRESST all nuclear recoils
CRESST W recoils only
EDELWEISS
CDMS Soudan
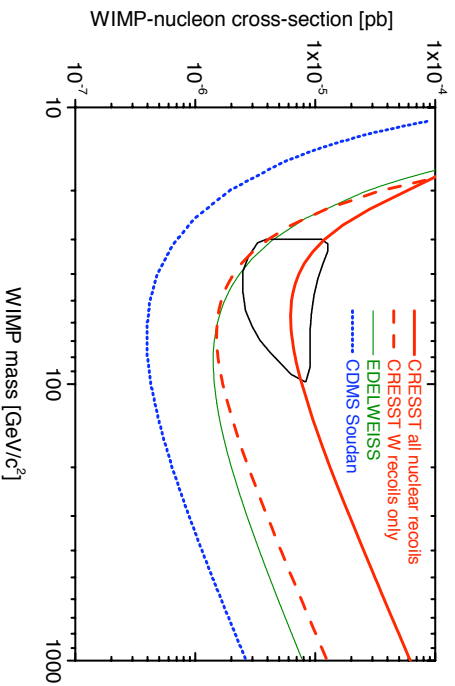
Figure 6: Exclusion plot for spin independent WIMP interaction, derived from 8.11 kg days of data from one 300 g CRESST-II detector module. The area above the curve is excluded at 90% c.l. For comparison, the DAMA positive evidence is shown and also the limits from other cryogenic experiments, CDMS and EDELWEISS.

Counts / (kg keV day)

Energy in Phonon Channel [keV]
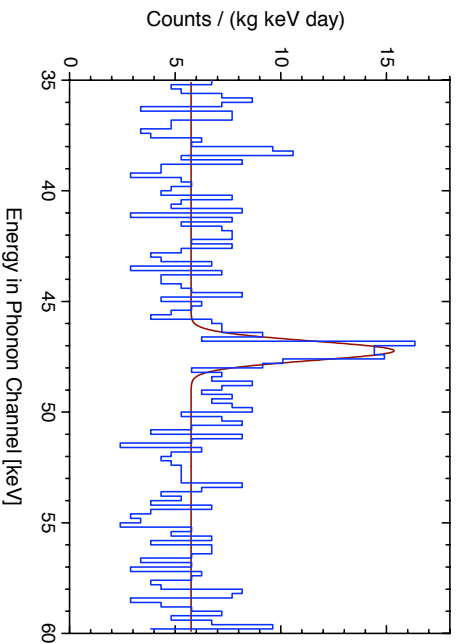
Figure 7: Energy spectrum of the phonon channel of a 300 g CaWO$_4$ detector. The peak at 46.53 keV, with a rate of 3.2 counts/day, is from an external ^{210}Pb contamination. The agreement with the nominal decay energy and the good resolution confirms the energy calibration and its stability.

of ^{180}W.A half-life of $T_{1/2} = (1.8 \pm 0.2) \times 10^{18}$ y and an energy release of Q = (2516.4 $\pm$ 1.1 (stat.) $\pm$ 1.2 (sys.)) keV have been measured. The limits on the decay of other Tungsten isotopes could be improved by more than a foactor 50 over present limits.

5   Publications

Limits on WIMP dark matter using scintillating CaWO cryogenic detectors with active background suppression G.Angloher et al. Journal of Astroparticle Physics 23 , 325-339 (2005)

Detection of Natural Alpha Decay of Tungsten C. Cozzini et al. Phys. Rev. C 70 (2004)

CRESST-II: dark matter search with scintillating absorbers

G. Angloher et al. NIM A Vol. 520 Nos. 1-3

Light detector development for CRESST-II,

F. Petricca et al. , NIM A Vol. 520 Nos. 1-3

CUORICINO and CUORE. Neutrinoless double beta decay searches with low temperature detectors

F. Alessandria[2], R. Ardito[1,3], C. Arnaboldi[1], D. R. Artusa[4], F. T. Avignone III[4], M. Balata[5], I. Bandac[4], M. Barucci[6], J.W. Beeman[7], F. Bellini[16], C. Brofferio[1], C. Bucci[3], S. Capelli[1], F. Capozzi[1], L. Carbone[1], S. Cebrian[8], M. Clemenza[1], C. Cosmelli[16], O. Cremonesi[1], R. J. Creswick[4], I. Dafinei[16], M. Diemoz[16], M. Dolinski[7,11], H. A. Farach[4], F. Ferroni[16], E. Fiorini[1], S.J. Freedman[7,11], C. Gargiulo[16], E. Guardincerri[10], A. Giuliani[9], P. Gorla[8], T.D. Gutierrez[7], E. E. Haller[7,13], K. Heeger[14], I. G. Irastorza[8], E. Longo[16], G. Maier[3], R. Maruyama[11], S. Morganti[16], S. Nisi[5], C. Nones[1], E. B. Norman[15], A. Nucciotti[1], E. Olivieri[5], P. Ottonello[10], M. Pallavicini[10], V. Palmieri[14], E. Pasca[5], M. Pavan[1], M. Pedretti[9], G. Pessina[1], S. Pirro[1], E. Previtali[1], B. Quiter[6,11], L. Risegari[6], C. Rosenfeld[4], S. Sangiorgio[9], M. Sisti[1], A. R. Smith[7], L. Torres[1], G. Ventura[6], N. Xu[7], and L. Zanotti[1]

1. Dipartimento di Fisica dell'Università di Milano-Bicocca e Sezione di Milano dell'INFN, Milano I-20126, Italy

2. INFN - Sezione di Milano, Milano I-20133, Italy

3. Dipartimento di Ingegneria Strutturale del Politecnico di Milano, Milano I-20133, Italy

4. Dept.of Physics and Astronomy, University of South Carolina, Columbia, South Carolina, USA 29208

5. Laboratori Nazionali del Gran Sasso, I-67010, Assergi (L'Aquila), Italy

6. Dipartimento di Fisica dell'Università di Firenze e Sezione di Firenze dell'INFN, Firenze I-50125, Italy

7. Nuclear Science Division, Lawrence Berkeley National Laboratory, Berkeley, CA 94720, USA

8. Laboratorio de Fisica Nuclear y Altas Energias, Universidàd de Zaragoza, 50009 Zaragoza, Spain

9. Dipartimento di Fisica e Matematica dell'Università dell'Insubria e Sezione di Milano dell'INFN, Como I-22100, Italy

10. Dipartimento di Fisica dell'Università di Genova e Sezione di Genova dell'INFN, Genova I-16146, Italy

11. Department of Physics, University of California, Berkeley, CA 94720, USA

12. Department of Materials Science and Mineral Engineering, University of California, Berkeley, CA 94720, USA

13. Physics Division, Lawrence Berkeley National Laboratory, Berkeley, CA 94720, USA

14. Laboratori Nazionali di Legnaro, I-35020 Legnaro (Padova), Italy

15. Lawrence Livermore National Laboratory, Livermore, California, 94550, USA

16. Dipartimento di Fisica dell'Università di Roma La Sapienza e Sezione di Roma dell'INFN, Roma I-00185, Italy

Abstract

CUORE is a bolometric experiment which aims at searching for neutrinoless double beta decay of ^{130}Te with a sensitivity on the Majorana neutrino effective mass of the order of 20-30 meV. The CUORE detector will consist of an array of 988 TeO$_2$ bolometers arranged in a cylindrical configuration of 19 towers of 52 5×5×5 cm^3 crystals each. A slightly modified tower of CUORE, named CUORICINO, has been already built in 2002 and is taking data at LNGS since 2003. It consists of 44 cubic TeO$_2$ crystals of 5×5×5 cm^3 and 18 crystals of 3×3×6 cm^3 arranged in a single 13 storey tower. With a mass of 40.7 kg it is the largest mass detector operating at low temperature ($\sim$ 10 mK). Besides being a crucial test of the CUORE concept, CUORICINO is also a sensitive experiment on $\beta\beta(0\nu)$ of ^{130}Te. The progress achieved during 2005 for CUORE and CUORICINO is reported.

1 Introduction

The results of the neutrino oscillation experiments have provided convincing evidence that neutrinos undergo flavor-changing oscillations and therefore have non-zero mass. However, these experiments are only sensitive to the squared differences in the masses of the neutrinos and cannot therefore fix the absolute scale of neutrino mass which, on the contrary, can only be directly inferred by beta decay end point spectral shape measurements, or in the case of Majorana neutrinos, by the observation and measurement of the neutrinoless double-beta decay half-life. By using the mixing angles and mass differences yielded by the oscillation experiments it is possible to predict with good accuracy a range of values of the effective mass of the Majorana electron neutrino which could be tested by the next generation $\beta\beta(0\nu)$ experiments. In particular it is possible to conclude that at least one species of neutrino has a mass greater than 55 meV while nothing can be deduced about the important issue of whether the neutrino and anti-neutrino are distinct

particles (i.e. Dirac type) or not (Majorana type). Neutrinoless double beta decay (DBD) experiments seem therefore to be still the only way to answer both the question of the neutrino mass scale and of its nature.

Consisting of an array of 988 TeO_2 bolometers (750 g each) operating at ~ 10 mK, the CUORE experiment is designed with a sensitivity capable of probing most of the range suggested by oscillation experiment results. The large natural abundance of ^{130}Te (33.87%) eliminates the requirement for the very expensive isotopic enrichment required in all of the other proposed next generation experiments. The proposed array has a cylindrical structure consisting of 19 towers of 52 detectors each (Fig.**??**).

One such tower has been successfully constructed and is being operated at LNGS as an independent experiment called CUORICINO since spring 2003. The CUORICINO 3 year sensitivity on the half-life for neutrinoless double-beta decay is 6.4×10^{24} years (1σ), corresponding to an average value of $|\langle m_\nu \rangle|$ of the order of 0.3 eV. This is superior to the present upper bound on the effective electron-neutrino mass set by the ^{76}Ge experiments.

During current year (2005) CUORICINO has increased the collected statistics to ~ 6 kg y of Te^{130} taking data with a duty cycle better than 60%. On the other hand, CUORE, already approved by the LNGS Scientific Committee in April 2004 and by the INFN Scientific Committee in September 2004, received the first funding, mainly for the cryostat construction.

2 Neutrinoless Double Beta Decay and Low Temperature Detectors

Neutrinoless double beta decay is a very rare process in which a nucleus (A,Z) decays into its isobar (A,Z+2) with the emission of two electrons and no neutrino thus violating lepton number conservation. This leads to a sharp line in the sum energy spectrum of the two electrons, while the decay rate of this process can be expressed as

$$\tau_{1/2}^{-1} = G^{0\nu}(Q,Z)|M^{0\nu}|^2|\langle m_\nu \rangle|^2 \tag{1}$$

where $G^{0\nu}(Q,Z)$ is the exactly calculable phase space factor while $|M^{0\nu}|^2$ is the nuclear matrix element whose calculation is still quite uncertain. $\beta\beta(0\nu)$ observation would therefore allow a direct measurement of the effective neutrino mass $|\langle m_\nu \rangle|$, which can be expressed in terms of the elements of the neutrino mixing matrix as follows:

$$|\langle m_\nu \rangle| \equiv ||U_{e1}^L|^2 m_1 + |U_{e2}^L|^2 m_2 e^{i\phi_2} + |U_{e3}^L|^2 m_3 e^{i\phi_3}|, \tag{2}$$

where $e^{i\phi_2}$ and $e^{i\phi_3}$ are the Majorana CP–phases ($\pm$ 1 for CP conservation), $m_{1,2,3}$ are the Majorana neutrino mass eigenvalues and U_{ej}^L are the coefficients of the Pontecorvo-Maki-Nakagawa-Sakata (PMNS) neutrino mixing matrix, determined from neutrino oscillation data. Recent global analyses of all oscillation experiments [1, 2, 3, 4, 5, 6, 7, 8, 9, 10] yield on average:

$$|\langle m_\nu \rangle| = |(0.70 \pm 0.03)m_1 + (0.30 \pm 0.03)m_2 e^{i\phi_2} + +(< 0.05)m_3 e^{i\phi_3}| \tag{3}$$

while, being sensitive to the square of the neutrino mass differences, neutrino oscillation experiments can give no direct information on the neutrino mass scale. Two possible patterns, or hierarchies, the normal ($m_1 \approx m_2 \ll m_3$) and the inverted one ($m_1 \ll m_2 \approx m_3$) are then possible.

It should be stressed that in the inverted hierarchy, a minimum value of the order of 0.045 eV is expected for $|\langle m_\nu \rangle|$ according to oscillation results. This implies a minimum sensitivity acceptable for next generation experiments on neutrinoless DBD.

No evidence for neutrinoless DBD has been reported so far [11, 12, 13, 14], with the only exception of a claimed discovery of the decay of ^{76}Ge reported by a subset of the Heidelberg-Moscow collaboration [15]. This claim has been disputed by various authors [1, 16, 17] and also by other members of the same Heidelberg-Moscow Collaboration [18]. It was however confirmed by a new recently published analysis [19, 20]. Due to the smallness of the signal and to the presence of not completely understood peaks in the same energy region (with similar statistical significance) it is possible to conclude that only new results from the presently running (CUORICINO and NEMO3) or from the next generation experiments will possibly turn off the discussion.

As can be easily deduced from the 1σ sensitivity formula

$$S_{0\nu}^{1\sigma} = \ln 2 \frac{N_A \eta \epsilon}{A} \sqrt{\frac{Mt}{B\Gamma}} \qquad (4)$$

where η is the isotopic abundance, ϵ the detection efficiency, M the detector mass, t the measure time, B the background level (per unit mass, energy and time) and γ the energy resolution, the most effective approach to $\beta\beta(0\nu)$ is represented by direct experiments based on the use of "calorimeters" [21] in which the detector itself is made of a material containing the double beta active nucleus.

Suggested in 1984[22] in order to enlarge the number of $\beta\beta(0\nu)$ active isotopes for which the calorimetric approach could be possible, cryogenic detectors have shown a constantly improving performance. In a very naive approach they consist of a suitable (massive) absorber in good thermal contact with a proper phonon detector (temperature sensor). When made of diamagnetic and dielectric crystals, these bolometers are characterized by a heat capacity which, at low temperature, is proportional to the cube of the ratio between the operating and Debye temperatures [23, 24, 25] and can become so small that even the small energy released by a single particle interaction in the form of heat generates a measurable increase of temperature. Cryogenic detectors offer therefore a wide choice of DBD candidates, since the only requirement is that the candidate nucleus be part of a compound which can be grown in the form of a crystal with reasonable thermal and mechanical properties, low temperature detectors (LTD) offer a wide choice of DBD candidates. In particular, because of its high transition energy (2528.8 ± 1.3 keV) [26] and large natural isotopic abundance (33.8 %)[27], ^{130}Te is the best candidate and was chosen for CUORE and CUORICINO. Other isotopes (e.g. ^{100}Mo and ^{150}Nd) seem however of particular interest for $\beta\beta(0\nu)$ searches and their inclusion as a part the CUORE project is under study.

20
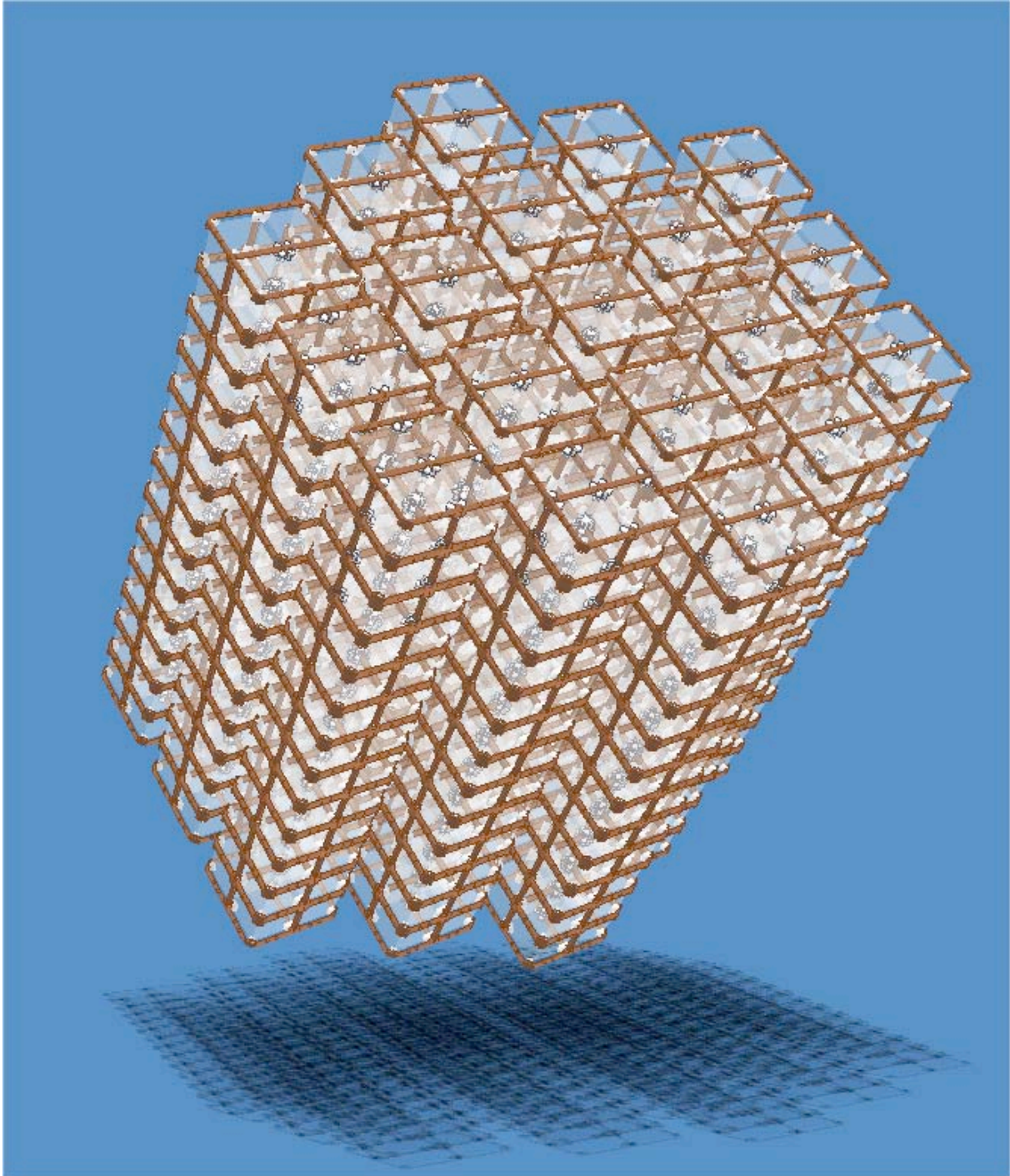
Figure 1: The CUORE detector.

3   CUORE (Cryogenic Underground Observatory for Rare Events)

Consisting of an array of 988 TeO$_2$ bolometers arranged in a cylindrical configuration of 19 towers of 52 crystals each (Fig. **??**), CUORE will be a second generation experiment on $\beta\beta(0\nu)$ with a sensitivity in the $|\langle m_\nu \rangle|$ range suggested by neutrino oscillation experiments. The single CUORE detector will consist of a 5×5×5 cm^3 crystal of TeO$_2$ acting both as a detector and source of the decay. The detectors will be supported in a copper frame and grouped in modules of 4 bolometers, so that each tower will be a stack of 13 modules. The crystal temperature change will be recorded with Neutron Transmutation Doped (NTD) germanium thermistors. All TeO$_2$ bolometers will be housed in a common dilution refrigerator and operated at a temperature of 8–10 mK. The total mass of ^{130}Te contained in CUORE will be approximately 203 kg.

The CUORE dilution refrigerator will be built with selected, low activity materials and shielded from environmental and material radioactivity by means of heavy shields held both at low and room temperature. The relevant details of the CUORE detector as well as the background issues, electronics, DAQ and data-analysis can be found in the CUORE proposal [28].

The expected CUORE $\beta\beta(0\nu)$ sensitivities according to different detector performance and background levels are summarized in table 1. The actual background level that can be presently foreseen just rescaling the CUORICINO results (i.e. assuming to simply assemble 13 CUORICINO towers without any improvement) but taking into account the different structure of the CUORE cryogenic setup is shown in table 2.

A straightforward reduction of this background, to a level of the order of 0.01 counts/keV/kg/y, is expected as a result of the improvement of the surface cleaning techniques, currently under investigation (a reduction by about an order of magnitude of the crystal and copper surface contamination is required). A more radical change of the surface treatment procedures or the development of active methods for the suppression of surface contributions, resulting in a further improvement by an order of magnitude, cannot be excluded but will require a more extensive and long dedicated R&D. In this respect, the preliminary results concerning the development of Surface Sensitive TeO$_2$ Detectors [29] looks very promising.

Table 1: Expected CUORE $\beta\beta(0\nu)$ sensitivity (5 years). B is the background rate and Δ is the FWHM energy resolution. The $|\langle m_\nu \rangle|$ interval is evaluated according to different QRPA nuclear matrix element calculations.

B(counts/keV/kg/y)	Δ(keV)	T$_{1/2}$(y)	$|\langle m_\nu \rangle|$ (meV)
0.01	10	1.5×10^{26}	23–118
0.01	5	2.1×10^{26}	19–100
0.001	10	4.6×10^{26}	13–67
0.001	5	6.5×10^{26}	11-57

The CUORE experiment was proposed to the LNGS Scientific Committee (LNGSSC) and to the INFN *Commissione Nazionale Scientifica II* (CSN2) in September and November 2003, repectively. It was approved by the LNGSSC in March 2004 subject to the possibility to demonstrate that, compared to CUORICINO, copper (TeO$_2$ crystal) surface contamination can be reduced by about a factor of 10 (4) within one (two) year. An area of about $10{\times}10$ m^2 in the southern wing of Hall A (just near CRESST, in the region once occupied by GNO) was accorded for the location of the CUORE setup inside the underground laboratories.

Scientific approval of the CUORE project was accorded by CSN2 in June 2004 followed, in September 2004 by the complete approval of the CUORE plan of activities and costs. Complete funding for the CUORE cryostat was received during this year (2005) and a tender was called for that.

An R&D program aiming at the construction of an enriched core of CUORE (144 central crystals) was presented in July 2004 to the American National Science Foundation. It is worthwhile to mention that this option would practically double the CUORE sensitivity on the half-life for $\beta\beta(0\nu)$ of ^{130}Te .

3.1 CUORE activities in 2005

CUORE activities in 2005 were mainly devoted to complete the design of the hut and of the shielding structure while a detailed design of the CUORE dewar and of the CUORE cryostat was discussed with the companies involved in the refrigerator tender. A final design of the detector copper structure was achieved and a prototype tower with 3 planes was succesfully tested in the Hall C. Improvements on surface contamination of both copper and TeO$_2$ crystals were obtained, while a first test of an array of 4 $5{\times}5{\times}5$ cm^3 crystals coupled with Surface Sensitive Bolometers (SSB) was constructed as well. The first prototype of the CUORE DAQ card was tested. The material selection program for all the CUORE setup components, already started during year 2004, continued and extremely good results were obtained exploiting α and γspectroscopy toghether with neutron activation analysis. Here we will summarize only the activities concerning the optimization of the detector structure, the SSB detector test and the analysis of the surface backgrond contributions.

Table 2: Expected CUORE background contributions in the $\beta\beta(0\nu)$ energy region for different sources. Background rates are obtained by assuming the presently available limits for material bulk contaminations and simply rescaling to the CUORE structure the CUORICINO results on surface contamination.

	B(10^{-3} counts/keV/kg/y)
Detector and setup material bulk	2.39 ± 0.07
TeO$_2$ crystal surface	16 ± 8.4
Copper surface	58 ± 6.6
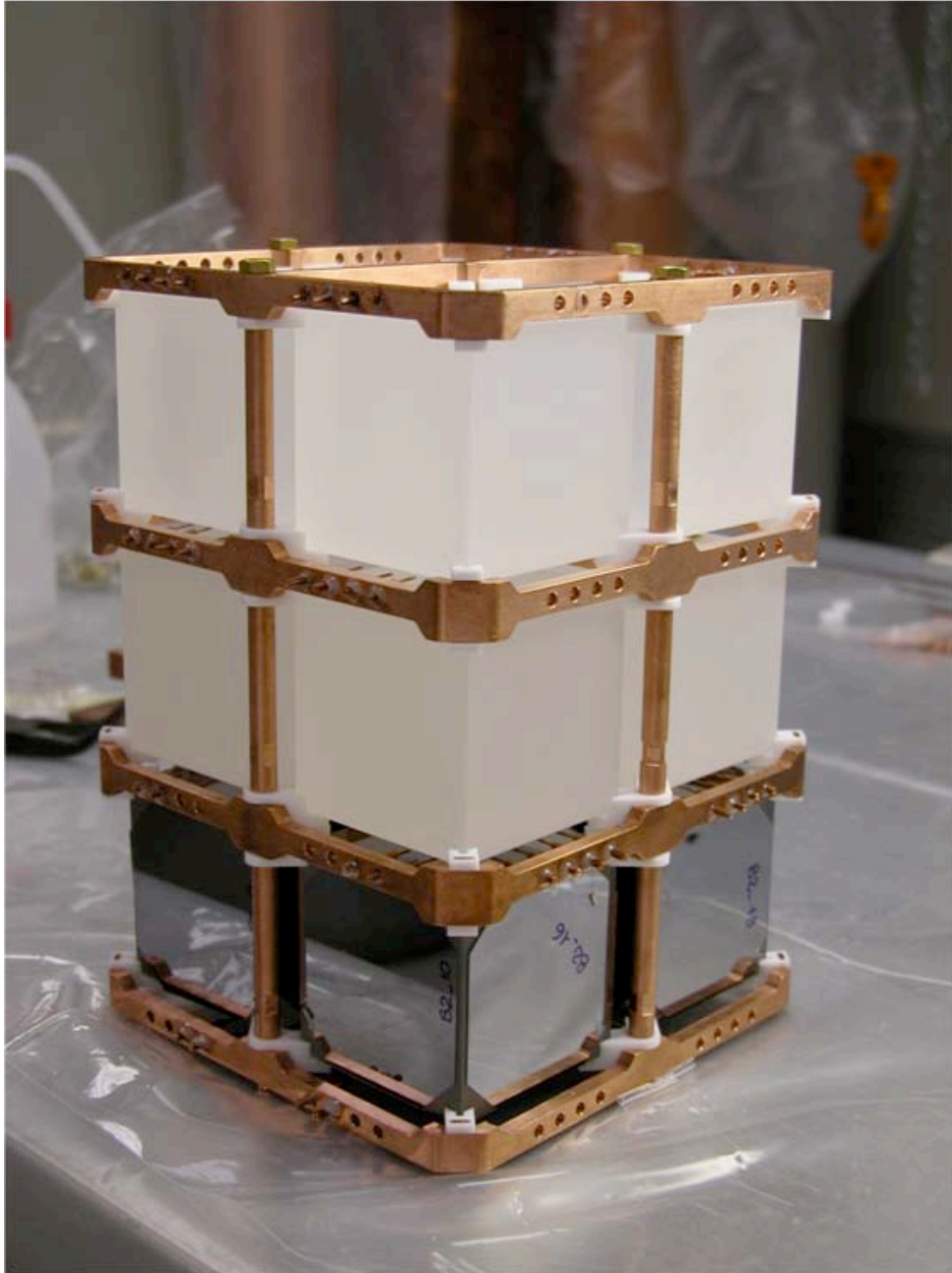
Figure 2: The 3-planes prototype tested in hall C. The top and middle planes host four 5×5×5 cm^3 crystals while the top plane hosts four 5×5×5 cm^3 crystals coupled with SSB detectors.
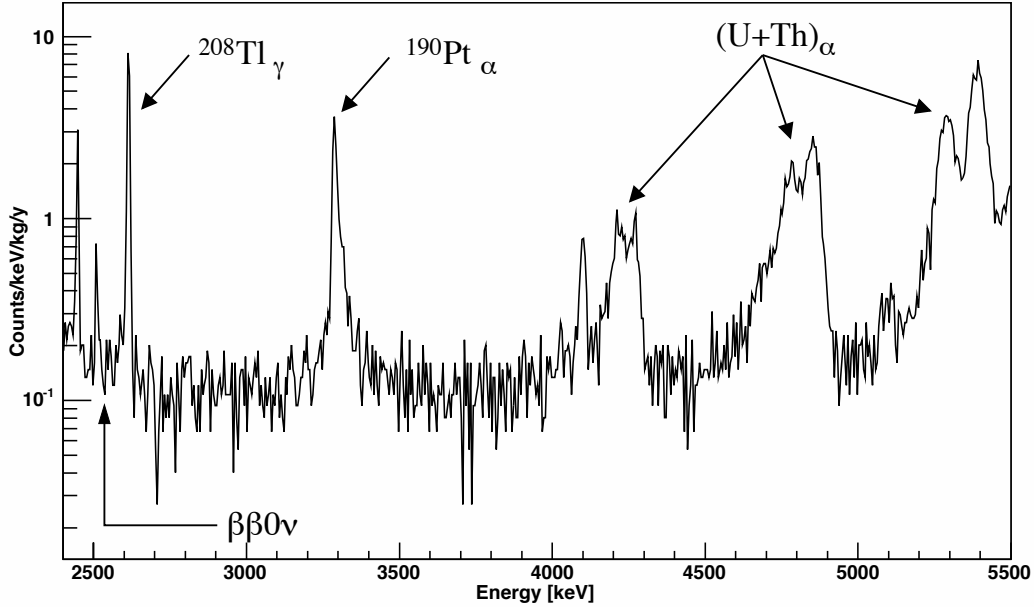
Figure 3: Cuoricino background in the $\beta\beta$ region. The 2505 ^{60}Co and the 2615 keV ^{208}Tl line are clearly visible in the left side of the plot, the $\beta\beta$ decay should appear at 2530 keV. In the right side α peaks due to U and Th chains are evident. The α peak centered at ~ 3200 keV is ascribed to an internal contamination of the TeO$_2$ crystals in the long living isotope ^{190}Pt.

3.1.1 Optimization of the CUORE detector structure

The baseline detector structure described in the CUORE proposal [28] is based on the experience gathered in the course of several years of development of TeO$_2$ bolometers of increasing mass, culminated with the CUORICINO detector. However, several aspects of the CUORE detectors can be improved substantially (e.g. single element reproducibility) with a contained effort. An intense program of optimization of the detector structure was therefore started in 2004, involving all aspects of the single module structure and of its assembly procedure in the final CUORE towers. Dedicated measurements of the mechanical response of the structure and calculations of the expected response of various alternate solutions were carried out. A new design for the single tower structure was finally produced during year 2005, this structure should guarantee a high degree of reproducibility in its mechanical features as well as a simple assembly and a reduced amount of inert material in between the detectors. Mechanical tolerances for all the detector parts (TeO$_2$ crystals and copper mounting structure) were consequently fixed: if this will be the final design of the CUORE structure these will be the tolerance requirements for both crystals and copper frames. A test prototype, a tower of 3 planes, each containing 4 5×5×5 cm^3 crystals, was finally constructed and cooled to base temperature in our R&D setup at LNGS (see fig. 2).

25

The tower included 8 "traditional" bolometers (top and central planes) consisting in $5\times5\times5$ cm^3 TeO$_2$ crystals each provided with its own NTD thermistor and Si heater, held in the copper structure with newly designed PTFE tips. In the bottom plane 4 $5\times5\times5$ cm^3 TeO$_2$ crystals coupled to 6 SSB (each covering one of the 6 faces of the crystal) were mounted. The eight crystals of the top and central planes showed quite good performances and reproducibility: the average energy resolution measured during a calibration (~ 6 keV FWHM at 2615 keV) was perfectly compatible with that of Cuoricino $5\times5\times5$ cm^3 crystals with a rather lower spread. The test was completely successful and - although a further test is forseen for year 2006 - the CUORE assembly structure can now be considered well defined.

The SSB coupled detectors were not used to study the performances of the bolometers in the new mounting system either because of the deep changes in the detector structure and because the $5\times5\times5$ cm^3 crystals of the SSB-plane did not fit perfectly with the geometry requirements asked for. Description and results of this SSB-plane are discussed later.

3.1.2 Reduction of background contributions

The most important objective of the CUORE activities program consists in the development of methods to control and reduce the radioactive background in the $\beta\beta(0\nu)$ region. As shown in fig. 3 the background measured by Cuoricino on the left side of the 2615 keV ^{208}Tl line and on its right side differs by about 30%. The ^{208}Tl line is the highest natural γ line due to environmental contamination and appears as the only possible γ contribution (through Compton events) to the $\beta\beta(0\nu)$ background. The background measured on the right side of the ^{208}Tl line is ascribed mainly to degraded alphas, coming from U and Th radioactive chains, due to surface contamination of the crystals or of the inert material facing them. This continuum clearly extends below the ^{208}Tl line thus partecipating to the to the $\beta\beta(0\nu)$ background counting rate.

While the heavy shielding forseen for CUORE will guarantee a deep reduction of the γ background (and therefore of the ^{208}Tl contribution), for α background (that comes only form the very inner part of the detector, i.e. the crystal themselves and the material directly facing the crystals) only a severe control of bulk and surface contaminations can guarantee the fulfillment of the sensitivity requirements for CUORE. To do that a correct identification and localization of the sources of the continuous α background is mandatory. Indeed alpha peaks can be identified very clearly in bolometers spectra. The peak position gives strong indication on the location of the contamination: external to the crystal if the energy corresponds to the alpha energy and in/on the crystal if it corresponds to the transition energy of the decay (i.e. alpha+recoil). The peak shape gives information as well: sharp gaussian peaks indicate contamination of either the crystal bulk or an extremely thin surface layer (could it be on the crystals surface or on the inert material surface facing the crystal). On the contrary asimmetric, "long-tailed" peaks are produced by thick contamination of surfaces. Finally a bulk contamination of an inert material facing the detector should produce just a continuum without any αpeak (but several, visible gamma peaks).

Unfortunately while α peaks are clearly evident and their origin rather easily un-

derstood the continuous background underlying the peaks and extending toward the $\beta\beta(0\nu)$ region cannot be easily correlated to the one or the other peak (i.e. to the one or the other contamination). Different hypoteses can be checked against Monte Carlo simulations that however require as input a contamination intensity and a density profile, both unknown. Side information, useful in this study, comes from the analysis of coincidence events in the array and from the study of gamma peaks. In Cuoricino the amount of coincidences in the 3-4 MeV range indicates a large contribution coming from outside the crystals while the reduced rate of low (hundred keV) energy gamma peaks indicates that U and Th bulk contaminations of copper cannot account for the αbackground.

Excluding important contribution form the bulk contamination of the small parts of the detector (thermistors, heaters, bonding wires, PTFE parts ...) on the basis of the radioactive measurements made before the construction of Cuoricino and excluding neutrons on the basis of both Monte Carlo simulations and experimental results (MiDBD experiment didn't see any change in the $\beta\beta$ background rate when the borated polyethylene shield was added) we have concluded that most of the background measured by Cuoricino should come from crystal and copper surfaces. The surface background contribution extrapolated in Table 2 was obtained on the basis of this background model. It is however worth to note that minor contribution from small parts and neutrons cannot be excluded, and have to be investigated.

To get rid of this puzzle three main solutions were devised:

- improvement of the quality of the copper and TeO_2 crystal surface treatment;

- further check the radioactive contamination of the small parts of the detector structure;

- development of bolometers able to identify events originated at the detector surface.

A program of optimization of the surface treatment, combined with a more sensitive diagnostic method for low surface contamination levels, was continued with promising results in 2005. A severe bulk contamination selection of the small parts started in 2005 with "ad hoc" bolometric measurements, improving the already obtained limits with HPGe spectroscopy and neutron activation analysis. Finally the development of active shields in the form of thin, large-area, ultrapure, Si or TeO_2 bolometers, surrounding the TeO_2 crystals and allowing for the identification of events originating from material surface begun.

3.1.3 Surface treatment

The program of surface cleaning of the detector materials close to the TeO_2 bolometers, was originally started in the second run of MiDBD and has been perfectioned in CUORICINO with satisfactory results in terms of background reduction. As described above however, the background level obtained in CUORICINO is not enough to guarantee the CUORE sensitivity goal and an improvement of the cleaning methods of both the TeO_2 crystals and of the copper parts directly faced to them is necessary.

A dedicated measurement with a bolometric setup ("Radioactivity Array Detector" or RAD) cleaned with an improved procedure based on the use of ultrapure materials

was carried out at LNGS at the end of summer 2004. The RAD consists in a 2-plane array made of 8 5×5×5 cm³ TeO₂ crystals, with a structure almost identical to that of CUORICINO (fig. 4). A nice feature of the RAD is that it can be mounted inside the hall C cryostat, as a standalone system, together with other detectors housed in an independent mounting structure. In this manner it is possible to exploit the hall C facility simultaneously for different CUORE measurements. The preparation of the first run of the RAD started in June 2004 (RAD-1). The crystals were etched with nitric acid (removing about 10 micron on the surfaces) and then polished with a SiO_2 powder. The copper mounting structure was etched and successively treated through electroerosion removing from 10 to 30 microns on the surfaces.

The result of RAD-1 was quite successful from the point of view of crystal cleaning: the TeO₂ surface contamination in U and Th was drastically reduced as proved by the disappearance of the U and Th peaks. The extremely low background reached so far allowed us for the first time to disentangle the bulk vs. surface contamination of the crystals: once the large spread peaks due to surface contamination disappeared the gaussian sharp peaks of the internal contamination of TeO₂ were visible. Apparently the crystals are contaminated with long living Th isotopes (to a level of about 10^{-13} g/g) while the other isotopes of the U and Th chains are present at a much reduced level (their peaks are not visible in the RAD-1 measurement and only upper limits could be extracted, for the chains in secular equilibrium the limits are of the order of 10^{-14} g/g). The only other alpha peaks visible in RAD-1 are the two 5.3 and 5.4 peaks due to ^{210}Po decay (usually the contamination is not in ^{210}Po that has a very short half-life but its father ^{210}Pb). When compared to Cuoricino the intensity of these two lines results to be: comparable in the case of the line due to the deposition of the entire transition energy (α+recoil = 5.4 MeV), 3 times higher in the case of the line due to the deposition of the only α particle energy (5.3 MeV). Finally, despite the strong reduction of the U and Th crystal contamination, no improvement is observed in the flat background spanning the 3-4 MeV region.

RAD-3 was operated at the end of 2005, the only change with respect to RAD-1 was the almost complete coverage of the copper faced to the crystals with a selected radio-clean polyethylene film. The result was the dramatic reduction of the 5.3 MeV peak (by more than a factor 3) that has now the same intensity as measured in Cuoricino. The 5.4 peak on the other hand appears unchanged (proving that it is due to ^{210}Pb and not directely ^{210}Po).

The continuous background extending below the alpha peaks toward the $\beta\beta(0\nu)$ region appeared unchanged in RAD-1 with respect to Cuoricino while it is reduced in RAD-3 (the 3-4 MeV counting rate of Cuoricino is 0.12±0.01 c/keV/kg/y while that of RAD-3 is 0.07±0.03 c/keV/kg/y). A validation of this result, whose significance is unfortunately limited by the high statistical error of RAD-3 counting rate, will be obtained by the statistics collected in the second run of RAD-3, beeing started at the beginning of 2006.

An interesting point concerning the residual continuous background is obtained when comparing Cuoricino with RAD-3: in the region above the ^{210}Po peaks the reduction of contaminations has improved the background figure of RAD-3 with respect to Cuoricino by a factor 10 while the reduction in the 3-4 MeV region is at most by a factor 2 and that in the 4-5 MeV region is of about 2.5 (although the peaks that in Cuoricino dominate this region are reduced by a factor 4). This looks like if the continuum have a large
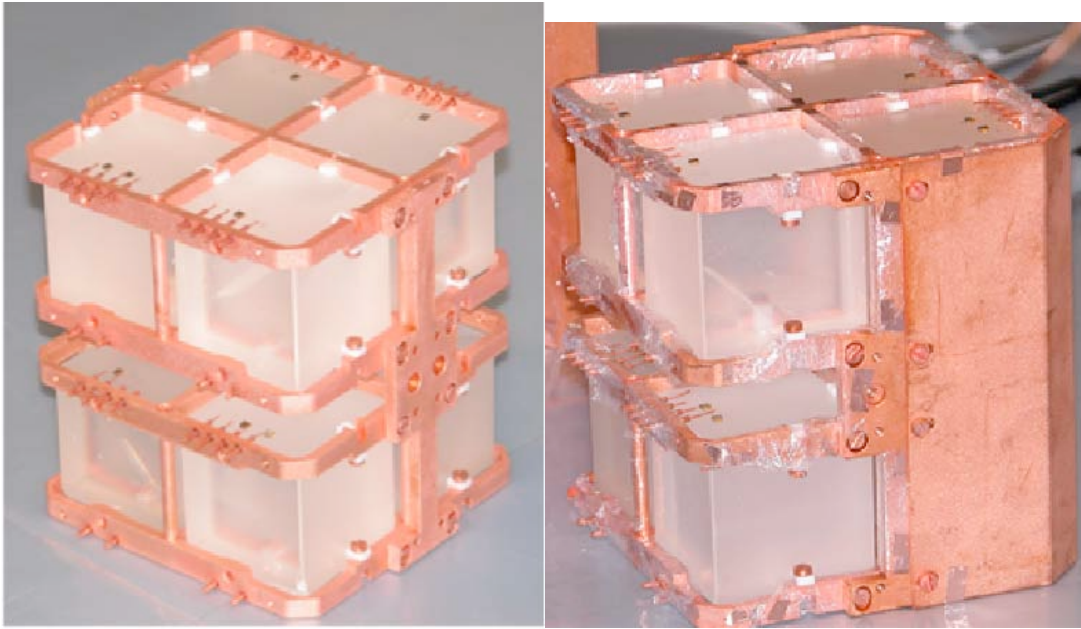
Figure 4: The RAD detector in run 1 (left) and run 2 (right).

contribution only below the ^{210}Po as beeing due to a long rather flat tail undelying this peak.

In conclusion while the quantitative result concerning copper surface contamination is not yet available a quite good result concerning crystal surface contamination has been established, fullfilling completely the CUORE requirement on this point. Indeed the TeO$_2$ contamination measured with the RAD yields a contribution to the overall background in the DBD region of CUORE of less than few 10^{-3} c/keV/kg/y. Finally a somehow clear indication that the continuous background extending to the 3-4 MeV region comes from ^{210}Pb contaminations have been obtained, this agrees with the preliminary result we got with a dedicate measurement on a Rn contaminated bolometer and what we got from background measurement in ultraclean Si surface barrier detectors. The first months of year 2006 will likely give us an answer on that.

3.1.4 Development of surface sensitive TeO$_2$ elements

The basic idea of the method consists in the construction of Surface Sensitive Bolometers (SSB) characterized by active shields: six slabs (of Si or of TeO$_2$) operated as bolometers (Surface Sensitive Elements or SSE) surround the TeO$_2$ crystal (Main) creating an active veto. Events generated on the surface of the crystal or of the SSE itself are in this way tagged and rejected. The implementation of this technique in CUORE is possible by thermally coupling these active shields to the main TeO$_2$ detector: six thin slabs would be attached to the Main TeO$_2$ crystal providing almost complete coverage without requiring a dedicated holder. In this way, a composite bolometer is realized with multiple read-out, capable to distinguish the origin of the event (SSE or Main) by means of a comparison between pulses coming from the different elements or by an analysis of the pulse shapes. Since a thermal link exists between the Main and the SSE, any particle interaction in one

29
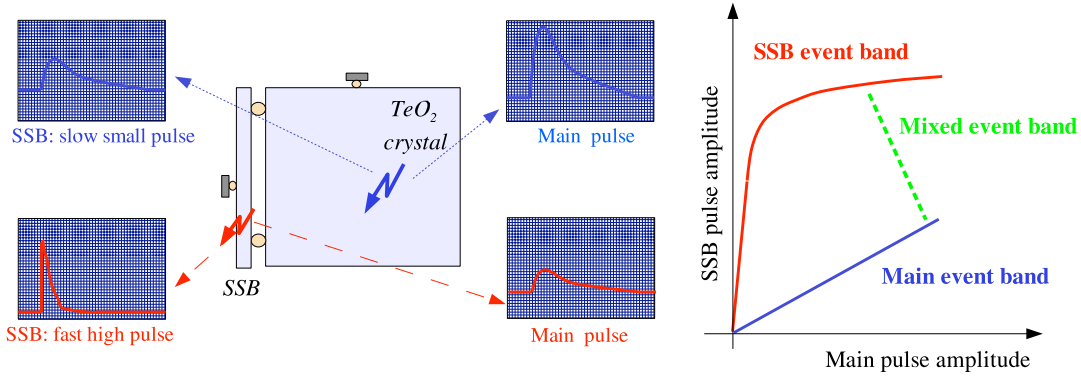
Figure 5: The behaviour of composite bolometers with respect to a signal produced by interaction in the slab or in the TeO$_2$ crystal. The scatter plot shows the different shapes of the curves drawn by pure SSE events and pure Main ones. The curve originated by a monochromatic alpha sharing its energy between SSE and Main is also shown.

of the 7 bolometers yields a signal in each of them. The response (amplitude and shape) is however quite different in bolometers directly hit by the particle or in bolometers heated, through the thermal link, by the others.

The size of the auxiliary bolometers (SSE) would be of $50\times50\times0.3$ mm^3: therefore, the main crystal plus the shields would form a cube with a side only 0.6 mm larger than the main crystal alone, preserving the general CUORE structure and rendering the assembling procedure substantially unchanged. This proposed solution has the potential to control the problem of the surface radioactivity relying on a technological improvement of the detector rather than on a better cleanness of the employed materials.

Figure 5 outlines the main feature of such a detector: any particle depositing its energy only in the Main, as a $\beta\beta(0\nu)$ decay event, produces a *large particle-induced* signal on the Main and a *small slow thermally induced* signal in the SSE (due to temperature rise of the Main). A similar pattern is obtained for alpha particle interactions due the bulk contamination of the Main, and for gamma rays. Indeed the probability that a gamma ray interacts also in the SSE is negligible due its small mass. On the contrary any particle interacting just in the SSE, as an alpha particle due to a bulk contamination of the SSE or emitted by the surface of a faced element, yields a *fast high particle induced* signal in the SSE and a *small thermally induced* signal in the Main. Particles that share their energy between the Main and the SSE are an intermediate case between the two described above: for both Main and SSE a "particle" and a "thermal" contribution to pulse formation are present. The scatter plot of signal amplitudes as measured by the Main and by the SSE allows to clearly distinguish these different event tipologies (sse fig. 5 right panel).

In order to test the method, several small scale prototype detectors were succesfully tested during 2004, using Ge, TeO$_2$ and Si slabs. While good performances were obtained with both Ge and TeO$_2$ slabs, Si slabs showed some unexplained features that lead us to consider them less safe than the other two devices. According to these considerations and to the fact that the optimal SSE material should have thermal contraction coefficients as

30

near as possible to the Main crystal ones, TeO_2 slabs should be the final choice for a SSB.

In the year 2005 a large scale test was realized in Hall C. Indeed, as already mentioned, the 3-planes prototype built according to the new design of the CUORE assembly included, in its bottom plane, an array of 4 SSB (fig. **??** and fig. 2). Due to a delay in the delivery of the TeO_2 slabs the four detectors were realized gluing (with a vacuum grease spot at the center of the slab in order to prevent possible breaks) on each face of the 5×5×5 cm^3 crystals a Si slab (50×50×0.3 mm^3). For three crystals the coverage was not exactly complete (an almost triangular area near each vertex was not faced by the slab, being then partially convered by the PTFE tips used to held the crystal in the copper frame) while for the fourth of them the Si slabs covered almost completely the crystal and the teflon tips were positioned on the slab themselfes. This crystal was the smallest one, with dimensions by far lower that those foreseen for this mounting system, and the interposition of the slab between the crystal and the PTFE tips increased the size of the detector, helping in keeping the crystal firmly held in the mouting. Unfortunately that was not enought and this crystal, as well as the other with particularly small dimensions resulted to be loosely held in the mounting with a consequent deterioration of their performances.

Each slab was provided with its own NTD Ge thermistor used to read-out the thermal signal. In order to reduce the readout channels, the six thermistors of the SSEs were connected in parallel. In this way, for each 5×5×5 cm^3 detector, two channels were read out: the Main (the 5×5×5 cm^3 TeO_2 crystal) and the SSEs.

The two detector with smaller dimensions (responsible for the excess noise due to their vibrations) showed a rather poor performance, while for the other two a good energy resolution, compatible with that of the Cuoricino detectors, was measured. Unfortunately only for one of these detectors the SSE could be read-out because during the cooling the electrical connections to the slabs thermistors of the other were broken. A long background measurement, as well as few day calibration, were used to understand the beheaviour of these detectors and to study the rejection efficiency for surface alpha contamination. The detector with complete read-out was used for an extensive study of the main features of the composite bolometer. Signal were acquired on both Main and SSE (here we use SSE to indicate just the parallel of the 6 SSEs) with an independent trigger and trigger threshold. Once only signal above the common maximum threshold are considered (equalizing then the thresholds on SSE and Main) only coincident events are observed. The amplitude measured on the Main was calibrated in energy exposing the detector to a gamma source, this provides a correct conversion of the Main pulse amplitude if and only if the considered signal corresponds to a pure interaction in the Main (i.e. the SSE pulse is induced by the thermal heating of the Main). A similar calibration was not possible for signals produced in the SSE.

Fig 6 shows in the right panel the scatter plot of coincident events as measured by the Main and by the SSEs.

Signals produced by particles interaction in the Main are clearly identified as those belonging to the straight line ("Main band" in the following) in the lower part of the plot (they correspond to small-slow signals in the SSE) while signals produced by particle interaction in the SSE belong to the multiple (because we have 6 different SSEs) curves ("SSE band" in the following) identified by a high SSE amplitude and low Main amplitude. When the energy of the particle is shared between the SSE and the Main, as it is for a
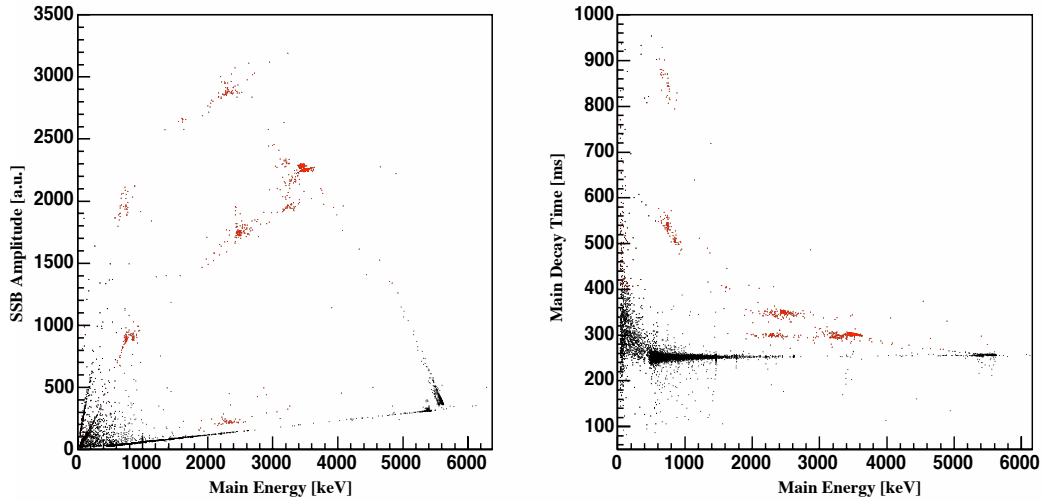
Figure 6: Scatter plot of the pulse amplitudes from TeO$_2$ thermistor versus the pulse amplitudes from shield thermistor obtained with a 12 g TeO$_2$ surface sensitive detector.

surface alpha event originating in between the SSE and TeO$_2$ surface, a line connecting the Main band and the SSE band is produced. Few (probably two) similar lines are evident in the scatter plot and are ascribed to a surface alpha contamination between the slab and the crystal.

The left panel of fig. 6 shows, for the same events, the decay time vs. amplitude as measured on the Main. What is clearly evident is that the events belonging to the Main band have the usual distribution while events that belong to the SSE band or to the so called mixed events are clearly distinguishable having a much slower decay time. The conclusion is that the presence of the slabs thermally connected on the TeO$_2$ crystal modify the response of the bolometer in such a way that bulk events are distinguishable from surface events just looking to their decay time. Indeed in fig. 6 the pulse rejection efficiency obtained by separating the bulk from surface events just using a cut on the Main decay time is shown by different colors. A plot similar to that shown in the left panel of fig. 6 is obtained for the other well working detector (the one with the SSE electrical contact disconnected) proving that this is a characteristic feature of these composite bolometers. The rejection efficiency for alpha events, in the region of the $\beta\beta(0\nu)$ signal, appears to be in both cases quite high.

This measurement demonstrates therefore the power of this technique in identifying surface events, and opens moreover a new way of using the composite bolometers that do not require them to be read out (this is particularly important for CUORE because means that SSB could be mounted without increasing the number of thermistors necessary and the number of wires and channels to be biased and read-out). As in this run no cleaning procedure of the detector and mounting system was applied a quantification of the background reduction obtained by the composite bolometers cannot be obtained. At the beginning of 2006 a new run with an array of 4 crystals (having this time the correct

dimension to fit into the assembly) covered with TeO_2 slabs will be constructed. The detector will be mounted with the same cleaning procedure used for the RAD (crystal and copper etching, clean room assembly ...), the answer on the background reduction attainable with composite bolometer will then obtained toghether with a unique cross check of our background model (important surface contribution).

4 CUORICINO

Besides being a conclusive test of CUORE, CUORICINO is also a sensitive experiment on $\beta\beta(0\nu)$ of ^{130}Te . Installed at LNGS during 2002 and cooled down for the first time in January 2003, CUORICINO is providing important results concerning both the technical performance of the bolometric tower, the $\beta\beta(0\nu)$ background level and origin, and the $\beta\beta(0\nu)$ of ^{130}Te [30, 31].

CUORICINO is a tower of 13 planes containing 62 crystals of TeO_2 ; 44 of them are cubes of 5 cm on a side while the dimensions of the others are $3\times3\times6$ cm^3 . All crystals are made with natural paratellurite, apart from two $3\times3\times6$ cm^3 crystals, which are enriched in ^{128}Te and two others of the same size enriched in ^{130}Te , with isotopic abundance of 82.3 % and 75 %, respectively. The total mass of TeO_2 in CUORICINO is 40.7 kg, the largest by more than an order of magnitude than anycryogenic detector.

In order to shield against the radioactive contaminants from the materials of the refrigerator, a 10 cm layer of Roman lead, with ^{210}Pb activity of <4 mBq kg^{-1} [32], was inserted inside the cryostat immediately above the CUORICINO tower. A 1.2 cm lateral layer of the same lead is framed around the array to reduce the activity of the thermal shields. The cryostat is externally shielded by two layers of Lead of 10 cm minimal thickness. The background due to environmental neutrons is reduced by a layer of Borated Polyethylene of 10 cm minimum thickness. The refrigerator operates inside a Plexiglass anti-radon box flushed with clean N_2, and inside a Faraday cage to reduce electromagnetic interference.

Thermal pulses are recorded by means of Neutron Transmutation Doped (NTD) Ge thermistors thermally coupled to each crystal. Possible detector response instabilities are controlled by means of voltage pulses generated across heater resistors attached to each bolometer by high stability pulse generators. A tagging of these stabilizing signals is made by the acquisition system. The detector temperature is stabilized by means of a dedicated feedback circuit.

The front-end electronics for all the $3\times3\times6$ cm^3 and for 20 of the $5\times5\times5$ cm^3 detectors is maintained at room temperature while a *cold electronics* stage (located in a box at $\sim$100 K near the detector to reduce the noise due to microphonics) is used for the remaining 24 crystals.

CUORICINO is operated at a temperature of $\sim$8 $\pm$ 1 mK. A routine energy calibration is performed at the beginning and at the end of each background measurement period ($\sim$two weeks) by irradiating the detector with ^{232}Th and/or ^{60}Co sources placed in immediate contact with the refrigerator (fig. 8).

The total statistics so far collected and analyzed corresponds to an effective exposure of 5.87 kg of ^{130}Te $\times$year. The background spectra, after the anticoincidence cut, are

Figure 7: Background sum spectra, after anticoincidence cut, for 5×5×5 cm³ (black line) and 3×3×6 cm³ CUORICINO crystals.

Figure 8: Calibration sum spectra (^{232}Th γ-source), after anticoincidence cut, for 5×5×5 cm³ (black line) and 3×3×6 cm³ CUORICINO crystals.
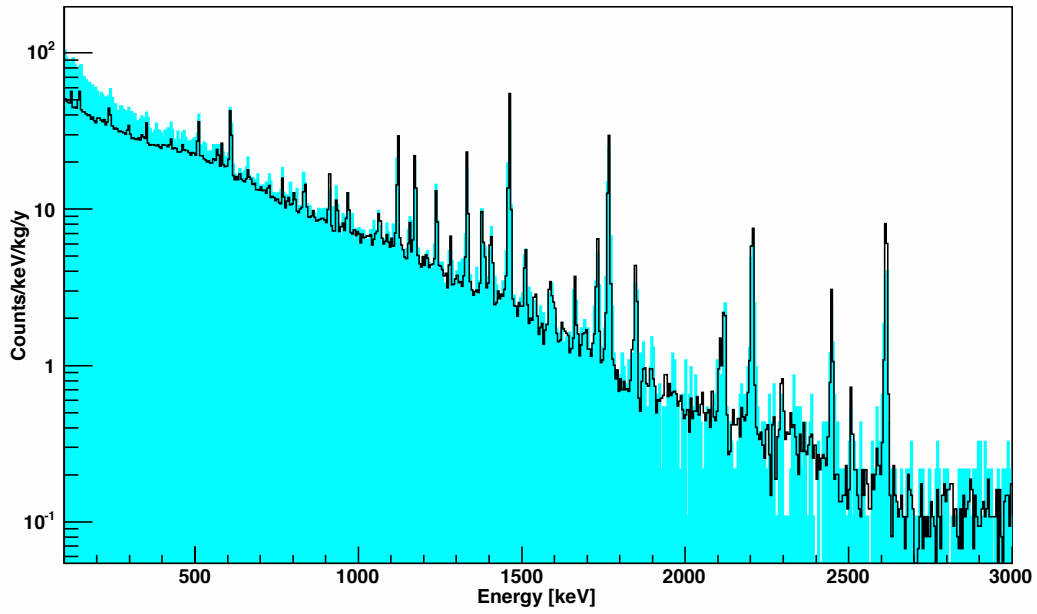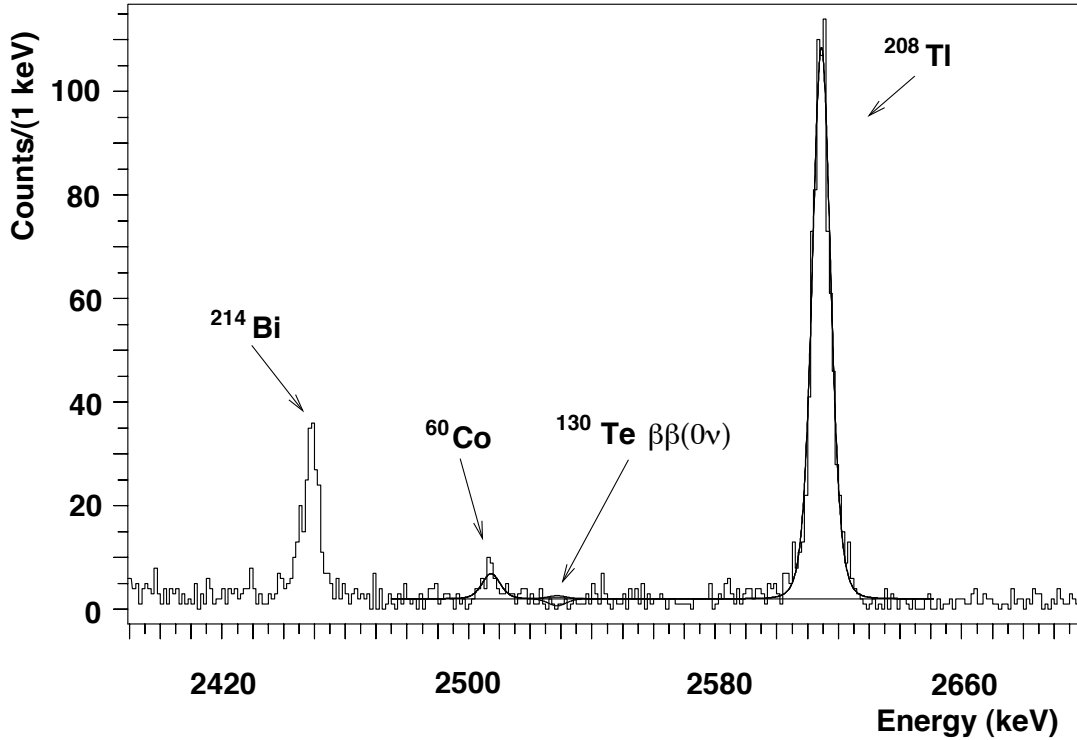
Figure 9: Spectrum of the sum of the two electron energies in the region of neutrinoless DBD

separately shown for the 5×5×5 cm^3 and 3×3×6 cm^3 detectors in fig. 7). The detail of the sum spectrum of the 5×5×5 cm^3 and 3×3×6 cm^3 crystals in the $\beta\beta(0\nu)$ region is shown in Fig. 9. The lines at 2447 and 2615 keV from the decays of ^{214}Bi and ^{208}Tl, and also the weak line at 2505 keV due to the sum of the two γ lines of ^{60}Co are clearly visible. The background at the energy of neutrinoless DBD is of 0.18 ± 0.01 counts kg^{-1} keV^{-1} y^{-1}.

No peak was observed at the ^{130}Te $\beta\beta(0\nu)$ energy implying a 90% C.L. lower limit of 2×10^{24} years on the lifetime for this decay. The upper bounds on the effective mass of the electron neutrino that can be extracted from this result depend strongly on the values adopted for the nuclear matrix elements. Considering all the theoretical calculations apart from those based on the shell model whose validity for heavy nuclei is sill under discussion, it is possible to indicate an interval of 0.2 to 1.1 eV, which partially covers the mass range of 0.1 to 0.9 eV indicated by H.V. Klapdor-Kleingrothaus et al. [20].

4.1 Conclusions

The excellent results of CUORICINO in terms of detector performance and $\beta\beta(0\nu)$ sensitivity are the best proof of the actual feasibility of a larger scale experiment like CUORE. Improvements with respect to the present CUORICINO design are however required and still under investigation. In particular sizeable improvements of the background level

originated by TeO$_2$ crystal and structure copper surfaces were obtained thanks to a new improved surface cleaning technique. Excellent results were moreover obtained in the first test measurement with an array of 4 SSB. This recently proposed technique demonstrated to be a powerful diagnostic tool for surface background source identification while allowing the implementation of an active background rejection method in the CUORE structure without requiring major changes.

5   List of 2005 Publications

1. S. Pirro et al., *Cleanliness, backgrounds and surface contamination in CUORE* Proc. "Low Radioactivity Technique 2004", Sudbury, Canada, 12-14 December 2004, AIP Conf. Proc. vol.785 (2005) p. 177.

2. S. Pirro et al., Nuclear Physics B (Proc. Suppl.) 138 (2005) 210-213.

3. C. Arnaboldi et al. Physical Review Letters 95 (2005) 142501(4).

4. C. Arnaboldi et al, Nuclear Instruments and Methods in Physics Research A 554 (2005) 300

5. L. Foggetta et al., Applied Physics Letters 86 (2005) 134106

6. C. Nones et al. *A new method for background rejection with surface sensitive bolometers*, presented at "11th International Workshop on Low Temperature Detectors" (LTD-11), TOKYO, Japan, 31 July-5 August 2005, to be pubblished on Nuclear Instruments and Methods in Physics Research, Section A.

7. E. Previtali al, *CUORE* "SNOLAB IVth Workshop", Lively, Canada, 15-17 Agust 2005

8. C. Nones et al. *Development of new bolometers for rare avents with background active discrimination*, presented at "International School of Nuclear Physics" - 27th course - Neutrinos in Cosmology, in Astro, Particle and Nuclear Physics, Ettore Majorana Center for Scientific Culture, Erice, Sicily, Italy, 16-24 September 2005, to be pubblished in Progress in Particle and Nuclear Physics

9. C. Nones et al. *Status of Cuoricino and prospects for CUORE*, presented at "Virtual Institute for Dark Matter und Neutrino Physics", 1-2 December 2005, DESY-Hamburg.

References

[1] F. Feruglio, A. Strumia and F.Vissani, Nucl.Phys.B 637 (2002) 345

[2] F. Feruglio et al., Nucl.Phys.B 659 (2003) 359.

[3] F. Joaquim, Phys.Rev. D 68 (2003) 033019.

[4] C. Giunti, hep-ph/0308206.

[5] S. Pascoli and S.T.Petkov, Phys.Lett. B 544 (2004) 239.

[6] S. Pascoli and S.T.Petkov, Phys.Lett. B 580 (2004) 280.

[7] J. Bahcall and C.Pena-Garay, J.High En.Phys JHEP 11 (2004) 4.

[8] J. Bahcall et al., Phys.Rev.D 70 (2004) 033012.

[9] H. Murayama and C.Pena-Garay, Phys.Rev.D 69 (2004) 031301.

[10] J. Suhonen and O.Civitarese, Phys.Rep. 300 (1998) 123.

[11] V.I. Tretyak and Yu.G.Zdesenko, At.Data Nucl.Data Tables 80 (2002) 83.

[12] A.S. Barabash, Phys.of Atom.Nuclei 27 (2004) 438.

[13] S.R.Elliott and P.Vogel, Ann.Rev.Part.Sci. 53 (2002) 115.

[14] S.R. Elliott and J.Engel, J.Phys.G:Nucl.Part.Phys. 30 (2004) 183.

[15] H.V. Klapdor-Kleingrothaus et al., Mod.Phys.Lett.A 16 (2001) 2409.

[16] C.E. Aalseth et al., Mod.Phys.Lett.A 17 (2002) 1475.

[17] C.E. Aalseth et al., Phys.Lett.B 546 (2002) 206.

[18] A.M. Bakaliarov et al., hep-ex/0309016.

[19] H.V. Klapdor-Kleingrothaus et al., Phys.Lett.B 586 (2004) 2004.

[20] H.V. Klapdor-Kleingrothaus et al., Nucl.Instrum.and Meth. 522 (2004) 367.

[21] G.F. Dell'Antonio and E. Fiorini, Suppl. Nuovo Cim. 17 (1960) 132.

[22] E. Fiorini and T. Niinikoski, Nucl. Instrum. and Meth. 224 (1984) 83.

[23] D. Twerenbold, Rep. Prog. Phys. 59 (1996) 349; N. Booth, B. Cabrera and E. Fiorini, Ann. Rev. of Nucl. Sci. 46 (1996) 471.

[24] Proc. of the IX International Workshop on Low Temperature Detectors, Ed. by F. Scott Porter, D. McCammon, M. Galeazzi and C.K. Stahle, Madison (Wisconsin) 22-27 July 2001. Amer. Inst. of Phys. Vol. 605 (2002)

[25] Proc. of the X International Workshop on Low Temperature Detectors, Ed. by F.Gatti Genoa 6-11 July 2003, to be published on Nucl. Instrum. and Meth.A

[26] G.R. Dyck et al., Phys. Lett. B 245 (1990) 343

[27] R.B. Firestone, C. Baglin and S.F. Chu: Tables of Isotopes (eight edition), 1998 CD-ROM update (1998)

[28] CUORE Collaboration, *CUORE (Cryogenic Underground Observatory for Rare Events): A proposal submitted to the INFN, the us doe and the us nsf by the international CUORE Collaboration*, http://crio.mib.infn.it/wig and hep-ex/0501010.

[29] L. Foggetta et al., Applied Physics Letters 86 (2005) 134106.

[30] S. Pirro et al., Nuclear Physics B (Proc. Suppl.) 138 (2005) 210-213.

[31] C. Arnaboldi et al.,Physical Review Letters 95 (2005) 142501(4).

[32] A. Alessandrello et al., Nucl.Instrum.and Meth. A 142 (1998) 454.

ERMES
Measurements of environmental radioactivity

Matthias Laubenstein[a], Wolfango Plastino[b,c]

[a] I.N.F.N.-Laboratori Nazionali del Gran Sasso,
S.S. 17/bis, km 18+910, I-67010 Assergi (AQ) - Italy
[b] Department of Physics, University of Roma Tre,
Via della Vasca Navale, 84, I-00146 Rome - Italy
[c] I.N.F.N., Sezione Roma Tre,
Via della Vasca Navale, 84, I-00146 Rome - Italy

Abstract

In the framework of the ERMES (Environmental Radioactivity Monitoring for Earth Sciences) research project many samples were analysed by means of gamma spectroscopy in the Low Background Laboratory of the National Laboratories of Gran Sasso (LNGS). A summary of these measurements is presented.

1 Introduction

The ERMES research project includes radioactive analyses of environmental samples like sea water, soils, sediments and volcanic material ([1], [2]). In its framework in the period from 2004 to 2005 a series of samples has been measured in the Low Background Laboratory (LBL), situated in the underground labs of the LNGS. Five sets of samples were provided by the National Institute for Geophysics and Vulcanology (I.N.G.V.) of Italy within a scientific collaboration, and two sets of samples were measured in collaboration with the International Atomic Energy Agency (I.A.E.A.) in a preliminary study for new standardised materials for radionuclide analysis.

In the LBL nine high purity germanium (HPGe) detectors are currently installed. The laboratory is dedicated principally to material screening measurements for all the underground research projects installed in the LNGS. Since those experiments must have very low intrinsic radioactive backgrounds in order to detect the extremely weak signals they are looking for, the intrinsic concentration of natural radioactivity in the materials used for the experimental set-up has to be extraordinarily low. The HPGe detectors and their shielding used for the material screening have been designed and built especially for

165

the purpose to detect very small amounts of radioactivity (in the order of 10^{-10} g/g for uranium and thorium, and 10^{-7} g/g for potassium), and if not detecting it, to put at least very low limits of detection. An extensive description can be found in [3], [4] and [5] .

Nevertheless, these specialised detectors can also be used to measure easily natural radioactivity which is occurring usually in concentrations of approximately 10^{-6} g/g in uranium and thorium and 10^{-2} g/g in potassium, which is four to five orders of magnitude higher than the sensitivity of those detectors.

2   Sample preparation and measurement procedure

2.1   Samples of the I.N.G.V.

Five sets of samples have been measured for the I.N.G.V.:

1. the BIOZAIRE 03 set: 23 sea water samples, 15 sea sediment samples;

2. the ORION set: 17 sea water samples;

3. the PATRASSO set: 4 sea water samples; 7 sea sediment samples;

4. the SACLANT set: 4 sea water samples;

5. the mud volcano set: 15 samples from mud volcanoes.

i.e. an overall number of 85 samples has been measured.

These samples have been collected in the framework of I.N.G.V. campaigns in the Mediterranean sea for what is concerning the first four sets. The mud volcano set consists in three subsets coming from regions with mud volcano activity in Italy (3 samples), Romania (6 samples) and Azerbeijan (6 samples).

2.2   Samples of the I.A.E.A.

Two sets of samples have been measured in the framework of a feasability study for new reference materials for radionuclide measurements. The sets were:

1. IAEA-434: 5 phosphogypsum samples from Poland;

2. IAEA-RM-05: 2 soil samples;

The crucial point in measuring these samples was that traceability of all measured parameters (i.e. mass, time, radioactivity) had to be guaranteed.

2.3   The sample preparation

The sample preparation for the different types of samples was performed as follows:

2.3.1 Sea water samples

The sample size is rangeing from 60 g to 120 g. The water, which arrived already filtered, is filled into polystyrene containers of cylindrical shape, with 70 mm diameter. The height inside the box is of course varying according to the volume of the sample. The length of the measurement varies from 7 to 10 days, according to the sample size, i.e. smaller samples having a longer measurement time than larger ones.

2.3.2 Solid samples

The sample size is usually between 50 g and 300 g. The sample has first to be dried in the oven at approx. 150 ºC for at least 48 hours. Then it is powderised as best as possible manually, using mortar and pestle, in order to homogenise the whole sample, which reduces uncertainties due to a non uniform radioactivity distribution inside the sample. After this step, the powder is filled into polystyrene boxes with various dimensions rangeing from 65 mm diameter and max. 7 mm height for small samples to 90 mm diameter and max. 34 mm height for the largest samples. The measurement time varies from 2 to 4 days according to the sample size. The I.A.E.A. samples arrived already powderised by using a mill (particle size 0.7 micrometers), and they only had to be dried.

2.4 Measurement and data analysis procedures

2.4.1 Measurement geometry

The samples are placed in a central position in front of the detector endcap at a fixed distance, which ranges from 3 mm to 6 mm depending on the detector set-up used for the measurement. The I.A.E.A. samples had to be measured five times on the same detector in order to check the repeatability of the result, and had to be analyzed with two different techniques in order to check the reproducibility of the measurement. The I.N.G.V. samples were checked less systematically for repeatability repeating occasionally a sample measurement.

2.4.2 Data analysis

The efficiency determination of each measurement is done via software using the Monte-Carlo technique. The computer code written is using the GEANT 4 software package [6] and was validated comparing its results with measurements performed using certified extended radioactive sources with different geometries and in different distances from the detector endcap. The spectrum analysis is done using a thoroughly tested fitting routine developed at the University of Milano. The peak shape is fit with a Gaussian peak and linear background, having the possibility to perform also the unfolding of up to 10 peaks. In case of low counting rates, where statistics is poor or where actually no net activity can be seen, the analysis is done manually summing simply the number of counts per energy channel the regions of interest (ROI) of peak and background, choosing the appropriate width of the ROI to 2.5 times the full width of half the maximum (FWHM) of the full energy peak, which is determined by calibration with radioactive standards.

The overall uncertainty budget for the gammaspectroscopy measurements is reported in table 1. The given total uncertainty is referring to the analysis of one full energy peak (e.g. ^{40}K). In case the radionuclide analysed has more than one gamma energy emission the single results of each photopeak can be combined statistically by averaging, which of course decreases the uncertainty for the combined result somewhat (e.g. ^{228}Ra).

Table 1: *Uncertainty budget for the gammaspectrometric measurements (relative uncertainties).*

counting	1.5%
background	1.5%
efficiency	10.0%
total	10.2%

3 Discussion

For each sample the radioactivity concentration of thorium, uranium, potassium and caesium has been analysed. The uncertainties stated are the expanded uncertainties obtained by multiplying the combined standard uncertainty by a coverage factor of $k = 1$ [9]. The data was compared to the decision thresholds, which were calculated according to [10] using $\alpha = 0.5$, and $b = 2.5$ FWHM.

3.1 The radionuclides

3.1.1 ^{232}Th-series

The nuclides analysed in this naturally occurring decay chain are the gamma emitting nuclides ^{228}Ac, ^{212}Bi and ^{208}Tl. The results obtained from these nuclides give also the possibility to determine whether secular equilibrium is present in the decay chain (from ^{228}Ra on) or not.

3.1.2 ^{238}U-series

The nuclides analysed in this naturally occurring decay chain are the gamma emitting nuclides ^{234m}Pa, ^{226}Ra, ^{214}Pb and ^{214}Bi. These nuclides give also the possibility to determine whether secular equilibrium is present between ^{238}U and ^{226}Ra, which due to the long half-life of the latter one ($t_{1/2} = 1600$ a [7]) could show some disequilibrium, given the different chemical behaviour of the elements uranium and radium, which could for example cause depletion of one nuclide with respect to the other.

3.1.3 ^{235}U-series

The nuclides analysed in this naturally occurring decay chain are the gamma emitting nuclides ^{235}U, ^{227}Th, and, if detectable, ^{219}Rn. The latter two radionuclides are important in order to disentangle the contribution in the 185.71 keV gamma ray of ^{235}U from the contribution of ^{226}Ra with an emission at 186.2 keV.

3.1.4 Potassium

The concentration of this element is determined by measuring its primordial radioactive isotope ^{40}K. This nuclide emits with 10.67 % probability during its decay also gamma rays with an energy of 1460.83 keV. The natural abundance of ^{40}K is (1.17 ± 0.01) % [8].

3.1.5 ^{137}Cs

The concentration of this radionuclide ($t_{1/2} = 30.17$ a [7]) is determined by its emission of gamma-rays with an energy of 661.67 keV. Produced solely by human activity (release by nuclear power plants and reprocessing plants, nuclear bomb test fall-out) it can be accompanied by the isotope ^{134}Cs ($t_{1/2} = 2.062$ a [7]). In all samples no evidence for ^{134}Cs could be found.

3.2 Measurement results

3.2.1 Results of the I.N.G.V. sea water samples

In tables 2 and 3 are reported the measurement results of the sea water samples of the various INGV sample sets. No other radionuclide than ^{40}K could be positively identified, a part from occasionally occurring spurious ^{137}Cs. Possible contamination coming from ^{222}Rn-daughters from the air introduced during the sample preparation was minimised, by erasing and restarting the measurement after approximately one day. After this time almost all radon daughters introduced had decayed away, due to their short half lives which are of the order of several tens of minutes.

3.2.2 Results of the I.N.G.V. sediment and mud volcano samples

In tables 4 and 5 are reported the measurement results of the sea sediment samples and the mud volcano samples of the I.N.G.V. sample sets. Only naturally occurring radionuclides could be positively identified, a part from occasionally occurring spurious ^{137}Cs. Possible loss of ^{222}Rn-daughters due to diffusion out of the sample containers was excluded at a 2% level. True coincidence summing effects occurring in the ^{238}U- and ^{232}Th-series were estimated to be less than 2%, well below the overall uncertainty of the measurement.

3.2.3 Results of the I.A.E.A. samples proposed as preliminary standardization materials

A table of the measurements concerning the two materials investigated as possible candidates for standard materials for radionuclide analysis of the I.A.E.A. will not be presented,

because the program is still ongoing and data release is not yet allowed. A detailed analysis of this data will be performed in the next months and possibly published in an I.A.E.A. official report. Nevertheless, it can be said, that the uncertainties involved in the measurement and the data analysis procedures are well understood.

4   Summary

In this report of the ERMES research project a summary of the gammaspectrometry measurements performed during 2004 and 2005 has been presented. During data analysis no other radionuclide than the ones reported was identified. Of course, this measurement technique can only provide information about gamma emitting radionuclides. A direct determination of uranium, thorium and potassium as a complementary measurement (e.g by means of ICP-MS) has not yet been performed. As for now only the raw data is presented and no detailed analysis and interpretation has been performed in order to investigate possible deviations from secular equilibrium in the decay chains and possible correlations between sampling points and results. The work is still ongoing. Interesting and innovative results are expected for the fields of geology and geophysics, where until now the use of radiometric methods has not been applied in its full capability.

Acknowledgements

References

[1] Plastino, W. et al., ERMES, Annual Report 2003 - Laboratori Nazionali del Gran Sasso, LNGS/EXP-01/04 (2004) p. 203.

[2] Etopie, G. et al., The Benthic Boundary Layer: geochemical and oceanographic data from the GEOSTAR-2 observatory, submitted to Ann. of Geophysics (in press).

[3] Arpesella, C., A low background counting facility at Laboratori Nazionali del Gran Sasso, Appl. Rad. Isot., 47 (1996) p. 991.

[4] BOREXINO collaboration, Measurements of extremely low radioactivity levels in BOREXINO, Astropart. Phys. 18 (2002), p. 1

[5] Laubenstein, M. et al., Underground measurements of radioactivity, Appl. Rad. and Isot. 61, 2-3 (2004), p. 167

[6] Geant4 Collaboration, GEANT4: A Simulation Toolkit, Nucl. Instr. Meth. A 506 (2003), 250-303

[7] Chu, S.Y.F., Ekström L.P. and Firestone R.B., WWW Table of Radioactive Isotopes, database version 1999-02-28 from URL http://nucleardata.nuclear.lu.se/nucleardata/toi/

[8] Commission on Atomic Weights and Isotopic Abundances, Report for the International Union of Pure and Applied Chemistry, Isotopic Composition of the Elements 1989, Pure and Applied Chemistry **70** (1998).

[9] ISO/IEC/OIML/BIPM, Guide to the expression of uncertainty in measurement, (1st corrected edition), International Standard Organisation, Geneva, Switzerland (1995).

[10] ISO 11929-3, Determination of the detection limit and decision threshold for ionising radiation measurements Part 3, International Standards Organisation, Geneva, Switzerland, (2000).

Table 2: *Measurement results for the naturally occurring radionuclides thorium, uranium, potassium and the antropogenic nuclide ^{137}Cs in the I.N.G.V. sea water samples (part 1).*

sample	Thorium [10^{-9} g/g]		Uranium [10^{-9} g/g]			Potassium [10^{-6} g/g]	^{137}Cs [mBq/kg]
	^{228}Ra	^{228}Th	^{234m}Pa	^{226}Ra	^{235}U		
BIOZAIRE 03							
9 fondo	< 11	< 9	< 78	< 3	< 29	291 ± 42	< 15
9 50 m	< 11	< 9	< 98	< 3	< 32	330 ± 35	< 14
11 fondo	< 8	< 7	< 69	< 2	< 23	236 ± 35	< 13
11D 50 m	< 14	< 14	< 142	< 4	< 47	307 ± 45	< 13
12D fondo	< 15	< 14	< 126	< 4	< 40	288 ± 32	< 17
12D 50 m	< 9	< 8	< 95	< 2	< 21	359 ± 39	< 9
14 fondo	< 9	< 7	< 72	< 2	< 24	288 ± 42	< 11
14 50 m	< 11	< 10	< 109	< 3	< 38	300 ± 42	< 11
23 fondo	< 4	< 3	< 39	< 1	< 10	368 ± 39	5 ± 2
23 50 m	< 7	< 6	< 51	< 2	< 19	310 ± 32	< 8
27 fondo	< 10	< 9	< 83	< 2	< 32	310 ± 45	< 9
27 50 m	< 9	< 7	< 57	< 2	< 35	295 ± 43	< 11
27 3000 m	< 6	< 6	< 55	< 2	< 22	293 ± 42	< 6
28 fondo	< 12	< 12	< 109	< 3	< 44	333 ± 48	< 11
28 50 m	< 12	< 11	< 88	< 3	< 34	323 ± 35	< 14
28 3000 m	< 5	< 5	< 49	< 2	< 15	313 ± 32	< 6
32 fondo	< 6	< 4	< 53	< 2	< 13	362 ± 35	12 ± 4
32 50 m	< 9	< 8	< 78	< 2	< 26	313 ± 32	< 11
34 fondo	< 5	< 5	< 43	< 2	< 15	288 ± 42	< 7
34 50 m	< 7	< 6	< 62	< 2	< 20	304 ± 32	< 8
36 fondo	< 6	< 6	< 55	< 2	< 22	310 ± 45	< 6
36 50 m	< 12	< 11	< 109	< 3	< 45	284 ± 42	< 11

Table 3: *Measurement results for the naturally occurring radionuclides thorium, uranium, potassium and the antropogenic nuclide ^{137}Cs in the I.N.G.V. sea water samples (part 2).*

sample	Thorium [10^{-9} g/g]		Uranium [10^{-9} g/g]			Potassium [10^{-6} g/g]	^{137}Cs [mBq/kg]
	^{228}Ra	^{228}Th	^{234m}Pa	^{226}Ra	^{235}U		
ORION							
01RN	< 6	< 7	< 53	< 2	< 14	297 ± 32	< 6
03RN	< 8	< 7	< 89	< 2	< 19	397 ± 42	< 8
05RN	< 11	< 9	< 113	< 2	< 23	417 ± 45	< 12
07RN	< 10	< 8	< 97	< 2	< 26	426 ± 45	< 11
09RN	< 11	< 8	< 97	< 2	< 25	420 ± 459	< 10
11RN	< 17	< 18	< 162	< 5	< 49	323 ± 36	< 20
15RN	< 12	< 10	< 97	< 4	< 39	342 ± 36	< 15
17RN	< 21	< 16	< 170	< 5	< 55	359 ± 39	< 22
19RN	< 17	< 15	< 130	< 4	< 46	342 ± 36	< 19
21RN	< 9	< 9	< 68	< 2	< 46	323 ± 32	< 9
23RN	< 9	< 9	< 72	< 2	< 46	313 ± 32	< 8
27RN	< 12	< 10	< 105	< 3	< 33	336 ± 36	< 14
29RN	< 21	< 16	< 154	< 4	< 92	333 ± 39	< 19
31RN	< 26	< 23	< 243	< 5	< 67	339 ± 39	< 29
33RN	< 10	< 8	< 68	< 2	< 42	333 ± 36	< 8
35RN	< 11	< 9	< 89	< 3	< 30	339 ± 36	< 12
37RN	< 10	< 9	< 78	< 2	< 46	336 ± 36	< 8
PATRASSO							
GMM 1	< 16	< 15	< 122	< 4	< 44	391 ± 42	< 19
GMM 2	< 12	< 11	< 89	< 3	< 62	233 ± 26	< 10
GMM 3	< 15	< 13	< 113	< 3	< 76	368 ± 39	< 13
GMM 4	< 17	< 14	< 113	< 4	< 42	388 ± 42	< 18
SACLANT							
#1	< 15	< 13	< 105	< 4	< 41	342 ± 36	< 17
#2	< 14	< 13	< 105	< 3	< 67	339 ± 36	< 12
#3	< 14	< 13	< 105	< 4	< 41	352 ± 39	< 16
#4	< 15	< 13	< 105	< 4	< 69	349 ± 36	< 15

Table 4: *Measurement results for the naturally occurring radionuclides thorium, uranium, potassium and the antropogenic nuclide ^{137}Cs in the sea sediment and mud volcano samples supplied by I.N.G.V. (part 1)*

sample	Thorium [10^{-6} g/g]		Uranium [10^{-6} g/g]			Potassium [10^{-3} g/g]	^{137}Cs [Bq/kg]
	^{228}Ra	^{228}Th	^{226}Ra	^{234m}Pa	^{235}U		
BIOZAIRE 03							
MTB25 (0-5)cm	6.1±0.4	8.1±0.5	1.61±0.07	2.2±0.5	2.9±0.4	9.7±1.0	1.5±0.2
MTB25 (10-15)cm	5.6±0.3	8.8±0.5	1.59±0.07	2.7±0.5	2.5±0.3	9.7±1.0	1.7±0.2
MTB26 (0-5)cm	9.5±0.6	9.8±0.6	2.68±0.12	2.6±0.5	3.5±0.4	10.1±1.0	< 0.09
MTB26 (10-15)cm	10.2±0.6	9.8±0.6	3.10±0.13	3.4±0.5	4.2±0.5	11.5±1.3	0.27±0.05
MTB28 (0-5)cm	9.4±0.6	8.8±0.5	3.11±0.13	2.9±0.5	3.8±0.4	11.2±1.1	< 0.20
MTB28 (25-30)cm	10.1±0.6	9.6±0.6	2.65±0.12	3.2±0.6	5.0±0.6	10.9±1.1	< 0.15
MTB29 (0-5)cm	7.0±0.4	6.2±0.4	1.79±0.08	2.8±0.6	3.9±0.4	10.5±1.1	< 0.12
MTB29 (40-50)cm	9.2±0.5	9.3±0.6	1.31±0.06	4.2±0.5	5.5±0.6	9.9±1.0	< 0.08
MTB30 (0-5)cm	11.0±0.7	9.7±0.6	3.54±0.16	1.7±0.7	3.7±0.5	10.6±1.1	< 0.15
MTB30 (40-51)cm	11.2±0.7	11.0±0.6	3.40±0.15	3.6±0.5	6.5±0.7	11.9±1.2	< 0.09
MTB31 (0-5)cm	9.8±0.6	9.9±0.6	3.31±0.15	2.5±0.8	3.8±0.6	9.8±1.0	0.19±0.04
MTB31 (40-50)cm	11.6±0.7	10.6±0.6	3.34±0.15	3.8±0.7	7.1±0.7	12.1±1.2	< 0.13
MTB32 (0-5)cm	12.0±0.7	11.7±0.7	2.27±0.10	2.9±0.8	5.5±1.0	10.1±1.0	< 0.14
MTB32 (40-47)cm	10.2±0.6	9.9±0.6	1.43±0.06	3.2±0.5	3.5±0.5	10.4±1.1	< 0.10
MTB33 (10-15)cm	6.5±0.4	6.6±0.4	1.37±0.06	2.9±0.6	2.8±0.4	9.0±0.9	1.5±0.2

174

Table 5: *Measurement results for the naturally occurring radionuclides thorium, uranium, potassium and the antropogenic nuclide ^{137}Cs in the sea sediment and mud volcano samples supplied by I.N.G.V. (part 2)*

sample	Thorium [10^{-6} g/g]		Uranium [10^{-6} g/g]			Potassium [10^{-3} g/g]	^{137}Cs [Bq/kg]
	^{228}Ra	^{228}Th	^{226}Ra	^{234m}Pa	^{235}U		
PATRASSO							
Malta C13	2.7±0.2	2.4±0.2	0.71±0.03	3.4±0.4	2.6±0.4	4.1±0.4	0.08±0.03
Malta #19	2.3±0.4	7.5±0.4	1.39±0.06	1.3±0.3	3.0±0.4	13.1±1.3	< 0.08
# 1	4.7±0.3	5.4±0.3	1.11±0.05	1.5±0.4	2.1±0.4	14.2±1.4	7.3±0.7
# 2	4.7±0.3	5.4±0.3	1.08±0.05	2.0±0.5	1.7±0.3	14.3±1.4	7.0±0.7
# 3	5.0±0.3	5.8±0.3	1.13±0.05	1.5±0.3	2.1±0.4	15.2±1.5	7.7±0.8
2005 # 1	6.8±0.4	6.9±0.4	1.47±0.06	1.2±0.4	1.8±0.3	18.3±1.8	4.3±0.5
2005 # 2	7.2±0.4	6.5±0.4	1.31±0.06	2.2±0.4	2.2±0.4	18.1±1.8	0.21±0.04
mud volcanoes							
Fango 1	5.3±0.3	5.6±0.4	1.45±0.07	2.7±0.7	2.0±0.3	10.2±1.0	0.14±0.06
Fango 2	6.2±0.4	6.2±0.4	1.64±0.07	2.6±0.6	1.7±0.2	12.8±1.3	< 0.11
Pineto	8.6±0.5	8.8±0.6	2.52±0.11	2.7±0.7	3.4±0.3	13.6±1.4	< 0.13
Dashgil 1	5.4±0.3	5.4±0.3	1.64±0.07	2.2±0.5	2.1±0.2	13.5±1.4	< 0.08
Dashgil 2	6.0±0.4	5.7±0.4	1.95±0.09	2.7±0.7	2.4±0.2	13.3±1.3	< 0.11
Banar	5.7±0.3	5.7±0.3	1.73±0.07	1.9±0.4	2.4±0.2	14.2±1.4	< 0.06
Kechaldag 1	9.2±0.5	9.2±0.5	5.73±0.24	8.7±1.0	6.8±0.7	23.6±2.4	< 0.12
Kechaldag 2	7.9±0.5	7.6±0.5	4.5±0.20	6.0±1.1	6.7±0.7	19.8±2.0	< 0.09
Lokbatan	6.1±0.4	5.9±0.4	2.13±0.10	2.5±0.8	2.8±0.3	14.2±1.4	< 0.83
FI1A	12.8±0.7	11.5±0.7	4.01±0.17	2.2±0.5	2.6±0.3	12.0±1.2	< 0.09
FI1B	7.0±0.4	7.5±0.5	2.09±0.09	1.7±0.5	2.8±0.3	16.1±1.6	< 0.08
FI2A	11.1±0.7	9.8±0.6	3.33±0.14	2.9±0.5	2.7±0.3	17.4±1.7	< 0.08
FI2B	11.8±0.7	9.9±0.6	3.54±0.15	2.6±0.4	2.2±0.2	16.4±1.6	0.13±0.04
PMA1	8.1±0.5	7.8±0.5	2.56±0.11	1.8±0.6	3.0±0.3	16.5±1.7	< 0.11
PMA2	7.1±0.4	7.0±0.4	2.06±0.09	3.8±0.8	2.9±0.3	17.3±1.7	< 0.11

TELLUS. Ground deformations and their effects on the near-Earth Space

V. Sgrigna [a], A.Buzzi[a], L. Conti [a], C.Stagni[a], D.Zilpimiani[b]

a Dipartimento di Fisica "E. Amaldi", Universitá and Sezione INFN Roma Tre- Italy.

b Institute of Geophysics, Georgian Academy of Sciences (GAS) and National Space Agency, Tbilisi, Republic of Georgia.

Abstract

This report describes the activities carried out by the TELLUS team during 2005. These activities have been continuing those concerning ground aseismic creep strain events, observed by the TELLUS tilt network, the ESPERIA space mission project planned and designed for studying Earth near-Earth space interactions, and the construction of particle detector ARINA to be installed on board the Russian satellite RESURS-DK1, which launch is scheduled for mid-2006 within the PAMELA mission. ARINA is part of the ESPERIA payload. Another one is LAZIO-SiRad-EGLE. During 2005 this magnetic and particle experiment has been tested in space on board the International Space Station and used for collecting particle and magnetic data. The two instruments have been built during 2004 within a collaboration of Università and Sezioni INFN Roma Tre, Perugia and Roma Tor Vergata, with the Lazio Region and Polytechnic of Moscow (MEPhI). LAZIO-SiRad-EGLE thermal, vibration and electromagnetic emission tests were performed in laboratory both in Italy and in Russia. Launch was made on April 15, 2005. Also a study of intense fluxes of high-energy particles precipitating from the inner Van Allen radiation belt has been carried out in 2005 and correlated with seismic activity. Data were collected by the SAMPEX/PET NASA mission.

1 The aim of the TELLUS Experiment

The main scientific objective of the TELLUS experiment is the study of Earth's surface deformation events (particularly, earthquakes) and their possible effects in the atmospheric, ionospheric, and magnetospheric regions of our Planet. Electromagnetic emissions (EME) associated with seismic events appear to be an efficient coupling element between Earth's surface and surrounding near space. At this purpose continuous mechanical measurements are performed at three tilt sites of LNGS, while pre-seismic EME-wave investigations demand for specific space experiments to be carried out on board of LEO (Low-Earth-Orbit) satellites. Within the TELLUS experiment, a space mission project (ESPERIA) has already been performed for the Italian Space Agency (ASI) and one of the ESPERIA instruments (the ARINA particle detector) has been built during 2002. They have been described in the 2002, 2003 LNGS Annual Reports [1],[2]. During 2004 another ESPERIA instrument (the EGLE magnetometer) has been built and tested in laboratory [3].

2 Activities carried out by the TELLUS team during 2005

The experimental apparatus consists of three bi-axial tiltmeters, one ESPERIA satellite configuration resulting from a phase A study, and one ARINA particle detector design. During 2005, was designed and built the space model of the LAZIO-SIRAD-EGLE experiment (coordinated by R. Battiston) within the ENEIDE space mission for the International Space Station (ISS). This mission was managed by the European Space Agency (ESA). This space experiment was developed within a collaboration between Universities and related Sezioni INFN of Roma Tre, Perugia and Roma Tor Vergata, Regione Lazio and Polytechnic of Moscow (MEPhI). The experiment includes the LAZIO particle detector, developed by the Perugia team (Roberto Battiston, Principal Investigator); the SIRAD detector, made by the Roma Tor Vergata team (Piergiorgio Picozza, Principal Investigator), and the broad-band EGLE search-coil magnetometer made by the Roma Tre team (Vittorio Sgrigna, Principal Investigator). These instruments have been built to check instruments in space for a future LEO satellite mission and to monitor the radiation and magnetic environment inside the ISS. The EGLE Laboratory Model was space qualified and launched in space on April 15, 2005 on board the ISS. The EGLE laboratory model has been illustrated in the previous 2004 LNGS report [3]. The space instrument has also reported in international Conferences [4],[5] together with LAZIO-SIRAD detectors [6],[7].

Another work we carried out in 2005, was the analysis of high-energy particles detected by the Proton Electron Telescope (PET) of the SAMPEX NASA space mission. The study pointed out a correlation between high-energy burts of particles precipitating from the inner Van Allen radiation belt and seismic activity. Results have been published in an international journal [8], and presented in International Conferences [9],[10].

184

3 A short-description of the space Experiment

The monitoring of electromagnetic environment on board the ISS needs of an appropriate observation methodology and of a corresponding suitable experimental equipment design. The continuous monitoring of EM environment on board the ISS by an advanced magnetic experiment in the ULF-HF band is important in the following scientific areas:

a. Search of space weather conditions in equatorial, middle-latitude and sub-auroral ionosphere.

b. Geophysical research of plasma-wave processes connected to solar - magnetosphere - ionosphere - atmosphere-lithosphere interactions

c. Investigation of possible relationships between seismic activity and ULF-VLF EM phenomena that may be related to earthquakes.

d. Continuous monitoring of ULF-ELF-VLF EM activity in the near-Earth space including ELF-VLF EM pollution.

e. Monitoring of natural and man-made variations of the plasmasphere caused by whistlers.

f. Study of the EM background and space weather phenomena.

g. Investigation of effects of the large ISS structure on the propagation of EME-wavw front.

LAZIO-SIRAD-EGLE experiment aims at performing measurements involving:

1. radiation environment

2. magnetic environment inside the ISS.

This experiment (figure 1) livioincludes the high-precision low-frequency magnetometer EGLE (Esperia's Geo-magnetometer for a Low-frequency wave Experiment).

EGLE is used to measure the intensity and variations of the magnetic field within the ISS, and to correlate these measurements with those of particle fluxes. The study of these effects is important to detect electromagnetic field variations and particle pitch angle distribution of the precipitating particles. EGLE experiment is also the first test in space of a data acquisition system based on the 1-Wire®technology. EGLE is constituted by:

- a single axis search-coil probe, the EGLE Magnetometer Head (MH),

- an electronic interface with amplifiers, filtering and data acquisition unit (EGLE MB box),

- a 2m long cable to connect LAZIO Main Electronic Box and EGLE Magnetometer Box,

Figure 1: Egle box and Egle magnetometer head

- a 1-Wire®to RS232 serial adapter on the LAZIO PC tower. EGLE has been built for automatic measurements of the low-frequency magnetic field component. The instrument performs high accuracy measurements. The advantages in using such a device are:

- small dimensions and mass; low power consumption;

- data acquisition via 1-Wire®technology;

- a standard power supply of the device.

The Egle data acquisition board is shown in figure 2.

A schematic representation of EGLE magnetometer and characteristic amplitude-frequency response are reported in figure 3.

Figure 4 shows the preparation and launch of the ENEIDE mission.

Figure 5 shows the installation of EGLE inside the PIRS Module of the ISS.

An example of data recorded on board ISS is shown in figures: 6-9.
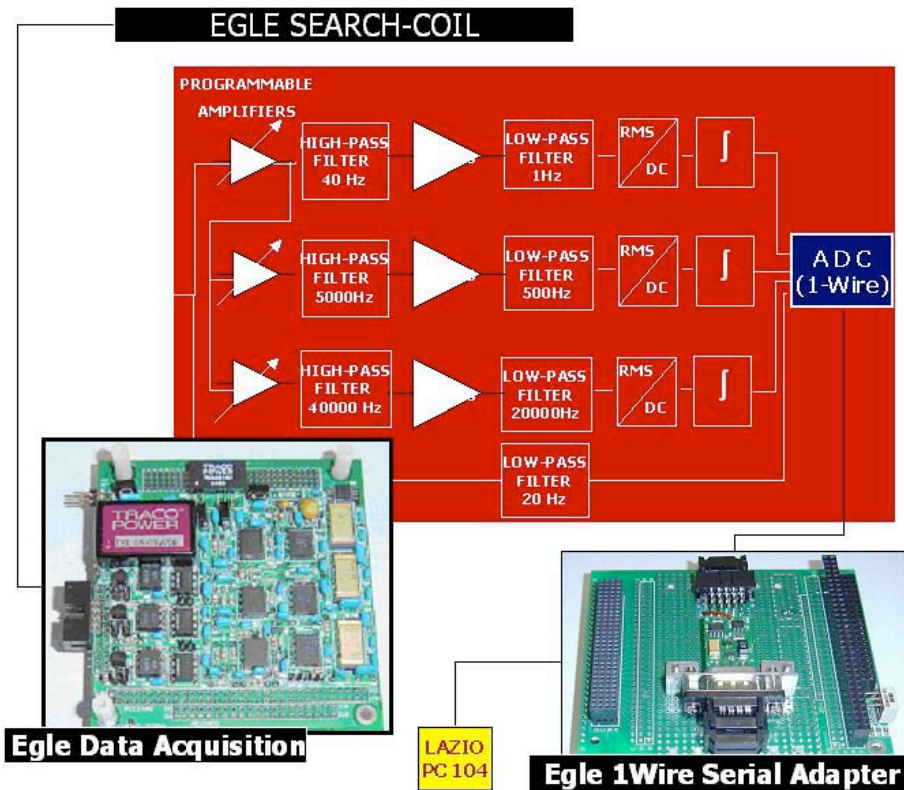
Figure 2: Egle data acquisition board
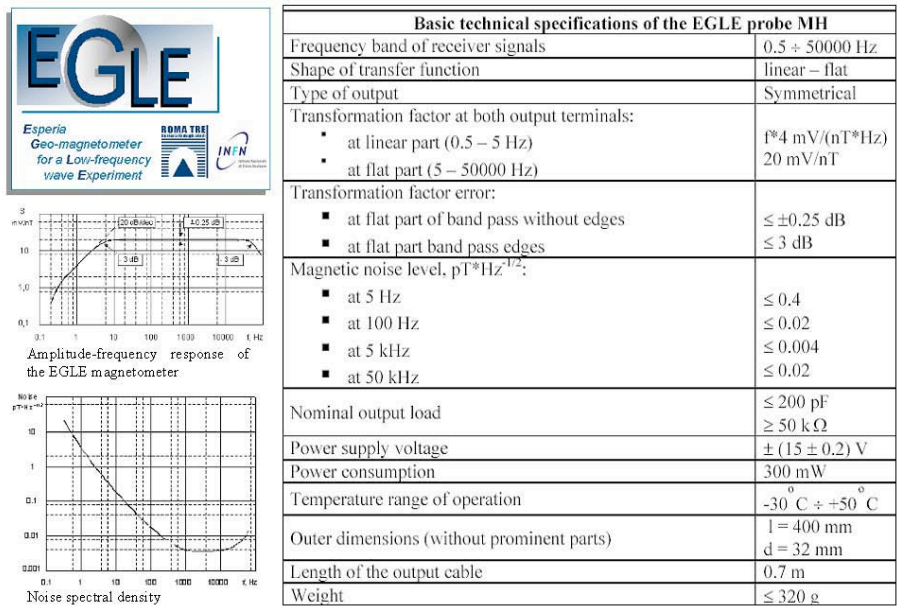
Figure 3: Egle magnetometer characteristics
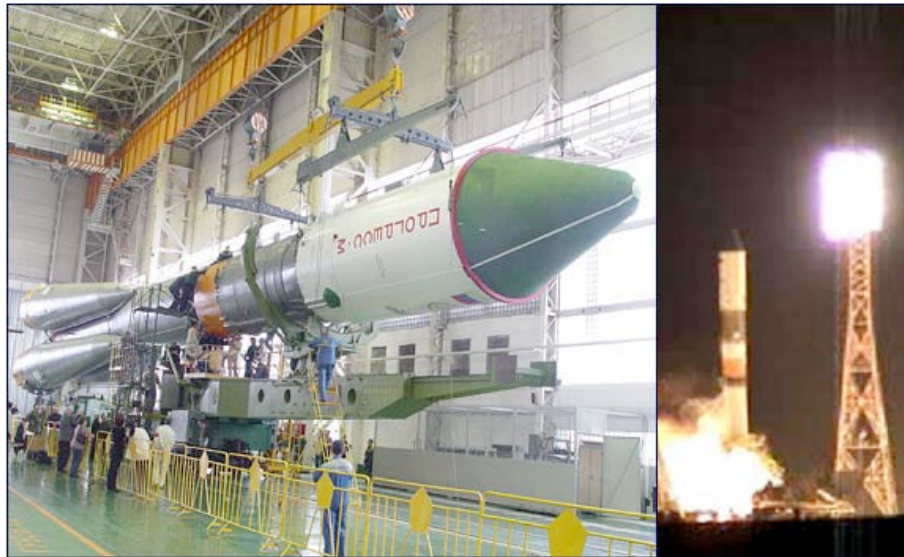
Figure 4: Preparation and launch of the ENEIDE mission

Figure 5: Egle and Lazio installation on board the ISS, inside the PIRS module.
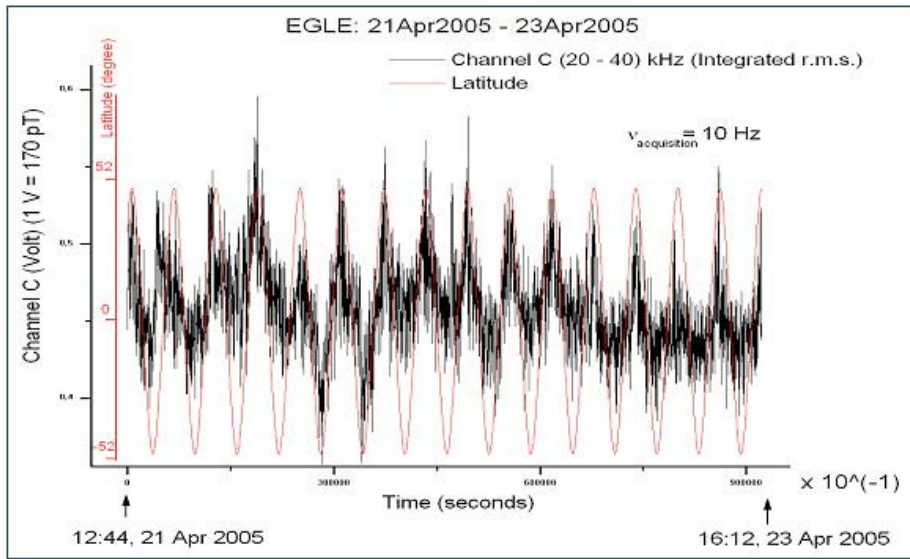
Figure 6: An example of Egle data recording: latitude vs time. (Channel C; $\simeq 60pT\pm3\%$).
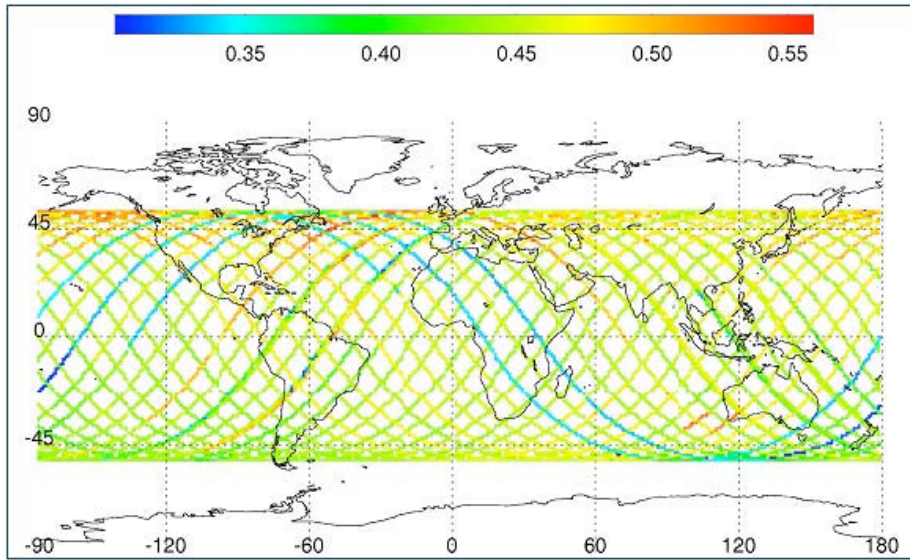
Figure 7: Geographic distribution of magnetic Egle data.

189
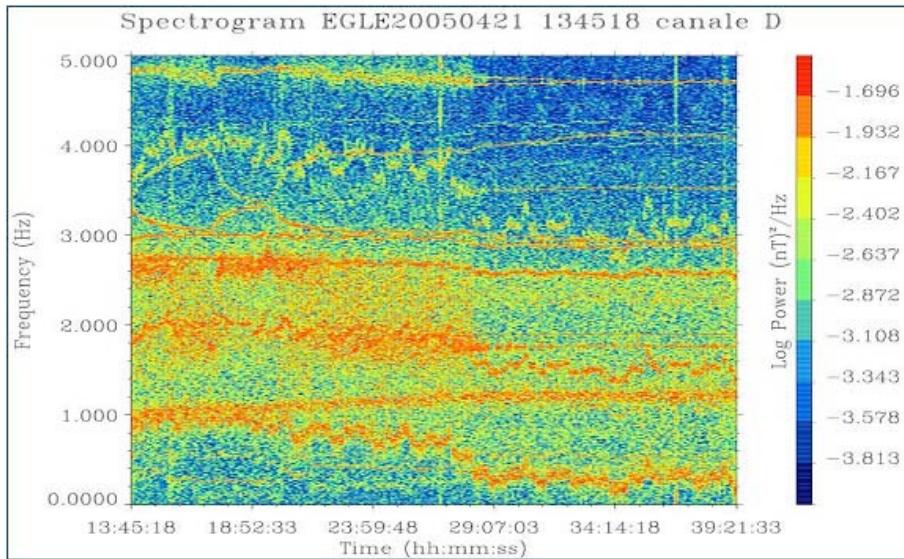
Figure 8: A spectrogram of magnetic Egle data.
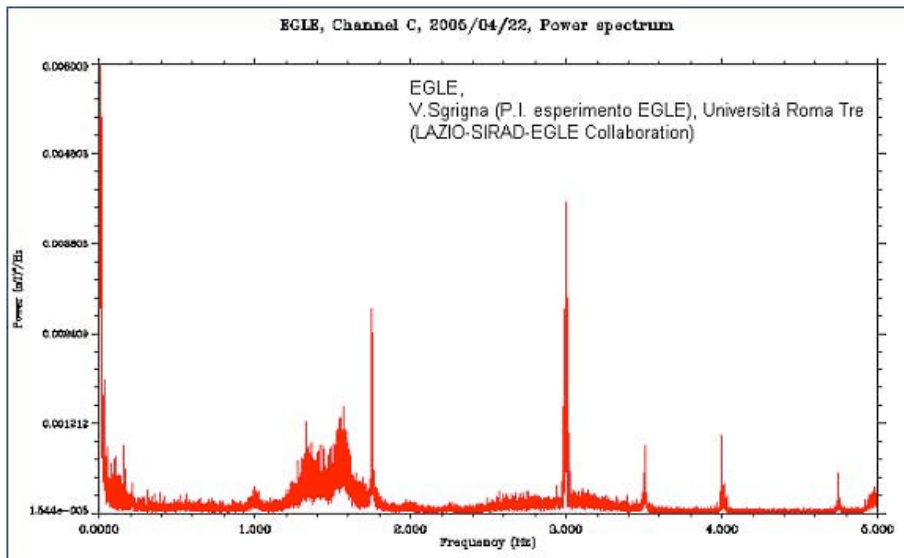
Figure 9: A spectrum of Egle magnetic data.

References

[1] Sgrigna, V., Conti, L., Malvezzi, V., 2002. TELLUS. Ground deformations and their effects in the near-Earth space, Laboratori Nazionali del Gran sasso, INFN, Annual Report, 2002, pp. 217-232.

[2] Sgrigna, V., A. Buzzi, A. Cirella, L. Conti, V. Malvezzi, 2003. TELLUS. Ground deformations and their effects in the near-Earth space, Laboratori Nazionali del Gran sasso, INFN, Annual Report, 2003, pp. 221-228.

[3] Sgrigna V., Buzzi A., Conti L., Stagni C., Zilpimiani D,, 2004. TELLUS. Ground deformations and their effects in the near-Earth space, Laboratori Nazionali del Gran sasso, INFN, Annual Report, 2004, pp. 189-200.

List of Publications in 2005

[4]] Sgrigna V, 2005. Description and Testing of ARINA and LAZIO/EGLE instruments in Space within the ESPERIA mission project and the DEMETER Guest Investigation Programme. DEMETER Guest Investigator Workshop, CNES, Paris, France, 2-4 May 2005.

[5] Conti, L., A. Buzzi, V. Sgrigna, C. Stagni, D. Zilpimiani, 2005. The EGLE experiment. (within the LAZIO-SIRAD-EGLE Collaboration: Conti, L., A. Buzzi, V. Sgrigna, C. Stagni, D. Aisa, A. Alvino, S. Ascani, P. Azzarello, R. Battiston, S. Bizzaglia, M. Bizzarri, S. Blasko, L. Di Masso, G. Chiocci, D. Cosson, G. Esposito, S. Lucidi, A. Papi, V. Postolache, S, Rossi, G. Scolleri, M. Ionica, F. Altamura, R. Bencardino, V. Bidoli, L. Bongiorno, M. Casolino, M. P. De Pascale, G. Mazzenga, M. Minori, M. Ricci, P. Picozza, D. Zilpimiani, A. Abramov, M. C. Korotkov, A. M. Galper, A. V. Popov, A. Kalmikov, A. Ivanova, A. Franceschi, S. Dell'Agnello, C. Falcone, S. Tassa, A. Potetti, L. Valentini). 10th Scientific Assembly of the International Association of Geomagnetism and Aeronomy (IAGA 2005), Toulose, France, July 18-29, 2005, Session Division II, C085: Low Latitude atmosphere-ionosphere-magnetosphere coupling, dynamics and energetics; IAGA2005-A-01522, p.83.

[6] R.Bencardino, F.Altamura, V.Bidoli, M.Casolino, M.P. De Pascale, P.Picozza, A. Alvino, S.Ascani, P.Azzarello, R.Battiston, S.Bizzaglia, M.Bizzarri, S.Blasko, G. Chiocci, D.Cosson, L.Di Masso, G.Esposito, L.M.Farnesini, M.Ionica, S.Lucidi, A.Papi, V.Postolache, S.Rossi, G.Scolieri, L.Bongiorno, S.Dell'Agnello, A. Franceschi, M. Ricci, C. Falcone, S. Tassa, A. Abramov, A. Ivanova, A.M. Galper, A. Kalmikov, M.C. Korotkov, A.V.Popov, A. Buzzi, L. Conti, V. Sgrigna, C. Stagni, D. Zilpimiani, A. Pontetti, L. Valentini. Response of the LAZIO-SiRad detector to low energy electrons. Proc. ICRC 2005, Pune(India). 00,101-104,ita-bencardino-R-abs1-sh36-poster.

[7] F. Altamura, R. Bencardino, V. Bidoli, L. Bongiorno, M. Casolino, M.P. De Pascale , M. Minori, P. Picozza, D. Aisa, A. Alvino, S. Ascani, P. Azzarello, R. Battiston, S. Bizzaglia, M. Bizzarri, S. Blasko, L. Di Masso, G. Chiocci, D. Cosson , G. Esposito,

S. Lucidi ,A. Papi, V. Postolache, S. Rossi, G. Scolieri, M. Ionica, A. Franceschi, S. Dell'Agnello, M. Ricci, C. Falcone, S. Tassa, A. Kalmikov, A.V. Popov, A. Abramov, M.C. Korotkov, A.M. Galper, A. Ivanova, L.Conti, V.Sgrigna , C.Stagni , A.Buzzi , D. Zilpimiani, A.Pontetti , L.Valentini. Preliminary results from the LAZIO-Sirad experiment on board of the International Space Station. Proc.ICRC 2005, Pune (India). 00,101.104, ita-casolino-M-abs2-sh35-poster

[8] Sgrigna, V., Carota, L., Conti, L., Corsi, M., Galper, A., Picozza, P., Stagni, L., 2005. Correlations between earthquakes and anomalous particle bursts from SAMPEX/PET satellite observations, J. Atm. Solar-Terrestrial Phys., 67, 1448-1462, 2005a.

[9] Sgrigna V., Buzzi, A.; Conti, L.; Picozza, P.; Stagni, C.; Zilpimiani, D 2005. Ground rock deformation events and their possible effects in the near-Earth space. General Assembly of the European Geosciences Union, Vienna, Austria, 24-29 April, 2005. Session Natural Hazards, NH 4.02: Deformation processes accompanying mechanical and electromagnetic phenomena, for rocks and other materials, from laboratory to geophysical scale, EGU05-A-06210, NH4.02-1FR3P-0043, p. 450.

[10] Conti, L., A. Buzzi, A. M. Galper, S. V. Koldashov, A. M. Murashov, P. Piccozza, R. Scrimaglio, V. Sgrigna, L. Stagni, 2005. Influence of the seismic activity on the inner Van Allen radiation belt. 10th Scientific Assembly of the International Association of Geomagnetism and Aeronomy (IAGA 2005), Toulose, France, July 18-29, 2005, Session Division I, GA101: Monitoring earthquakes and volcanic activity by magnetic, electric and electromagnetic methods; IAGA2005-A-01518, p.46.